

CENTRO DE INVESTIGACIÓN Y DE ESTUDIOS
AVANZADOS DEL INSTITUTO POLITÉCNICO NACIONAL

UNIDAD ZACATENCO

DEPARTAMENTO DE INGENIERÍA ELÉCTRICA

SECCIÓN BIOELECTRÓNICA

**“Evaluación de la efectividad de la electroquimioterapia para el
tratamiento de cáncer de mama primario con base en el desarrollo de
una planeación de tratamiento *in silico* y su validación *in vitro*”**

T E S I S

Que presenta

M. en T. A. ADRIANA LETICIA VERA TIZATL

Para obtener el grado de

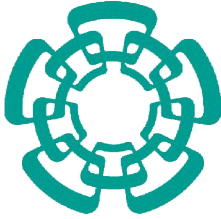
DOCTORA EN CIENCIAS

EN LA ESPECIALIDAD DE INGENIERÍA ELÉCTRICA

Director de Tesis: Prof. Dr. Arturo Vera Hernández

Ciudad de México

DICIEMBRE, 2019



CENTER FOR RESEARCH AND ADVANCED STUDIES OF
THE NATIONAL POLYTECHNIC INSTITUTE

ZACATENCO CAMPUS

DEPARTMENT OF ELECTRICAL ENGINEERING

BIOELECTRONICS SECTION

***“Effectiveness assessment of electrochemotherapy for the treatment of
primary breast cancer based on the development of patient-specific
treatment planning in silico, and its validation in vitro”***

Ph. D. THESIS

by

M. S. A. T. ADRIANA LETICIA VERA TIZATL

In Fulfillment of the Requirements for the degree of

Ph. D. ELECTRICAL ENGINEERING SPECIALTY

Doctoral Advisor: Prof. Dr. Arturo Vera Hernández

Mexico City

DECEMBER, 2019

ACKNOWLEDGEMENTS

To the **National Council for Science and Technology (CONACYT, Mexico)** for the support and the scholarship granted during my doctoral program in which I was given the CVU/scholar number:388502/593152. I hope this dissertation contributes to your aim and to the scientific growth of our nation.

To the reviewers of this thesis; Dr. Juan Manuel Gutiérrez Salgado, Dr. Sergio Rodríguez Cuevas, Dr. Damijan Miklavčič, Dr. Lorenzo Leija Salas and Dr. Arturo Vera Hernández. Your comments and observations highly impacted on the quality of the work. I deeply appreciate your time on reviewing the contents.

To my dear mentor, professor, **Dr. Arturo Vera Hernández**, for taking me in as your student, and for trusting me and this project regardless of its newness and unexplored application in Mexico. For your support and empathy in all circumstances, but mainly when questionings, challenges and hard times for the project had to be overcome.

To my dear assessor, professor, **Dr. Lorenzo Leija Salas**, for admitting me as a member of your laboratory. For motivating me and propelling me to explore academic opportunities abroad, and for sharing with me a bit of your ambitious and visionary mind. I will always remember our days together and talks in Nancy, France.

To my dear assessor, **MD, Oncologist Sergio Rodríguez Cuevas**, for conceiving the project, and for being with me, guiding and supporting me from the very start of the work, since my masters until now. Without your vision, this project would not exist.

To my beloved sister, colleague and active member of the project, **MD, M. Sc. Claudia Elizabeth Vera Tizatl**, for your invaluable contributions on the medical and biological fields of the project. For your hard work while designing and carrying out all the experiments. For guiding me, supporting me and healing me anytime, anywhere, regardless of the distance.

To professor **Dr. Damijan Miklavčič**, for accepting me as a scholar intern in the Laboratory of Biocybernetics at the Faculty of Electrical Engineering in Ljubljana, Slovenia. For everything I learnt from you, and for being a valuable member of my evaluation committee. You have been and will be an inspiration, both as a human being and as a professional.

To professor **Dr. Bor Kos**, for guiding me and training me during my stay in the Laboratory of Biocybernetics. For working hardly with me during the publication process of our JCR paper in spite of the distance between us.

To professor, **Dr. Rafael V. Davalos**, for accepting me as a scholar intern in the Laboratory of Bioelectromechanical Systems at the Institute for Critical Technology and Applied Science, Virginia Tech, USA. For trusting me and supporting my project during my stay with you. Your work, humanity and humbleness are inspirational and motivating to me.

To professor, **Dr. Daniel Martínez Fong**, who belongs to the Department of Physiology, Biophysics and Neurosciences, Cinvestav, Mexico, and who allowed us to use of the electroporation device for the experiments carried out in cell suspensions and adhered cells.

To **M. Sc. José Hugo Zepeda**, for your technical support and guidance during my stay in the Laboratory of Electromagnetic Radiation and Ultrasound (LAREMUS). For the nice talks and coffee/tea breaks we shared.

To my beloved youngest sister **M. A. T. Pamela Patricia Vera Tizatl**, for hearing me and advising me in every discussion we had about my project. For supporting me and helping me to continue my professional road in a postdoc position.

To my parents, **Bertha Leticia Tizatl Juárez, and Patricio Vera Lauriano**, for educating me, leading me, propelling me, inspiring me, walking with me and loving me in spite of my many deficiencies and imperfections as your daughter. You have been and always will be my reason to be a better person and professional.

CONTENTS

CHAPTER	PAGE
1. RESUMEN	1
1. ABSTRACT	3
2. INTRODUCTION	
2.1. LITERATURE SURVEY	4
2.1.1. Electroporation	4
2.1.2. Reversible electroporation	5
2.1.3. Electrochemotherapy	6
2.1.4. Irreversible electroporation	7
2.2. STATE OF THE ART	
2.2.1. Electroporation-based treatment planning of deep-seated tumor	
2.2.2. Electrochemotherapy of deep-seated tumors	11
2.2.3. Irreversible electroporation in the clinical practice	12
2.2.4. High Frequency Irreversible electroporation	13
2.3. STATEMENT OF THE PROBLEM	14
3. OBJECTIVES	
3.1. General objective	17
3.2. Specific goals	17
4. CONTRIBUTIONS	
4.1. Evolution of computational modeling; from ideal geometries to realistic models	

4.2. Needle-electrode arrays for deep-seated targets	19
4.3. Use of hydrogels as mimics for breast tumors	19
4.4. Electroporation protocols for the treatment of breast cancer	20
4.5. Use of Paclitaxel in electrochemotherapy of invasive ductal carcinoma	
4.6. Visualization of cell membrane after electroporation of adhered cell	

5. METHODOLOGY

5.1. Target tumors establishing	22
5.2. Patient-specific treatment planning for electrochemotherapy of invasive ductal carcinoma	22
5.2.1. ECT treatment planning for MRI-based realistic computational breast models; static conductivity approach	23
5.2.2. Electroporation modeling optimization	26
5.2.3. ECT treatment planning for MRI-based realistic computational breast models; dynamic conductivity approach	37
5.2.4. Realistic computational breast models base on DBT imaging	38
5.2.5. Novel needle-electrode design for electrochemotherapy	45
5.2.6. ECT treatment planning for DBT-based models	49
5.3. Reversible Electroporation <i>in vitro</i>	51
5.3.1. Electroporation of cell suspensions	53
5.3.2. Electroporation of two-dimensional cell cultures; adhered cells	
5.3.3. Electroporation of three-dimensional cell cultures; hydrogels	59
5.4. Breast Electrochemotherapy <i>in vitro</i> with paclitaxel	62
5.5. Complementary Investigation	63

5.5.1. Cell morphology and Cell-specific Induced Transmembrane Voltage in adhered cells	64
5.5.2. Monitoring and visualization of disturbances on the cell membrane after electroporation of adhered cells	65
5.5.3. Irreversible Electroporation of three-dimensional cell cultures; hydrogels	66
5.5.4. Pilot study of high-frequency electroporation of three-dimensional cell cultures; hydrogels	67

6. RESULTS

6.1. Electric field distribution in the MRI-based model (static conductivity)	69
6.2. Electric field distribution in the MRI-based model (dynamic conductivity using a sequential model)	72
6.3. Patient-specific electroporation protocols establishing for DBT-based models	75
6.4. Cell-specific electroporation protocols for breast-cancer cell suspensions	
6.5. Cell-specific electroporation protocols for breast-cancer adhered cells	
6.6. Establishing reversible electroporation thresholds in three-dimensional cell cultures	88
6.7. Effectiveness of ECT with paclitaxel in breast-cancer cells	89
6.8. Cell-specific Induced Transmembrane Voltage for suspended and adhered cells.	92
6.9. Visualization of mechanical disturbances on the cell membrane	94
6.10. Findings on irreversible electroporation of breast-cancer hydrogels	96

6.11. Findings on high frequency electroporation of breast-cancer hydrogels

7. DISCUSSION	102
8. PERSPECTIVES	115
9. CONCLUSIONS	118
10. PRODUCTIVITY	122
11. APPENDIXES	126
12. REFERENCES	177

1. RESUMEN

La electroquimioterapia ha sido investigada como un potencial tratamiento mínimamente invasivo y altamente eficiente para tumores cutáneos y subcutáneos. Actualmente se investiga activamente su efectividad en el tratamiento de diversos tumores profundos. Sin embargo, el tratamiento de cáncer de mama primario con electroquimioterapia ha sido escasamente abordado. Por tal motivo y con base en alta incidencia y mortalidad en mujeres jóvenes en México debido a esta enfermedad, se describe en esta tesis, la investigación *in silico* e *in vitro* sobre el uso de la electroporación y la electroquimioterapia en el tratamiento del carcinoma ductal invasor. Computacionalmente, se diseñaron doce arreglos de electrodos de aguja que buscan minimizar la invasividad del tratamiento y aseguran la cobertura de los tejidos de interés con un campo eléctrico entre 400 V/cm y 800 V/cm. Con estos electrodos, se planearon tratamientos con electroquimioterapia en modelos computacionales anatómicos realistas de tres pacientes mexicanas a través de un modelo numérico secuencial de electroporación. Los resultados *in silico* mostraron que tres arreglos de electrodos con 4, 5 y 6 agujas respectivamente, garantizan la cobertura de carcinomas mamarios entre 1 cm³ y 5 cm³. Experimentalmente, la electroporación se demostró en tres arreglos de cultivos celulares; suspensiones, cultivos bidimensionales y cultivos tridimensionales (hidrogeles) que proveen un medio experimental análogo a un tejido. Se utilizaron tres líneas celulares mamarias cancerosas (BT-20, MCF-7 y HCC1419) y una línea celular epitelial mamaria (MCF-10A), es decir no cancerosa. Particularmente se observó, que la electroquimioterapia puede representar una alternativa prometedora como tratamiento adyuvante de tumores metastásicos y como terapia neoadyuvante a tumores Her-2/neu. Por el contrario, los tumores mamarios triple negativo mostraron una alta sensibilidad a electroporación y por tanto la electroporación irreversible podría representar una técnica efectiva de tratamiento. Por otra parte, las células de mama no cancerosas demandaron el mayor voltaje en todos los arreglos celulares para ser electroporadas. Los

resultados *in vitro* demuestran que la respuesta a la electroporación depende del protocolo eléctrico utilizado y de la histología y morfología celular. Además, son congruentes con los obtenidos en las planeaciones de electroquimioterapia *in silico*.

1. ABSTRACT

Electrochemotherapy has been investigated as a highly efficient, minimally invasive treatment for cutaneous and subcutaneous tumors. Currently, its efficiency in the treatment of diverse deep-seated tumors is actively investigated. However, the treatment of primary breast cancer with electrochemotherapy has been scarcely addressed. Consequently, and based on the high incidence and mortality in young women due to this disease in Mexico, this dissertation describes the investigation *in silico* and *in vitro* on the use of electroporation and electrochemotherapy in the treatment of invasive ductal carcinoma. Computationally, twelve needle-electrode arrays aimed to minimize the invasiveness of the treatment, and to guarantee the coverage of target tissues with an electric field between 400 V/cm y 800 V/cm. These electrodes were evaluated in the treatment planning of electrochemotherapy in realistic computational models of three mexican female patients, using a sequential model of electroporation. The *results in silico* showed that three needle-electrode arrays with 4, 5, and 6 needles respectively, ensure the coverage of breast carcinomas ranging from 1 cm³ to 5 cm³. Experimentally, electroporation was demonstrated in three cell cultures platforms; cell suspensions, bidimensional cultures, and three-dimensional cell cultures (hydrogels) that mimics a tissue. Three breast cancerous cell lines (BT-20, MCF-7 and HCC1419) and a non-cancerous breast cell line (MCF-10A) were used. Particularly, it was found that electrochemotherapy may represent a promising alternative as an adjuvant treatment of metastatic breast tumors, and as a neoadjuvant therapy for Her-2/neu tumors. Oppositely, triple negative breast tumors showed a high sensitivity to electroporation and therefore, they may be efficiently treated with irreversible electroporation. On the other hand, non-cancerous breast cells demanded the highest voltage in all cell culture platforms in order to be electroporated. The results *in vitro* showed that the cell response to electroporation depends on the electric protocol, and on the histology and cell morphology. They are in addition congruent with the results obtained from the treatment planning *in silico*.

2. INTRODUCTION

Based on the increasing incidence of Breast cancer in Mexico, which has become the first cause of death in women caused by cancer, the *Feasibility Assessment of Electrochemotherapy Use as a Treatment Alternative for Primary Deep-Seated Breast Carcinomas* is described as a dissertation thesis in the following chapters. In this chapter, fundamental definitions regarding electroporation and electrochemotherapy shall be presented.

2.1. LITERATURE SURVEY

2.1.1. Electroporation

In 1982, the term “Electroporation” (EP) was introduced to describe the induced permeability of the cell membrane to low permeant or non-permeant molecules that do not diffuse across the plasma membrane and for which there are no active transporters. EP refers to a phenomenon in which the permeability of the cell membrane is increased due to the formation of hydrophilic pores in the lipid bilayer. Electroporabilization is a related term that ascribes this permeability increase to a wide range of biophysical and biochemical mechanisms caused by the exposure of the cells to electric pulses and hence, to an external electric field [Kotnik T. 2019]. Electric pulses are delivered to cells/tissues through electrodes. During the application of this electric field, an induced transmembrane voltage (ITV) proportional to the strength of the electric field, results as an additional component superimposed on the resting transmembrane voltage (TMV) [Pavselj & Miklavcic, 2008, Kotnik T. 2019]. The increase in membrane permeability results in an inflow/outflow of molecules, originally non-permeable to the cell membrane [Zupanic, Kos, & Miklavcic, 2012]. The critical electric field and the corresponding TMV that must be exceeded in order to detect permeabilization of the cell membrane is not a universal constant but a variable dependent on several factors: cell type, cell size, local membrane curvature, transported

molecule, exposure duration, temperature, osmotic pressure, and artifacts caused by the sensitivity of the detection technique [Kotnik T. 2019]. EP is currently used in biotechnological applications (for microbial deactivation and shelf life time prolongation of beverages) and in medical applications such as gene transfection, gene therapy, DNA vaccination, cell electrofusion, drug delivery and tissue ablation [Kanduser M and Miklavcic D, 2008, Miklavcic D. et al., 2012]. Regarding cell viability, there are two types of electroporation: reversible electroporation (REP) and irreversible electroporation (IRE) [Mir L. M, 2008].

2.1.2. Reversible electroporation

In reversible electroporation, cell membrane permeabilization to molecules deprived of transmembrane transport mechanisms is a transient phenomenon, since after some time membrane reseals and reestablishes its homeostatic semipermeable properties, allowing ions and other small molecules to passively cross [Miklavcic, D. and Davalos R. V., 2015]. The kinetics of transmembrane transport mediated by electropermeabilization have reported that membrane electrical conductivity and permeability increase detectably within less than a microsecond after the onset of the electric pulse. The kinetics of transmembrane transport can be roughly divided by into five stages: the initiation of a permeable state (μs), its expansion (ms), stabilization with partial recovery (ms), the resealing of the membrane (s) and finally gradual cessation of residual memory effects (cell viability is preserved, but membrane structural and physiological properties recover on a much longer time) reflected in cells' altered physiological processes and reactions to various stressors (h) [Kotnik T. 2019].

2.1.3. Electrochemotherapy

Electrochemotherapy (ECT) involves the combination of reversible electroporation and chemotherapy, allowing this latter to be successfully used as a nonthermal local antitumor treatment in which electric pulses are applied to a target tumor after injection of a membrane-impermeant cytotoxic drug, [Corovic, Zupanic, & Miklavcic, 2008; Miklavcic, D. and Davalos R. V., 2015]. Some chemotherapeutic drugs targeting intracellular material have poor membrane permeability, requiring high doses for antitumor effectiveness producing pronounced side effects. Since electroporation increases the permeability of the cell membrane, the dose of chemotherapeutic agents can be reduced by using ECT. For an efficient ECT, it is necessary that the entire tumor tissue is subjected to a local electric field in the range between reversible and irreversible electropermeabilization threshold values. In addition, another effect increasing the efficacy of ECT is drug retention in the tumor for longer periods of time due to vascular lock after electric pulse application [Corovic, Zupanic, & Miklavcic, 2008; Haberl, S. et al., 2013].

ECT was carried out for the first time *in vivo* by L. M. Mir in 1989. Since then many treatment protocols and high voltage pulse generators were developed and ECT have been successfully used in Europe in the treatment of cutaneous and subcutaneous metastases regardless of its histological origin [Hoffman A. G. 1999; Ivorra A. 2009; Pavliha D. et al. 2012]. First clinical trials with ECT using bleomycin and cisplatin were presented during 1990s, for the treatment of head and neck squamous cell carcinoma and malignant melanoma. Despite ECT efficacy was demonstrated, differences among treatment procedures, the lack of defined operating procedures and the use of different pulse generators raised a concern to standardize ECT use in the clinical practice. Therefore, the European Commission funded two projects: Cliniporator™ (IGEA, SpA, Italy) in 2000 for the development of a medical grade device for EP and, in 2006, the Standard Operating Procedures (SOP) for electrochemotherapy [Zupanic, Kos, & Miklavcic, 2012; Cadossi, R. et al., 2014]. The SOP consisted of a

decision tree offering treatment guidelines to ensure patient safety and to achieve optimum treatment results regarding (i) the selection of chemotherapeutic drug, (ii) drug delivery route (intravenous or intratumoral), (iii) electrode shape (plate or needle), and (iv) pulse parameters (usually 8 pulses, 100 μ s in duration, 1 Hz to 5 kHz pulse repetition frequency). These procedures were developed to be used specifically with the pulse generator Cliniporator and the maximum lesion size to be treated was \leq 3cm [Mir, L. M. et al., 2006]. About three thousand patients has been treated since SOP publication with an objective response rate of 68% to 86% and complete response rate of 33% to 60% [Zupanic A, Kos B and Miklavcic D, 2012; Haberl, S. et al., 2013; Probst U. et al., 2018]. Currently, ECT clinical application is mostly limited to Europe and is routinely applied in everyday clinical practice in 130 clinical centers [Miklavcic, D. et al., 2014]. Current research aims now to translate the application of ECT from easily accessible lesions to the treatment of nonsuperficial tumors which requires addressing the critical importance of achieving complete EP of the target lesion(s) in order to treat deep-seated tumors [D. Milavcic et al., 2010].

2.1.4. Irreversible electroporation

Irreversible electroporation (IRE) uses an energy regime much higher than that of reversible electroporation and induces cell death via various mechanisms. [Meijerink M. R, 2018, Chapter 2]. When a cell is exposed to a large number of electric pulses, or the pulse duration is too long, or the electric field amplitude to which the cell is exposed is too intense, the cell becomes permanently permeabilized, and therefore resulting in cell death due to a loss of its homeostasis caused by irreversible electroporation (IRE). Normally, IRE demands a higher number of pulses than reversible electroporation. Yet it is beneficial to reduce the electric field strength to achieve ablation, this fact increases the treatment duration. [Miklavcic D. and Davalos, 2015; Kos B, 2017].

The field of electroporation has become dominated mainly by reversible electroporation applications whereas irreversible electroporation was viewed as an undesirable side effect and was studied only to define the upper limit of the electrical parameters that induce reversible electroporation, and in food industry for sterilization and preprocessing of food. Nonetheless, during the last decades, IRE has emerged as a non-thermal ablation method for normal and tumor tissue caused by either necrotic or apoptotic cell death, considered as an important medical technology. Its use as an independent modality for ablation of substantial volumes of tissue has been confirmed in studies on cells, small animal models and in large animal models in the liver and the heart. The most attractive properties of IRE are (1) the resultant sharp demarcation between ablated tissue and untreated tissue, without areas in which the extent of damage changes gradually as during thermal ablation, since a cell is destroyed by IRE or not, (2) IRE induces apoptotic cell death and these apoptotic cells are promptly removed by immune cell derived phagocytosis and replaced by intrinsic cellular regeneration, in contrast to coagulative necrosis and protein denaturation induced by thermal ablation modalities, where necrotic cell death does not get replaced by intrinsic cellular regeneration but rather by fibrosis and scarring of cellular and tissue remnants and finally (3) IRE is not affected by blood flow, (4) it has the ability to spare connective structures, bile ducts and large blood vessels. Sparing of vascular structures makes IRE a promising technique in the treatment of tumors abutting large blood vessels. In addition, IRE can be performed as a real-time percutaneous image-guided intervention, with observation and measurements of the treated area during real-time monitoring correlating well with pathological measurements of the lesion, in contrast to thermal ablation techniques which creates hyperechoic microbubbles from the thermally injured tissue in ultrasound (US) images, significantly hindering the possibility of real-time monitoring. Moreover, the extent of IRE ablation can be also confirmed with computed tomography (CT) and magnetic resonance imaging (MRI). However, IRE electroporation devices present technical challenges in

designing devices for the delivery of the appropriate electric fields [Rubinsky B, 2007; N. Jourabchi N. et al., 2014]. IRE is currently performed *in vivo* with a medical device approved for clinical use, Nanoknife (AngioDynamics, Queensbury, NY, USA).

2.2. STATE OF THE ART

2.2.1. Electroporation-based treatment planning of deep-seated tumors

A successful electroporation-based treatment of a deep-seated tumor demands the whole tumor to be covered with the sufficiently strong electric field exceeding the reversible or irreversible electroporation threshold depending on the treatment to be performed; ECT or tissue ablation by IRE, respectively. For deep-seated tumors, electric field pulses are delivered to the target area by needle electrodes, which can be fixed in an array or as individual electrodes inserted in the vicinity of the tumor, or inside the tumor. The electric field strength at a given point in a tissue is dependent on the distance between the electrodes, the shape of the electrodes, the applied voltage, the electrical properties of the tissue(s) in which the electrodes are inserted, and the number of needles used since normally, more than one electrode pair is activated depending on the imitations of the electroporation pulse generator, in terms of voltage and current. Based on the number of variables affecting the electric field distribution in a tissue, it is advisable to establish a treatment planning in order to determine the best electroporation-based procedure [Kos B. 2017].

A key factor increasing the complexity of planning ECT or IRE treatments of deep-seated tumors is the remarkably different electrical properties of the tissues in the human body. In addition, tissue conductivity increases as a function of the electric field and hence, the exact electric field in the non-homogeneous tissues cannot be calculated analytically and instead computational methods are required. A numerical method frequently used in

electroporation research is the finite element method (FEM) in order to calculate the electric field distribution during an electroporation pulse. This problem may be considered as a steady state problem since most electroporation pulses for ECT and IRE use 100 μ s long pulses which are long compared to the cell charging constant. Therefore, it can be assumed that the transient phenomena occur in the beginning of the pulse and have settled out before the end of the pulse [Kos B. 2017].

An individualized numerical treatment planning is based on the treatment planning in radiotherapy and consists of several phases; patient medical imaging in order to determine the anatomy of the patient and delimitate the clinical target volume including the tumor volume and a surrounding safety margin, image preprocessing, image segmentation into different tissues in order to confer the electrical properties of different tissues, three-dimensional anatomical model generation, electrode placement, implementation of the mathematical model of electroporation, and optimization of results as described in [Pavliha, D. et al., 2012]. The coverage of the target tissues with a sufficient electric field above reversible or/and irreversible electroporation thresholds, depends on the maximum voltage and current that the pulse generator can provide. Currently, the most widely used generators for ECT and IRE allow the activation of six individual electrodes, which yield a total of 15 possible pairs. Consequently, visualization tools for the consecutive coverage by multiple pairs of needle electrodes have been developed, including electroporation cross-section images overlaid on original CT images showing the regions where the conductivity increased and which is directly related to the maximum electric field strength and to the degree of electroporation. A second visualization tool is a cumulative coverage plot, analogous to dose-volume histograms typically used in radiotherapy, which shows the fraction of tissue volume covered by electric fields above electroporation threshold after the complete sequence of pulses has been applied [Zupanic , Kos, & Miklavcic, 2012; Kos B. 2017].

2.2.2 Electrochemotherapy of deep-seated tumors

Based on the effective outcomes obtained with ECT application in the treatment of cutaneous and subcutaneous tumors regardless of histological origins, the treatment of internal tumors is currently a new scope. It is hypothesized that ECT may be used in the treatment of tumors located in surgically difficult to reach regions, or in the treatment of lesions resistant to chemotherapy or radiotherapy. To this purpose, new standard operating procedures for deep-seated tumors are needed and hence, treatment planning design for ECT has been developed taking as a basis, radiotherapy treatment planning [Pavliha, D. et al., 2012; Pavliha, D. et al., 2013; Miklavcic, D. et al., 2014; Cadossi, R. et al., 2014].

A novel application of Electrochemotherapy for the treatment of liver and bone metastases, soft tissue sarcomas, brain tumors and colorectal esophageal tumors has been described along with the electrodes proposed to be used for each target tissue [Miklavcic D, 2012]. However, treatment of deep-seated tumors become a more complex procedure. The current challenges in performing ECT in this type of tumors are (1) the determination of tissue conductivity, (2) the amount of dynamic conductivity changes due to EP, (3) the determination of thresholds for reversible and irreversible electroporation, also as a function of duration and number of pulses, and (4) the accuracy for treatment planning and positioning of long needle electrodes based on intraoperative imaging such as X-ray, ultrasound, computed tomography (CT) or magnetic resonance imaging (MRI) [Miklavcic D. and Davalos R. V, 2015].

The implementation of ECT in treatment of deep-seated tumors requires the development of new electrodes. Up to now, three types of electrodes have been manufactured and are being tested: long needle electrodes (127 mm length) for treatment of metastases of colorectal tumors in liver, bone metastases and soft tissue sarcomas, endoluminal electrodes (plate) for Colorectal, gastric and esophageal tumors and expandable electrodes for the treatment of brain tumors [Miklavcic, D. et al., 2014].

To the best of our knowledge, there are only 2 works that address the treatment of primary breast cancer with ECT, that is, (1) an infiltrative lobular carcinoma in a single elderly patient, inoperable for neoplastic infiltration of the chest wall and undergoing preoperative (attempt of cytoreduction) and intraoperative ECT prior to radical mastectomy [Cabula C, 2012] and (2) a single clinical case of unifocal ductal breast cancer that reports reduced efficacy of the ECT treatment with 5 needle electrodes [Denzi A. et al., 2015]. Both studies performed ECT through Cliniporator (IGEA SpA, Carpi, Italy) and operating standard procedures for Electrochemotherapy. These encourage the development of better electrode configurations along with an adequate pretreatment planning based on numerical models for the treatment of invasive breast ductal carcinoma with ECT.

2.2.3. Irreversible electroporation in the clinical practice

Because of IRE's non-thermal mechanism to induce cell death, IRE represents an attractive modality to safely treat unresectable tumors, opposite to traditional ablative-thermal technologies [Meijerink M. R, 2018, ch. 2]. Conversely to thermal-ablation modalities, IRE is presumed to be safely used for treating tumors in the vicinity of large vascular structures and heat-sensitive structures including nerves and bile ducts [Jourabchi N, 2014]. Consequently, there has been an increasing research on IRE, moving from *in vitro* studies, to *in vivo* animal studies, and finally to human patients through clinical trials.

In 2010, the first human clinical trial on treatment of prostate cancer with IRE was published in which 94% showed cancer remission. Since then, patients with advanced liver, lung, kidney and pancreatic tumors have enrolled different clinical trials. Among these four types of neoplasia, only liver tumors were suggested to be an optimal target for IRE ablation. Recently, the treatment of renal tumors with IRE has been evaluated and the results of two phase I and II clinical trials are still to be gathered. [Meijerink M. R, 2018, ch. 2].

Regarding the treatment of breast malignancies with IRE, only a preclinical study has been reported, in which breast cancer tumors (MDA-MB231) were implanted in female Nu/Nu mice. Tumor regression was observed in five out of seven tumors. These outcomes suggest that IRE could be an advantageous alternative to surgical resection for breast conserving therapy [Jourabchi N, 2014].

The success of treatments with IRE depends on a number of electrical parameters (number of pulses, length, shape, interval between pulses, field amplitude and polarity). Equally important, it depends on cell parameters (type, morphology). In addition, the most challenging parameter to optimize so far is an accurate electrode placement even with laparotomy. Therefore, a new design of electrode, electrode stabilizer, and multi-imaging modality guidance have been implemented and currently active research projects are being conducted [Jourabchi N, 2014].

2.2.4. High Frequency Irreversible Electroporation (H-FIRE)

Traditional IRE ablation is achieved through a series of unipolar electric pulses that result in muscle contraction which is undesirable during the procedure since electroporation-based therapies require the patient to remain motionless. In order to mitigate this drawback, Arena et al. (2012) developed an approach known as high-frequency irreversible electroporation (H-FIRE) that uses high frequency bipolar bursts to eliminate/minimize muscle contractions. Unlike conventional IRE, H-FIRE protocols involve the use of microsecond bursts of bipolar pulses on the order of 500 ns to 5 μ s, delivered at a pulse repetition rate of 1 Hz. Histopathological studies on tissues revealed that H-FIRE at 250 kHz or 500 kHz was indistinguishable from IRE regarding the ablation efficacy and precision. Moreover, it has been reported that H-FIRE may enable the creation of substantially larger ablations by allowing the use of significantly higher treatment voltages. The clinical application of H-FIRE may eventually

eliminate the need to administer neuromuscular agents during IRE procedure [Jourabchi N, 2014].

H-FIRE has been recently used in mammary tumor ablation using a mouse model (4T1 metastatic human breast cancer cell line) demonstrating that H-FIRE treatment shifts the local immunosuppressive mammary tumor microenvironment to one that is more pro-inflammatory and facilitates improved adaptive immune system engagement, resulting in the targeting and elimination of metastatic cells. H-FIRE is effective in the induction of a systemic anti-tumor immune response that is capable of eliminating metastases in location distal to the primary tumor treatment site. H-FIRE may be a valuable tool as a pre-treatment strategy to prime the immune system to eliminate metastases prior to conventional or emerging therapeutic approaches. [Ringel-Scaia V. M, et. al., 2019].

So far, there is one single clinical trial on the treatment of prostate cancer with H-FIRE. The procedure was performed with a device tested at the Shanghai Testing and Inspection Institute for Medical Devices. The efficacy of ablation at a cellular level was analyzed in eight patients who underwent complete resection of the prostate four weeks after treatment. During this clinical trial, low-dose muscle relaxants were injected before treatment [Dong S. et al., 2018]

2.3. STATEMENT OF THE PROBLEM

Since 2006, breast cancer represents in Mexico the first cause of death due to malignant tumors in women older than 25 years. Its recurrence has increased 49.5% during the last two decades. About 45% of total cases are diagnosed in stages III and IV and 11% are younger than 40 years old. The survival rate for this latter group is lower compared to the one for older population [Masson Doyma México S. A. 2015]. The detection methods combine imaging and corroboration techniques (biopsy with histopathologic studies). Imaging

monitoring include mammography, ultrasound (US), magnetic resonance (MR), positron emission tomography (PET) and digital breast tomosynthesis (DBT). Mammography has been used as the primary solving tool for breast abnormalities but despite its benefits it is limited by tissue superimposition. On one hand, overlying dense tissues can mask tumors, potentially leading to a missed cancer and on the other, overlapping structures can mimic the appearance of a tumor and thereby cause a false-positive. Therefore, DBT is becoming increasingly accepted since it can reduce the tissue overlap effect and structure noise in single slice two-dimensional mammography imaging [Reiser & Sechopoulos, 2014; Smith, 2012] and it is nowadays the main detection tool used in the Institute of Breast Diseases-FUCAM. Regarding the treatment techniques used for breast cancer, neoadjuvant chemotherapy, radiotherapy, hormonal therapy and surgical procedures including lumpectomy and mastectomy may be mentioned. Since breast cancer has become a rising problem concerning public health, current efforts are aimed to the control of known risk factors, the establishment of early detection programs and the development of new minimally invasive and conservative treatment procedures to this disease [Masson Doyma México S. A. 2015].

Studies in minimally invasive tumor ablation of breast cancer have been relatively limited so far. Therefore, this dissertation addresses the assessment of electrochemotherapy as a minimally invasive alternative treatment of breast primary tumors in Mexico. For this purpose, technological challenges must be overcome including the design of new electrodes in order to reach the target tissue while preserving the minimally invasiveness of the procedure and the implementation of a treatment planning algorithm considering the electric field distribution, the insertion depth of electrodes. Special emphasis regarding numerical methods has to be made since they represent the only current way of prediction of electric field distribution applied to deep-seated tumors which are most likely to be non-homogeneous, non-linear and anisotropic, thus dielectric properties of target and surrounding tissue must be accurately determined. Since distribution of external electric field is the most important

factor to predict in order to control electroporated and/or ablated zone, the appropriate electrical parameters of the electric pulses must be determined for specific tissues. In turn, based on these parameters, new electric field threshold values for ECT in deep-breast tissues must be calculated in order to be further considered in the new standard operating protocols for electrochemotherapy of deep-seated malignancies.

Since ECT is not an accepted clinical procedure for the treatment of any disease in Mexico, experimental media need to be generated in order to validate the investigation regarding the treatment of breast cancer with ECT.

3. OBJECTIVES

3.1. General objective

Feasibility assessment of electrochemotherapy as a novel treatment alternative of primary deep-seated breast carcinomas based on the development of patient-specific treatment planning and the proposal of an application protocol of this therapy in breast tumors.

3.2. Specific goals

1. Determination of the target lesions based on the most frequent malignancies treated in the FUCAM.
2. Design of a new electrode aimed to reach deep-seated breast tumors, based on the finite element modelling of different configurations of electrodes, simulating the application of electrochemotherapy in breast tumors.
3. Development of realistic computational breast models for simulation of electroporation of breast tumors with the electrodes designed.
4. Development of patient-specific treatment planning for electrochemotherapy of deep-seated breast tumors through the finite element method.
5. Design of an experimental medium that mimics a breast tumor and surrounding breast tissue in order to provide a more realistic breast model for experimental electroporation.
6. Establishing of the electric field threshold for reversible electroporation of deep-seated breast tumors, based on the outcomes of the treatment planning.

4. CONTRIBUTIONS

The general contribution in this dissertation is the evaluation of electrochemotherapy as a potential treatment alternative of primary breast tumors, which has been little investigated worldwide. The particular contributions were achieved thanks to the collaboration with researchers who belong to different departments and institutions; M.Sc. Claudia Elizabeth Vera Tizatl and Dr. Patricia Talamás Rohana who are part of the Department of Infectomics and Molecular Pathogenesis (CINVESTAV-IPN, México); Dr. Damijan Miklavčič and Dr. Bor Kos as part of the Laboratory of Biocybernetics (Faculty of Electrical Engineering, Slovenia), and Dr. Rafael V. Davalos as part of the Institute for Critical Technology and Applied Sciences (Virginia Tech, United States of America).

4.1. Evolution of computational modeling; from ideal geometries to realistic models

Primary breast tumors have not been the main target tissue in ECT. It has been recently addressed and hence, little literature on the issue is currently available. A couple of publications have reported two-dimensional geometries considering a breast tumor and a surrounding healthy tissue in order to numerically determine an appropriate electric field for the treatment with ECT [Vera-Tizatl A. L, 2013; Agoramurthy P. et al., 2011]. Additionally, some three-dimensional models considering simple ideal geometries have been suggested [Vera-Tizatl A. L, 2013, Neal R. E, and Davalos R. V. 2009, Vera-Tizatl A. L, 2017 ERK]. As a main requirement for developing a patient-specific treatment planning for ECT of deep-seated tumors, realistic anatomical models of breast target tissues are presented in this work, which are focused on the development of geometries closer to those that can be found in the clinical practice. Hence, the reconstruction of volumes based on clinical images corresponding to real breast neoplasia were developed. These models

provide, in addition, a basis for evolution of the current models used in the Laboratory for Ultrasound and Electromagnetic Radiation (LAREMUS) in the CINVESTAV, for simulating treatment of breast malignances with thermal ablation, high intensity focused ultrasound and microwave ablation.

4.2. Needle-electrode arrays for deep-seated tumors

Three types of needle electrodes have been designed and manufactured so far for the treatment of deep-seated tumors with ECT [Miklavcic, D. et al., 2014]. In order to ensure an optimal electric field coverage of a deep-seated tumor and a surrounding non-tumoral tissue, new needle-electrode configurations were proposed in this dissertation. These configurations differ from the commercial ones on the number of needles, the inter-needles distance, needle geometrical positioning, and the active length of needles. The aim of the variation of these parameters was to minimize the invasiveness of the treatment, and to evaluate whether a sufficient electric field can be generated with the minimal number of needles positioned in a strategic configuration. If manufactured, these electrodes might be used in any deep-seated neoplasia.

4.3. Use of hydrogels as mimics for breast tumors

Hydrogels, which consist of swollen networks of polymers represent an alternative mimic for the native extracellular matrix. Hydrogel formation consists on encapsulating viable cells within a polymer-network substrate overcoming a transition of liquid precursor solutions into solid materials. They provide a better biological environment than conventional cell cultures, and are more similar to complex native *in vivo* scenarios. 3D hydrogels provide milieus that lead to more realistic cellular responses, especially in the context of pathophysiological environments [Caliari S. R. and Burdick J. A, 2016]. 3D Collagen-based hydrogels have been used as models of non-malignant and malignant tissues for targeted ablation with pulsed electric fields (PEFs). These models have been designed mostly to mimic brain, pancreatic and hepatic tissues in order to evaluate the effects of IRE and HFIRE on these

tissues [Caliari S. R. and Burdick J. A, 2016; Arena C. B. et al., 2012]. A complementary study on the effects of reversible electroporation and IRE in hydrogels seeded with breast cancer cell lines is presented in this dissertation as a contribution on the application of electroporation on mimics of breast tissues.

4.4. Electroporation protocols for the treatment of breast cancer

In order to address the reported current necessity of determining cancer-type-specific voltages in the treatment decision tree of the new modified Standard Operating Procedures (SOP) for Electrochemotherapy [Zhao, D et. al., 2018], a contribution on establishing breast electroporation protocols is to be described in sections 9.4 to 9.6. It is hypothesized that breast cells may respond differently to electroporation depending on the cell type and malignant or non-malignant origin.

4.5. Use of Paclitaxel in electrochemotherapy of invasive ductal carcinoma

Bleomycin has been reported as one of the most promising drugs used in ECT since its cytotoxicity has been reported to be augmented 100-fold approximately by electroporation [Gothelf A, Mir L. M, Gehl J, 2003]. On the other hand, Paclitaxel is the preferred drug for the particular treatment of the invasive ductal carcinoma with conventional chemotherapy based on its low cost and its possible combination with targeted therapies. Therefore, a pilot study on the potentiation of Paclitaxel's effect specifically in breast cancer cell lines was conducted.

4.6. Visualization of cell membrane after electroporation of adhered cells

Electropermeabilization has been assessed indirectly depending on the nature of the molecules used [Batista N and Miklavcic D, 2018; Kamensek et al., 2018; Kotnik et al., 2015; Kotnik et al., 2019]. Generation of rough structures, intense groupings of lipids due to irreversible electroporation [Spugnini et al., 2007], and suggestive images of the formation of volcano-shape defects in

erythrocytes membrane exposed to electric fields have been reported. However, these images were a consequence of sample preparation [Kotnik et al., 2012]. The methodology for electroporation of adhered cells furthered discussed in section 8.3, allowed visualizing disturbances on the cell membrane by means of microscopy techniques. This represents an important contribution which may be further useful in the understanding of pore formation phenomenon attributed to electroporation.

5. METHODOLOGY

5.1. Target tumors establishing

Statistically, the most common histologic subtypes of breast cancer are ductal carcinoma, *in situ* (DCIS) and invasive (IDC) and lobular carcinoma, *in situ* (LCIS) and invasive (ILC). Both of them represent 80% and 10% of all breast cancer types respectively [Masson Doyma México S. A, 2015]. This is in agreement with the morbidity reported by the Institute for Breast Diseases – FUCAM, which consequently sets the invasive ductal carcinoma as the target lesion discussed in this dissertation.

5.2. Patient-specific treatment planning for electrochemotherapy of invasive ductal carcinoma

The first breast models used for the evaluation of an optimal electrode array for the treatment of deep-seated breast tumors with ECT consisted of ideal spherical tumors of 10 mm in diameter surrounded by a sphere of 30 mm in diameter which simulated the safety margin. Both spheres were embedded in a 50 mm x 50 mm x 50 mm block of surrounding healthy tissue [Vera-Tizatl, A. L, et al., 2017, ERK].

Contrary to the spherical breast geometries, three-dimensional realistic breast models were performed considering non-homogeneity of breast, thus containing fatty tissue, fibroglandular breast tissue, skin and neoplastic tissue. For this purpose, two methodologies are described in this section. On the one hand, initial breast models were based on the use of magnetic resonance images, provided on-line, for further three-dimensional reconstruction. On the other hand, a second methodology is presented for modeling of breast malignancies imaged by DBT.

5.2.1. ECT treatment planning for MRI-based realistic computational breast models; static conductivity approach

Three-dimensional reconstruction of tissues was based on medical interpretation, segmentation, and processing of DICOM (Digital Imaging and Communication in Medicine) data provided online by the Cancer Imaging Archive (TCIA) [Smith, K et al.]. The image collections provided by The Cancer Genome Atlas for Breast Invasive Carcinoma (TCGA-BRCA), within the TCIA, correspond to images obtained to assess breast cancer response to neoadjuvant chemotherapy. The scanning modality for these studies is Magnetic Resonance Imaging (MRI) with and without contrast agent, and spin-echo (SE) sequence using a Siemens 3T TIM Trio system. Each study is made of sequences of the axial, sagittal and coronal planes [Smith, K et al.]. Among 164 collections provided by the TCGA-BRCA, a single clinical case, Fig. 1, corresponding to a T2 left breast series of a woman, was selected after clinical guidance taking into account: adequate contrast, optimal resolution of images in each anatomical plane and visible neoplasia. The MRI series were taken on December 20th, 2003.

The sagittal plane, in Fig. 1A, shows a hypodense image corresponding to a fibrocystic pattern, suggestive of a tumor localized in the top right quadrant. In the same image, a second suggestive tumoral mass and a hyperdense image are found in the bottom right quadrant. This latter is consistent with a cystic lesion. Such interpretation was inferred based on a visual inspection due to the lack of data regarding clinical history of the patient. For the collection selected, semiautomatic segmentation based on threshold application was not possible. Due to the low resolution of medical images, pixels corresponding to breast tissue, fatty tissue, and skin own similar intensities. Consequently, voxels in the different volumes overlap. Therefore, manual segmentation of 52 slices was carried out.

Breast tumor reconstruction was carried out with 3D Slicer (National Cancer Institute, USA) which is an open source platform aimed to research and hence,

owning no Food and Drug Administration (FDA) approval. Three labels were used to differentiate three main tissues: fatty tissue (blue), breast tissue (green) and tumoral tissues (yellow) as shown in Fig. 1D. In spite of the achievement of a proper reconstruction for all tissues of interest, only the tumor volumes could be exported for its analysis with FEM since all its faces were adequately parameterized. The rest of the reconstructed volumes appeared as open structures unsuitable to be meshed for FEM analysis [Vera Tizatl A. L. et al.,CCE 2016]

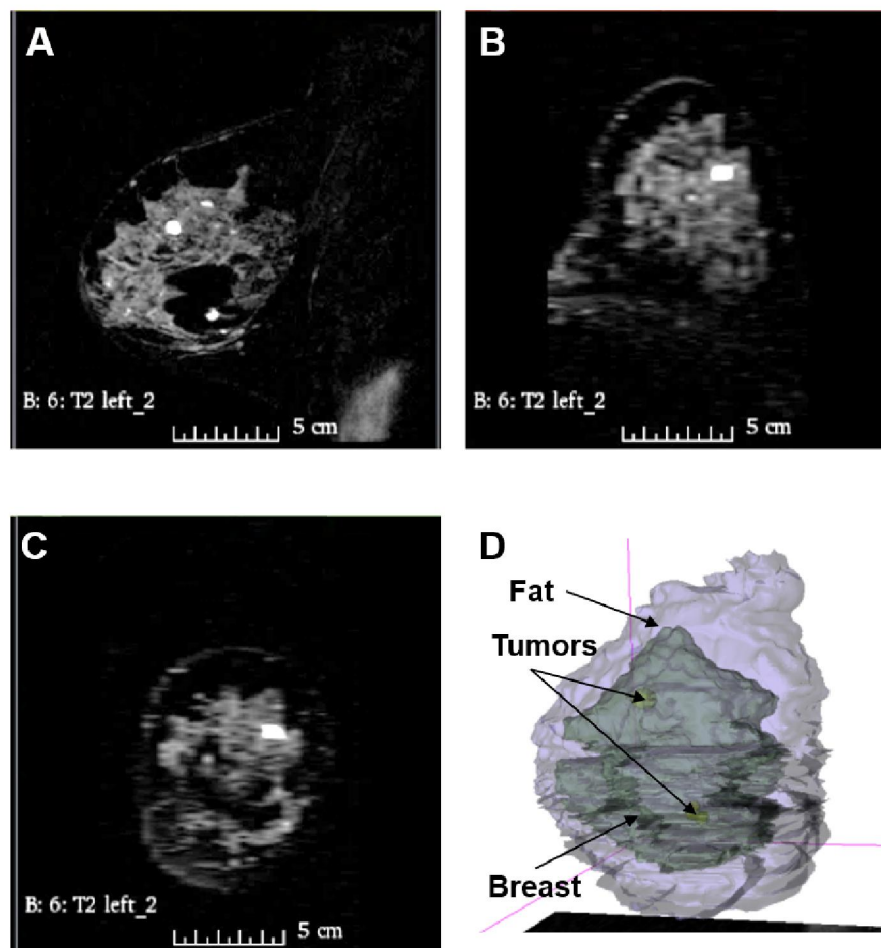


Figure 1. T2 left breast of a woman where two tumors are evident. (A) sagittal plane, (B) axial plane, (C) coronal plane, and (D) target tissue reconstruction in 3D slicer. Three labels were used to differentiate tissues: fat (blue), breast tissue (green) and tumoral tissues (yellow).

The electric field distribution caused by two needle electrodes in the largest tumoral volume (approximately 0.8 cm x 1.0 cm x 0.7 cm) was modeled with FEM (COMSOL Multiphysics®). For this purpose, two conductive cylinders with 1 mm in diameter corresponding to steel needle electrodes were inserted into the tumor, Fig 2A. The simulated electrical properties of tumoral tissue are shown in Table II. Regarding boundary conditions, one electrode was set to electric potential and the second one was grounded. A parametric study was performed ranging the voltage from 100 V to 1500 V with voltage increments of 100 V. This work was presented during the 13th International Conference on Electrical Engineering, Computing Science and Automatic Control, CCE 2016 [Vera Tizatl, A. L et al, CCE 2016]

In order to complement this model, a reconstructed volume of healthy breast surrounding tissue with dielectric properties in Table 1, was filtered and added to the previous model to be analyzed in COMSOL Multiphysics® as shown in Fig. 2B. The electric field distribution within the tumor and the surrounding breast tissue was calculated for 500 V only because of the computational requirements to solve this model [Vera Tizatl A. L. et al., (EBTT), 2016]

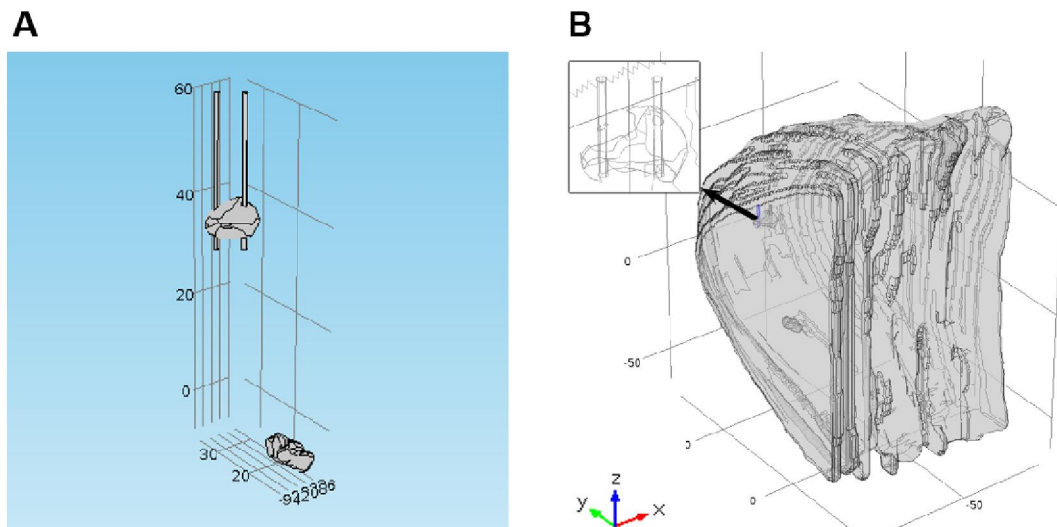


Figure 2. Realistic computational model of two deep-seated breast carcinomas based on MRI imaging. (A) breast carcinomas and two cylindrical conductive

electrodes, and (B) a complete model of a left breast and two needle electrodes [Vera Tizatl A. L. et al., (EBTT). 2016].

Table 1. Electric properties of tissues reconstructed from MRI images.

Property	Value			Unit
	Symbol	Tumor	Healthy breast tissue	
Heat capacity	C_p	3700	3420	J/(kg·K)
Density	ρ	1044	1090	Kg/m ³
Thermal conductivity	k	0.564	0.49	W/(m·K)
Electrical conductivity	σ	0.5	0.05	S/m

5.2.2. Electroporation modeling optimization

The model described in the previous section represented a closer approach to the development of realistic anatomical models than those using spherical geometries to simulate target tissues. However, many aspects to be improved were evident. The manipulation of reconstructed volumes, corresponding to different tissues, in Comsol Multiphysics and positioning of electrodes into the imported geometries was a difficult and time/memory consuming process.

In order to enhance the previous methodology, research activities were carried out at the Laboratory of Biocybernetics, University of Ljubljana, Faculty of Electrical Engineering, Slovenia. Manipulation of models to be solved by the finite element method in COMSOL Multiphysics® was enhanced through LiveLink™ for Matlab. This optimization methodology allowed the insertion of multiple needle electrodes in order to ensure a complete coverage of the target tissues. Main functions were used in Matlab in order to program geometries, boundary conditions, and to extract results instead of using the user interface of Comsol.

For this purpose, three numerical models were developed and compared: (i) a reference model created in COMSOL Multiphysics, Fig. 3A, (ii) an interpolated

model, both considering static conductivity, and (iii) an interpolated model considering an electric field dependent conductivity which represents better the electroporation phenomenon. Interpolated models were programmed in Matlab, as shown in Fig. 3B. Geometrical traits, material properties, boundary conditions and mesh size were varied in order to establish their effects in the resultant electric field during electrochemotherapy.

The geometries for all models consisted of a tumoral volume of 2 cm in diameter embedded in a block of 4 cm x 4 cm x 4 cm surrounding tissue. Four cylinders of 1 mm of diameter and 4 cm length simulate the electrodes positioned orthogonally into the block 2.5 mm away from tumor quadrants. Each pair of electrodes (E1E2, E2E3, E3E4, E4E1, E1E3 and E2E4) was activated sequentially. Regarding the interpolated models, electrical conductivity of the tumor and the surrounding tissue was programmed through interpolation functions defined as grids as shown in Fig. 4. The distance between the points in the interpolation function grid was varied from 0.5 mm (Fig. 4A), 1 mm (Fig. 4B), 2 mm (Fig. 4C), and 4 mm (Fig. 4D).

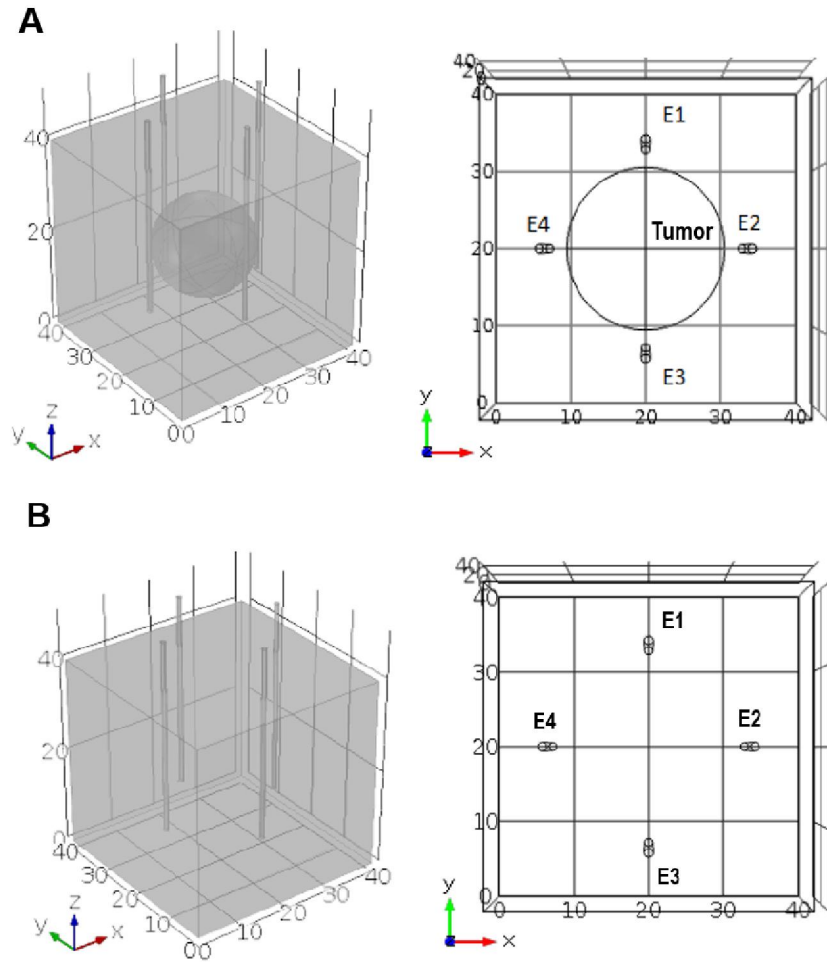


Figure 3. Geometries for electroporation modeling optimization. (A) Reference model of a tumor embedded in healthy surrounding tissue and four needle electrodes (E1, E2, E3 and E4) created in COMSOL Multiphysics interface. (B) Interpolated model of a tumor, defined by a grid of conductivities programmed in Matlab, embedded in a block of healthy surrounding tissue.

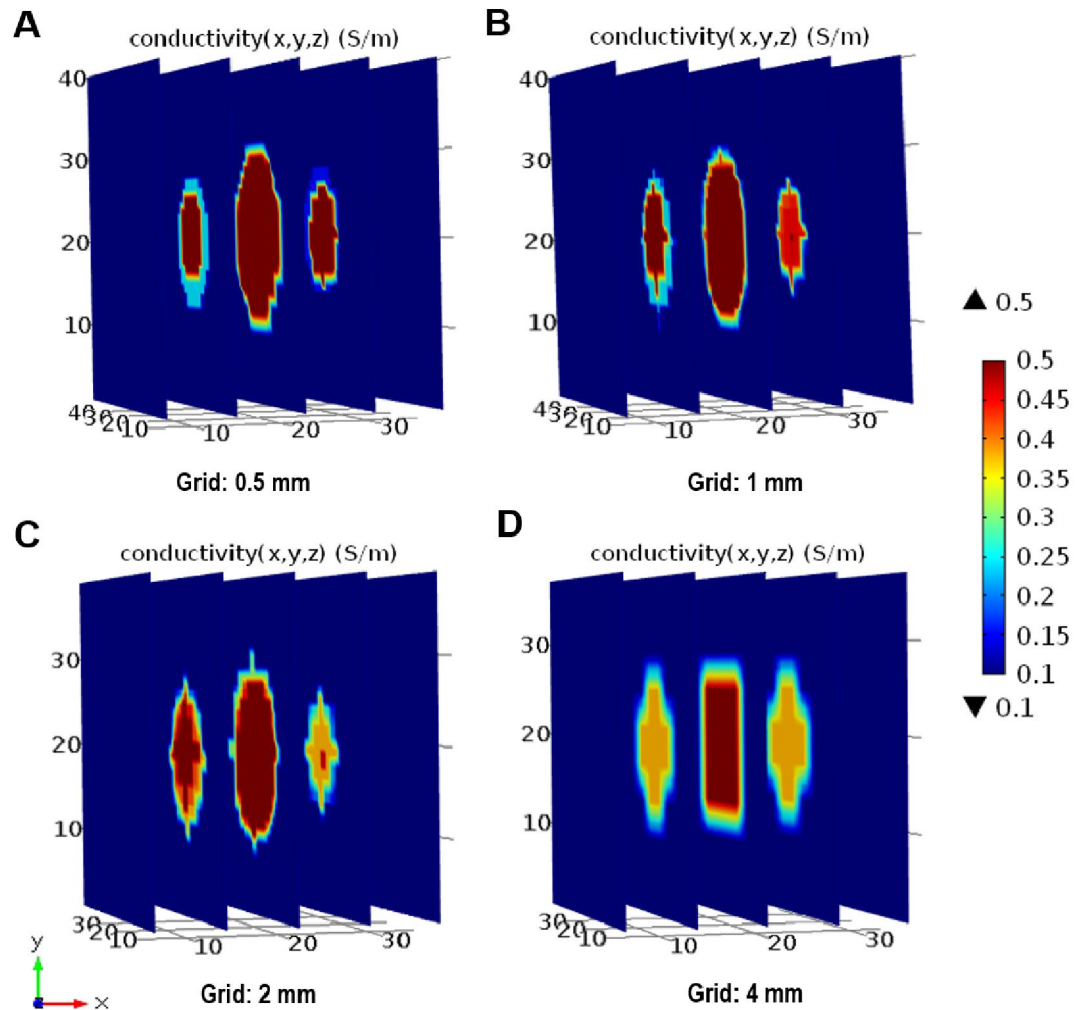


Figure 4. Grid of conductivities programmed in Matlab for defining the tumoral volume embedded in a healthy surrounding tissue. Conductivity grids varied in points spacing; A) 0.5 mm, B) 1 mm, C) 2 mm and D) 4 mm [Vera Tizatli, A. L. et al., (GMEPE/PAHCE) 2017].

For the static conductivity models, the electrical conductivity assigned to tumoral and healthy tissue were 0.5 S/m and 0.1 S/m respectively. Each pair of electrodes was set to 1500 V. Two mesh qualities were used, i. e., a normal mesh (NM) and a finer mesh (FM).

The resultant electric field for each model was read in Matlab through the use of LiveLink™ for Matlab. The electric field distribution for the reference model

and for the models with interpolation functions are shown quantitatively in Table 2 and graphically in Fig. 5. Figures. 5B and 5C show that a grid of conductivities with a spacing of 0.5 mm and 1 mm produce an electric field distribution approximating better to the one obtained for the reference model (Fig. 5A). Despite the distorted geometry generated by the coarser grids of 2 mm and 4 mm (Fig. 5D, Fig. 5E) the electric field magnitudes were similar for all the grids.

Table 2. Electric field distribution in reference model and interpolated models.

Active Pair of Electrodes	Comsol mesh	Maximum Electric Field (V/m) x 10 ⁶				
		Ref. Model	0.5 mm	1 mm	2 mm	4 mm
E1E2	Normal	1.48	2.12	2.13	2.13	2.14
E2E3	Normal	2.57	2.40	2.37	2.28	2.34
E3E4	Normal	2.60	2.39	2.41	2.45	2.47
E4E1	Normal	1.07	2.11	2.16	2.28	2.25
E1E3	Normal	2.42	2.26	2.24	2.15	2.20
E2E4	Normal	1.39	0.76	0.78	0.80	0.77
E1E2	Finer	2.93	1.66	1.67	1.67	1.68
E2E3	Finer	1.97	1.67	1.65	1.59	1.66
E3E4	Finer	1.96	1.64	1.66	1.70	1.74
E4E1	Finer	2.94	1.63	1.67	1.77	1.75
E1E3	Finer	2.74	1.57	1.57	1.67	1.65
E2E4	Finer	2.94	1.63	1.67	1.77	1.75

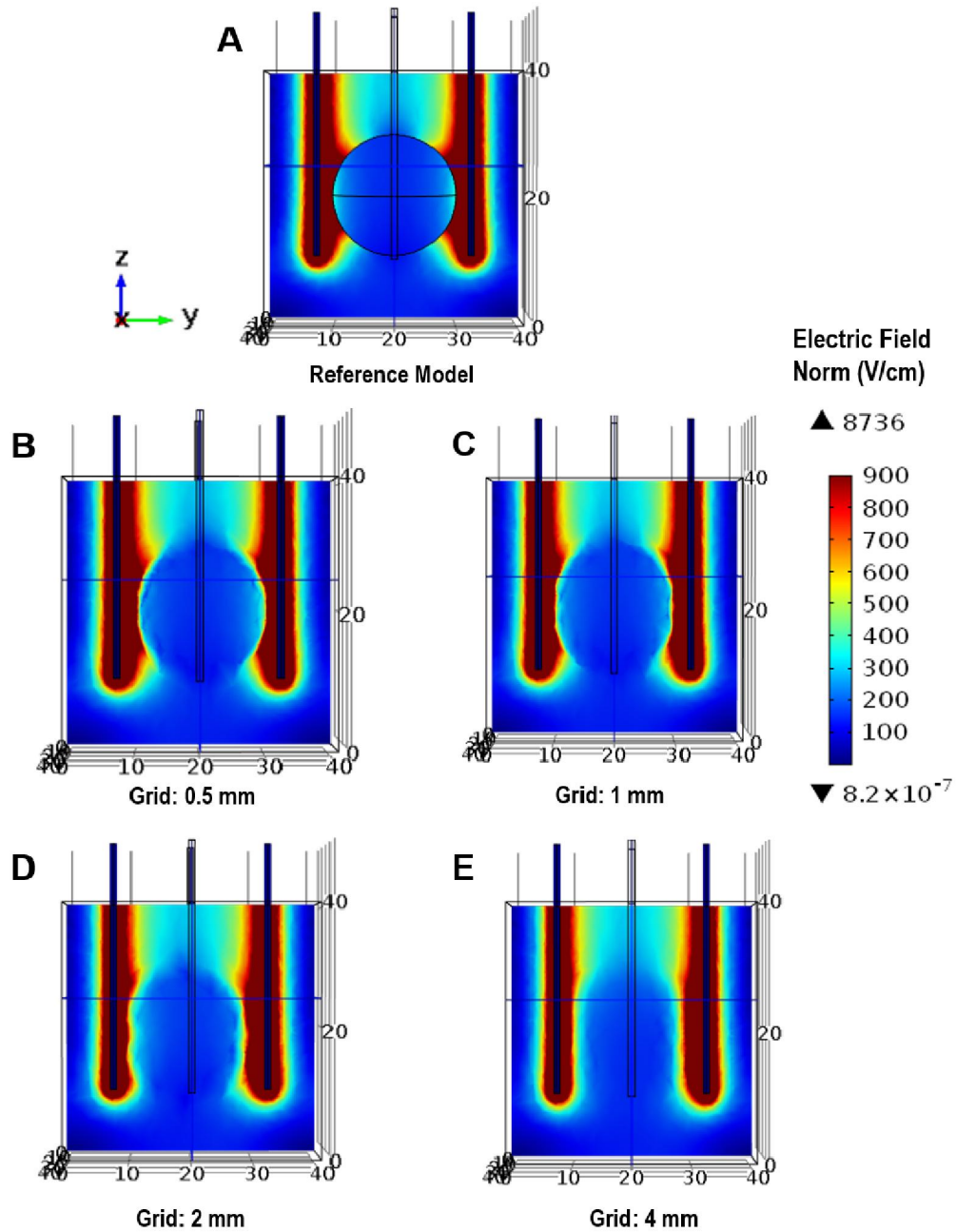


Figure 5. Electric field distribution obtained for (A) the reference model and for (B) 0.5 mm, (C) 1 mm, (D) 2 mm and (E) 4 mm grid spacing in the interpolated model [Vera Tizatl, A. L. et al., (GMEPE/PAHCE) 2017].

The comparison between both models (reference and interpolated model) is based on the correlation factor, the root-mean square error (RMSE), and the

normalized crossed-correlation factor (NCC) as shown in Table 3 and in Fig. 6. In Fig. 6A, B, it can be seen that the most accurate results are obtained for the interpolation function grids of 0.5 mm and 1 mm and the finest mesh. Despite the high correlation factors obtained for the finest mesh, its use seems unsuitable due to the longer solution time than the use of a finer mesh demands. The solution time increased from 15 s to 3.5 min when the geometry mesh was varied from a normal mesh to a finer mesh. In order to determine the similarity between the reference model and the interpolated model with a 1 mm grid, the normalized cross correlation (NCC) was calculated using a normal mesh as shown in Fig. 6C. NCC was calculated along the z axis with a 1 mm spacing for 40 slices representing the complete geometry. E12, E23, E34, E41, E13 and E24 denote the active pair of electrodes E1E2, E2E3, E3E4, E4E1, E1E3 and E2E4 respectively.

Table 3. Comparison between reference model and interpolated models.

Active Pair of Electrodes	Comsol Mesh	Correlation factor				RMSE (V/cm)			
		0.5 mm	1 mm	2 mm	4 mm	0.5 mm	1 mm	2 mm	4 mm
E1E2	Normal	0.9170	0.9225	0.9190	0.9166	119.58	114.60	106.06	117.40
E2E3	Normal	0.9417	0.9445	0.9380	0.9387	103.29	100.81	106.36	105.71
E3E4	Normal	0.9642	0.9626	0.9530	0.9555	79.29	81.30	92.03	89.27
E4E1	Normal	0.9397	0.9411	0.9297	0.9312	100.01	99.01	108.14	106.31
E1E3	Normal	0.9422	0.9438	0.9319	0.9334	92.85	91.55	100.41	98.87
E2E4	Normal	0.9288	0.9321	0.9226	0.9237	97.29	95.02	101.24	100.34
E1E2	Finer	0.9722	0.9791	0.9770	0.9757	77.18	67.98	72.51	75.00
E2E3	Finer	0.9893	0.9930	0.9861	0.9871	46.64	38.19	52.80	51.25
E3E4	Finer	0.9931	0.9927	0.9838	0.9861	39.08	39.07	56.97	52.70
E4E1	Finer	0.9751	0.9788	0.9727	0.9735	73.97	68.64	77.19	76.42
E1E3	Finer	0.9720	0.9764	0.9694	0.9702	70.95	65.47	73.87	73.36
E2E4	Finer	0.9886	0.9929	0.9844	0.9857	43.34	34.65	50.37	48.90

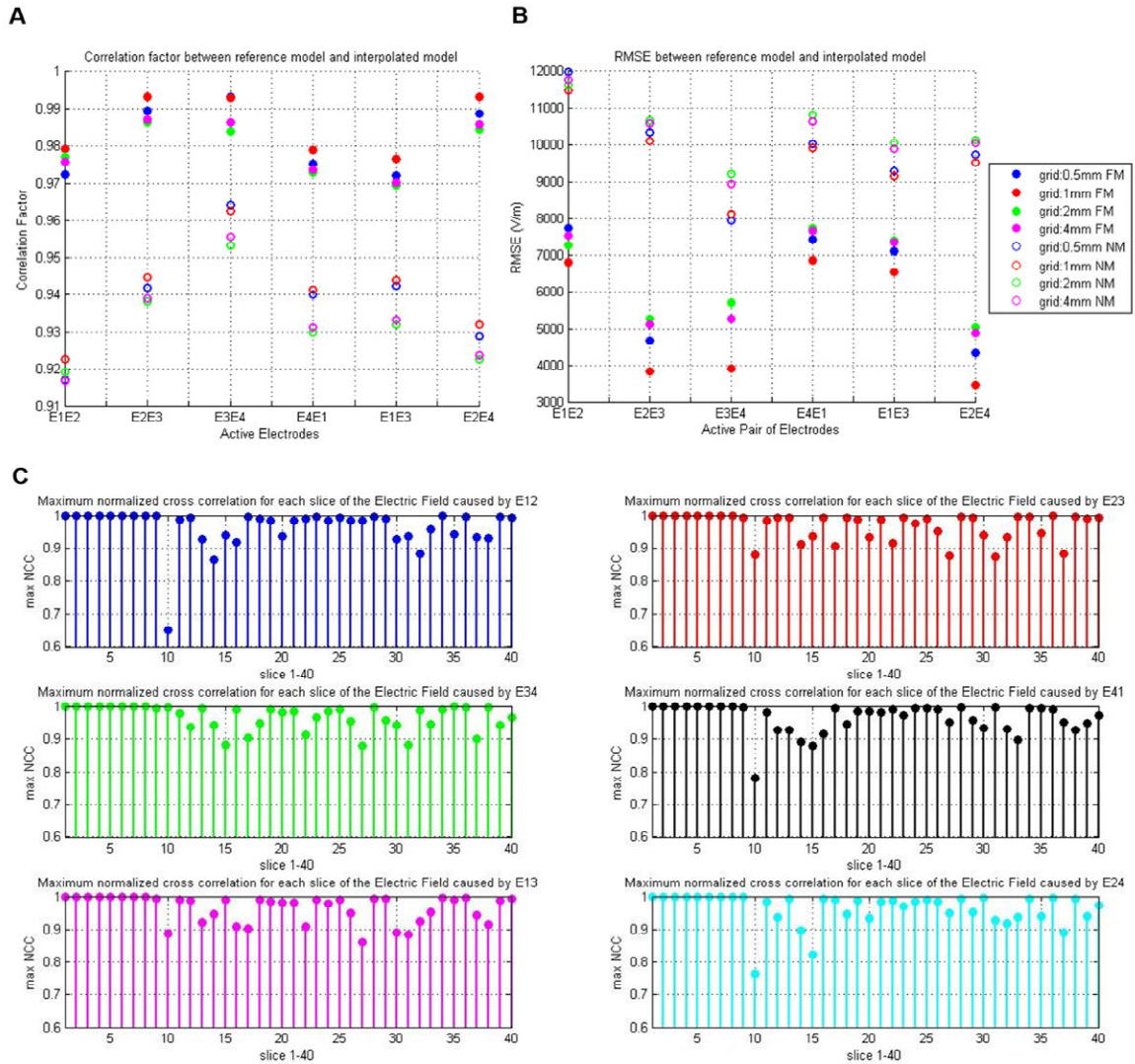


Figure 6. Comparison between the electric field distribution obtained with the reference model and the interpolated model based on the calculation of (A) the correlation factor, (B) the RMSE, for different grid spacing and meshes, and (C) the maximum normalized cross-correlation (NCC) for the electric field distribution between the reference model and the interpolated model of 1 mm grid spacing.

Regarding the electric field dependent conductivity model, conductivity values ranged from 0.5-1.5 S/m for the tumoral tissue and from 0.1-0.3 S/m for the surrounding healthy tissue, since electroporation phenomenon has been reported to increase tissue conductivities from three to four times the initial values. Two functions were used to define a dynamic conductivity behaviour: (i) smooth step functions were defined in Comsol Multiphysics interface as shown in Fig. 7A, and (ii) increasing-conductivity ramp functions were programmed in Matlab as shown in Fig. 7B, according to Eq. (1) and (2).

$$\sigma_{ti}(E_i) = \begin{cases} \sigma_{t0} & E_i > E_{rev} \\ \frac{\sigma_{tf} - \sigma_{t0}}{E_{irr} - E_{rev}} E_i & E_{rev} \leq E_i \leq E_{irr} \\ \sigma_{tf} & E_i > E_{irr} \end{cases} \quad (1)$$

$$\sigma_{pi}(E_i) = \begin{cases} \sigma_{p0} & E_i > E_{rev} \\ \frac{\sigma_{pf} - \sigma_{p0}}{E_{irr} - E_{rev}} E_i & E_{rev} \leq E_i \leq E_{irr} \\ \sigma_{pf} & E_i > E_{irr} \end{cases} \quad (2)$$

where $i=1, 2, 3, 4$ and define the number of iterations programmed, $\sigma_{t0}=0.5$, $\sigma_{tf}=1.5$ define initial and final tumoral conductivity and $\sigma_{p0}=0.1$ and $\sigma_{pf}=0.3$ are the initial and final peripheral healthy tissue conductivity. E_{rev} and E_{irr} represent the threshold electric field values for reversible (400 V/cm) and irreversible electroporation (600 V/cm), respectively.

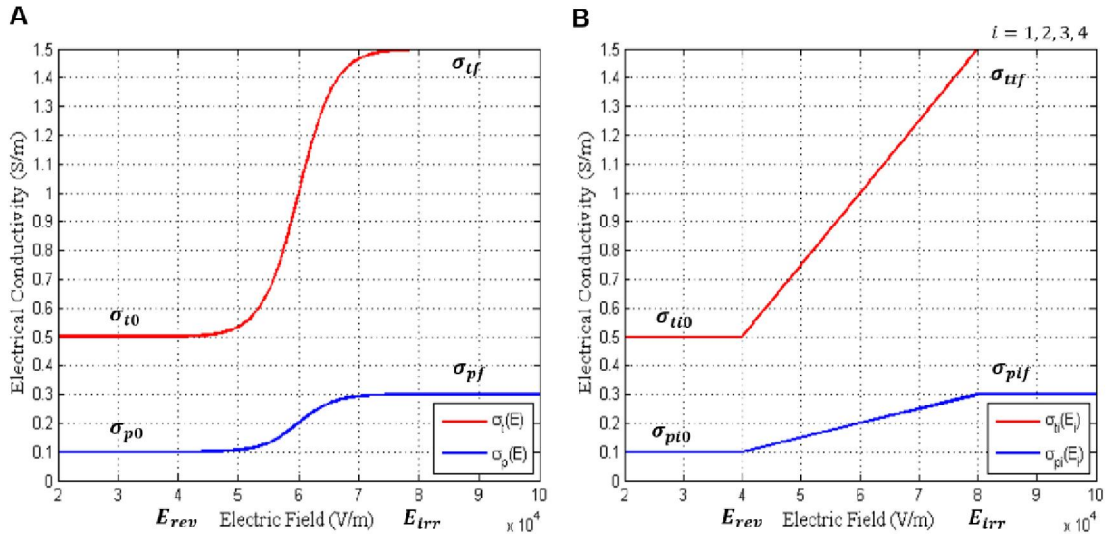


Figure 7. Dynamic conductivity curves. (A) Sigmoidal electrical conductivity as a function of the electric field defined for the reference model in COMSOL Multiphysics. (B) Iterative electrical conductivity as a function of the electric field defined for the interpolated model in Matlab.

The best results showing the similarity between the reference model and the interpolated model were obtained by using a grid spacing of 1 mm and a normal mesh based on the high correlation factors, low root square error values and the solution time of the models. Therefore, an iterative dynamic conductivity study according to (1) and (2) was carried out only for a spacing grid of 1 mm. For the first iteration, E_1 is the resultant electric field corresponding to the static conductivity study in the reference model. A new increased conductivity matrix is generated after each iteration depending on the conditions stated in (1) and (2). Electric field E_2 , E_3 and E_4 are obtained after solving the model for the conductivity matrix generated in their precedent iterations. The electric field dependent conductivity for the reference model and the iterative increased conductivity programmed in Matlab are shown in Fig. 8. Interestingly, a smoother incremental behavior is obtained through iterative processes (Fig. 8B) compared to the increased conductivity obtained with step functions defined in COMSOL user interface (Fig. 8A).

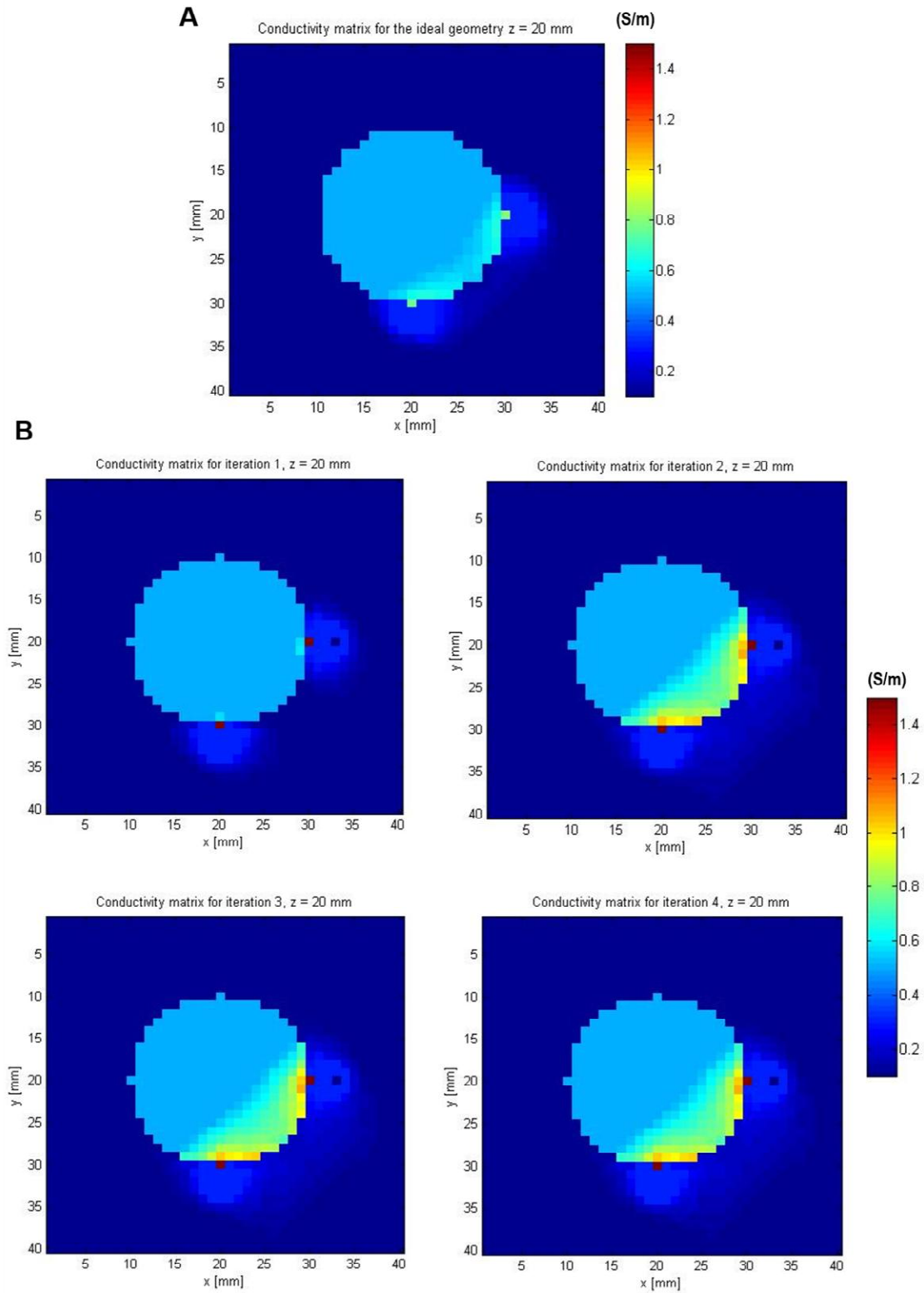


Figure. 8. Electric field dependent conductivity for (A) COMSOL Multiphysics step functions and for (B) the iterative increasing conductivity in Matlab.

The results show that the use of an interpolation function with a grid spacing of 1 mm and a normal mesh are suitable for further more complex models considering the solution time for the electric field distribution calculation, and the similarity between the models created in the COMSOL user interface and the ones manipulated in Matlab. Results in Fig. 8 show that an iterative increasing conductivity is preferred over the step functions that can be defined in the COMSOL Multiphysics user interface since it describes better the increasing conductivity phenomenon caused by electroporation. This work was presented during the Global Medical Engineering Physics Exchanges/Pan American Health Care Exchanges (GMEPE / PAHCE) conference [PAHCE 2017].

5.2.3. ECT treatment planning for MRI-based realistic computational breast models; dynamic conductivity approach

A sequential model for electroporation of tissue, developed by the members of the Laboratory of Biocybernetics at the Faculty of Electrical Engineering, Slovenia, which is a method for personalized treatment planning procedure, was used to analyze breast cancer treatment with electrochemotherapy. This model was implemented in COMSOL Multiphysics and is able to determine the electric field distribution generated in the tissues of interest, to predict the electric current during treatment and the electroporated tissue volumes. The computational simulation of electroporation in this model includes three steps: 1) solving the Laplace Equation for static electric currents, 2) irreversibly changing electrical conductivity due to electric fields above electroporation threshold and 3) sequentially repeating previous steps until a steady state (non-changing conductivity) is reached. This sequential model of electroporation is described in detail in Zupanic, Kos, & Miklavcic (2012).

This sequential model was used to analyze the MRI collection taken from the TCGA-BRCA, previously described in section 5.2.1. For this analysis, the two breast carcinomas and surrounding healthy breast tissue were treated with two

needle electrodes of 4 cm in length, inserted close to the tumor boundaries to treat each tumor as shown in Fig. 9. In addition, an increasing conductivity behavior was conferred to the tissues of interest, i. e., an initial conductivity $\sigma_{it}(E)=0.4$ and a final conductivity $\sigma_{ft}(E)=1.2$ for both tumors, and an initial conductivity $\sigma_{ip}(E)=0.1$ and final conductivity $\sigma_{fp}(E)=0.4$ for the surrounding breast tissue. A voltage of 500 V was used to start the studies based on the results reported in section 5.2.1, in order to determine the appropriate voltage to assure a complete coverage of the tumors to cause electroporation.

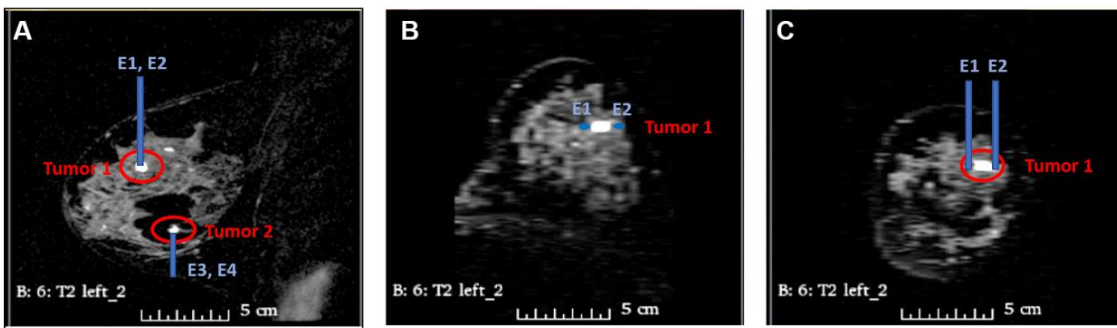


Figure 9. Insertion of four needle electrodes (E1, E2, E3 and E4) for treating two breast carcinomas segmented from MRI images. (A) Electrode insertion parallel to the sagittal plane, (B) normal to the axial plane, and (C) electrode insertion represented on the coronal plane.

5.2.4. Realistic computational breast models base on DBT imaging

Digital Breast Tomosynthesis (DBT) is a diagnosis tool which is becoming increasingly accepted since it can reduce the tissue overlap effect and structure noise in single slice two-dimensional mammography imaging [Reiser & Sechopoulos, 2014; Smith, 2012] and it is nowadays the main detection tool used in the Institute of Breast Diseases-FUCAM. DBT is a three-dimensional method in which images are acquired at a limited number of different x-ray source angles while the breast is statically compressed [Smith, 2012]. It differs from other 3D imaging modalities in that orthogonal multiplanar reconstructions cannot be generated from the transverse tomosynthesis image sets. Instead,

Cranial-caudal (CC) and Medio-lateral oblique (MLO) views are obtained with DBT. Due to the lack of orthogonal multiplanar views, this imaging technology represents a challenge for the development of 3D breast reconstruction [Zastrow E. et al., 2008; Sechopoulos, 2014; Ertas M, 2013; Smith, 2012]. The development of tridimensional reconstruction algorithms of DBT projections is beyond the scope of this dissertation, and hence, realistic breast modeling, alternatively carried out in a 2-step process, is presented in this section.

DBT collections, corresponding to patients treated in the Institute of Breast Diseases – FUCAM, were analyzed over physician guidance. Diagnosis was done by DBT, Giotto Tomo, IMS (slice thickness 1 mm and pixel size 0.1 mm). All DBT Imaging studies were approved by the Scientific-Ethics Committee FUCAM (approval number 2017/14). All patients provided verbal consent to be subjected to the imaging studies. Three representative clinical cases of women diagnosed with invasive breast ductal carcinoma without previous treatment, hence corresponding to primary deep-seated tumors, Fig 10, were analyzed to evaluate their treatment with electrochemotherapy.

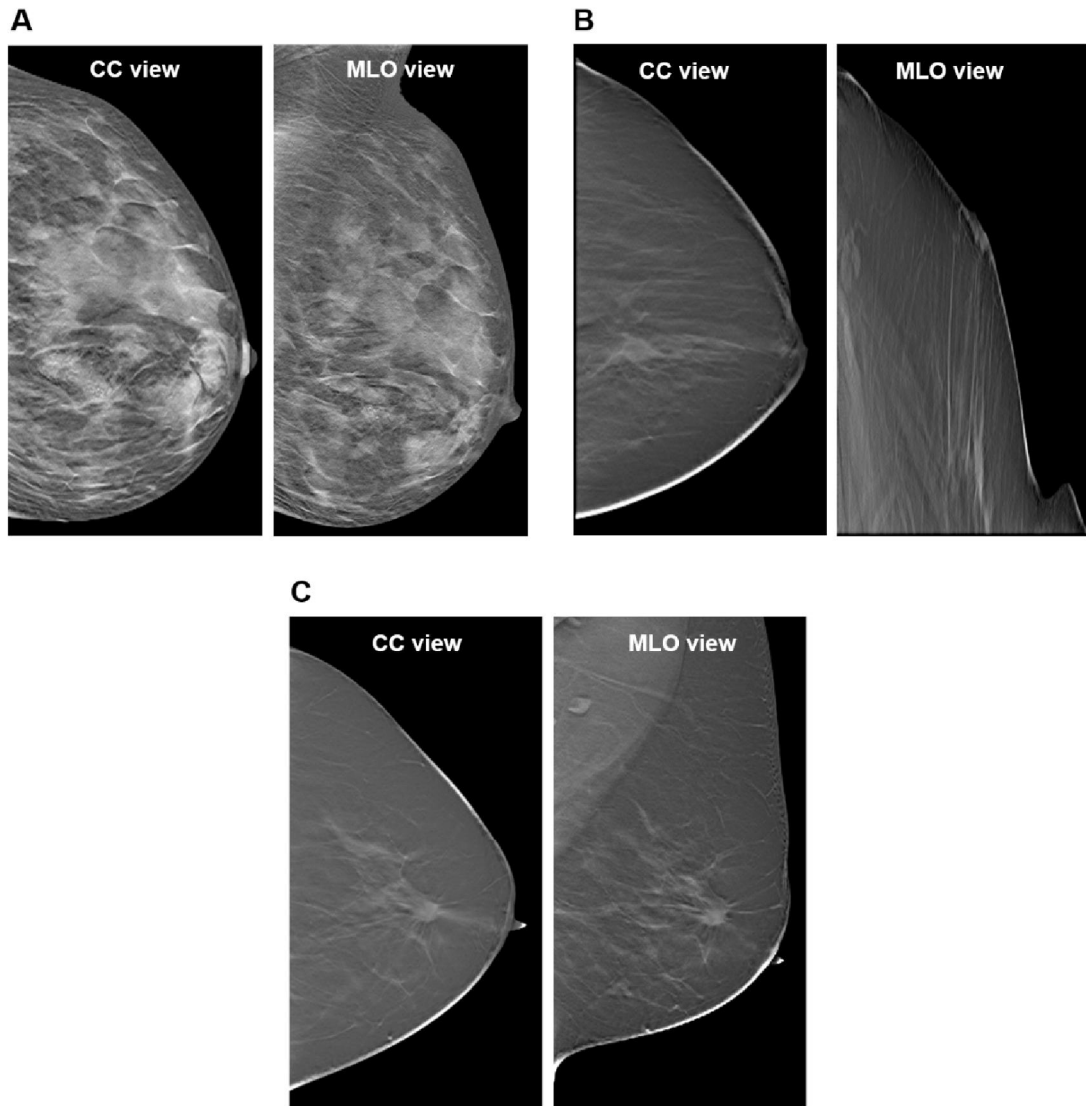


Figure 10. Clinical cases of women diagnosed by Digital Breast Tomosynthesis (DBT) with invasive breast ductal carcinoma without previous treatment. A Cranial-caudal (CC) view and Medio-lateral-oblique (MLO) view is shown for (A) patient 1, (B) patient 2, and (C) patient 3.

In order to deal with the breast-deformation issue of DBT due to tissue compression, breast modeling was done in two steps. First, the target tissues (tumoral tissue, fibroglandular tissue, and fatty tissue) in the region of interest were determined and marked out by physicians in both CC and MLO views in

which dimensions, breast density, and the center of the tumor were determined. Tumor segmentation and 3-D reconstruction were carried out in 3-D Slicer in the original DBT images. Second, numerical breast phantoms available in a repository [Numerical Breast Phantoms Repository] and derived from T1-weighted magnetic resonance images of patients with no malignancy or other abnormalities were used to provide a decompressed model for the rest of the tissues of interest (fibroglandular and fatty tissue).

Each phantom consists of a 3-D grid of cubic voxels of 0.5 mm x 0.5 mm x 0.5 mm. The database of numerical phantoms was classified based on the standard tissue composition descriptors used by radiologists to classify X-ray mammograms according to the radiographic density of the breast. Four categories, listed in Table 4, were defined for the computational phantoms according to the breast imaging reporting and data system (BI-RADS) [Jossinet J, 1996; Moran MS et al., 2014].

Table 4. Computational phantoms categories according to the BI-RADS system.

Description	Glandular Tissue (%)	Phantom type
Almost entirely fat	< 25	I
Scattered fibroglandular	25 – 50	II
Heterogeneously dense	51 -75	III
Very dense	> 75	IV

Breast tissue consists mainly of glandular parenchyma, connective tissue, and fatty tissue. Breast tissue and glandular parenchyma are radiologically considered as dense tissue. A computational phantom was radiologically assigned to each patient based on the correlation of patient’s breast density grading with the categories of the BI-RADS. Patient 1 DBT images showed whitish appearance that pointed to a major glandular parenchyma proportion; hence, a very dense phantom was selected for this patient. A scattered

fibroglandular phantom was used for patient 2, since dense tissue in DBT images showed a scattered pattern, which corresponded to a minor amount of glandular parenchyma. On the other hand, nondense mammographic areas (dark regions) were observed for patient 3, and therefore, a mostly fatty phantom was selected to represent this case.

Three main tissues were considered for phantoms segmentation: skin (beige pixels, Fig. 11), fibroconnective/glandular tissue (pink pixels, Fig. 11), and fatty tissue (yellow pixels, Fig. 11). Finally, in order to build a model of a realistic-anatomical breast with malignancies, the scale of the tumor segmentation corresponding to each patient was adjusted to fit the dimensions of the selected phantom; then, the reconstructed tumor (red pixels, Fig. 11) was embedded into the selected computational breast phantom, keeping its original position inside the breast. This position was determined in its corresponding DBT image.

This methodology allowed the development of a 3-D anatomical model of a decompressed breast for the three patients as shown in Figure 11. Table 5 shows the patients' and tumors' anatomical properties considered in order to build the breast models.

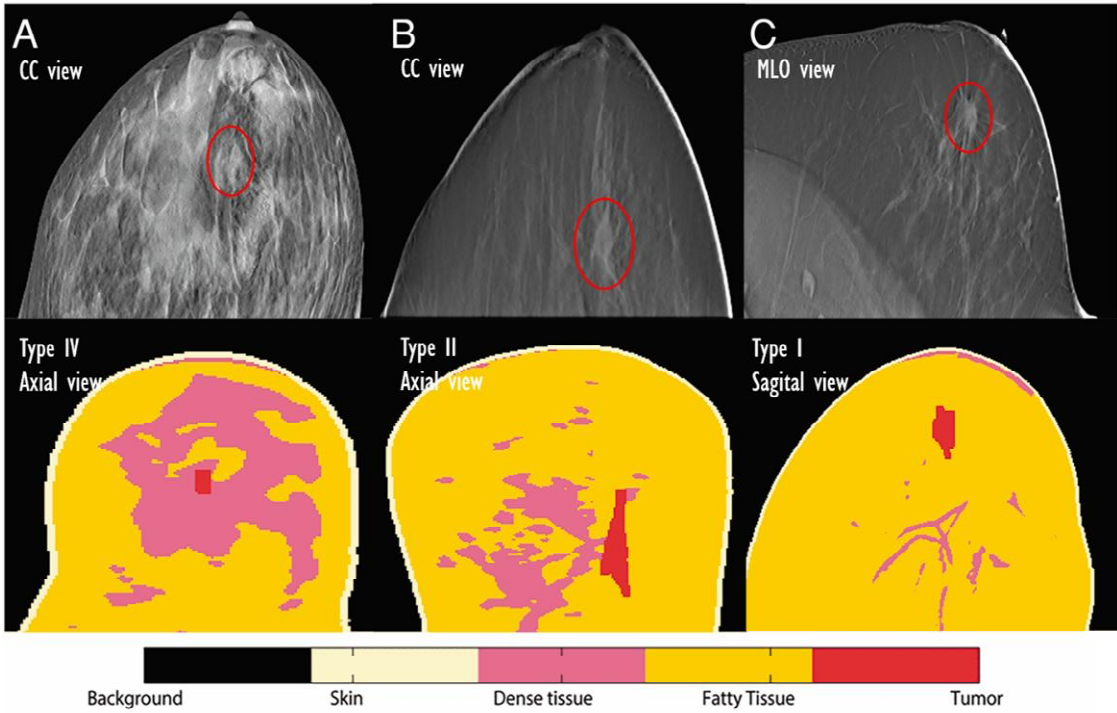


Figure 11. Computational Breast Models based on DBT images. (A) Craniocaudal (CC) view of a digital breast tomosynthesis of patient 1 and corresponding axial view of a very dense phantom analogue to CC view. (B) CC view of patient 2 and corresponding axial view of a scattered fibroglandular phantom. (C) Mediolateral-oblique (MLO) view of patient 3 and the corresponding sagittal view of a mostly fatty phantom analogue to mediolateral oblique (MLO) view [Vera-Tizat et al., 2018].

Table 5. Properties of the computational breast models.

P ^a	Age	Location	Tumors			Phantom		
			#	Size [mm]	Volume [cm ³]	Type	Density	Volume Size [pixels]
1	67	Left Breast	1	4.4 x 9.1 x 11.5	0.46	III	Very dense	215 x 328 x 212
2	55	Left Breast	1	38 x 9.6 x 8.5	3.10	II	Scattered fibroglandular	258 x 253 x 251
3	54	Left Breast	1	29 x 9.5 x 18.5	5.10	I	Almost entirely fat	310 x 355 x 253

^a Patient

The aims for these realistic breast models are to determine first, whether the deep-seated invasive ductal carcinomas along with tissue into a safety margin of 10 mm may be eligible for their treatment with electrochemotherapy through the use of an universal electrode array, and second, the most effective electrode configuration and the electric protocol to be applied for a particular patient and electrode. It has been reported that successful medical application of ECT requires the achievement of optimal parameters in the whole target tissue while keeping healthy tissue damage at a minimum [Neal R. E, Davalos R. V, 2009]. Nevertheless, in this work, healthy tissue constituting the safety margin was subjected to electroporation for the treatment of potential micro-metastases or tumor outgrowths not visible in imaging. For this purpose, the investigation regarding the design of different needle electrode arrays for ECT is presented in the next section.

5.2.5 Novel needle-electrode design for electrochemotherapy

It has been suggested that any target tissue in any location may be treated by ECT with appropriate electrodes and an accurate positioning provided by image guided assistance since tissue electroporation depends on local electric field distribution and this is in turn a function of the electrode geometry and positioning, tissue anatomy and tissue dielectric properties [Zupanic, 2012]. In clinical practice, the handle of electrodes must remain the same for all electrode arrays, and the selection of a particular electrode array shall depend on the dimensions of the target tumor.

In order to establish a suitable electrode array with a fixed geometry configuration, which may cover target tissues in any clinical scenario of patients with IDC, four different needle-electrode arrays in three geometrical configurations were computationally tested for the treatment of breast tumors and a surrounding safety margin. The needle electrodes are arranged in three geometrical configurations: delta (three needles forming a triangle, diamond (four needles forming a plain rhombus, and five needles forming a rhombus with a central needle), and star (five needles forming a pentagon with a sixth needle in the center) as shown in Fig. 12A, where it can be seen that a maximum of one needle is intratumorally inserted and the rest of the needles are positioned into the safety margin. It is worth noting that for the diamond configuration, 2 electrode arrays were derived, that is, a 4-needle array without a central needle and a 5-needle array considering an intratumoral needle. The number of needles ranges from 4 to 6 in order to investigate whether a sufficient electric field can be generated through the minimal number of electrodes and hence requiring fewer needle punctures. The distance between the needles in these electrode arrays are shown in Table 6 (see set 1).

These four electrode arrays were initially tested in an ideal breast-model geometry which consisted of a spherical tumor of 10 mm in diameter surrounded by a sphere of 30 mm in diameter which simulated the safety margin. Both spheres were embedded in a 50 mm x 50 mm x 50 mm block of

surrounding healthy tissue. Cylinders of 1.2 mm diameter and 30 mm length were used to simulate the needles. Initial conductivity values of the tumor, safety margin and healthy-breast surrounding tissue were conferred in each point of the model by interpolation functions as 0.4 S/m, 0.03 S/m respectively. An electric field dependent conductivity was considered as suggested Langus et. al., (2016) and Corovic et. al., (2013). Hence final conductivity values for the tumor, safety margin and healthy-breast surrounding tissue were 1.2 S/m, 0.09 S/m respectively. Modeling was performed in COMSOL Multiphysics and Live link for Matlab as reported in Marcan et. al., (2015).

The four original electrode configurations were afterwards adjusted to be used in the realistic computational models of three patients described in section 5.2.4. Hence, three sets of electrodes corresponding to twelve electrode arrays were proposed, as shown in Fig. 12 and Table 6. The electrodes in these three sets keep the same number of needles (4, 5, and 6) and the original geometrical configurations: delta (three needles forming a triangle), diamond (four needles forming a plain rhombus, and five needles forming a rhombus with a central needle), and star (five needles forming a pentagon with a sixth needle in the center). Conversely, they differ in distance among the needles as described in Fig. 12 and Table 6, in order to improve the target tissue coverage in the three patients. Variation in distance among the electrodes was proposed to fulfill a complete coverage of the tumors in the three patients according to their tumor dimensions and geometries. Needles' diameter in all arrays was 1.2 mm, and their active length varied depending on the tumor size as shown in Table 6, where the symbols indicate the number of needles (4, 5, 6), the array configuration (De = Delta, Di = Diamond, St = Star) and the electrode set marker (1 refers to the original electrode array, 2 refers to the enlarged electrode array, 3 refers to the ellipse electrode array), C-P refers to the distance from the intratumoral–central electrode to the peripheral electrodes, P-P refers to the distance between peripheral electrodes only, and D refers to the distance between electrodes forming diagonals. The twelve

electrode arrays were tested, *in silico* by FEM, in the three patients described in the previous section.

In general, the electrodes with an intratumoral needle were activated considering first the electrode pairs formed by the central electrode and the electrodes into the safety margin tissue and then the electrode pairs into the safety margin only. On the other hand, the needles in the electrode with no intratumoral needle were activated in the 6 possible combinations in order to cover the complete regions of interest.

After all needle combinations are activated, the total coverage of the tumor and the safety margin with electric field between reversible (400 V/cm) and irreversible (800 V/cm) electroporation thresholds values are determined. For all the electrodes arrays, an initial voltage protocol is first simulated. The resulting tissue coverage obtained for this first simulation allows the adjustment of the voltage to improve the tissue coverage. Therefore, different voltage values are simulated until an efficient coverage close to the reversible electroporation threshold for both tissues of interest is obtained.

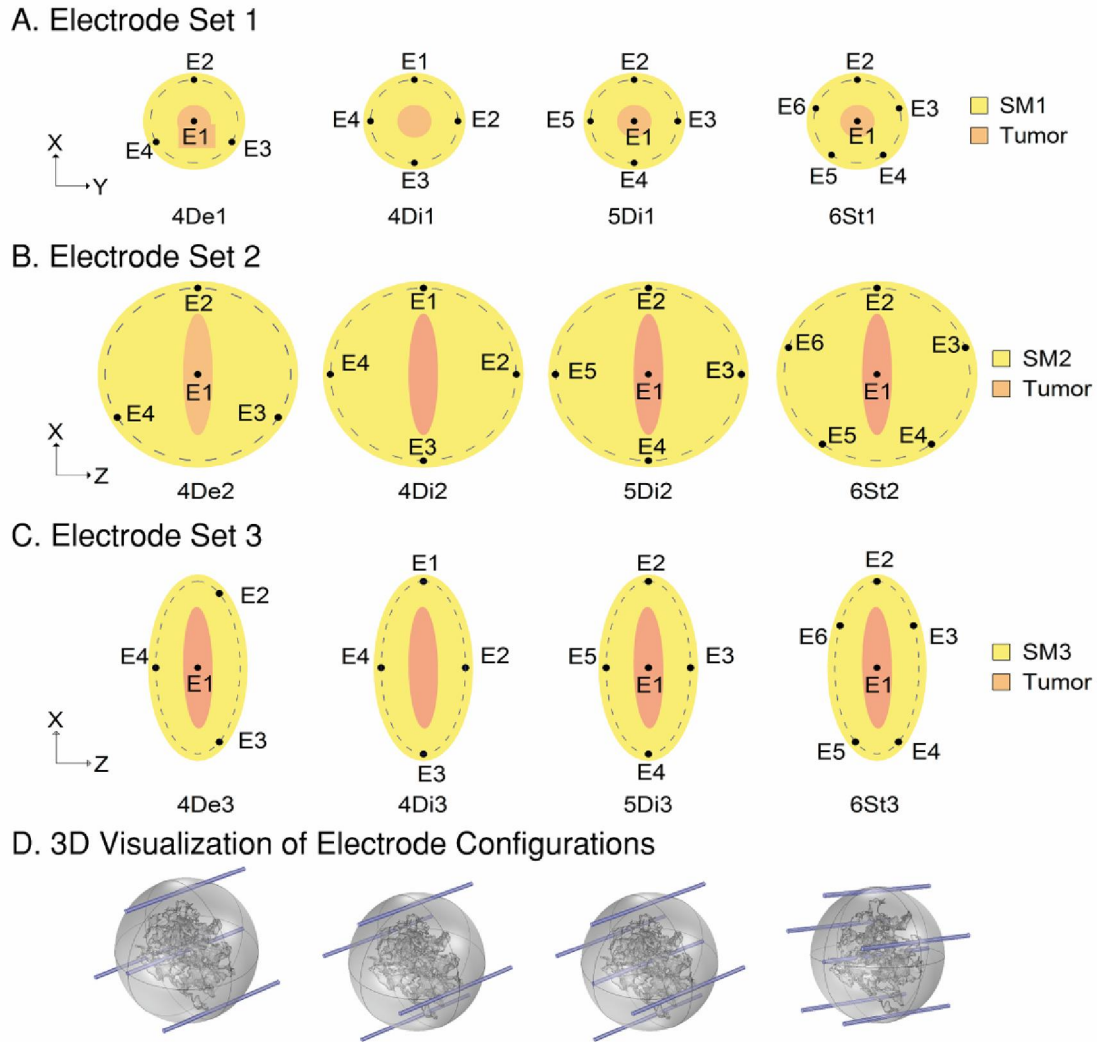


Figure 12. Topside view of (A) electrode set 1 for the treatment of a breast tumor (red) in patient 1 and a spherical safety margin tissue (SM1), (B) electrode set 2 for the treatment of a breast tumor (red) in patient 2 and a spherical safety margin tissue (SM2), and (C) electrode set 3 for the treatment of a breast tumor (red) in patient 2 and an elliptic safety margin tissue (SM3). (D) Three-dimensional visualizations of the tumor embedded into a safety margin and the 4 electrode configurations; delta configuration, 4-needle diamond configuration, 5-needle diamond configuration, and 6-needle star configuration [Vera-Tizatl A. L, 2018].

Table 6. Geometric properties of the needle-electrode arrays.

# needles	Configuration	Electrode Set	Symbol	Active length (mm)	Needle spacing (mm)		
					C-P	P-P	D
4	Delta	1	4De1	15	13.0	22.5	--
		2	4De2	20	27.0	46.8	--
		3	4De3	20	24.1 12.2	29.7 46.5	--
	Diamond	1	4Di1	15	--	18.4	26.0
		2	4Di2	20	--	38.2	54.0
		3	4Di3	20	--	29.6	54.0 24.5
5	Diamond	1	5Di1	15	13.0	18.4	--
		2	5Di2	20	27.0	38.2	--
		3	5Di3	20	27.0 12.2	29.6	--
6	Star	1	6St1	15	13.0	15.3	--
		2	6St2	20	27.0	31.7	--
		3	6St3	20	27.0	17.4	--
					17.0	36.7	
			24.1	12.5			

5.2.6. ECT treatment planning for DBT-based models

The electric field coverage of target tissues in the three patients described in section 5.2.4 was modeled by FEM. All the electrode described in the previous sections were tested in the three patients. Therefore, a simulation per patient

and per electrode array was carried out. Based on the location of the tumor in the breast and the ease of needle insertion into the target tissue, the electrode arrays were determined to be inserted normal to the axial plane for patients 1 and 2 and normal to the sagittal plane for patient 3.

Methodology for activation of needle-electrodes: the pairs of needles in the different electrode arrays were sequentially set to voltage until all possible combinations were activated (needles already activated are disregarded), setting boundary conditions for voltage as an anode and a cathode during each simulation. The central needle in the electrode arrays considering an intratumoral needle was first set as an anode paired off with peripheral needles considered as cathodes in the safety margin; subsequently, only peripheral electrodes were switched as anode and cathode, respectively. For configurations lacking a central needle (i.e., 4Di1, 4Di2, and 4Di3), electrodes were commuted as anode and cathode in 6 possible combinations formed by adjacent and opposite needles.

FEM Modeling: All models were computed in COMSOL Multiphysics with an algorithm written in Matlab. Initial voltage values were applied between each pair of electrodes in the different arrays. Depending on the tissue coverage resulting from this first simulation, voltage was varied until the target volumes were covered by an electric field magnitude above the reversible electroporation threshold in order to find the most appropriate treatment protocol for each patient. Electric field visualization methodology reported by Zupanic et al. (2012) was used to extract the results and quantitatively compare the models based on the electroporation cross-section images, and the cumulative coverage of tissues by electric fields after the complete sequence of pulses were applied. Electric field cumulative coverage curves were calculated for the target tissues. All tissues were considered as isotropic with initial electrical conductivity values reported in the literature [Neal R. E, Davalos R. V, 2009; Surowiec A. J et al., 1988; Gabriel S. et al., 1996]. An

electric field dependent conductivity due to electroporation was taken into account as shown in Table 7.

Table 7. Dielectric properties of tissues in the breast models

Tissue	Initial conductivity (σ_0) [S/m]	Final conductivity (σ_f) [S/m]	Threshold Electric Field [V/cm]	
			RE ^a	IRE ^b
Skin	0.170	0.170	400	800
Fibroconnective/glandular	0.085	0.340		
Fatty	0.025	0.100		
Tumor	0.425	1.700		

5.3. Reversible Electroporation *in vitro*

As previously mentioned, ECT is an accepted procedure for the treatment of cutaneous and subcutaneous tumors in the clinical practice only in Europe. Since it is not yet applied in America, and the treatment of primary deep-seated tumors with ECT is in its early stages worldwide, three methodologies for reversible electroporation *in vitro* are described in this section in order to experimentally assess its effects on breast malignancies.

On the one hand, traditional electroporation of cell suspensions is compared with an alternative methodology implemented for electroporation of adhered cells which allows the preservation of cell morphology opposite to a cell suspension environment. For this purpose, three cell lines representative for the most common molecular types of breast cancer were used; a Triple Negative Breast Cancer (TNBC) cell line BT-20, a Her2/neu cell line

HCC1419, both derived from a primary ductal carcinoma, and a metastatic cell line, MCF-7 expressing hormonal receptors derived from pleural effusion.

On the other hand, reversible electroporation of hydrogels, as a three-dimensional culture, is presented as a closer approach to an *in vivo* scenario. For this purpose, four cell lines were used; two breast cell lines (MCF-7 and a non-tumoral mammary gland cell line MCF-10A), and two additional non-breast cell lines; a glioblastoma cell line U251, and a hepatocellular carcinoma cell line HEPG2

A universal electroporation voltage cannot be effectively applied to all tissues. Therefore, establishing cancer-specific electroporation voltages is encouraged in order to be included in the decision tree in the new modified Standard Operating Procedures (SOP) [Miklavcic D. et al., 2014; Zhao D. et al., 2014]. We rely on the assumption that *in vitro* optimized electrical parameters may be used as a basis for *in vivo* ECT [Larkin J. O. et al., 2007; Miklavcic D. et al., 2000; Sersa G. and Miklavcic D. 2008; Zhao D. et al., 2018].

Cell-specific electroporation protocols were predicted by FEM in COMSOL Multiphysics, on an Intel(R) Core (TM) i5-6500, 3.20GHz, 4-core processor. A dynamic electric-field-dependent conductivity for cell suspensions, adhered cells and hydrogels was assumed for the electroporation phenomenon through a step function.

A commercial electroporation device BTX830 Square Wave Electroporation System (ECM® 830) was used to apply electric pulses for reversible electroporation *in vitro* in all cell cultures. An electrochemotherapeutic protocol of 8 pulses, 100 μ s duration and 1 Hz repetition frequency has been demonstrated as an effective protocol applied *in vitro* with comparable effects *in vivo* [Maček A. et al., 2002]. Therefore, the experimental electric protocols applied to cell suspensions, adhered cells and hydrogels consisted of 8 pulses, 100 μ s duration and 1 Hz repetition frequency, and the specific voltage was tuned for each cell line and cell culture.

The work presented in this section, regarding electroporation of cell suspensions and adhered cells, resulted from a collaboration made with the Department of Infectomics and Molecular Pathogenesis, CINVESTAV-Mexico. The work corresponding to electroporation of three-dimensional cell cultures resulted from a collaboration made with the Department of Biomedical Engineering, Virginia Tech, USA.

5.3.1. Electroporation of cell suspensions

Cell cultures: the BT-20 cell line (ATCC® HTB-19™) was cultured with Eagle's Minimum Essential Medium (EMEM) (ATCC® 30-2003™), the MCF-7 cell line (ATCC® HTB-22™) was cultured with Dulbecco's Modified Eagle's Medium (DMEM) (ATCC® 30-2002™), and the HCC1419 cell line (ATCC® CRL-2326™) was cultured with RPMI-1640 Medium (ATCC® 30-2001™). All medium cultures were completed with fetal bovine serum at 10%. Cell cultures were maintained in T-75 flasks at 37°C with a humidified atmosphere and 5% of CO₂, when the cell confluence reached approximately 80%, cultures were harvested with a solution of Trypsin-EDTA (0.25%-0.034%). Subsequently, cells were placed in commercial electroporation cuvettes for electroporation (0.4 cm electrode gap, GENE PULSER®/MICROPULSER™, Fig.13A).

In silico prediction of electroporation protocols: the distribution of the electric field in cell suspensions was predicted by FEM, through the Laplace equation solution. A model of cells suspended in an electroporation buffer, contained in an electroporation cuvette was created in COMSOL Multiphysics. The electroporation cuvette was modeled as a polycarbonate block containing two aluminum blocks which simulated parallel-plate electrodes with an inter-plate distance of 4 mm (Fig.13B). One plate was set as a voltage terminal and the other was grounded in order to simulate the application of electric pulses. An initial electrical conductivity of 0.75 S/m was measured at 37°C with a conductivity meter HANNA HI8633 in a BT-20 cell suspension. Considering cells in suspension as insulating spheres placed in a saline solution, the

effective initial conductivity was calculated as 0.7475 S/m for a cell volume fraction $f=0.00225$ [Broncino J. D, 1995]. This value was assumed for the three cell lines (MCF-7, BT-20, HCC1419). An increment of 8% on the initial effective electrical conductivity was considered based on the colloid-osmotic swell in our high conductive cell suspensions after the application of 8 pulses, 100 μ s duration and 1 Hz repetition frequency [Pavlin M, 2005]. Table 8 summarizes the dielectric properties for the domains in this model. A parametric study was performed varying the input voltage between the electrodes from 100 V to 450 V with increments of 50 V. A stationary parametric non-linear solver was used. The solution for the model of cell suspension electroporation converged at 10 s for an 18190 free tetrahedral element mesh. The resultant electric in the center of the cell suspension is listed in Table 9 and shown in Fig. 13C. These results provided a basis treatment protocol to be experimentally applied, suggesting that suspended cells would be reversibly permeabilized between 150 V and 250 V in order to be reversibly electroporated between 400 V/cm and 600 V/cm.

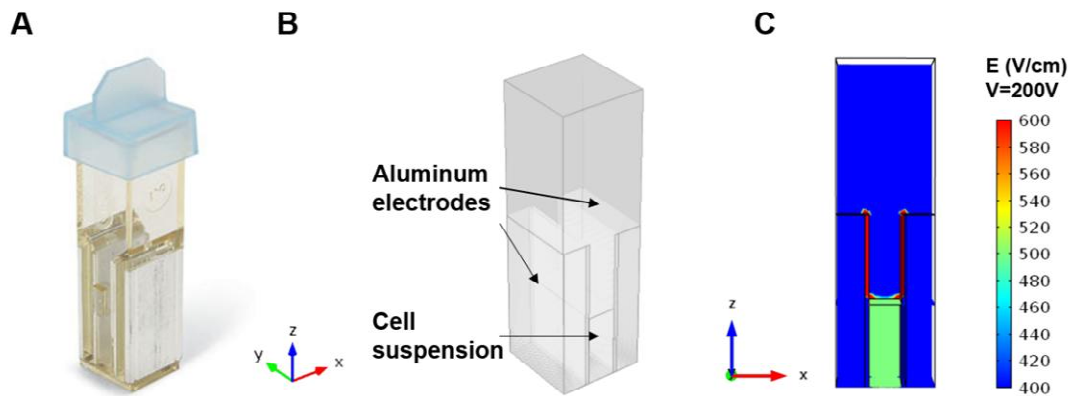


Figure 13. Computational model of a cell suspension. (A) electroperoration cuvette (0.4 cm electrode gap, GENE PULSER®/MICROPULSER™), (B) computational geometry of the cell suspension, and (C) the electric field distribution in the cell suspension for 200 V.

Table 8. Dielectric properties considered for cell suspensions.

Domain	Dielectric Property	Value
Electroporation buffer	Electrical conductivity	0.75 [S/m]
	Relative permittivity	80
Cell suspension	Initial electrical conductivity	0.7475 [S/m]
	Final electrical conductivity	0.8073 [S/m]
	Relative permittivity	80
Aluminum electrode	Electrical conductivity	3.774e7 [S/m]

Table 9. *In silico* prediction for cell suspensions electroporation.

Voltage [V]	Electric field [V/cm]
100	250
150	375
200	500
250	625
300	750
350	875
400	1000

Experimental electroporation: Cells (1.5×10^5) were electroporated in an electroporation cuvette (0.4 cm electrode gap, GENE PULSER®/MICROPULSER™) using a BTX830 Square Wave Electroporation System (ECM® 830). In order to monitor the membrane permeabilization caused by electroporation, the uptake of external molecules was determined. Therefore, 5 μ l of Propidium Iodide (PI, P4170, SIGMA-ALDRICH) was added per sample. Cell suspensions were placed in a 24 well plate and they were observed 30 min, 24 h, and 48 h after treatment with an epifluorescence microscope (Nikon Eclipse Ti-U). An experimental group consisting of five samples was generated; four samples treated with voltages ranging from 100

V to 250 V and one sample unexposed to electric pulses, which was used as a control. The experiments were repeated 3 times.

Establishing final efficient electroporation protocols for cell suspensions: the efficiency of an electroporation protocol was based on qualitative PI uptake, and quantitative cell viability of cells that remained undamaged and metabolically active after electric pulsing. Cell viability was determined by the 3-(4, 5-dimethylthiazol-2)-2,5 diphenyltetrazolium bromide (MTT) assay by removing the culture medium and washing cells with PBS twice. Then, 1 ml of PBS was added with 100 μ l of MTT stock solution (5 mg/ml) (No. M 5655 SIGMA-ALDRICH). Cells with MTT solution were incubated 4 h at 37°C. After incubation, the solution was removed, and the formazan crystals were solubilized with acidic isopropanol (0.04-0.1 N HCl in absolute isopropanol). The absorbance of the dye was measured at 570 nm wavelength.

5.3.2. Electroporation of two-dimensional cell cultures; adhered cells

Cells were grown following the same procedure described for cell suspensions in section 5.3.1. When the cell confluence reached approximately 80%, cultures were harvested with a solution of Trypsin-EDTA (0.25%-0.034%). Cells were afterwards placed on Indium Tin Oxide (ITO)-coated glasses for electroporation of adhered cells, respectively. An electrode for electroporation of attached cells was implemented as illustrated in Fig. 14A. Commercial ITO-coated glasses (25 x 25 x 1 mm SIGMA-ALDRICH) were cut and clamped by double headers in order to fit wells in a 12-well plate.

In silico prediction of electroporation protocols: the distribution of the electric field in adhered cells was predicted by FEM, through the solution of the Laplace equation. A model of a monolayer of cells adhered to an ITO-coated glass substrate was created in COMSOL Multiphysics. Because of the

irregular shape that cells acquire when adhered on a substrate, and on the number of cells, electroporation of a cell monolayer was roughly modeled by a block of 20 μm thickness tissue on a block of ITO-coated glass as a cathode. These blocks were embedded into a cylinder simulating the electroporation buffer contained by a polypropylene well. A block of aluminum was inserted 5 mm above the ITO-coated glass in order to simulate the anode (Fig. 14B). Table 10 summarizes the dielectric properties for the domains in this model. A parametric study was performed varying the input voltage between the electrodes from 100 V to 450 V with increments of 50 V in order to determine the voltage values which will generate an electric field between 400 V/cm and 600 V/cm for reversible electroporation *in vitro*. A stationary parametric non-linear solver was used. The solution for the model of adhered cell electroporation converged at 26 min and 45 s solving 4204874 degrees of freedom. The resultant electric in the center of the cell monolayer on the ITO glass surface is listed in Table 11 and shown in Fig. 14C. These results provided a basis treatment protocol to be experimentally applied, suggesting that adhered cells would be reversibly permeabilized between 200 V and 300 V in order to be reversibly electroporated between 400 V/cm and 600 V/cm.

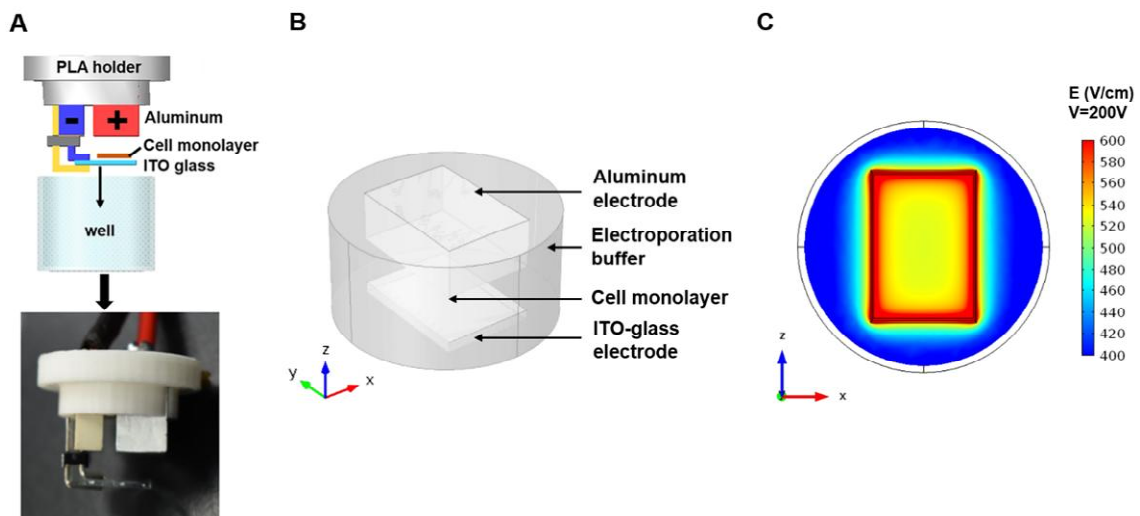


Figure 14. Computational model of adhered cells electroporation. (A) An electrode designed for electroporation of adhered cells consisting of a holder

(white) printed in polylactic acid (PLA) used to house a cathode header (blue) clamping an ITO-coated glass (light blue) with cells adhered on it, and an anode aluminum bar (red). Electrode assembly and (B) mounting inside a 12-well plate, and (C) the electric field distribution in the cell monolayer for 200 V.

Table 10. Dielectric properties considered for cell suspensions.

Domain	Dielectric Property	Value
Electroporation buffer	Electrical conductivity	0.75 [S/m]
	Relative permittivity	80
Cell monolayers	Initial electrical conductivity	0.75 [S/m]
	Final electrical conductivity	2.25 [S/m]
	Relative permittivity	1
Aluminum electrode	Electrical conductivity	3.774e7 [S/m]
ITO-coated glass	Electrical conductivity	250000 [S/m]
	Relative permittivity	3.3378
	Density	0.00714 [kg/m ³]
	Thermal conductivity	3.95 [W/(m·K)]

Table 11. *In silico* prediction for adhered cells electroporation.

Voltage [V]	Electric field [V/cm]
100	208
150	311
200	415
250	519
300	622
350	726
400	830

Experimental electroporation: An electrode for electroporation of adhered cells consisted of a holder (white) printed in polylactic acid (PLA) used to

house a cathode header (blue) clamping an ITO-coated glass (light blue) with cells adhered on it, and an anode aluminum bar (red), as illustrated in Fig. 14A. Over the free glass surface, 1.5×10^5 cells were cultured and incubated during 24 h in order to allow their adaptation and arrangement in monolayers or multilayers according to their nature. When cells reached 80% of confluence, they were electroporated in presence of a potassium phosphate buffer (KPB) in order to reduce the conductivity of the medium and PI was added to the buffer. The cells were observed with an epifluorescence microscope (Nikon Eclipse Ti-U) 30 min, 24 h and 48 h after electroporation. An experimental group consisting of five samples was generated; four samples treated with voltages ranging from 100 V to 250 V and one sample unexposed to electric pulses, which was used as a control. The experiments were repeated 3 times.

Final efficient electroporation protocols for adhered cells was determined by following the same methodology described for cell suspensions.

5.3.3. Electroporation of three-dimensional cell cultures; hydrogels

Hydrogels are currently used as tissue scaffolds in regenerative medicine, for cell encapsulation, immobilization, and drug delivery [Caliari S. R, 2016]. Therefore, in order to assess electrochemotherapy effects in a suitable drug testing model *in vitro*, reversible electroporation protocols in three-dimensional cell cultures (hydrogels) are described in this section.

Fabrication of hydrogels consists on the fabrication of substrates (using molds) which are seeded with cells. For electroporation application, collagen was selected as the substrate for hydrogels since it is a natural matrix polymer which is the predominant extra-cellular matrix component of most connective tissues within the mammalian body, comprising one third of all protein found within tissues. Hydrogel formation involves the transition of liquid precursor solutions into solid materials. Hydrogel mechanical properties are important

towards the stability of the material in culture and may also influence cellular mechanotransduction (the conversion of mechanical information from the microenvironment into biochemical signaling), which in turn has consequences for cellular behaviors like spreading, migration, and stem cell differentiation [Caligari S. R, 2016]. These hydrogels provide an engineering platform for 3D tumor growth that mimics an *in vivo* tumor microenvironment which allows the cells to respond to electroporation-based therapies in a manner that can be directly related to an *in vivo* response and therefore have direct clinical impact [Arena C. B. et al., 2012].

Hydrogels preparation: a methodology similar to that developed and used in the Laboratory of Bioelectromechanical Systems (BEMS) of the Virginia Tech, USA [Arena C. V. et al., 2012] was followed to fabricate hydrogels seeded with MCF-7, MCF-10A, U251, and HEPG2 cells. A neutralizing buffer containing 10xDMEM (Mediatech, Manassas, VA), 1N NaOH, and medium according to the cell line, was used resuspend a pellet of cells to obtain a final seeding density of 1×10^6 cells/ml, forming a cell suspension. This cell suspension was then gently mixed with an appropriate volume of collagen I in order to achieve a concentration of 5 mg/ml, which provides a matrix stiffness close to that of measured values for *in vivo* tumors. This process was carried out in a conical tube contained on ice for the hydrogel not to polymerize. 100 μ l of the liquid hydrogel was deposited into 10-mm-diameter cylindrical polydimethylsiloxane (PDMS) molds, as shown in Fig. 15A. These PDMS molds are fabricated to fit the wells in 24-well plates. After a 20-min polymerization period at 37°C, the cancer-cell seeded hydrogels were removed and cultured in complete media overnight before electroporation delivery.

Reversible electroporation protocols for hydrogels: four voltages were used to assess cell permeabilization due to electroporation, as shown in Table 12. Hydrogels not exposed to electric pulses were used as controls. Five replications were performed per condition and cell line.

Table 12. Parameters for reversible electroporation of hydrogels.

Hydrogels traits		Electric protocol for reversible electroporation	
Collagen I concentration	5 mg/ml	Pulse duration	100 μ s
Cell seeding	1x10 ⁶ cells/ml	Number of pulses	8
Diameter	10 mm	Repetition frequency	1 Hz
Thickness	1 mm	Monitoring timepoints	3 h, 24 h, 48 h
Cell lines	MCF-7	Voltage	150 V
	MCF-10A		250 V
	U251		350 V
	HEPG2		450 V

FEM modeling of hydrogels electroporation: the distribution of the electric field in hydrogels was modeled by FEM, through the Laplace equation solution. A model of a cylinder 10 mm in diameter and 1 mm height, simulating the hydrogel, in which two cylinders 0.8 mm in diameter and 3 mm height are inserted simulating needle stainless steel, was created in COMSOL Multiphysics, as shown in Fig. 15B. One needle was set as a voltage terminal and the other was grounded in order to simulate application of pulses. An electric field dependent conductivity was assumed for the hydrogel. Initial electrical conductivity was 0.98 S/m [Ivey J. W. et al., 2015]. A parametric study was performed varying the input voltage between the needle-electrodes from 250 V to 450 V with increments of 50 V. A stationary parametric non-linear solver was used. The solution for the model of cell suspension electroporation converged at 7 s for an 8481 free tetrahedral element mesh. The resultant electric Fig. 15C, was computed in order to further determine the cell-specific electric field thresholds for reversible electroporation in hydrogels.

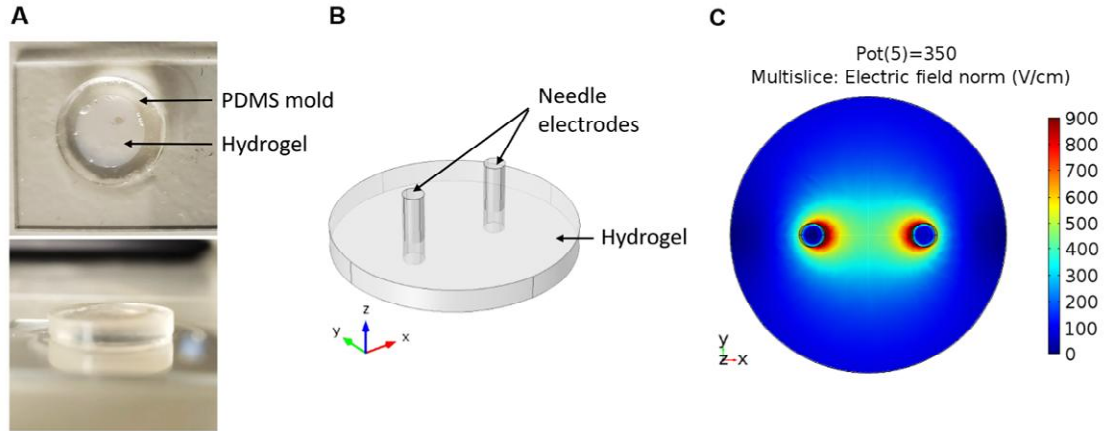


Figure 15. Hydrogels properties for reversible electroporation. (A) Hydrogel deposited on a PDMS mold for electroporation. (B) Computational model for electroporation of hydrogels. (C) Electric field distribution caused by electroporation with needle electrodes in hydrogels.

Protocol for permeabilization assessment: since reversible electroporation is expected to occur in hydrogels for further ECT, two fluorescent dyes were used to stain hydrogels in order to verify cell membrane permeabilization and cell viability. Similar to the permeabilization methodology described for cells suspensions and adhered cells, PI was used to corroborate cell membrane permeabilization in the timepoints reported in Table 12. On the other hand, calcein acetomethoxy (AM) was used to verify cell viability 48 h after treatment. Imaging of hydrogels was carried out through a Zeiss LSM510 (Carl Zeiss Microscopy LLC, Thornwood, NY) laser scanning confocal microscope.

5.4. Breast Electrochemotherapy *in vitro* with paclitaxel

Cell membrane permeabilization and cell viability were demonstrated *in vitro* in the previous sections. Therefore, this section is focused on the assessment of complete ECT in breast malignancies models provided by MCF-7, BT-20 and HCC1419 adhered cells.

Paclitaxel is a chemotherapeutic drug used for the treatment of breast tumors. Consequently, it was used in combination with the most efficient reversible protocols in the breast cell lines obtained with the methodology reported in section 5.3.2. In order to assess ECT with paclitaxel, four experimental groups were used consisting of samples treated with ECT (EP + paclitaxel), samples treated with paclitaxel only, samples exposed to EP (no drug) and samples neither exposed to electric pulses, nor treated with paclitaxel which were used as controls.

Assessment of the effectiveness of ECT with paclitaxel in breast-cancer cell lines was based on the cell death monitoring. The detection of phosphatidylserine localization in the plasmatic membrane has been used to determine cell death by apoptosis. Phosphatidylserine is an internal phospholipid in the cellular membrane in healthy cells. Once an apoptotic process begins, phosphatidylserine migrates outwards the membrane, where it can be easily recognized by Annexin V in a calcium dependent reaction. Annexin V is combined with different fluorophores to be detected by epifluorescent microscopy. In the late stage of apoptosis, cell undergoes a plasmatic membrane and DNA fragmentation, this latter is detected by the fluorescent nucleic acid dye Ethidium Homodimer III (EthD III).

5.5. Complementary Investigation

The methodology for electroporation of adhered cells presented in section 5.3.2. allowed on the one hand, the determination of morphological cell parameters which were used to analytically calculate the ITV for cells in suspension, and microscopy images were used to obtain realistic three-dimensional models of cells in order to numerically determine the ITV in adhered cells. On the other hand, it allowed visualizing some disturbances on the cell membrane by means of microscopy techniques which may be further useful in the understanding of pore formation phenomenon in electroporation.

5.5.1. Cell morphology and Cell-specific Induced Transmembrane Voltage

Cell morphometric properties were determined for MCF-7, BT-20 and HCC1419 cells, by the measurement of membrane thickness and the maximum and minimum radius of all cell lines. Membrane thickness was determined in samples of adhered cells containing 1.5×10^6 cells by transmission electron microscopy (TEM), with a JEOL JEM-1011 microscope (JEOL-LTD-Tokyo Japan) and cell radii were measured in the digitized images taken by a confocal microscopy LSM 700 Microscope (CARL ZEISS GmbH, Germany), by using the software ZEN 2012 (blue edition). Radii of 15 cells selected from random visual fields in each cell line and the membrane thicknesses determined in three random points on TEM images using ImageJ software as shown in Fig 16. The average radius and thickness were calculated for each cell line and are reported in Table 13.

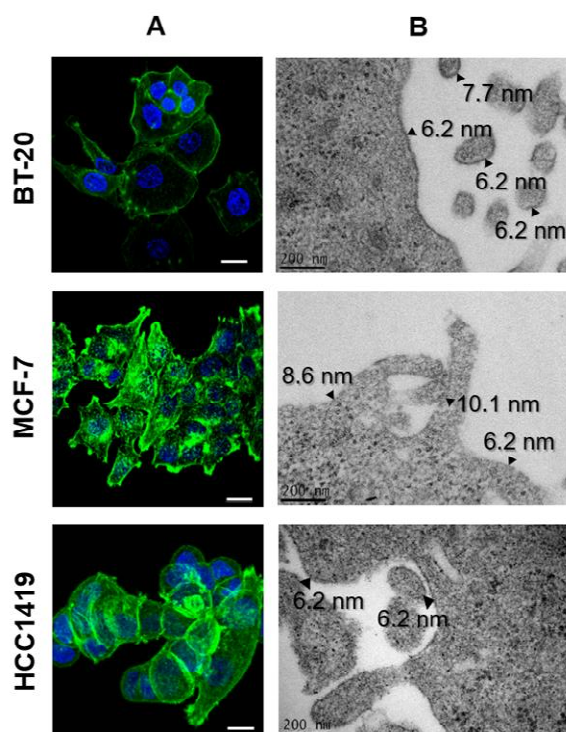


Fig. 16. Cell morphometry imaged by (A) confocal microscopy and (B) transmission electron microscopy. Confocal images were taken with a Carl

Zeiss LSM-700 confocal microscope. Objective 40x, scale bar = 20 μm . Transmission electron microscopy images taken with a JEOL JEM-1011 microscope (JEOL-LTD-Tokyo Japan), scale bar = 200 μm

Table 13. Cell morphometric properties of breast-cancer cells.

Cell line	Cell radius [μm]		Membrane thickness [nm]	
	Average	Standard deviation	Average	Standard deviation
MCF-7	38.7	6.7	10.0	4.1
BT-20	59.8	28.9	6.6	0.5
HCC1419	9.1	1.3	6.6	1.1

Cell morphometric properties in addition to the cell-specific electric field threshold numerically determined (as described in section 5.3.2.) were used as inputs in the steady state Schwann's equation in order to address the complexity that experimental measurements of ITV would demand and to analytically calculate the cell-specific ITV induced after the onset of the electric field in suspended cells. ITV in adhered cells was numerically determined based on realistic cell modeling following a methodology similar to that described in [Pucihar G. et al., 2006]. Confocal images of all cell lines were imported in 3D-Slicer in order to generate a three-dimensional cell model, which was further exported to COMSOL Multyphysics and combined with geometries simulating the electrodes in order to solve the electric potential.

5.5.2. Monitoring of mechanical disturbances on the cell membrane

The visualization of the mechanical electroporation effect was carried out through scanning electron microscopy (SEM) of adhered cells. Each cell line was placed on ITO-covered glasses and subjected to the most efficient electroporation protocol (described in section 5.3.2). In order to ascertain cell

membrane disturbances due to electroporation in attached cells, SEM images were analyzed for BT-20 cells due to their sensitive response to electric field.

5.5.3. Irreversible Electroporation of three-dimensional cell cultures; hydrogels

As a complementary activity, a study on the effects of irreversible electroporation *in vitro* was carried out. Irreversible electroporation protocols were applied to three-dimensional cell cultures (hydrogels). All the experiments reported in this section were performed in the BEMS laboratory at the Virginia Tech, USA.

Hydrogels preparation: the methodology corresponding to hydrogels preparation is the same reported in section 5.3.3. The cell lines used to seed the hydrogels for IRE were MCF-7, MCF-10A, U251, and HEPG2.

IRE protocols for hydrogels: two voltages were used to assess cell ablation due to IRE, as shown in Table 14. Hydrogels not exposed to electric pulses were used as controls. Five replications were performed per condition and cell line.

Table 14. Parameters for irreversible electroporation of hydrogels.

Hydrogels traits		Electric protocol for irreversible electroporation	
Collagen I concentration	5 mg/ml	Pulse duration	100 μ s
Cell seeding	1x10 ⁶ cells/ml	Number of pulses	100
Diameter	10 mm	Repetition frequency	1 Hz
Thickness	1 mm	Monitoring timepoints	3 h, 24 h, 48 h
Cell lines	MCF-7 MCF-10A U251 HEPG2	Voltage	400 V 600 V

FEM modeling of irreversible electroporation in hydrogels: the distribution of the electric field in hydrogels was modeled by FEM, through the Laplace equation solution. The geometry for the model described in section 5.3.3. was used for obtaining the electric field distribution in the hydrogel caused by irreversible electroporation pulses of a cylinder 10 mm in diameter and 1 mm height, simulating the hydrogel. The boundary conditions are the same reported in section 5.3.3., i. e., one needle was set as a voltage terminal and the other was grounded in order to simulate application of pulses. An electric field dependent conductivity was assumed for the hydrogel. Initial electrical conductivity was 0.98 S/m [Ivey J. W, 2015]. A parametric study was performed applying 400 V and 600 V as the input voltage between the needle-electrodes. A stationary parametric non-linear solver was used.

Protocol for ablation assessment: two fluorescent dyes were used to stain hydrogels in order to verify cell ablation and cell viability. On the one hand, PI was used to corroborate cell ablation. On the other hand, calcein acetomethoxy (AM) was used to verify cell viability. Both dyes were monitored in the timepoints reported in Table 14. Imaging of hydrogels was carried out with a Zeiss LSM510 (Carl Zeiss Microscopy LLC, Thornwood, NY) laser scanning confocal microscope.

5.5.4. Pilot study on high-frequency electroporation of three-dimensional cell cultures; hydrogels

A pilot study on the effects of high frequency electroporation in breast cells was carried out *in vitro*. High frequency reversible and irreversible electroporation protocols were applied to three-dimensional cell cultures (hydrogels) as described in Table 15. All the experiments reported in this section were performed in the BEMS laboratory at the Virginia Tech, USA.

Hydrogels preparation: the methodology corresponding to hydrogels preparation is the same reported in section 5.3.3. The cell lines used to seed

the hydrogels for H-FIRE were two breast cell lines (MCF-7 and MCF-10A), and two non-breast cell lines (U251 and HEPG2).

High-frequency electroporation protocols for hydrogels: four voltages were used to assess electroporation due to high-frequency reversible electroporation, and two voltages were used to assess cell ablation due to H-FIRE, as shown in Table 15. Hydrogels not exposed to electric pulses were used as controls. One replication was performed per condition and cell line.

Table 15. Parameters for high-frequency electroporation of hydrogels.

Hydrogels traits		Electric protocol for high-frequency EP		
Collagen I concentration	5 mg/ml	Bursts	reversible	Irreversible
			8	100
Cell seeding	1x10 ⁶ cells/ml	Pulse width	5 μ s	5 μ s
		Number of pulses	20	20
Diameter	10 mm	Interburst delay	1 s	1 s
Thickness	1 mm	Monitoring timepoints	3 h, 24 h, 48 h	3 h, 24 h, 48 h
Cell lines	MCF-7	Voltage	300 V	800 V 1200 V
	MCF-10A		500 V	
	U251		700 V	
	HEPG2		900 V	

Protocols for electroporation and ablation assessment: two fluorescent dyes were used to stain hydrogels in order to verify cell ablation and cell viability. On the one hand, PI was used to corroborate cell permeabilization after high-frequency reversible electroporation, and cell ablation due to H-FIRE. On the other hand, calcein acetomethoxy (AM) was used to verify cell viability. Both dyes were monitored in the timepoints reported in Table 15. Imaging of hydrogels was carried out with a Zeiss LSM510 (Carl Zeiss Microscopy LLC, Thornwood, NY) laser scanning confocal microscope.

6. RESULTS

6.1. Electric field distribution in the MRI-based model (static conductivity)

The electric field distribution obtained for the tumor (Fig. 17A) and the complete breast model (Fig. 17B) corresponding to the realistic breast model based on MRI images and considering a static conductivity described in section 5.2.1. are shown in Fig. 17.

As shown in Fig. 17A, two tumoral volumes were reconstructed but just the biggest tumoral volume could be solved by using FEM, in order to reduce computational requirements. The resultant electric field distribution in the tumor in Fig. 17A was analyzed based on the maximum, minimum and average electric field obtained for each voltage value as shown in Table 16. The solution time for the study was 8 s and 1170 degrees of freedom were solved. Based on these results, it was concluded for this first model, that for the size of the reconstructed tumor (0.8 cm x 1.0 cm x 0.7 cm), current positioning of the electrodes and the material properties conferred (Table 1), the electric potential suggested to be applied between the electrodes should range between 300 V and 500 V in order to cause reversible electroporation. Even if there are regions in which irreversible electroporation can be evidently generated, it is caused throughout the tumor which is the tissue to be damaged.

Table 16. Electric Field in the largest tumor of the MRI-based model.

Applied Voltage [V]	Electric Field [V/cm]		
	<i>Average</i>	<i>Minimum</i>	<i>Maximum</i>
100	130.76	0.87	1714.19
200	261.53	1.74	3428.39
300	392.29	2.61	5142.59
400	523.05	3.48	6856.79
500	653.82	4.35	8570.98
600	784.59	5.22	10285.28
700	915.35	6.09	11999.38
800	1046.12	6.97	13713.58
900	1176.88	7.84	15427.77
1000	1307.65	8.71	17141.97
1100	1438.41	9.58	18856.17
1200	1569.18	10.45	20570.37
1300	1699.94	11.32	22284.56
1400	1830.71	12.19	23998.76
1500	1961.47	13.07	25712.96

Regarding the complete model including a tumoral volume and a surrounding healthy tissue in Fig. 17B, the resultant electric field for both tissues when a 500 V voltage is applied between the electrodes are shown in Table 17 and Fig. 17B. It can be seen that an average electric field magnitude of 654.26 V/cm is achieved when 500 V are applied through two needle electrodes. Assuming an electric field of 400 V/cm as necessary for ECT of tissues, it was concluded that a voltage of approximately 500 V may be consider as suitable for this specific model. Details about these models may be found in Vera Tizatl, A. L. et al. (EBTT), 2016; Vera Tizatl, A. L et al. (CCE), 2016.

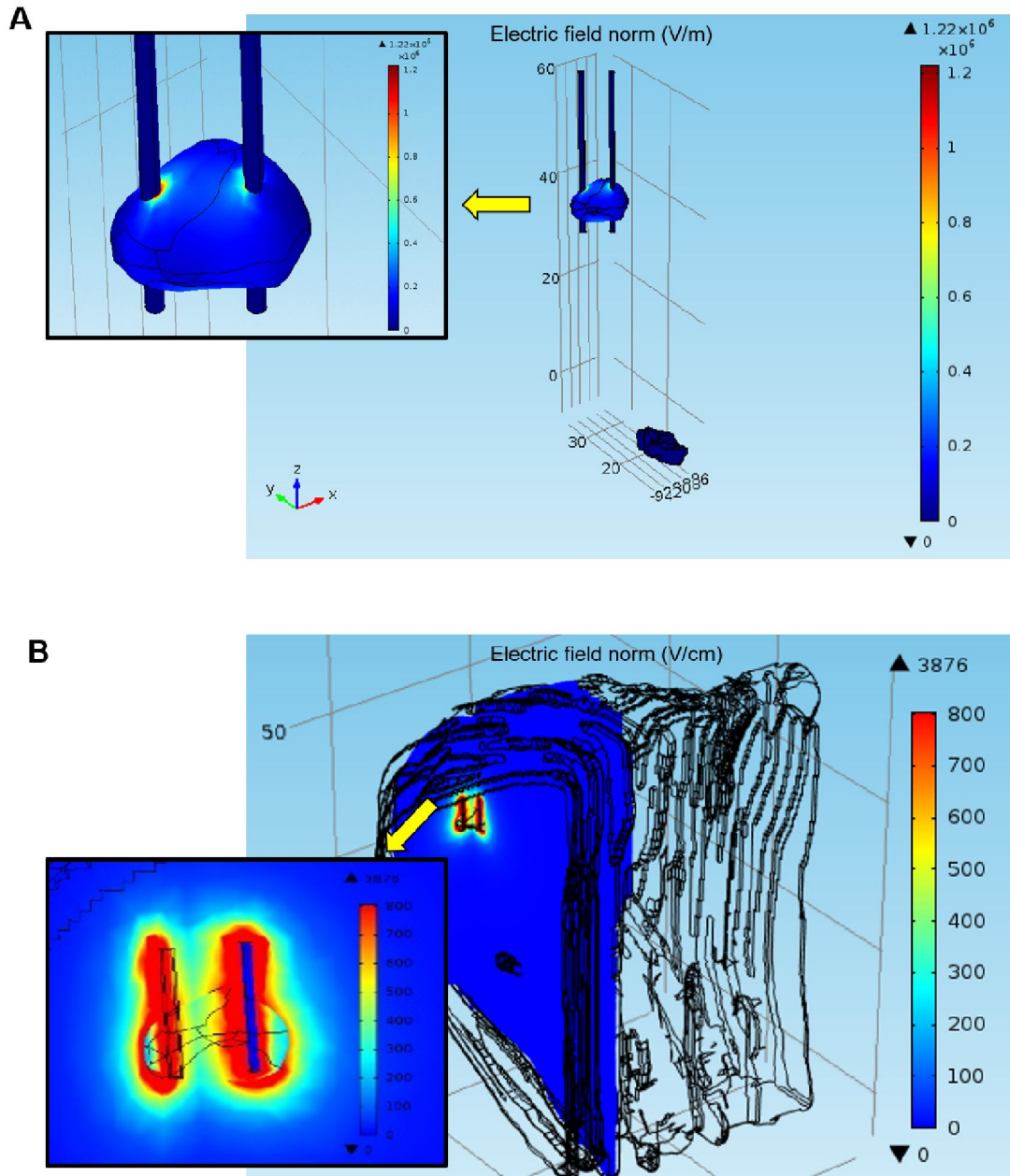


Figure 17. Electric field distribution generated in (A) the largest tumor in the MRI-based model, and in (B) the complete breast model. The tumor coverage is zoomed in for the “zx” plane.

Table 17. Electric field obtained for MRI-based breast model.

Electric Field [V/cm]	Healthy breast tissue	Breast carcinoma
Average	2.37	654.26
Minimum	0	9.35
Maximum	43.17	900.42

6.2. Electric field distribution in the MRI-based model (dynamic conductivity using a sequential model)

The electric field distribution obtained for the MRI-based model, solved by a sequential electroporation model and considering an electric field dependent conductivity, is represented through a gray-scale map proportional to the electric field magnitude as shown in Fig. 18, where both tumors are treated simultaneously by a pair of electrodes.

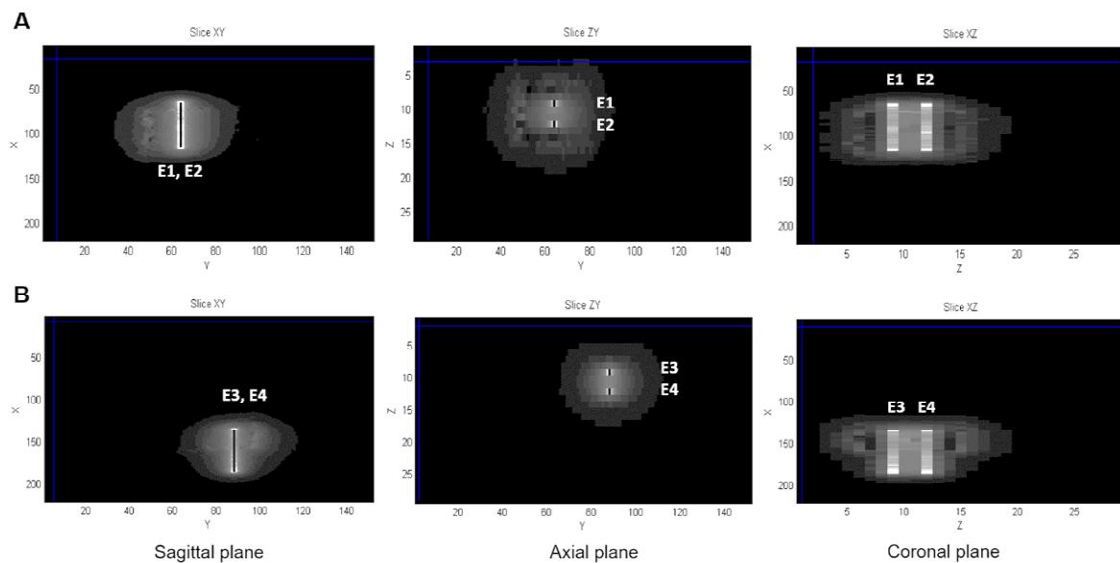


Figure 18. Electric field distribution represented through a gray-scale map for (A) tumor 1, and (B) tumor 2 in addition to their corresponding surrounding tissue. The electric field magnitude is proportional to the brightness on the map, i. e., the brighter a point in the map, the higher the electric field in that point.

In order to visualize the coverage of both tumors, the cumulative coverage curves for the tumoral tissue were obtained for two voltages applied between the electrodes (500 V and 600 V), as shown in Fig. 19A and Fig. 19B. It can be seen that a voltage of 600 V produces better tumor coverage producing 100% tumor coverage with 412.8 V/cm, in contrast with 100% tumor coverage with 331.7 V/cm when 500 V voltage is applied. These results are in agreement with the results obtained for the model solved only with COMSOL Multiphysics but the solution time was considerably decreased from 3 hours to a couple of minutes when the sequential electroporation model is used.

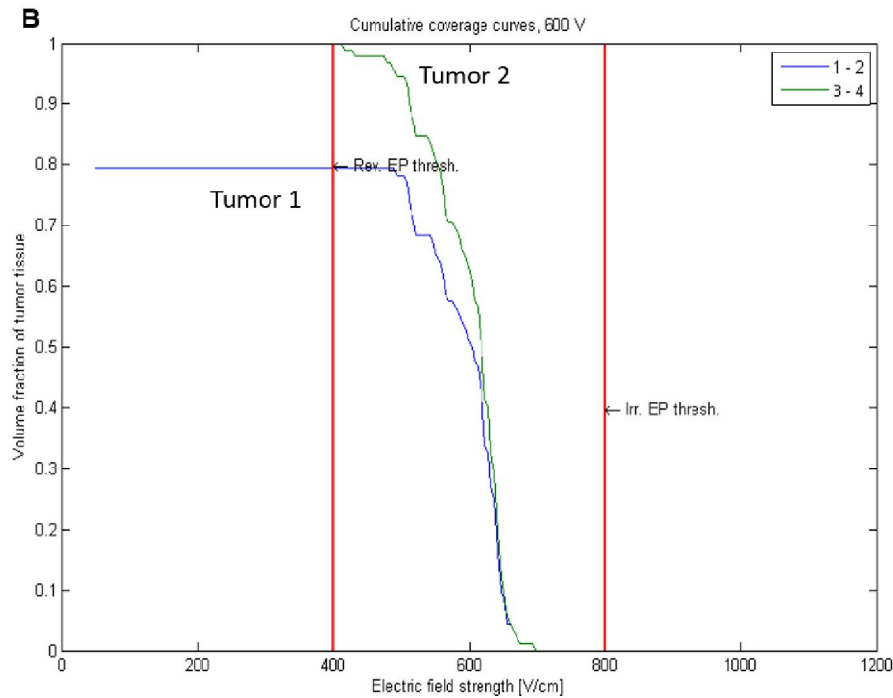
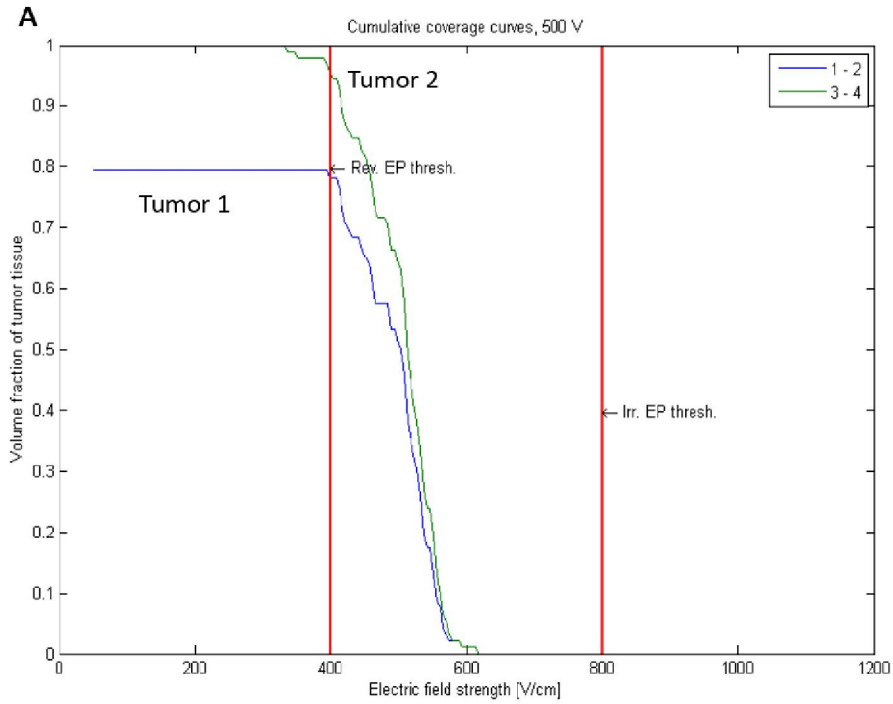


Figure 19. Cumulative coverage curves for MRI-based breast model for (A) 500 V, and (B) 600 V applied between electrodes. Green and blue lines define the coverage generated by electrodes E1 and E2 for the upper tumor (T1) and the coverage generated by electrodes E3 and E4 for the bottom tumor (T2).

A comparison between the model solved in COMSOL Multiphysics and the optimized model programmed in Matlab is reported in Table 18. It is worth noting that an estimation of electric current necessary to cause electroporation is possible with the use of a sequential model of electroporation. In addition, an increasing conductivity behavior was conferred to the tissues of interest.

Table 18. Comparison between models.

Model	COMSOL		COMSOL + Matlab		
	Tumor 1	Surrounding tissue	Tumor1	Tumor 2	Surrounding tissue
Electrical conductivity [S/m]	$\sigma = 0.4$	$\sigma = 0.1$	$\sigma_i = 0.4$ $\sigma_f = 1.2$	$\sigma_i = 0.4$ $\sigma_f = 1.2$	$\sigma_i = 0.1$ $\sigma_f = 0.4$
Electrode activation	E1E2	--	E1E2	E3E4	--
Voltage [V]	500	--	600	600	--
Current [A]	--	--	6.9	4.41	--
Distance between electrodes [mm]	--	--	E1E2 = 9.0 E3E4 = 9.0		

6.3. Patient-specific electroporation protocols establishing for DBT-based models

The total volumes of each target tissue expected to be treated with ECT are listed in Table 19. Global electroporation results obtained for each patient and the twelve electrode arrays are presented in detail in Appendix B.

Table 19. Target tissue volumes on the DBT-based models.

Patient	Volume of target tissues[cm ³]		
	Breast Tissue	Fatty Tissue	Tumor
1	10.20	3.76	0.46
2	5.16	19.73	3.10
3	1.05	26.58	5.10

The three most efficient electrode arrays for each patient were hierarchically selected based on the following criteria which are in accordance with the literature [Neal R. E. et al., 2010].

- 1) percentage of tumor volume reversibly electroporated,
- 2) percentage of tumor volume irreversibly electroporated,
- 3) percentage of treated safety margin volume,
- 4) minimal invasiveness given by the number of electrodes inserted,
- 5) minimal activated electrode pairs, and
- 6) minimal electric current.

The most efficient electroporation protocols are listed in Table 20, according to the hierarchic selection criteria applied to the global results described in Appendix B. These protocols are reported as the electrode configuration, the voltage applied between the activated needles, the percentage of the target tissue covered between reversible (400 V/cm) and irreversible electric field thresholds (800 V/cm), and the average electric current between all pairs of activated electrodes.

Table 20. Effective electroporation protocols for the treatment of target tissues.

P ^a	Electrode Array	Voltage ^b [V]			Tissue Coverage [%]						\bar{I}^e [A]
		C-P	P-P	D	Tumor		Breast		Fat		
					RE ^c	IRE ^d	RE	IRE	RE	IRE	
1	4Di1	--	1000	2000	100	0	95.1	22.9	99.8	48.4	3.5
	4De2	2000	1500	--	100	30.2	85.3	11.0	90.6	10.1	3.2
	6St2	1500	3000	--	100	33.5	85.0	6.2	91.8	6.6	4.3
2	5Di2	2000	--	--	98.9	9.7	96.7	16.9	99.2	28.1	7.9
	6St2	2500	2000	--	99.9	29.9	100	51.0	100	64.0	5.8
	4De2	3000	3000	--	99.8	60.3	99.6	48.8	99.8	62.3	7.5
3	6St2	3000	--	--	98.6	14.9	94.0	29.0	100	80.5	8.2
	5Di2	3000	--	--	97.8	15.4	92.1	27.5	100	74.9	8.2
	4De2	3000	3000	--	95.7	14.2	88.2	22.7	100	59.4	6.1

a Patient.

b Voltage applied between central electrodes and peripheral electrodes (C-P), peripheral electrodes (P-P) and opposite electrodes (D) in 4-needle diamond configuration.

c Percentage of tissue covered at the reversible electroporation threshold (RE = 400 V/cm).

d Percentage of tissue covered at the irreversible electroporation threshold (RE = 800 V/cm).

e Average electric current between activated pairs of needles.

The best electroporation protocols highlighted in green in Table 20 were used to obtain the electric field cumulative coverage curves for the 3 target tissues (tumor, fatty, and breast tissue in the safety margin) as shown in Figures 20 to 22. Electric field cumulative coverage curves show the volume fraction of

tissue (1=100%) covered at a certain electric field strength. A complete coverage was expected to be reached above 400 V/cm, whereas the tissue volume covered above 800 V/cm had to be kept at the minimum to minimize IRE.

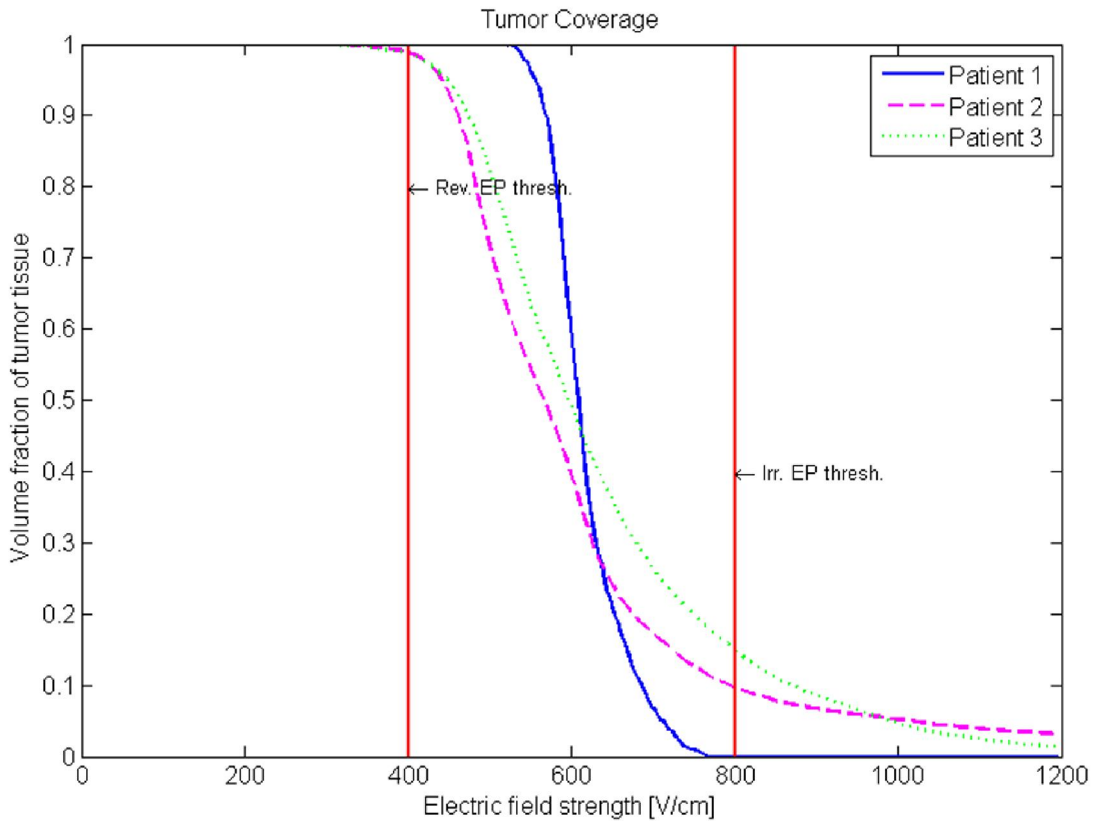


Figure 20. The most efficient tumor coverage for the 3 patients. Electrode 4Di1 covered 100% of tumor in patient 1 with 1000 V and 2000 V between peripheral and opposite needles. Electrode 5Di2 covered 98.9% of tumor in patient 2 with 2000 V between C-P needles. Electrode 6St2 covered 98.6% of tumor in patient 3 with 3000 V between C-P needles.

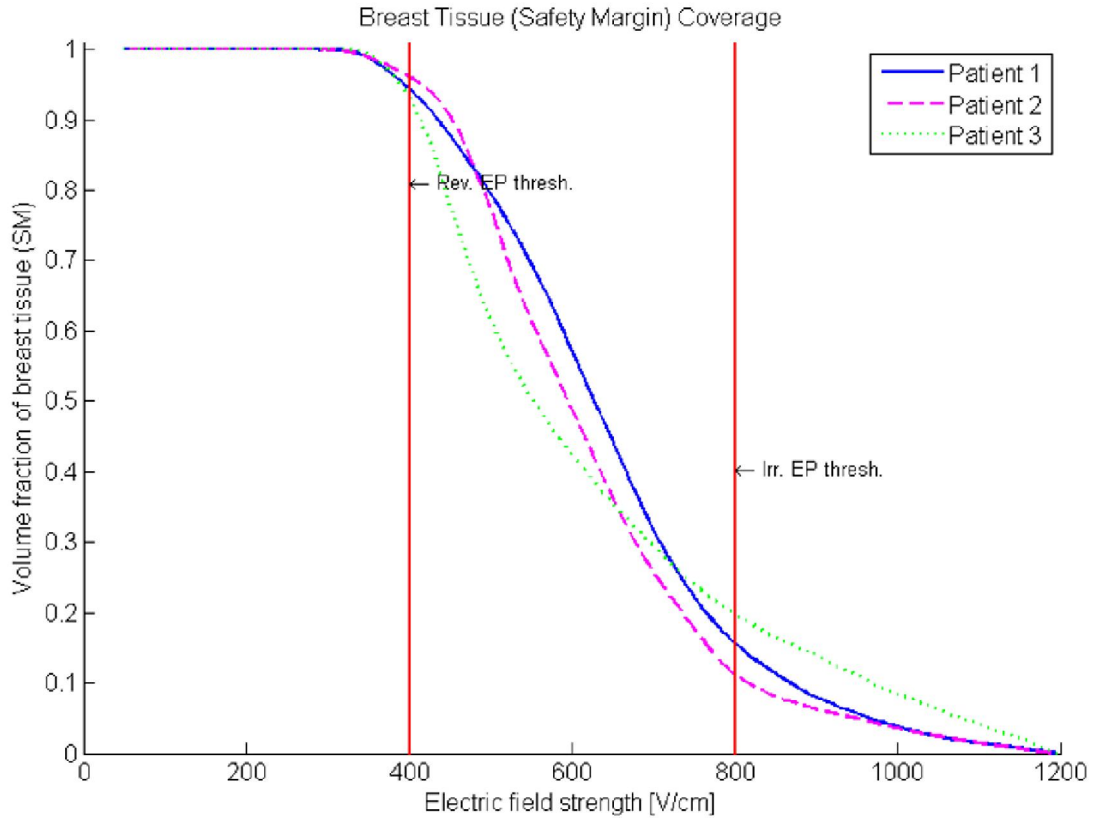


Figure 21. The most efficient coverage of breast tissue in the safety margin for the 3 patients. Electrode 4Di1 covered 95.1% of breast tissue in patient 1 with 1000 V and 2000 V between peripheral and opposite needles. Electrode 5Di2 covered 96.7% of breast tissue in patient 2 with 2000 V between C-P needles. Electrode 6St2 covered 94% of breast tissue in patient 3 with 3000 V between C-P needles.

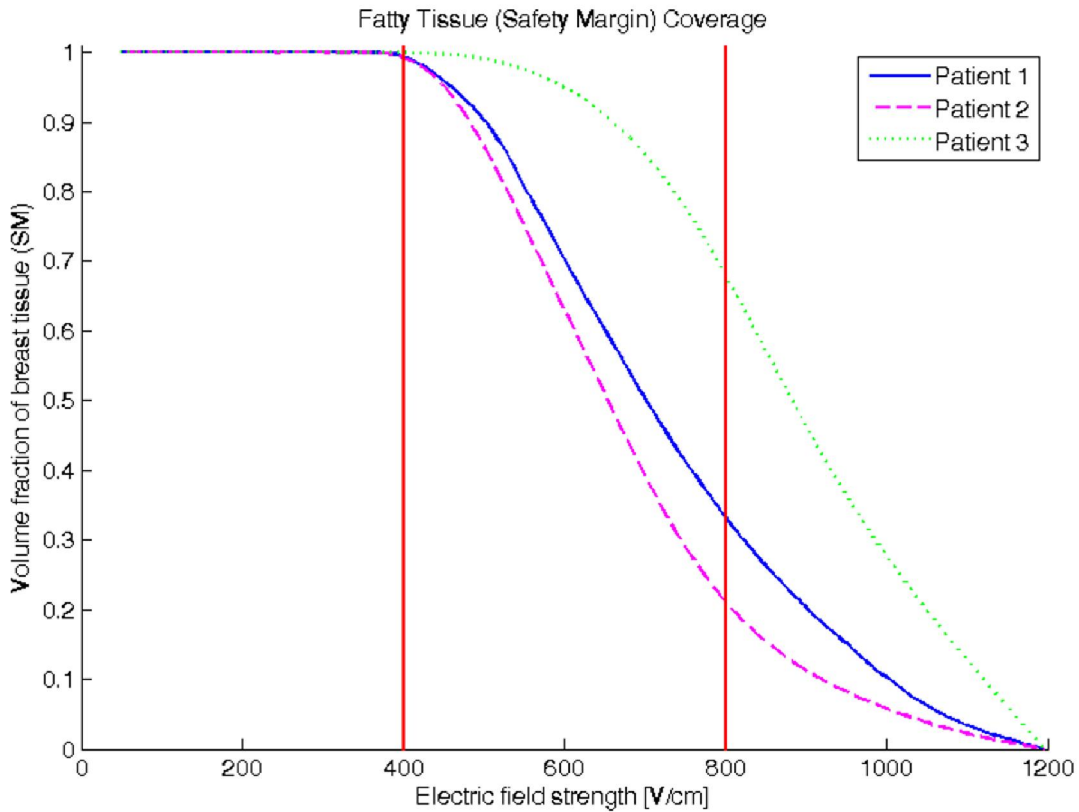


Figure 22. The most efficient coverage of fatty tissue in the safety margin for the 3 patients. Electrode 4Di1 covered 99.8% of fatty tissue in patient 1 with 1000 V and 2000 V between peripheral and opposite needles. Electrode 5Di2 covered 99.2% of fatty tissue in patient 2 with 2000 V between C-P needles. Electrode 6St2 covered 100% of fatty tissue in patient 3 with 3000 V between C-P needles.

Electroporation color maps were obtained for the most efficient electroporation protocol applied to the three patients as shown in Figure 23. Irreversibly electroporated areas are marked in magenta, color blue represents reversibly electroporated areas in the tumors, and green shows reversibly electroporated areas in the safety margin tissues. Nontreated areas, that is, points where reversible electroporation threshold was not reached, appear uncolored.

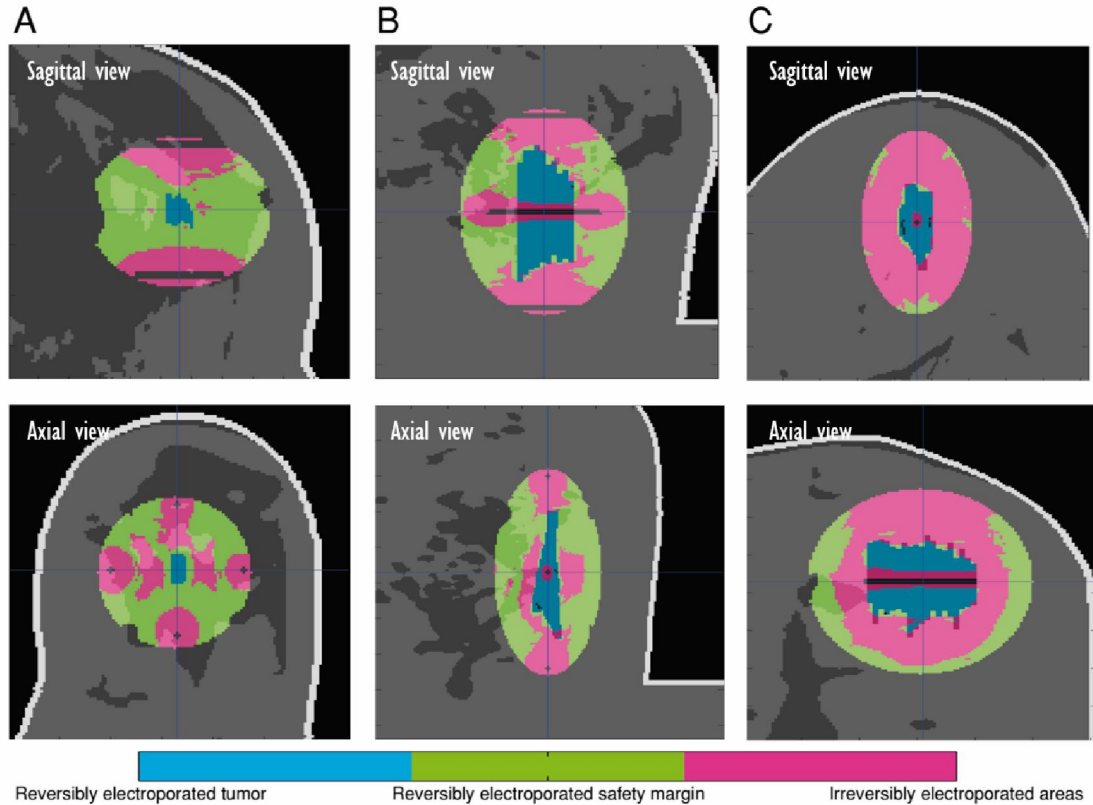


Figure 23. Visualization of electroporation reached in the target tissues of (A) patient 1 with 4Di1 electrode array, (B) patient 2 with 5Di2, and (C) patient 3 with 6St2. Magenta color represents irreversibly electroporated regions, green shows reversibly electroporated regions in the safety margin (fatty tissue and breast) and blue indicates reversibly electroplated areas in the tumors. Nontreated areas in the models are uncolored.

Results analysis for Patient 1: for a small tumor in patient 1, a 4-needle electrode array in diamond configuration (4Di1) was suitable to reversibly cover the complete tumor and more than 90% of the safety margin. Good results were obtained with a 4-needle electrode array in delta configuration (4De2) and 6-needle electrode array in star configuration (6St2), as they covered 100% of the tumor and more than 85% of the safety margin. Tumor coverage in Figure 20 shows that an efficient electroporation (100% coverage

above 400 V/cm) of a small tumor in patient 1 may be achieved with electrode 4Di1.

Results analysis for Patient 2: for this patient, 5Di2, 6St2 and 4De2 electrode arrays showed comparable results regarding reversibly electroporated tissue coverage. 5Di2 electrode array generated the lowest amount of IRE. The tumor in this patient is bigger than the tumor in patient 1 and hence, more difficult to reversibly electroporate, covering 98.9% of the tumor with an electric field above 400 V/cm with the 5Di2 electrode array.

Results analysis for Patient 3: similar to patient 2, for this patient, 6St2, 5Di2, and 4De2 resulted to be the most efficient electrode arrays in a comparable manner, but 5Di2 electrode array required fewer pairs of active electrodes. The tumor in this patient is bigger than the tumor in patient 1 and hence, more difficult to reversibly electroporate, covering 98.6% of the tumor with an electric field above 400 V/cm with the 6St2 electrode array.

It is worth noting that coverage of the tissues in the safety margin changed for the different breast densities due to the different dielectric properties of the tissues. Fatty tissue was easier to cover completely by fields above the reversible electroporation threshold (shown in Figure 21) than breast tissue (shown in Figure 22). At the same time, fatty tissue was also more susceptible to IRE than breast tissue.

6.4. Cell-specific electroporation protocols for breast cancer cell suspensions

Initially, pulse amplitudes listed in Table 9 were applied to cell suspensions. In order to determine the most effective protocol for each cell line, pulse amplitudes were afterwards refined for each breast-cancer cell line depending on cell viability.

The PI uptake in four qualitative effective protocols and in controls is shown, Fig. 24, which corresponds to the fluorescence emitted by cells that remained

unaffected after electroporation. Light microscopy images of controls, in Fig.24A, show the morphology and confluence of all cell lines in suspension. For cells suspensions, the PI uptake strongly differed among cell types and pulse amplitudes. MCF-7 cells were the most difficult to electropermeabilize, showing a weak PI uptake while demanding the highest voltage applied to the breast cancer cell lines. However, HCC1419 cells showed qualitatively similar PI uptake for lower voltages as predicted by computational simulation. BT-20 cells were, in contrast, the most sensitive to voltage and the easiest to be permeabilized with the lowest voltages which were computationally unexpected to cause electroporation. Moreover, PI uptake was observed in control suspensions due to the presence of damaged cells because of the trypsinization process which resulted in false positive signals. Nonetheless, the uptake difference between treated and control suspensions was evident.

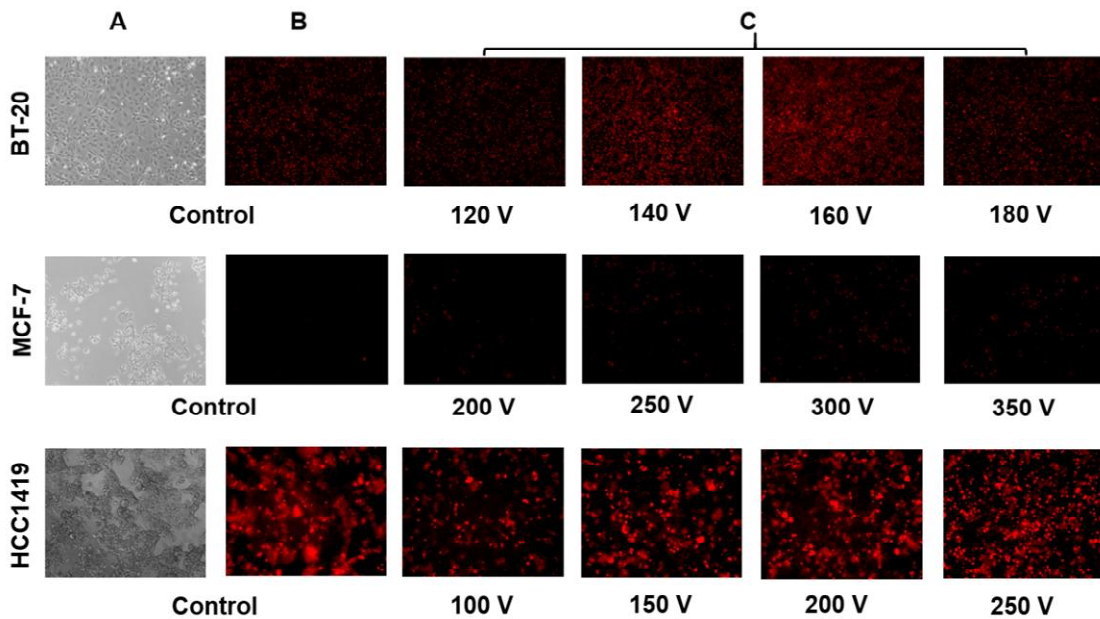


Figure 24. Electroporation of cell suspensions: (A) light and (B) epifluorescence microscopy which show the morphology, confluence, and PI uptake obtained in controls. False positive signals can be observed in the controls due to the presence of damaged cells because of the trypsinization process. (C) Epifluorescence microscopy of samples electroporated with different voltages. Images were taken with Nikon Eclipse Ti-U. Objective 40x.

Cell viability percentage served as the final criterion to select the most efficient cell-specific electroporation protocol. Figure 25 shows the average cell viability in three experimental replications for cell suspensions. High viability values were observed in all cell suspensions.

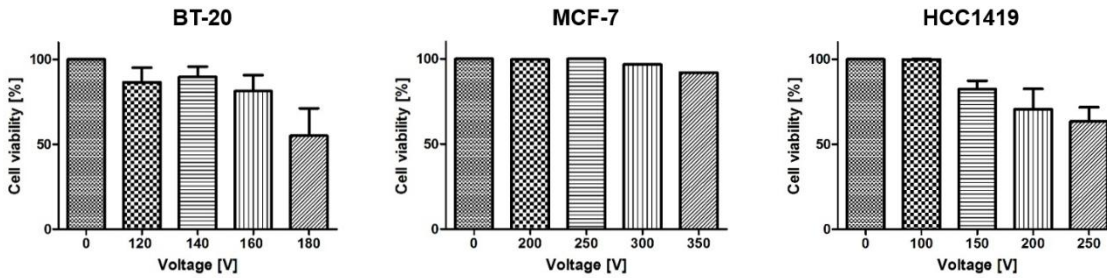


Figure 25. Cell viability percentage in cell suspensions. The plots correspond to the qualitatively effective voltages for each cell line and represent the average of three independent replications.

The best electroporation protocols for each cell line in suspension, along with their respective electric field threshold, are summarized in Table 21.

Table 21. Cell-specific electroporation protocols for cell suspensions.

Cell line	Voltage [V]	Cell viability [%]	Electric field threshold [V/cm]
MCF-7	250	100	625
BT-20	140	89.7	300
HCC1419	100	99.9	250

MCF-7 cells in suspension were hard to electroporate most probably because their plasmatic membrane was more resistant. This assertion is supported by the fact that their membrane was not affected after undergoing trypsinization and the absence of a false positive signal of PI in the control where they remained impermeable. The cell-specific protocols allowed establishing

reversible electroporation thresholds; 250 V/cm to 625 V/cm for breast-cancer cell suspensions.

6.5. Cell-specific electroporation protocols for breast-cancer adhered cells

Pulse amplitudes listed in Table 10 were applied to adhered cells. In order to determine the most effective protocol for each cell line, pulse amplitudes were afterwards modified for each breast-cancer cell line depending on cell viability.

The PI uptake in four qualitative effective protocols and in controls is shown in Fig. 26, which corresponds to the fluorescence emitted by cells that remained unaffected after electroporation. Light microscopy images of controls, in Fig. 26A, show the morphology and confluence of all cell lines in suspension. Conversely to electroporation of cell suspensions, electroporation of adhered cells resulted in an overall significant PI uptake increase in all cell lines. MCF-7 cells required again a higher voltage (in agreement with numerical simulation) than the other breast cancer cells to be electropermeabilized, but they showed a much more perceptible PI uptake with lower voltages than the required for the suspension platform. BT-20 and HCC1419 cells were more efficiently electroporated when adhered rather than suspended with lower voltages which were computationally unexpected to cause reversible electroporation. It is noticeable that no false positive signals were observed in the controls for adhered cells. A fluorescence decrease was noticed in some cell lines in transitions from low to high voltage due to the clearance of damaged cells (unable to adhere to a substrate) from the medium. These results imply that electropermeabilization is more reliable in adhered cells than in suspended cells.

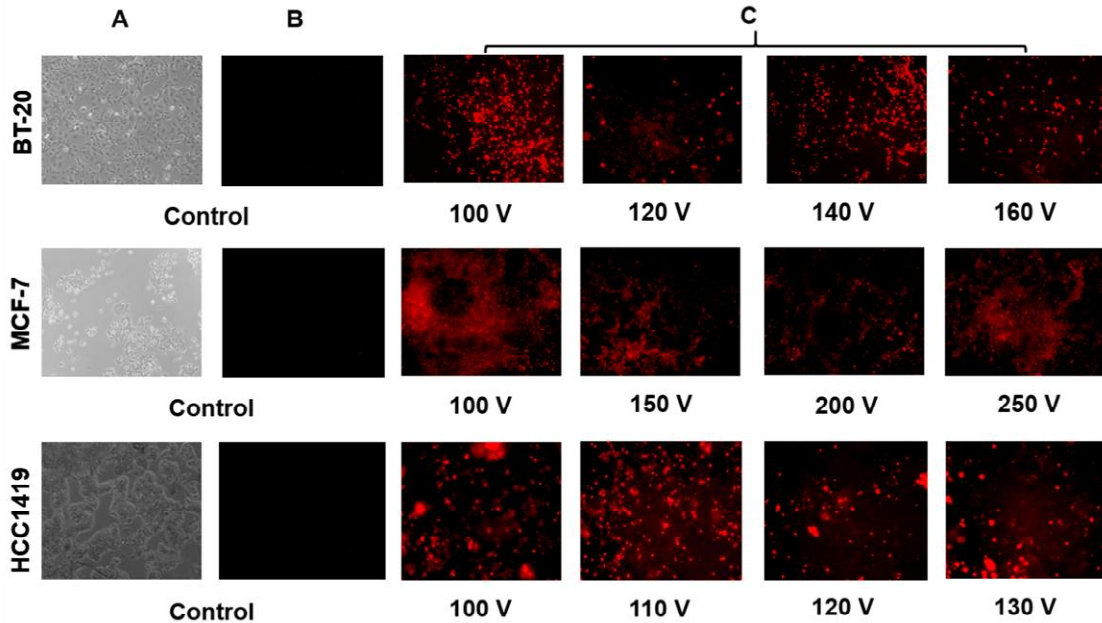


Figure 26. Electroporation of adhered cells: (A) light and (B) epifluorescence microscopy which show the morphology, confluence, and PI uptake obtained in controls. No false positive signals were observed in the controls which provide a reliable PI uptake signal. (C) Epifluorescence microscopy of samples electroporated with different voltages. Images were taken with Nikon Eclipse Ti-U. Objective 40X.

Cell viability percentage served as the final criterion to select the most efficient cell-specific electroporation protocol. Figure 27 shows the average cell viability in three experimental replications for adhered cells. Opposite to cells suspensions, lower cell viabilities were obtained in adhered cells probably caused by the larger cell membrane surface exposed to the external electric field due to attachment of cells.

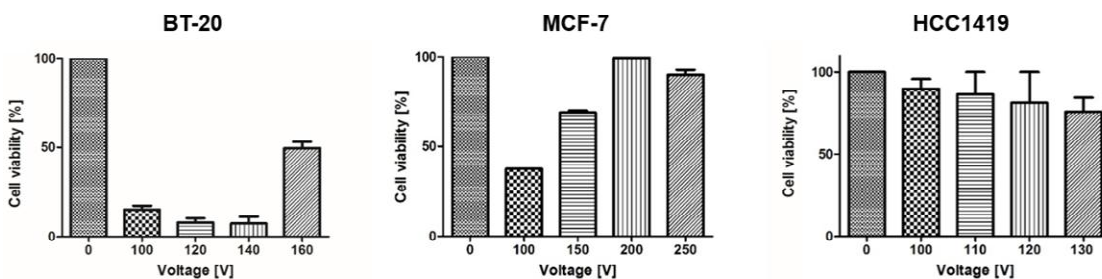


Figure 27. Cell viability percentage in cell suspensions. The plots correspond to the qualitatively effective voltages for each cell line and represent the average of three independent replications.

The best electroporation protocols for each cell line when adhered, along with their respective electric field threshold, are summarized in Table 22.

Table 22. Cell-specific electroporation protocols for adhered cells.

Cell line	Voltage [V]	Cell viability [%]	Electric field threshold [V/cm]
MCF-7	200	100	415
BT-20	160	50	332
HCC1419	110	86.5	228

Noticeably, the highest PI uptake in MCF-7 cells, associated with the highest cell viability were obtained with lower voltages when adhered rather than suspended. On the contrary, HCC1419 and BT-20 cells required, a higher voltage when adhered in order to be efficiently electroporated. The cell-specific protocols allowed establishing reversible electroporation thresholds; 228 V/cm to 415 V/cm for breast cancer adhered cells, which is lower to the reversible electroporation threshold for breast-cancer cells in suspension.

6.6. Establishing reversible electroporation thresholds in three-dimensional cell cultures

PI uptake was imaged by confocal imaging of hydrogels for cell lines MCF-7, MCF-10A, U251 and HEPG2 in three timepoints: 3 h, 24 h and 48 h after electroporation. Fig. 28A shows the cell permeabilization in all cell lines 24 h after electroporation. Similar to the results obtained for suspended and adhered cells, different PI uptake signals are obtained for each cell line and voltage. The breast metastatic cell line was permeabilized with high voltages (considering the four voltages used), which is in agreement with the results obtained for this cell line in suspension and adhered. This fact supports the implication of a resistant cell membrane in these cells. Non-breast cells lines were permeabilized similarly with 350 V. Interestingly, non-malignant breast cell line MCF-10A was permeabilized with the highest voltage. Based on this fact, it is hypothesized that healthy breast tissue in a safety margin will be harder to treat with ECT than tumoral tissue. Green pixels in Fig. 28B show the viable cells for all cell lines and red pixels represent dead cells within the hydrogels 48 h after treatment. The images in this figure confirm that mostly all cells in the hydrogels remain viable and undamaged after electroporation. Some dead cells are evident in the vicinity of the electrode-insertion points. This may be attributed to two main factors: irreversible electroporation which is characteristic around the electrodes and/or mechanical damage due to the insertion of the needles.

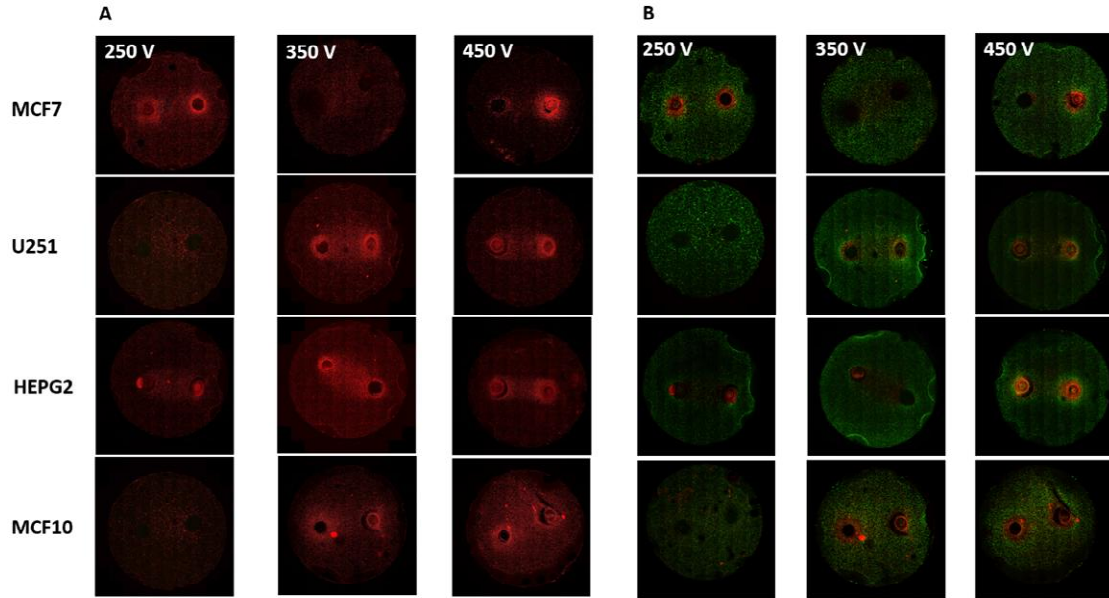


Figure 28. Reversible electroporation assessment in hydrogels. (A) PI fluorescence in red show the cell permeabilization in all cell lines 24 h after electroporation. (B) Calcein fluorescence in green show the viable cells and red pixels represent dead cells within the hydrogels 48 h after treatment.

Cell-specific reversible electroporation thresholds for hydrogels were obtained with a two-step process: first, confocal images corresponding to the PI uptake are analyzed with imageJ software in order to measure the permeabilization surfaces, per cell line, voltage, and timepoint. Second, these measurements are compared with the integration surfaces obtained in COMSOL Multiphysics for the electric field distribution related to different voltages applied between the electrodes.

6.7. Effectiveness of ECT with paclitaxel in breast-cancer cells

The effectiveness of ECT with paclitaxel in breast-cancer cells was assessed through fluorescent dyes indicating cell death and the corresponding death via. As shown in Fig. 29 and Fig. 30, the bright field indicate the cell confluence

and cell morphology after the application of the respective treatments, Hoechst dye labels total cell nuclei, Annexin V binds to phosphatidylserine thus detecting early apoptosis, and Later apoptosis was detected by the nucleic acids interleave EthD III.

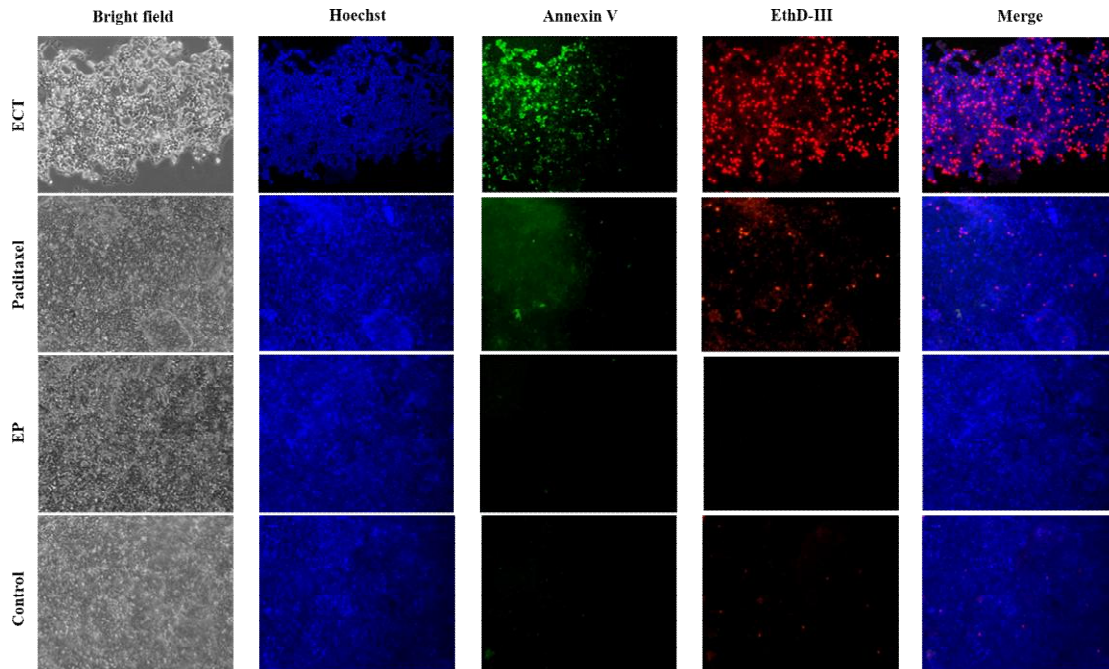


Figure 29. ECT with paclitaxel in MCF-7 cells. The bright field shows the cell confluence and cell morphology after the application of the respective treatments. Hoechst dye labels total cell nuclei. Annexin V binds to phosphatidylserine thus detecting early apoptosis. Later apoptosis was detected by the nucleic acids interleave EthD III. The use of Electrochemotherapy leads to a faster cell death compared to chemotherapy, removing a greater number of cells with an equal drug concentration.

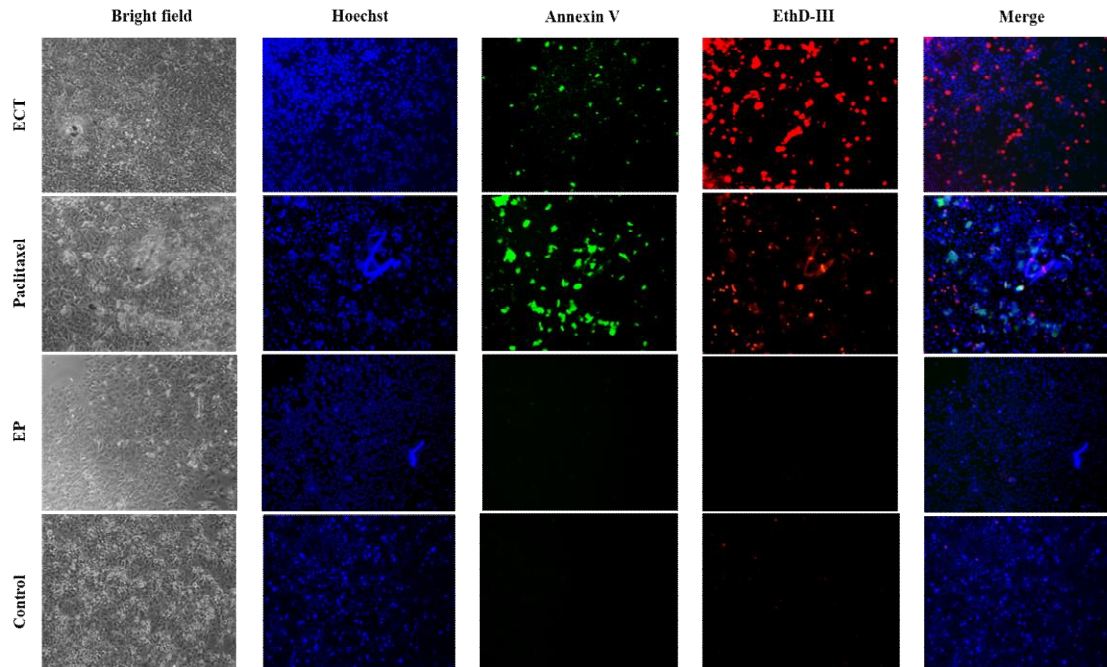


Figure 30. ECT with paclitaxel in BT-20 cell line. The bright field shows the cell confluence and cell morphology after the application of the respective treatments. Hoechst dye labels total cell nucleus, Annexin V binds to phosphatidylserine, thus detecting early apoptosis and the later apoptosis was detected by the nucleic acids interleave EthD III. The use of Electrochemotherapy in this cell line leads to a faster cell death compared to Chemotherapy.

Noticeably, ECT enhances the effect of paclitaxel in MCF-7 cells, leading to a faster apoptotic process compared to chemotherapy alone. It is worth noting the loss of the monolayer integrity due to ECT, 24 h after application of the treatment. Only few domes were found in different visual fields where most of the cells were in late apoptosis. This apoptotic process is slower in chemotherapy because of the low permeability nature of the antineoplastic drug and therefore, a significant loss of cells was not observed. The number of cells in early and late apoptosis is similar without a stage death predominance.

We also confirm the use of the most suitable and effective electroporation protocol, after the application of this protocol there is no cell death due to electroporation, which is comparable to the control condition.

Although the response to electrochemotherapy was less evident in the BT-20 cell line, a faster induction to late apoptosis was also found. The monolayer remained almost at the same degree of confluence as in chemotherapy condition. The applied electroporation protocol does not induce cell death compared to the control condition. In this case irreversible electroporation could be applied, instead of ECT, since no significant drug effect enhancement was observed.

6.8. Cell-specific Induced Transmembrane Voltage for suspended and adhered cells

Because of the complex geometry that cells acquire when they are adhered to a substrate, confocal images obtained for each breast cancer cell line (MCF-7, BT-20 and HACC1419) were used to build three-dimensional realistic models for adhered cells. A single cell for each cell line was reconstructed in 3D Slicer and exported to COMSOL Multiphysics in order to compute the electric potential in cells, as shown in Fig. 31.

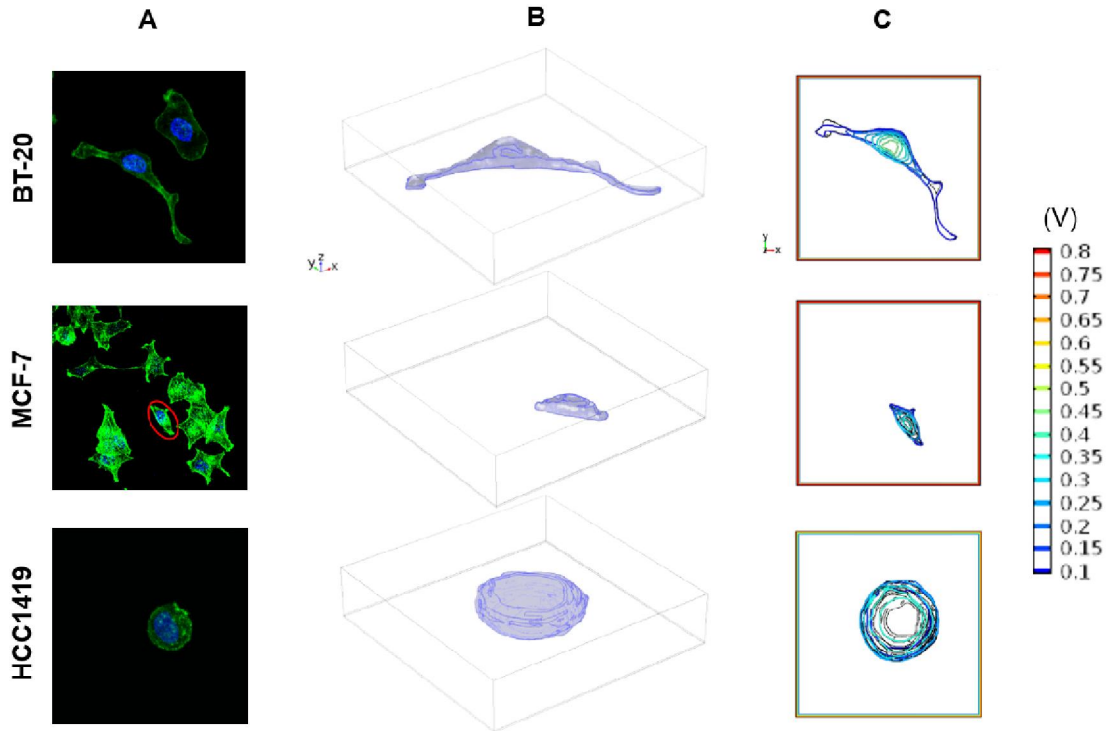


Figure 31. Cell-specific three-dimensional modeling of attached cells. (A) a single cell was selected (red bounded) on confocal slices and it was used to reconstruct (B) realistic cell models in order to calculate (C) the induced transmembrane potential.

The maximum ITV was calculated for all cell lines, analytically for suspended cells and numerically for adhered cells. Maximum ITV values are summarized in Table 23, from which it is evident that BT-20 and MCF-7 cells required lower transmembrane potentials when adhered rather than in suspension. In addition, no significant difference in ITV was found for adhered cells among cell lines. Interestingly, HCC1419 adhered cells exhibit a shape close to a sphere, similar to the shape they acquire in suspension and hence, ITV analytical and numerical values were equal.

Table 23. Cell-specific ITV.

Cell line	Maximum ITV [V]	
	Suspended cells	Adhered cells
MCF-7	3.6	0.4
BT-20	2.7	0.5
HCC1419	0.4	0.4

6.9. Visualization of electroporated cell membranes

A single BT-20 cell is shown in Figure 32A, x2,000 in magnification. A visual field was magnified x10,000 (Fig. 32B) in which a considerable number of disturbances were observed on the cellular surface compared to cells without electroporation (Fig. 32C) in whose magnification (Fig. 32D) no disturbances were detected.

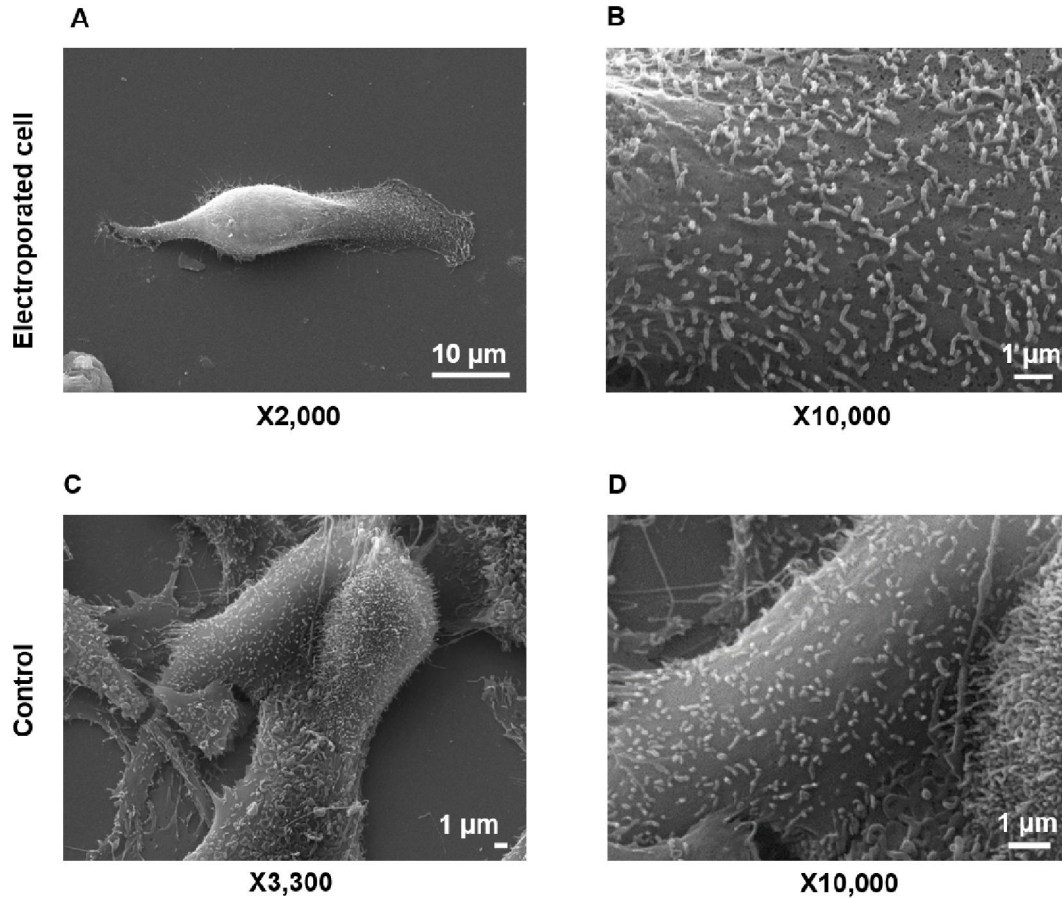


Figure 32. Scanning electron microscopy. (A) An electroporated BT-20 cell, optical zoom x2,000, bar = 10 μm. (B) x10,000 magnification, bar = 10 μm, where disturbances of different sizes are evident. (C) BT-20 cells without electroporation, optical zoom x3,300, bar = 1 μm. (D) x10,000 magnification, bar = 10 μm where no disturbances were found.

These findings may be further useful in the understanding of pore formation phenomenon attributed to electroporation. Further investigation is encouraged to confirm whether these disturbances can be considered as pores in the cell membrane.

6.10. Findings on irreversible electroporation of breast-cancer hydrogels

The results regarding the application of IRE in a breast cancerous cell line (MCF-7) and a non-malignant breast cell line (MCF-10A) are contrasted with the results obtained in two non-breast cell lines (U251 and HEPG2) in Fig. 33A and Fig. 33B respectively, for two voltages: 400 V and 600 V. Details on the irreversible electroporation protocols can be found in section 5.5.3. It can be noticed in Fig. 33, that the ablation regions in the hydrogels are well differentiated (red ellipsis) from the regions containing viable cells (green regions). Interestingly, among cancerous cell lines, breast cells (MCF-7) showed a smaller ablation surface than brain cells (U251) and comparable results with hepatocellular cells (HEPG2). On the other hand, non-cancerous breast cells (MCF-10A) showed the smallest ablation surface among the four cell lines. This fact provides evidence of the difficulty for treating healthy breast tissue with irreversible electroporation.

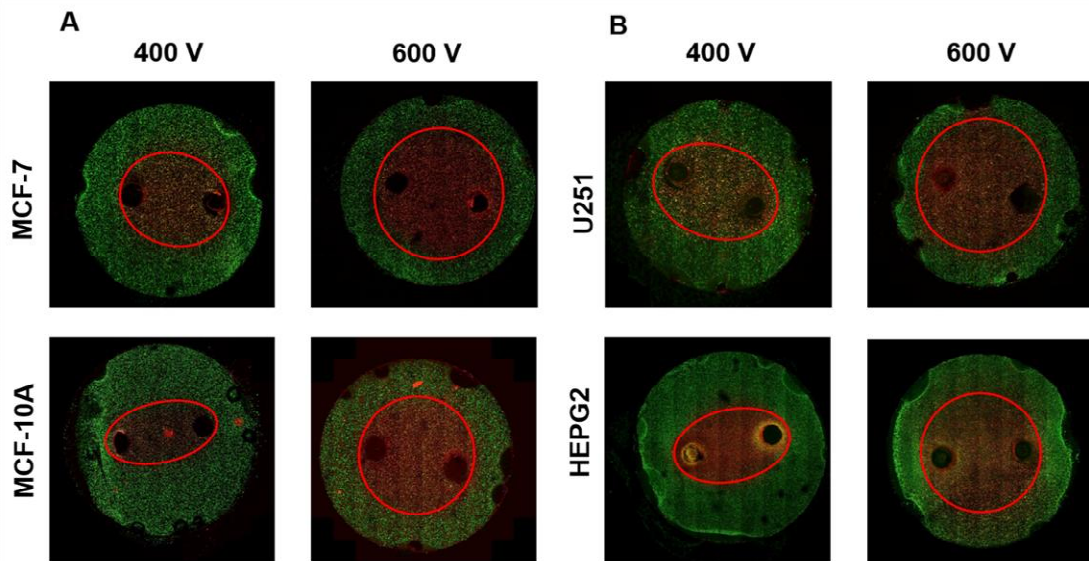


Figure 33. Irreversible Electroporation of hydrogels. (A) IRE in hydrogels seeded with cancerous (MCF-7) and non-cancerous (MCF-10A) breast cell lines. (B) IRE in hydrogels seeded with cancerous brain cells (U251) and cancerous hepatocellular cells (HEPG2).

6.11. Findings on high frequency electroporation of breast-cancer hydrogels

High-frequency reversible (H-FRE) and irreversible (H-FIRE) electroporation was evaluated in hydrogels seeded with four different types of cells: a breast cancerous cell line (MCF-7), a non-malignant breast cell line (MCF-10A) and two non-breast cell lines (U251 and HEPG2). The details regarding the electric protocols used in H-FRE and H-FIRE can be found in section 5.5.4. H-FRE was evaluated through cell permeabilization 3 h and 24 h after the treatment, and cell viability was monitored 48 h after the treatment as it was described in section 5.3.3. H-FIRE, in turn, was evaluated through the monitoring of the ablation zone 3 h, 24 h and 48 h after electric pulsing as it was described in section 5.5.3. The results for the different cell lines are presented per cell line in Figs. 34-37. It can be seen that H-FRE cause in general a more uniform permeabilization in all the hydrogel, in comparison with the results observed for reversible electroporation of hydrogels described in section 6.6. where the permeabilized regions were noticeably delimited depending on the cell type and voltage. In addition, a high cell viability was observed during the last timepoint. On the other hand, cell lines responded differently to H-FIRE. Noticeably, breast-cancer cells (MCF-7) resulted in a comparable ablation region for 800 V and 1200 V pulses, but the ablation size seems to decrease with time. This fact suggests that this type of cells is hard to eradicate, and that they might even repopulate a treated region. This finding is even more pronounced in non-malignant breast cell line (MCF-10) where the ablation regions obtained with 800 V and 1200 V seem comparable 3 h after treatment, but they remarkably decrease 24 h after treatment in a manner that all MCF-10A cells in hydrogels remain viable after the treatment with H-FIRE. This fact emphasizes the challenging process of treating breast tissues with electroporation either reversible, or irreversible.

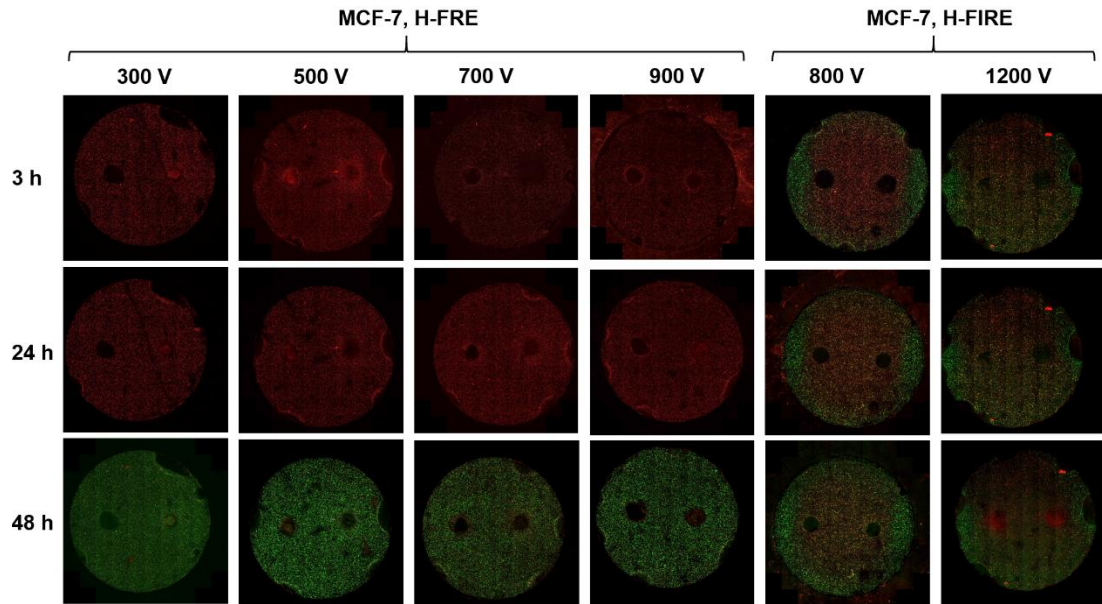


Figure 34. High-frequency reversible electroporation (H-FRE) and High-frequency irreversible electroporation (H-FIRE) of malignant breast cells (MCF-7) in three timepoints (3 h, 24 h, and 48 h).

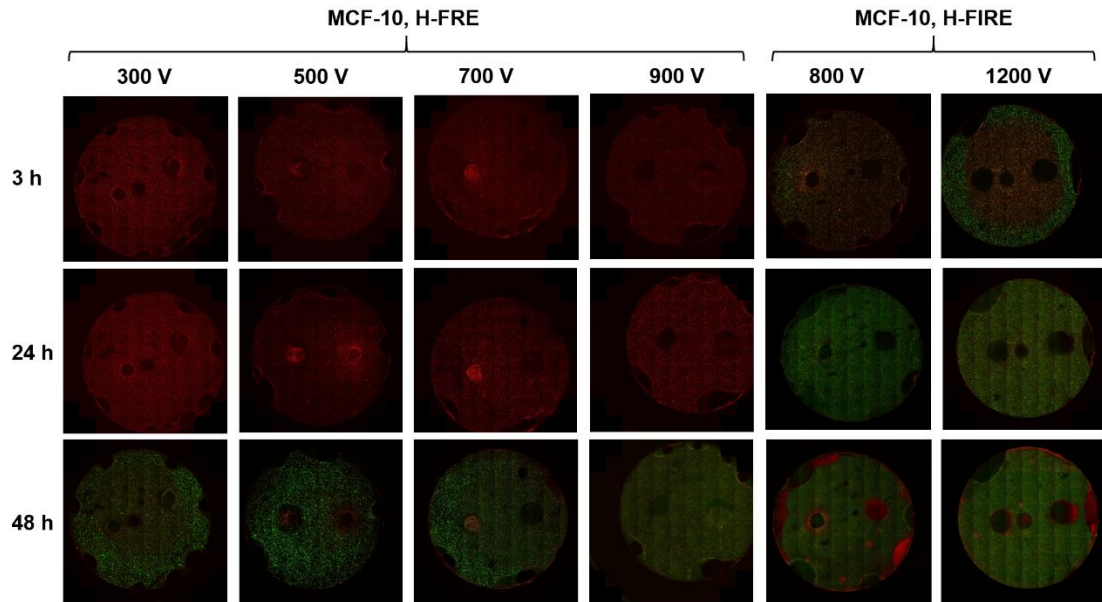


Figure 35. High-frequency reversible electroporation (H-FRE) and High-frequency irreversible electroporation (H-FIRE) of non-malignant breast cells (MCF-10A) in three timepoints (3 h, 24 h, and 48 h).

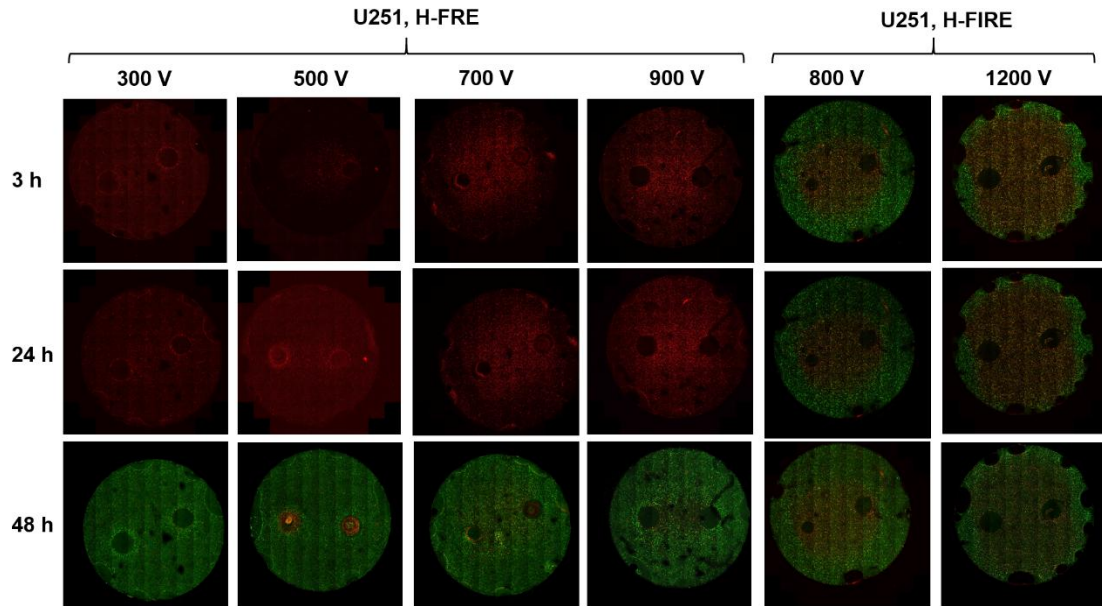


Figure 36. High-frequency reversible electroporation (H-FRE) and High-frequency irreversible electroporation (H-FIRE) of glioblastoma cells (U251) in three timepoints (3 h, 24 h, and 48 h).

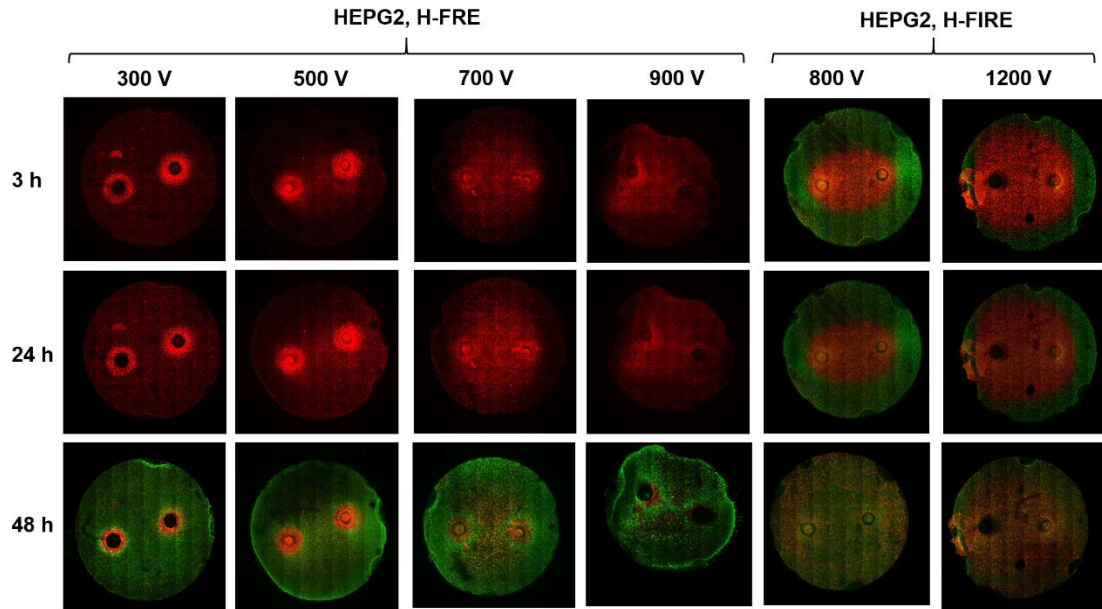


Figure 37. High-frequency reversible electroporation (H-FRE) and High-frequency irreversible electroporation (H-FIRE) of hepatocellular carcinoma cells (HEPG2) in three timepoints (3 h, 24 h, and 48 h).

7. DISCUSSION

Invasive ductal carcinomas as target tumors for electroporation-based therapies

IDC is the most frequent histologic subtype of primary breast tumors which demands new minimally invasive and conservative treatment therapies [Masson Doyma México S. A., 2015]. ECT has been an effective palliative treatment of tumors including: cutaneous tumors from breast cancer, chest wall recurrences of breast cancer [Campana L.G et al., 2014, Wichtowski M, 2017, Matthiessen L. W. 2012], and breast cancer metastases to the skin and subcutaneous tissues showing encouraging outcomes [Campana L.G et al., 2014; Wichtowski M, 2016; Kalavathy G, 2015; Sersa G, 2012; Schmidt, 2014]. In addition, ECT is currently investigated for its use in the treatment of internal tumors [Miklavcic D. et al., 2012; Edhemovic I, et al., 2014; Cadossi, R. et al., 2014; Granata V. et al., 2015; Biancchi G. et al., 2016]. To our best knowledge, there are only 2 works that address the treatment of primary breast cancer with ECT, that is, (1) an infiltrative lobular carcinoma in a single elderly patient, inoperable for neoplastic infiltration of the chest wall and undergoing preoperative (attempt of cytoreduction) and intraoperative ECT prior to radical mastectomy [Cabula C. 2012] and (2) a single clinical case of unifocal ductal breast cancer that reports reduced efficacy of the ECT treatment with 5 needle electrodes [Denzi A. et al., 2015]. Both studies performed ECT through Cliniporator (IGEA SpA, Carpi, Italy) and operating standard procedures for Electrochemotherapy [Campana L.G et al., 2014, Wichtowski M, 2017]. The treatment of breast cancer has also been addressed by IRE. Investigation on this issue has been carried out *in vitro* in order to establish a baseline estimate of electric field necessary for IRE treatment of breast carcinomas, and *in vivo*, in animal models comprising nude mice [Neal R. E. et al., 2010] and rabbits [Zhang W. et al., 2017]. The results reported in these works suggest that IRE may be a promising approach for patients with breast cancer who are not eligible for surgical excision. Based on this encouraging background of

electroporation of breast tumors, this thesis was aimed to the evaluation of ECT as a potential minimally invasive treatment for IDC. In addition, complementary investigation on the effects of IRE and high frequency electroporation on IDC was conducted in order to determine the most suitable electroporation-based treatment for a particular breast histology. For this to be accomplished, the methods were validated *in silico* and *in vitro* only, since electroporation-based therapies are not yet accepted *in vivo* in America. On the one hand, the results obtained *in silico* showed that electroporation of breast tumors may be a challenging process which require high-voltage values to achieve an efficient treatment. Nonetheless, breast tumors in the range of 1 to 5 cm³ resulted to be computationally eligible for complete coverage with: ECT and a one of two suitable needle-electrode arrays with 4 and 6 needles respectively. It is worth noting that usually, IDC targets are up to 2 cm in diameter which are therefore expected to be completely covered based on the *in silico* outcomes. Moreover, the electrode with only 4 needles represents a less invasive alternative than the 5-needle commercial electrode used in Denzi et al., (2015). On the other hand, the results obtained *in vitro* verified the demanding nature for permeabilizing and ablating malignant and non-malignant breast tissues.

Realistic computational breast models

Current ECT and IRE planning of many internal tumors (brain, liver, bone, etc.) is carried out in realistic computational models [Miklavcic D, 2012, Miklavcic, D. et al., 2014, Jourabchi N, 2014]. However, little literature regarding the modelling of deep-seated breast tumors is currently available since this type of malignancies have not been intensively investigated [Agoramurthy P. et al., 2011, Neal R. E, and Davalos R. V. 2009].

The first breast models used for the evaluation of an optimal electrode array for the treatment of deep-seated breast tumors with ECT consisted of ideal spherical tissues. The results in these models showed that the needle-electrode array in a delta configuration (4 needles) represents an effective

minimal invasive scenario due to the reduced number of needles. However, the required voltage and electric current for the coverage of this small tumor model (10 mm) are higher than the diamond (5 needles) and the star (6 needles) electrode arrays. For the diamond (5 needles) and star (6 needles) electrode configurations, a complete coverage was observed by activating the C-P electrode pairs only, i. e., the pairs of electrodes formed by the needles outside the tumor and inside the safety margin may remain inactive. Oppositely, the activation of needles inserted into the safety margin only (diamond configuration, 4 needles), and no electrode into the tumor, leads to a higher demand of voltage and consequently to the highest electric current required for the complete coverage of the target tissue volume which makes this electrode-array the least effective.

Interestingly, the results obtained in the realistic breast models agreed with the ones obtained in the ideal spherical models regarding delta and star configuration which caused an effective target coverage. Similarly, a diamond array (4 needles without intratumoral needle) was the least efficient configuration, but only for the case of big tumors, as for the case of a small tumor this configuration was the most efficient. Consequently, spherical models provided a good initial approach for determining potential effective needle-electrode arrays for ECT of breast tumors, and a guideline to further electroporation modeling of realistic breast tumors along with a safety margin tissue. Nevertheless, as it was expected, the voltage protocols and electric current requirements remarkably differed between spherical-tissue models and patient-specific realistic breast models in which the shapes of the target tissues are completely different to a sphere. In addition, non-homogeneity of breast was not assumed in the spherical models and hence, electric field distribution in realistic computational phantoms containing fatty tissue, fibroglandular breast tissue, skin and neoplastic tissue, led to discrepancies between the outcomes obtained in both models.

The breast models presented in this thesis provide a more realistic computational model for ECT planning than the models reported so far. However, their improvement may be implemented: development of MRI-based breast models seem to be not recommendable since detection and/or treatment of breast cancer by MRI imaging is not affordable, on the contrary, investigation on the reconstruction of DBT images is strongly encouraged, so that more accurate breast models can be obtained, since the breast models presented in this work consisted of interpolations of data in the DBT images in order to deal with the tissue compression issue.

Needle-electrode arrays for ECT of deep-seated targets

Long-needle electrode arrays have been described and used for the treatment of deep-seated tumors [Miklavcic, D. et al., 2014] with ECT and IRE. This thesis researched whether IDC may be efficiently treated with ECT by using a universal electrode array to assure the electroporation of the entire target volume [Zupanic, 2012]. Consequently, 12 electrode arrays with 3 different needle-spacing, and 4 geometric configurations (delta, diamond, and star) with 4, 5, and 6 needles per configuration were tested *in silico*, in realistic three-dimensional breast models. The results showed that the adequate electrode array to be used for ECT of IDC depends on the anatomical properties of the tissues of interest, that is, tumor size, breast density, and dielectric properties. The 12 electrodes were evaluated in realistic breast computational models of three patients, representative of clinical cases as described in section 5.2.6. The results showed that the treatment of a small tumor, for the case of the first patient, through an electrode with 4 needles in a diamond array (4Di1, set 1) and the activation of the peripheral needles only, was enough to cover the whole tissues of interest. In addition, delta and star configuration (4De2 and 6St2) in the electrode set 2 (enlarged version of set 1) resulted in effective target coverage. It is worth noting that as the tumors become bigger, as for the cases for the second and third patient, this electrode array (4Di1, set 1) was the least efficient configuration, since none of the tissues of interest got

completely covered. In turn, efficient protocols for the second patient were obtained with larger arrays in set 2 (6St2 and 4De2) and set 3 (4De3 and 6St3). It was observed that the use of an electrode array following a geometry of a tumor-specific safety margin which was selected based on the tumor dimensions (ideally elliptic for the tumor in patient 2) resulted in optimal outcomes. Finally, effective coverage of the target lesion in the third patient was obtained with electrode arrays in set 2 (6St2, 5Di2, 4De2). Contrary to the results obtained for patient 1 with the array 4Di1, 4-needle diamond configuration in any of the sets, that is, 4Di1, 4Di2, and 4Di3, resulted in the least effective arrays for the treatment of large target lesions even if the voltage was increased to the maximum value (3000 V) provided by current electroporation systems. Noticeably, an enlarged version of the original electrode set used in patient 1, was the most appropriate set of electrodes for both patients 2 and 3 and a good alternative for patient 1 also. It is worthy to mention that for big tumors such as those in patients 2 and 3, a complete coverage of target tissues was harder to obtain if compared to the coverage of small tumors, but efficient coverage is possible to achieve.

Patient-specific treatment planning for ECT of IDC

There are two articles addressing the treatment of primary breast cancer with ECT tumors, which in both cases can be reached by commercial electroporators and electrodes [Cabula C, 2012; Denzi A. et al., 2015]. However, this work researched the feasibility of using electrochemotherapy for the treatment of IDC in realistic breast models based on digital breast tomosynthesis (DBT) images with a universal electrode array to assure the electroporation of the entire target volume. In addition to the tumor treatment, eradication of some surrounding tumor tissue is desirable, since tumor cells that have an infiltrative-like histological type spread diffusely throughout the healthy tissue.

In order to establish a patient-specific treatment planning for electrochemotherapy *in vivo* of invasive ductal carcinoma, the acquisition of medical images possessing correct resolution is crucial to carry out an adequate segmentation of them. If clinical condition of patients allows it, a manual segmentation is recommended because guidance of a physician interpretation from the different slices constituting a sample is strongly suggested to locate the right region of interest.

A key factor for the treatment planning is establishing the appropriate conductivity of the tissues of interest and the consideration of its electric field dependent nature in an electroporation phenomenon. The dielectric property ratios of tissues considered in the three patients presented in section 5.2.4 were considerable ($\sigma_{tumor}/\sigma_{breast\ tissue}=5$, $\sigma_{tumor}/\sigma_{fatty\ tissue}=17$), which made electroporation a challenging process that required high-voltage values to achieve an efficient treatment. However, the complete coverage of target tissues with three strategic needle-electrode configurations, an optimized sequential model of electroporation based on the use of COMSOL Multiphysics linked with LiveLink™ for Matlab and visualization tools reported by Zupanic et al., 2012, strongly encourage the use of ECT in deep-seated breast tumors.

Future acceptance of electrochemotherapy into medical practice as a first-line treatment of primary deep-seated breast tumors and possible replacement of conventional neoadjuvant chemotherapy and surgical procedures shall depend on advantages, drawbacks, and limitations of this procedure. Advantages include the reduction in antineoplastic drug dosage, local therapy administration instead of a systemic route, and hence the reduction in adverse effect of conventional chemotherapy (myelosuppression), potential displacement of neoadjuvant chemotherapy and/or radical mastectomy, the treatment enhancement of triple negative lesions for which hormone therapy, and the use of drugs that target estrogen, progesterone, and HER-2 receptors are ineffective, an apoptotic process would be induced in the major part of the target tissues contributing to a beneficial immune response. On the other

hand, if multiple ECT sessions are required and an inflammatory response associated with necrosis found in irreversibly electroporated regions may provoke drug resistance because of the activation of multiple drug resistance pumps due to low-drug concentration, which may represent a drawback for the treatment. Some limitations to address include: determining patient-specific breast dielectric properties is crucial in order to accurately model electroporation of target tissues. Moreover, accomplishing of image-guided electrode positioning according to the treatment planning, and developing and manufacturing a suitable hardware and the electrode arrays that provide enough energy to deliver the electric protocol determined by the treatment planning is imperative.

Reversible electroporation *in vitro*

In order to validate the results obtained *in silico* for the treatment of IDC with ECT, experimental breast media were used to investigate the effects of electroporation (reversible, irreversible and high frequency electroporation) *in vitro*. For this purpose, experiments were performed in four breast cell lines; a TNBC cell line BT-20, a Her2/neu cell line HCC1419, MCF-7 expressing hormonal receptors, and a non-tumoral mammary gland cell line, MCF-10A. Three cell culture platforms were tested sequentially in order to evolve towards a more realistic breast model. That is, cell suspensions were used as a first model for experimental reversible electroporation. Afterwards, it was replaced with a model for electroporation of adhered cells which was more related to a tissue scenario since it avoided false permeabilization signals shown in suspended cells. Adhered cells model facilitated permeabilization while demanding much lower ITV; hence, it provides a more realistic model for *in vivo* conditions as reported by Duval et al. and Pehlivanova et al. (Duval et al., 2017, Pehlivanova et al., 2012). This platform may therefore represent a reliable means for establishing cell-specific electroporation potentials while addressing reported necessities (Delgado-Canedo et al., 2006, Dovgan et al.,

2017, Larkin et al., 2007, Markelc et al., 2018, Miklavcic et al., 2014, Miklavcic et al., 2000, Sersa and Miklavcic, 2008, Zhao et al., 2018). Finally, three-dimensional cell cultures (hydrogels) were used as mimics for breast tumors for the evaluation of the effects of irreversible electroporation and high frequency reversible and irreversible electroporation in addition to reversible electroporation for ECT.

Cell-specific electroporation protocols were established in suspended and adhered cells, which allowed us to establish reversible electroporation thresholds ranging from 250 V/cm to 625 V/cm for cells in suspension, and 228 V/cm to 622 V/cm for adhered cells. It can be noticed that the lowest limit in both electric field thresholds are lower than the reported reversible electroporation threshold, i. e., 400 V/cm *in vitro*, but the irreversible electroporation thresholds are in agreement with the literature (Kranjc and Miklavčič, 2017, Miklavcic et al., 2010). Interestingly, a reversible electroporation threshold of 207 V/cm was obtained for breast cancer hydrogels which is similar to the threshold obtained for suspended cells. Opposite to cancer-cells hydrogels, non-malignant (MCF-10) hydrogels were hard to electroporate even with the highest voltages tested, This fact supports that electroporation thresholds need to be tuned depending on the target tissue histology in order to observe an efficient electroporation phenomenon, as suggested by Miklavcic and Zhao (Miklavcic et al., 2014, Zhao et al., 2018).

MCF-7 cells in suspension were the most difficult to be permeabilized; they demanded the highest voltage for breast cell lines while undergoing a poor permeabilization, as demonstrated by a weak PI uptake and a high cell viability after electroporation. On the contrary, PI uptake was remarkably increased when adhered. The optimal permeabilization voltage for both models, is in agreement with the simulations for reversible electroporation. Similarly, MCF-7 three-dimensional cell cultures were harder to permeabilize than brain or hepatic hydrogels, demanding the highest voltage among cancerous hydrogels which is in accordance with the scenario observed for MCF-7 suspended and

adhered cells. The high voltage and the high cell viability obtained for these cells highlight the difficulty for the treatment of metastatic origin tumors for which hormonal therapy is nowadays a conventional treatment (Coates et al., 2015, Loibl et al., 2015). Based on these results, ECT might potentiate a systemic therapy efficacy along with a hormonal therapy while reducing its side effects (Miklavcic et al., 2014).

Conversely, BT-20 and HCC1419 cells were easier to permeabilize with lower voltages which were numerically not expected to cause cell permeabilization. Opposite to MCF-7 cells, BT-20 and HCC1419 cells required slightly higher voltage while adhered to a substrate rather than in suspension, and they responded to a narrow low voltage range in both cell-culture platforms. Consequently, TNBC tumors might be successfully subjected to electroporation as a potential treatment alternative, addressing thus the current lack of targeted treatments for this histological type (Coates et al., 2015). Particularly, based on the low cell viability obtained for this cell line in both cell-culture platforms, IRE might be an easier and more effective treatment rather than ECT since cell ablation could be reached without the use of a drug.

HCC1419 cells were easily permeabilized with the lowest voltage in both cell-culture platforms while resulting in a high cell viability. Since these cells are HER-2/neu representative, ECT might be efficiently used as an neoadjuvant therapy before a targeted treatment with trastuzumab (Loibl et al., 2015, Matthiessen et al., 2012). This may result in the complete eradication of remaining neoplastic cells regardless of the presence of other types of receptors that can be found in vivo; avoiding, therefore, the use of additional targeted therapies which are detrimental for patients (Grischke et al., 2017).

Opposite to cancerous cells, non-malignant breast cells MCF-10A were permeabilized with the highest voltage among all cell lines. The high cell viability that these cells exhibit in all monitored timepoints confirm that mostly all cells in these hydrogels remain viable and undamaged after electroporation. Some evidence of cell damage was found in the vicinity of the electrode-

insertion points. This may be attributed to two main factors: irreversible electroporation which is characteristic around the electrodes and/or mechanical damage due the insertion of the needles. These finding demonstrate that healthy breast tissue in a safety margin will be harder to treat with ECT that tumoral tissue.

Breast ECT *in vitro* with Paclitaxel

ECT was performed *in vitro* in adhered MCF-7 and BT-20 cells, with Paclitaxel rather than Bleomycin since the former is commonly used in the treatment of breast tumors. On the one hand, the effect of Paclitaxel was remarkably enhanced with electroporation compared to the use of Paclitaxel alone. This fact supports our statement suggesting that ECT applied *in vivo*, might potentiate a systemic therapy efficacy along with a hormonal therapy while reducing its side effects. On the other hand, the effect of Paclitaxel in BT-20 cells was less evident which supports our hypothesis that IRE might represent a better treatment alternative for TNBC, rather than ECT since cell ablation could be performed without any chemotherapeutic drug. Further experimental evaluation of ECT in HCC1419 and non-malignant MCF-10A adhered cells will be helpful to determine whether Paclitaxel effect on them may be enhanced with ECT.

Impact of cell morphology in electroporation of breast cells

The evaluation of MCF-7 cell morphology leads us to suggest that their thick membrane and their particular actin distribution might explain its particular demand of the highest voltage among neoplastic breast cells to be permeabilized. Hormonal receptors (ER/PR) in MCF-7 cells may contribute to the heterogeneity found in their membrane thickness, which was, at the same time, the thickest of all the mammary membranes handled in this work. Their

high actin reorganization which leads to numerous adhesion sites might cause a strong cell-to-substrate adhesion when adhered; consequently, this makes these cells harder to permeabilize when suspended rather than adhered because when adhered, the cells are evenly distributed along the electrode surface.

Conversely, BT-20 cells which are representative of TNBC tumors, possess a homogeneous thin cell membrane, but a very heterogeneous morphology. Although they were the biggest cells, they responded to a narrow low voltage range in both cell-culture platforms. They showed a low actin distribution and a high cytoplasmic content, which along with their thin membrane, may turn these cells more conductive and consequently more responsive to low voltages.

In turn, HCC1419 cells were the smallest cells with the thinnest cell membrane of all cancerous breast cell lines. They were homogeneous in terms of morphology and cell membrane thickness. Most probably their homogeneous thin membrane and conventional actin distribution allow them to be easily permeabilized with the lowest voltage in both cell-culture platforms while resulting in a high cell viability. When adhered, these cells exhibit a shape close to a sphere and hence, ITV analytical and numerical values resulted to be almost equal.

Further morphology analysis of non-malignant breast cells MCF-10A is encouraged, so that it might be useful to explain their high voltage demand in order to be permeabilized with electroporation.

Disturbances in the cell membrane

The methodology used for electroporation of adhered cells was used to visualize regions in the cell membrane of TNBC cells after the application of reversible electroporation through SEM. A x10,000 magnification showed noticeable visual differences between an electroporated and a non-

electroporated cell membrane. We referred to these visual differences as “mechanical disturbances” in the cell membrane that may represent an evidence of pore formation due to electroporation. However, the methodology followed to obtain these results is different to the one described by Spugnini et al., (2007), and therefore, further replication of these SEM analysis in the rest of the breast cell lines is mandatory in order to determine whether the disturbances found may be considered as pores in the cell membrane.

IRE of breast-cancer hydrogels

Regarding the treatment of breast malignancies with IRE, only a preclinical study has been reported, in which breast cancer tumors (MDA-MB231) were implanted in female Nu/Nu mice. Tumor regression was observed in five out of seven tumors. These outcomes suggest that IRE could be an advantageous alternative to surgical resection for breast conserving therapy [Jourabchi N, 2014]. The results presented in this thesis, regarding the application of IRE in breast-cancer hydrogels are part of an investigation additional to the objectives established for this work. Interestingly, breast cells (MCF-7) were harder to ablate compared to the other cancerous-cells hydrogels, showing a smaller ablation surface than brain cells (U251) and comparable results with hepatocellular cells (HEPG2). Similarly, non-cancerous breast hydrogels (MCF-10A) showed the smallest ablation surface among the four cell lines. These outcomes support that treating metastatic primary tumors either with reversible or irreversible electroporation may a challenging, but feasible process. Moreover, they provide evidence of the difficulty for treating healthy breast tissue with irreversible electroporation.

High frequency electroporation of of breast-cancer hydrogels

A pilot study consisting of a single replicate of high-frequency reversible (H-FRE) and irreversible (H-FIRE) electroporation of hydrogels was performed in

two breast cell lines and the outcomes were contrasted with the outcomes obtained in other two non-breast cell lines. It was found that H-FRE cause a more uniform permeabilization shape along the hydrogel, compared to the permeabilization regions observed in reversibly electroporated hydrogels. In addition, a high cell viability was observed during the last timepoint. These facts lead us to suggest that H-FRE may be a better treatment alternative for the treatment of metastatic breast tumors and the surrounding healthy tissue in the safety margin than traditional ECT. Oppositely, breast hydrogels exposed to H-FIRE resulted in comparable ablation regions for 800 V and 1200 V pulses three hours after treatment, but the ablation size remarkably decreases with time. This fact supports that breast cells are difficult to eradicate, and that they might even repopulate a treated zone. In order to avoid this repopulation, a thorough planning of treatment of breast tumors with H-FIRE is required. In general, the outcomes obtained in this pilot study, emphasizes the challenging process of treating breast tissues with electroporation either reversible, or irreversible.

8. PERSPECTIVES

The main perspective of this thesis is to achieve the acceptance of ECT for the treatment of breast cancer in the clinical practice in Mexico. The work developed regarding the patient-specific treatment planning *in silico*, based on DBT-image analysis along with the experimental work *in vitro*, provide evidence of the efficacy that ECT may exert on the treatment of breast cancer, and strongly encourage continuing the investigation on this topic in many aspects:

1. The methodology for developing a patient-specific treatment planning has to be validated for it to be accepted as a clinical routine procedure in the future, as reported by Pavliha D. et al., (2012). Therefore, expertise in the segmentation of breast target tissues on DBT images and the validation of these segmented tissues by an oncologist is highly recommended. Additionally, the determination of patient-specific breast dielectric properties, and an enhanced methodology for three-dimensional reconstruction of breast target tissues from DBT-imaging is required, so that the assignment of a computational breast phantom to every patient is not needed, and more realistic and accurate patient-specific breast models are obtained.
2. Whether MRI is the imaging tool for breast malignancies and financial resources are available, the software “Mimics (Materialise’s Interactive Medical Image Control System) Innovation Suite” is suggested in order to generate better anatomical three-dimensional models of breast tumors and surrounding tissue which can be adequately handled with CAD objects, such as cylindrical stainless-steel needles, since this software is aimed to the processing of high-resolution 2D cross-sectional medical images. Mimics provides a Finite Element Analysis (FEA) module which allows optimization of triangle meshes to prepare further analysis using FEA (Mimics Student Edition Course Book, s.f.).

3. The development and implementation of an electroporation device, which deliver enough energy (3000 V, 50 A) determined by the treatment planning for the application of ECT *in vivo*, is strongly recommended. It is worthy to mention that this type of device must be standardized and accepted by the COFEPRIS before it can be accepted in a clinical scenario, which can demand considerable time. An alternative, but expensive option is to acquire a FDA approved, commercial electroporation device for *in vivo* applications of ECT manufactured by IGEA S.p.a.
4. The evaluation of the effects of Paclitaxel in reversibly electroporated HCC1419 adhered cells is required to compare the results obtained so far with MCF-7 and BT-20 cells, and to verify whether ECT is efficient in the treatment of Her-2/Neu tumors.
5. A morphological study of MCF-10A cells is recommended in order to elucidate structural properties that can explain their high voltage demand to be either reversibly permeabilized or ablated.
6. Further experiments regarding reversible electroporation in hydrogels seeded with BT-20 and HCC1419 cells would be helpful to verify that IRE is a good option for TNBC tumors, and that ECT is a better option for Her-2/Neu tumors, as observed in two-dimensional cell cultures of these cells.
7. The development of hybrid three-dimensional cell cultures (hydrogel) which include a mimic for breast tumors (MCF-7, BT-20 and HCC1419 cells), and a mimic of surrounding healthy tissue (MCF-10A cells) would provide an excellent means for performing electroporation of breast target tissues more related to *in vivo* scenarios. They might be used for further investigation of reversible and irreversible electroporation applications.
8. The manufacturing of the three most effective needle-electrode arrays 4De2, 5Di2, and 6St2 is highly suggested, in order to experimentally validate their efficiency *in vitro*. A strongly recommended experiment is

to verify these electrodes specifically in the hybrid hydrogels described in the previous point.

9. A comparison between the most effective electrode arrays (4De2, 5Di2, and 6St2) and the commercial hexagonal electrode array with a central needle, manufactured by IGEA S.p.a (Carpi, Italy), would be useful in order to determine whether the number of needles may be reduced without jeopardizing the effectiveness of the treatment.
10. Further investigation about the use of IRE in the treatment of TNBC representative hydrogels is highly recommended in order to compare the results obtained in adhered BT-20 cells. It would be also worthy to perform IRE in HCC1419 hydrogels in order to confirm that reversible electroporation is a better option than IRE.
11. Additional experimental replication of H-FRE and H-FIRE in breast tumor hydrogels are remarkably encouraged since the results obtained in the pilot study indicated promising outcomes in the treatment of breast malignancies.
12. Intensive further research on the analysis of SEM images of electroporated breast cell membranes is encouraged in order to determine whether the visual modifications observed in this thesis correspond to actual pores.

9. CONCLUSIONS

In general, the outcomes obtained in this thesis exhibit the demanding process that treatment of breast cancer involves, computationally and technologically, Nonetheless, promising results obtained *in silico*, and verified *in vitro*, strongly encourage the use of electroporation-based therapies for the treatment of IDC.

The investigation in this thesis was mainly focused in the evaluation of ECT as a potential minimally invasive treatment for IDC. For this purpose, realistic breast models based on processing of DBT images are remarkably preferred over ideal simple models since they show discrepancies with realistic models that can lead to inaccuracies in the planning of ECT, resulting therefore in non-efficient outcomes. In addition, the design of new needle-electrode arrays configuration and a methodology for a patient-specific treatment for ECT of IDC were developed. Based on the results presented in section 6.3, a single electrode array seems unlikely to treat effectively all breast ductal carcinomas with ECT, but a group of 3 fixed electrode arrays (4De2, 5Di2, and 6St2) may be sufficient to cover invasive breast ductal carcinomas in the range of 1 to 5 cm³ with ECT. Regarding the electrode-manufacturing issue, our results indicate that producing 2 electrode arrays (4De2 and 6St2) would be enough to treat invasive breast ductal carcinoma. This reduces meaningfully the complexity of manufacturing and device certification processes. Although a complete coverage of target tissues in large tumors, as it was the case for patients 2 and 3, was difficult to achieve *in silico*, it should be considered that these tumor dimensions are representative of most of the current stages detected in Mexican patients with breast cancer. These outcomes could probably be extrapolated to any population with an effective response to the treatment; however, its effectiveness may be potentiated if the disease is detected at an early stage.

Particularly, experimental ECT with Paclitaxel was determined to be a promising treatment alternative for metastatic origin tumors. This adjuvant procedure,

along with a hormonal therapy, can remarkably reduce the unwanted side effects that systemic chemotherapy cause, such as high toxicity and myelosuppression. However, this type of tumors may require higher voltage pulses than the required for permeabilization of other breast cancer tumors. This high-voltage demand is attributed to their thick membrane and their particular actin distribution.

Similarly, Her-2/neu tumors may be effectively treated with ECT as a neoadjuvant therapy before the target tumor is treated with trastuzumab. Neoadjuvant ECT in these tumors, may eradicate the remaining malignant cells regardless of the presence of other types of receptors that can be found in vivo; avoiding, therefore, the use of additional targeted therapies which are detrimental for patients. However, the particular efficacy of Paclitaxel is yet to be determined. Contrary to metastatic tumors, Her-2/neu malignancies may be permeabilized with lower voltages. This trait is associated with their small size, their homogeneous thin cell membrane, and their conventional actin distribution.

Oppositely to metastatic and Her-2/neu tumors, TNBC seem to be eligible for their eradication with IRE, since noticeable low cell viability is obtained with a narrow low voltage range. There is a current lack of target treatments for TNBC tumors, and hence IRE may represent an effective treatment alternative. Although their cell size is the largest of the three types of malignant cells (MCF-7, HCC1419 and BT-20) their sensitivity to low voltages is attributed to their homogeneous thin cell membrane, low actin distribution and a high cytoplasmic content, which may turn these cells more conductive and consequently more responsive to low voltages.

Non-malignant breast cells in the target safety margin are expected to be the hardest cells to eradicate with electroporation, either reversible or irreversible. That is, healthy tissue may be treated with both ECT, or IRE. In both cases, very high voltage will be required. Therefore, IRE may represent a better alternative than ECT, since IRE requires no additional chemotherapeutic drug.

The use of realistic computational models for ECT planning *in silico*, and hydrogels as mimics of breast malignancies provided a powerful tool to validate this investigation. Consequently, further investigation on treatment planning of IDC must be based in realistic models, and experimental validation should be based on the use of hybrid hydrogels containing malignant and non-malignant breast cells in order to better mimic *in vivo* environments.

On the other hand, investigation on the use of H-FRE and H-FIRE for treating breast malignancies should be further explored since the outcomes obtained in metastatic malignant cells and healthy breast cells show that permeabilization region with H-FRE is larger and more homogeneous than the one obtained with traditional reversible electroporation. On the contrary, H-FIRE seems to be non-efficient for breast tissues, malignant or not, since a repopulation of apparently ablated region with viable cells was observed. A limitation for this issue is that there are no high-frequency electroporation devices available in Mexico, and hence, such a device should be either manufactured or purchased.

The comparison of SEM images of electroporated and non-electroporated breast cancer cells exhibited visual differences between them. Electroporated membranes showed clusters of tiny holes which in some regions conform a larger fissure. These visual disturbances were observed *in situ* in electroporated cell membranes after electroporation of samples exposed to the most effective electroporation protocol. We attribute these disturbances to pore formation due to electroporation which represent an important contribution on the investigation of the electroporation phenomenon since no evidence (scientifically accepted) of pore formation is available so far. Therefore, further investigation on this issue is mandatory in order to confirm whether these disturbances can be considered as real pores in the cell membrane.

We imply that it is possible that in future electroporation-based therapies may displace conventional chemotherapy and/or surgery in the treatment of breast cancer and probably be considered as a first-line treatment of primary tumors.

Nevertheless, enrollment of patients and experimental application of the methods presented in this work conducting a clinical trial will be required to validate this hypothesis.

10. PRODUCTIVITY

Different parts of the work described in this dissertation were presented/submitted in/to international conferences and JCR journals. In addition, three research stays abroad were carried out. All of them are described in this section and included in appendixes C to L.

PUBLICATIONS

JCR Journals:

1. A. L. Vera-Tizatl, C. E. Vera-Tizatl, A. Vera-Hernández, L. Leija-Salas, S. Rodríguez Cuevas, B. Kos, D. Miklavčič, “**Computational Feasibility Analysis of Electrochemotherapy with Novel Needle-Electrode Arrays for the Treatment of Invasive Breast Ductal Carcinoma**”, *Technology in Cancer Research and Treatment*, Volume 17, August 2018. doi.org/10.1177/1533033818794939.
2. C. E. Vera-Tizatl, P. Talamás Rohana, A. Vera-Hernández, L. Leija-Salas, S. Rodríguez Cuevas, B. Chávez Munguía, A. L. Vera-Tizatl, “Cell Morphology Impact on the Set-up of Electroporation Protocols for In-suspension and Adhered Breast Cancer Cells”, Under review.
3. A. L. Vera-Tizatl, R. V. Davalos, C. E. Vera-Tizatl, A. Vera-Hernández, L. Leija-Salas Evaluation of the effects of reversible electroporation, irreversible electroporation, and high frequency electroporation in hydrogels mimicking breast carcinomas.

International Conferences:

1. A. L. Vera Tizatl, S. Rodríguez Cuevas, L. Leija Salas and A. Vera Hernández. “**Review of Electrochemotherapy-based Treatment of Cutaneous, Subcutaneous and Deep-seated Tumors towards**

Specific Treatment Planning", 2016 GLOBAL MEDICAL ENGINEERING PHYSICS EXCHANGES/PAN AMERICAN HEALTH CARE EXCHANGES (GMEPE / PAHCE). 4-9 /04/ 2016. Spain.

2. A. L. Vera Tizatl, C. A. Ramírez Martínez, C. E. Vera Tizatl, M. I. Gutiérrez Velasco, S. Rodríguez Cuevas, L. Leija Salas and A. Vera Hernández. **"Electric Field Distribution in an Anatomical Model with the Finite Element Method based on the 3D Reconstruction of a Breast Carcinoma"**, 13th International Conference on Electrical Engineering, Computing Science and Automatic Control (CCE). 26-30/09/2016. Mexico City.
3. A. L. Vera Tizatl, C. A. Ramírez Martínez, C. E. Vera Tizatl, M. I. Gutiérrez Velasco, S. Rodríguez Cuevas, L. Leija Salas and A. Vera Hernández. **"Simulation of Electric Filed and Joule heating distribution in breast tumor"**, 13th International Conference on Electrical Engineering, Computing Science and Automatic Control (CCE). 26-30/09/2016. Mexico City.
4. A. L. Vera-Tizatl, C. A. Ramírez-Martínez, A. Vera-Hernández, L. Leija-Salas, S. A. Rodríguez-Cuevas, P. R. Hernández-Rodríguez, **"Electric Field Distribution Generated by Two Needle Electrodes in an Anatomical Model of a Deep-Seated Breast Carcinoma"**, presented at the Electroporation Based Technologies and Treatments (EBTT), International Scientific Workshop and postgraduate course, Ljubljana, Slovenia 2016.
5. A. L. Vera-Tizatl, B. Kos, D. Miklavčič, A. Vera-Hernández, L. Leija-Salas, C. E. Vera Tizatl, S. A. Rodriguez Cuevas, **"Investigation of numerical models for planning of electrochemotherapy treatments of invasive ductal carcinoma"**, presented at the GLOBAL MEDICAL

ENGINEERING PHYSICS EXCHANGES/PAN AMERICAN HEALTH CARE EXCHANGES (GMEPE / PAHCE), 20-25/03/2017, Chiapas, Mexico.

6. A. L. Vera-Tizatl, A. Vera-Hernández, L. Leija-Salas, B. Kos, D. Miklavčič. **“Comparison of different electrode arrays for treatment of breast tumors with electrochemotherapy”**, presented at the 26th International Electrotechnical and Computer Science Conference (ERK), 25, 26/09/2017, Portorož, Slovenia.
7. C. E. Vera-Tizatl, A. L. Vera-Tizatl, J. C. Osorio Trujillo, P. Talamás Rohana, A. Vera-Hernández, L. Leija-Salas, S. Rodríguez Cuevas. **“Establishment of Electroporation Protocols in BT-20 and SKOV-3 Cell Lines based on Finite Element Modeling”**, 15th International Conference on Electrical Engineering, Computing Science and Automatic Control (CCE). 05-07/09/2018. Mexico City.
8. C. E. Vera-Tizatl, A. L. Vera-Tizatl, P. Talamás Rohana, A. Vera-Hernández, S. Rodríguez Cuevas. **“Pilot study of Paclitaxel Enhancement with Electrochemotherapy for Breast Cancer Treatment”**, presented at the Electroporation Based Technologies and Treatments (EBTT), International Scientific Workshop and postgraduate course, Ljubljana, Slovenia 2019.

RESEARCH INTERNSHIPS ABROAD

2016 **University of Lorraine (UL), Center of Research in Automatics of Nancy (CRAN), Superior National School of Electricity and Mechanics (ENSEM), Nancy, France**

Supervisors: Dr. Didier Wolf – CRAN Principal
Dr. Christian Daul – CRAN – ENSEM - UL

Aim: Presentation of the dissertation work and workflow establishment for a further research stay aimed to the development of breast reconstructed models based on MRI imaging

2016-2017 **University of Ljubljana, Faculty of Electrical Engineering, Slovenia, Laboratory of Biocybernetics, Ljubljana, Slovenia**

Supervisors: Dr. Damijan Miklavčič – Head of the Laboratory of Biocybernetics.
Dr. Bor Kos – Faculty of Electrical Engineering.

Aim: Establishing a treatment planning for the Electrochemotherapy of breast carcinomas.

2018-2019 **Virginia Tech, Department of Biomedical Engineering, Laboratory of Bioelectromechanical Systems (BEMS), Virginia, USA.**

Supervisors: Dr. Rafael. V. Davalos – Head of the BEMS Laboratory

Aim: The establishing of reversible and irreversible electroporation thresholds in hydrogels.

APPENDIX A

High voltage pulse generator

Since in Mexico there are no commercial electroporators approved for its use in electrochemotherapy, the implementation of an electroporation system needs to be developed. An electroporation system requires the construction of a high voltage source. To this purpose, three regulated high voltage DC to DC programmable converters (EMCO H05P) of output voltage ranging from 0 V to 500 V were used. Description of this converter is shown in Fig. A1.

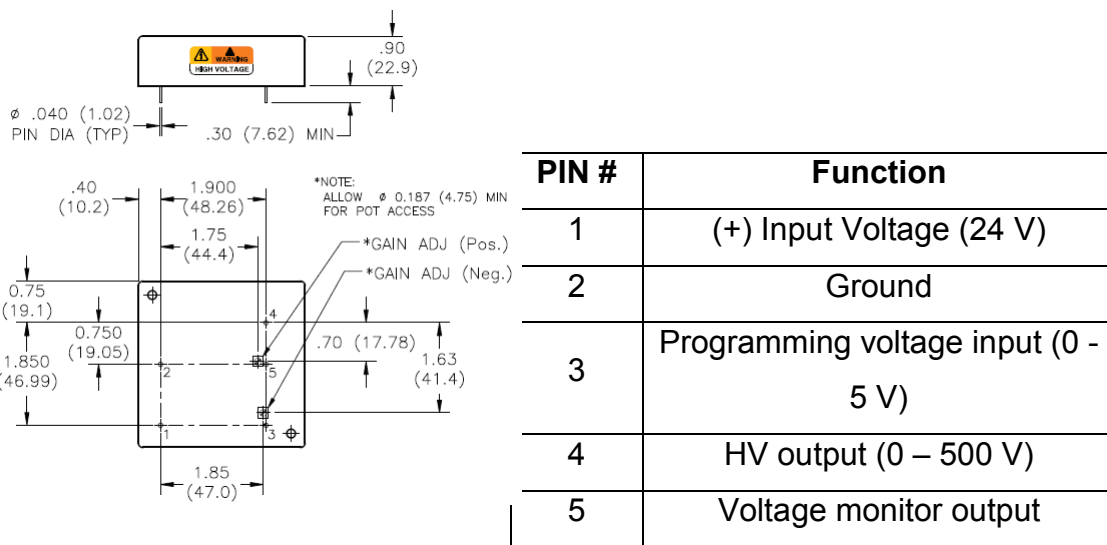


Fig. A1. EMCO high voltage DC to DC programmable converter, model: H05P.

Dimension are in inches (metric equivalent is in parenthesis).

These converters were connected in a serial configuration in order to generate 1500 V. Since more than one high voltage module is handled, Inter-Integrated Circuit (I²C) communication protocol was used to provide variable programming voltage input and hence to control output voltage. I²C communication was mainly chosen to simplify control electronics since it

requires only two communication wires and supports multiple devices on the same bus without additional select signal lines through in-communication device addressing.

To confer appropriate addressing to each one of the three high voltage converters, 8-bit input/output expanders for I²C (PCF8574) were used. To establish the programming voltage input for the high voltage converter, a digital to analog converter (DAC0808) along with an operational amplifier (TL082) were used.

A Texas Instruments microcontroller (MSP430G2552) was programmed in IAR Embedded Workbench as a master to address high voltage converters sequentially. A low-power bidirectional isolator (ISO1540) compatible with I²C interfaces was used to isolate I²C buses for each one of the high voltage DC-DC converters. High voltage source was designed as a modular device. Connection diagram for one of the three modules conforming the high voltage source is shown in Fig. A2.

In addition, the microcontroller was programmed as a PWM to generate pulses. A power MOSFET (2SK225) was used as a power switch to generate high voltage electric pulses as shown in Fig. A3.

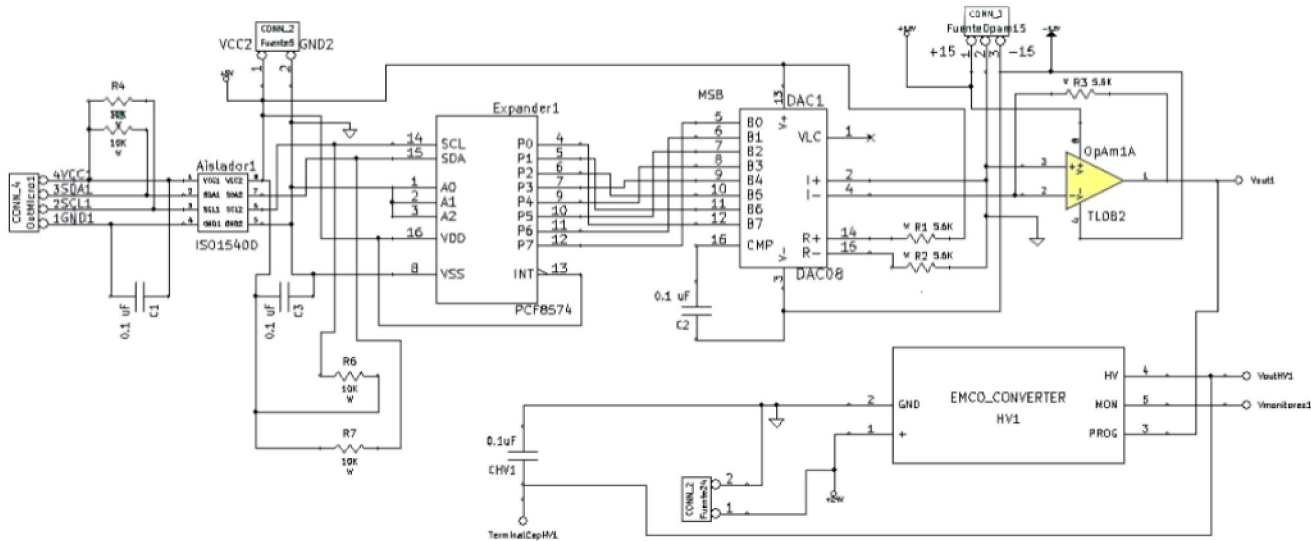


Fig. A2. High Voltage connection diagram. It is worth noting that three modules were used to control high voltage DC-DC converters depending on the address assigned to them.

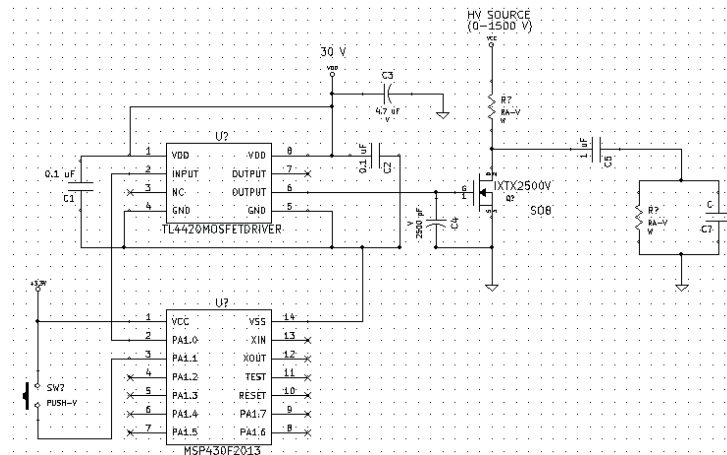


Fig. A3. High voltage pulse generator.

As it can be seen in Fig. A2 that four power supplies were required in this design as shown in Table A1.

Table AI. Voltage supplies for the high voltage source modules.

Voltage Supply	Electronic component	Description
+ 5 V	ISO1540	Bidirectional I ² C isolator
	PCF8574	Expander for I ² C bus
	DAC0808	8-bit Digital to analog converter
+ 15 V	TL082	Operational amplifier
- 15 V	TL082	Operational amplifier
	DAC0808	8-bit Digital to analog converter (Ref. voltage)
+ 24 V	EMCO H05P	High voltage DC to DC programmable converter

After testing and characterizing the modular high voltage, it was evident that four power supplies management was difficult to perform. In order to reduce the number of voltage supplies in the system, the expander for I²C bus, the digital to analog converter and the operational amplifier were replaced with an I²C voltage output digital to analog converter (LTC2631) supporting up to nine selectable addresses.

APPENDIX B

The results for all simulations computed for the DBT-breast models described in section 7.2.4, in which twelve electrode arrays described in section 7.2.5 were tested, are presented in Table B1. The first column indicates the patient, and acronyms in the second column stand for the electrode array used. Voltages between the different pairs of electrodes in the third column show the activation of electrode pairs. The percentage of tissue coverage in the fourth column indicates reversibly and irreversibly electroporated tissues, where breast and fat tissue correspond to the safety margin volume. Finally, the last column reports the electric current obtained for each electroporation protocol. The most efficient treatment protocols obtained for each patient regarding the generation of an electric field magnitude above the reversible electroporation threshold, and the coverage percentage of the tissues of interest are shown highlighted in green.

Table B1. Global results for twelve needle-electrode arrays

P ^a	Array	Voltage ^b [V]			Tissue Coverage [%]						I ^o [A]
		C-P	P-P	D	Tumor		Breast		Fat		
					RE ^c	IRE ^d	RE	IRE	RE	IRE	
1	4De1	800	2500	--	100	19.2	100	72.2	100	73.2	5.9
	4De2	2000	1500	--	100	30.2	85.3	11.0	90.6	10.1	3.1
	4Di1	--	1000	2000	100	0	95.0	22.9	99.8	48.4	3.5
	4Di2	--	3000	3000	5.91	0	32.6	0	73.4	0.3	4.4
	5Di1	--	3000	--	100	7.73	100	83.5	100	89.6	11.4
	5Di2	1500	3000	--	99.6	22.1	70.8	4.9	87.1	6.7	3.8
	6St1	800	3000	--	100	19.5	100	86.0	100	91.5	4.7
	6St2	1500	3000	--	100	33.5	85.0	6.2	91.8	6.6	4.3
2	4De1	3000	3000	--	98.1	88.2	94.9	64.1	94.1	67.5	13.9
	4De2	3000	3000	--	99.8	60.3	99.6	48.8	99.8	62.3	7.6
	4De3	2000	3000	--	99.8	33.0	99.9	46.2	100	49.6	7.4
	4Di1	--	1500	2500	99.8	83.9	94.3	45.6	92.3	48.1	5.9
	4Di2	--	3000	3000	16.1	0	73.0	1.8	85.2	17.7	5.4
	4Di3	--	3000	3000	78.1	4.81	100	36.8	100	65.2	6.2
	5Di1	3000	--	--	100	98.8	100	66.8	98.3	69.7	19.7
	5Di2	2000	--	--	98.9	9.7	96.7	16.9	99.4	28.1	7.9
	5Di3	2500	--	--	100	46.1	99.8	55.2	100	66.5	10.2
	6St1	--	3000	--	99.3	35.6	98.1	73.9	94.7	66.3	6.6
6St2	2500	2000	--	100	29.9	100	51.0	100	64.0	5.8	

	6St3	2000	--	--	99.7	30.7	99.6	46.3	99.8	56.7	6.8
3	4De1	3000	3000	--	99.9	70.2	65.7	12.5	94.7	53.5	9.2
	4De2	3000	3000	--	95.7	14.1	88.2	22.7	100	59.4	6.1
	4De3	3000	3000	--	98.5	30.7	83.3	27.9	100	67.1	7.4
	4Di1	--	3000	2000	100	26.1	40.1	2.60	93.9	47.4	5.2
	4Di2	--	3000	3000	5.7	0	13.4	0	77.9	11.7	4.5
	4Di3	--	3000	3000	22.0	1.70	52.6	2.95	98.0	54.5	5.3
	5Di1	--	3000	--	79.1	17.1	42.6	6.4	95.4	58.3	6.6
	5Di2	3000	--	--	97.8	15.4	92.1	27.5	100	74.9	8.2
	5Di3	2500	--	--	97.6	17.9	85.6	17.8	99.7	59.1	7.9
	6St1	1000	3000	--	71.3	11.7	30.9	10.6	93.9	63.0	4.5
	6St2	3000	--	--	98.6	14.8	93.9	28.9	100	80.5	8.2
	6St3	3000	--	--	99.6	53.6	91.6	31.7	100	80.9	9.5

^bVoltage applied between central electrodes and peripheral electrodes (C-P), peripheral electrodes (P-P) and opposite electrodes (D) in 4-needle diamond configuration.

^cPercentage of tissue covered at the reversible electroporation threshold (RE = 400 V/cm).

^dPercentage of tissue covered at the irreversible electroporation threshold (RE = 800 V/cm).

^eAverage electric current between activated pairs of needles.



APPENDIX C: JOURNAL PAPER (PRODUCTIVITY)

Electroporation Based Therapies-Original Article

Computational Feasibility Analysis of Electrochemotherapy With Novel Needle-Electrode Arrays for the Treatment of Invasive Breast Ductal Carcinoma

Technology in Cancer Research & Treatment
Volume 17: 1-13
© The Author(s) 2018 Article reuse guidelines: sagepub.com/journals-permissions DOI: 10.1177/1533033818794939 journals.sagepub.com/home/tct



Adriana Leticia Vera-Tizatl, MSAT¹, Claudia Elizabeth Vera-Tizatl, MSc², Arturo Vera-Hernández, PhD¹, Lorenzo Leija-Salas, PhD¹, Sergio Rodríguez, MD³, Damijan Miklavcic, PhD⁴ , and Bor Kos, PhD⁴ 

Abstract

Breast cancer represents a rising problem concerning public health worldwide. Current efforts are aimed to the development of new minimally invasive and conservative treatment procedures for this disease. A treatment approach for invasive breast ductal carcinoma could be based on electroporation. Hence, in order to determine the effectiveness of electrochemotherapy in the treatment of this disease, 12 electrode models were investigated on realistic patient-specific computational breast models of 3 patients diagnosed by Digital Breast Tomosynthesis imaging. The electrode models exhibit 4, 5, and 6 needles arranged in 4 geometric configurations (delta, diamond, and star) and 3 different needle spacing resulting in a total of 12 needle-electrode arrays. Electric field distribution in the tumors and a surrounding safety margin of 1 cm around the tumor edge is computed using the finite element method. Efficiency of the electrode arrays was determined hierarchically based on (1) percentage of tumor volume reversibly electroporated, (2) percentage of tumor volume irreversibly electroporated, (3) percentage of treated safety margin volume, (4) minimal invasiveness, that is, minimal number of electrodes used, (5) minimal activated electrode pairs, and (6) minimal electric current. Results show that 3 electrode arrays (4 needle-delta, 5 needle-diamond, and 6 needle-star) with fixed-geometry configuration could be used in the treatment with electrochemotherapy of invasive breast ductal carcinomas ranging from 1 to 5 cm³ along with a surrounding safety margin of 1 cm.

Keywords

breast cancer, computational breast model, electroporation, finite element modeling, safety margin

Abbreviations

BI-RADS, breast imaging reporting and data system; CC, cranial caudal; C-P, central to peripheral; D, diagonal electrodes; DBT, digital breast tomosynthesis; E, electrode; ECT, electrochemotherapy; ER, estrogen receptors; HER-2, hormone epidermal growth factor receptor 2; IDC, invasive ductal carcinoma; IRE, irreversible electroporation; MLO, medio-lateral oblique; P-P, peripheral to peripheral; PR, progesterone receptors; SM, safety margin; 2-D, 2-dimensional; 3-D, 3-dimensional; 4De1, 4 needle-delta configuration-set 1; 4Di1, 4 needle-diamond configuration-set 1; 5Di1, 5 needle-diamond configuration-set 1;

¹Department of Electrical Engineering, Centro de Investigación y de Estudios Avanzados del Instituto Politécnico Nacional (CINVESTAV-IPN), Mexico City, Mexico

²Department of Infectomics and Molecular Pathogenesis, Centro de Investigación y de Estudios Avanzados del Instituto Politécnico Nacional (CINVESTAV-IPN), Mexico City, Mexico

³Institute of Breast Diseases, FUCAM, Mexico City, Mexico

⁴Faculty of Electrical Engineering, University of Ljubljana, Ljubljana, Slovenia

Corresponding Author:

Bor Kos, University of Ljubljana, Trzaska 25, Ljubljana, N/A 1000, Ljubljana, Slovenia.
Email: bor.kos@fe.uni-lj.si

attributed as specified on the SAGE and Open Access pages (<https://us.sagepub.com/en-us/nam/open-access-at-sage>).



Creative Commons Non Commercial CC BY-NC: This article is distributed under the terms of the Creative Commons Attribution-NonCommercial 4.0 License (<http://www.creativecommons.org/licenses/by-nc/4.0/>) which permits non-commercial use, reproduction and distribution of the work without further permission provided the original work is

6St1, 6 needle-star configuration-set 1; 4De2, 4 needle-delta configuration-set 2; 4Di2, 4 needle-diamond configuration-set 2; 5Di2, 5 needle-diamond configuration-set 2; 6St2, 6 needle-star configuration-set 2; 4De3, 4 needle-delta configuration-set 3; 4Di3, 4 needle-diamond configuration-set 3; 6St3, 6 needle-star configuration-set 3

Received: December 27, 2017; Revised: June 24, 2018; Accepted: July 24, 2018.

Introduction

Breast cancer, due to malignant tumors in women older than 25, represents the first cause of death of women in Mexico since 2006. Its recurrence has increased 49.5% during the last 2 decades; about 45% of total cases are diagnosed in stages III and IV, and 11% are women younger than 40 years. Remarkably, the survival rate for the latter group is lower compared to the older population.¹

The most common histologic subtypes of breast tumors are ductal carcinoma, in situ and invasive (IDC), and lobular carcinoma, in situ and invasive. Both of them account for the 90% (80% and 10%, respectively) of all breast tumors.^{1,2} Breast cancer is a major problem concerning public health worldwide, and current efforts are aimed at controlling known risk factors, establishment of early detection programs, and the development of new minimally invasive and conservative treatment procedures for this disease.^{1,3}

The techniques currently used for treating breast cancer are neoadjuvant chemotherapy, radiotherapy, hormonal therapy, and surgical procedures, which include lumpectomy and mastectomy. Interestingly, 10% to 20% of diagnosed breast cancers are considered as triple negative breast cancer. For this type of tumors, treatments like hormone therapy and drugs that target estrogen, progesterone, and HER-2 receptors are ineffective, leaving chemotherapy as the only treatment. This characteristic makes these tumors more aggressive and difficult to treat.

Electroporation, or electropermeabilization, may be a novel approach for treating invasive ductal carcinoma because electroporation of the plasma membrane of living cells increases the uptake of nonpermeant or poorly permeant molecules once the cells had been exposed to short and strong electric pulses. Moreover, it is possible to permeabilize the cell plasma membranes while preserving their viability, which allows them to return to their natural state in a process called reversible electroporation.⁴ However, if the electric field is stronger than the irreversible threshold, it leads to cell death caused by irreversible electroporation (IRE).⁵ Reversible electroporation has been used for many clinical applications, such as the introduction of drugs into cells, electrochemotherapy, gene delivery to tissue, and transdermal delivery of drugs and genes.⁶⁻¹¹ Electrochemotherapy (ECT) enables the potentiation of effectiveness of chemotherapeutic drugs bleomycin by a factor of up to 1000 and cisplatin by a factor of up to 80.^{6-9,12} Electrochemotherapy is a local minimally invasive treatment that has been proven to be effective in cutaneous and subcutaneous tumors with different histologies.¹³⁻¹⁶ Most frequently, ECT represents

a palliative treatment in patients with cancer having progressive disease (stage IV); the therapeutic goal is improving the quality of life (bleeding and pain relief) during terminal phase due to the lack of suitable treatment to prolong overall survival.^{17,18} Electrochemotherapy has been proven to be highly effective in palliative treatment of cutaneous tumors including cutaneous tumors from breast cancer and chest wall recurrences of breast cancer.¹⁷⁻¹⁹ Because of its benefits, such as high specificity for targeting cancer cells and capacity for pre-serving the innate immune response, its use is therefore being extended to the treatment of internal tumors.²⁰⁻²⁴ Clinical experiences regarding the treatment of liver and bone metastases, soft tissue sarcomas, brain tumors, and colorectal and esophageal tumors have been reported.²⁰ Electrochemotherapy of breast cancer metastases to the skin and subcutaneous

tissues has also been reported showing encouraging outcomes.^{17,25-28} However, to our best knowledge, there are only 2 works that address the treatment of primary breast cancer with ECT, that is, (1) an infiltrative lobular carcinoma in a single elderly patient, inoperable for neoplastic infiltration of the chest wall and undergoing preoperative (attempt of cytoreduction) and intraoperative ECT prior to radical mastectomy²⁹ and (2) a single clinical case of unifocal ductal breast cancer that reports reduced efficacy of the ECT treatment with 5 needle electrodes.³⁰ Both studies performed ECT through Cliniporator (IGEA SpA, Carpi, Italy) and operating standard procedures for Electrochemotherapy.^{17,18} These results lead us to suggest that ECT may displace neoadjuvant chemotherapy and/or surgery in the treatment of breast cancer and have encouraged the development of better electrode configurations along with an adequate pretreatment planning based on numerical models for the treatment of invasive breast ductal carcinoma with ECT.³⁰

Treatment of breast cancer has also been addressed by IRE. Investigation on this issue has been carried out on one hand in vitro in order to establish a baseline estimate of electric field necessary for IRE treatment of breast carcinomas.³¹ On the other hand, in vivo studies have been reported in animal models comprising nude mice³² and rabbits.³³ The results reported in these works suggest that IRE may be a promising approach for patients with breast cancer who are not eligible for surgical excision. In addition, numerical modeling of electric field distribution represents a useful tool to validate the required voltage to fully expose the target to the electric field determined from in vitro experiments. Nonetheless, more experimental evidence regarding the treatment of breast cancer with IRE is required, since reports on this field remain limited.³¹⁻³⁴

This work researched the feasibility of using electrochemotherapy for the treatment of IDC in realistic breast models based on digital breast tomosynthesis (DBT) images with a universal electrode array to assure the electroporation of the entire target volume.³⁵ In addition to the tumor treatment, eradication of some surrounding tumor tissue is desirable, since tumor cells that have an infiltrative-like histological type spread diffusely throughout the healthy tissue. In order to achieve the destruction of the tumor and the eradication of some surrounding healthy tissue efficiently, 12 electrode arrays in 4 configurations were used for modeling electroporation of tumors corresponding to 3 representative clinical cases. Novel electrode arrays, which included a central intratumoral needle, are proposed in this work, and the results are compared to those obtained with electrode arrays without intratumoral needles in order to establish a suitable protocol for electrochemotherapy of invasive breast ductal carcinomas and a safety margin of healthy tissue.

Methods

Breast Computational Model

Imaging studies were approved by the Scientific-Ethics Committee of the Institute of Breast Diseases-FUCAM (approval number 2017/14). All patients provided verbal consent to be subjected to the imaging studies. Three representative clinical cases of women diagnosed with invasive breast ductal carcinoma without previous treatment, hence corresponding to primary deep-seated tumors, were analyzed to evaluate their treatment with electrochemotherapy. In all cases, diagnosis was done by DBT, Giotto Tomo, IMS (slice thickness 1 mm and pixel size 0.1 mm).

Mammography has been used as the primary detection tool for breast abnormalities, but nowadays it is being replaced by DBT. Digital Breast Tomosynthesis is a 3-dimensional (3-D) imaging technology that involves acquisition of images of a stationary compressed breast at multiple X-ray source angles during a short scan. Typically, the X-ray tube is rotated 10 to 20°, and 10 to 20 exposures are made approximately at every 1° of rotation during a total scan of 5 seconds or less. Individual images are then reconstructed into a series of thin, high-resolution slices with a separation of 1 mm. Tissues that overlap in 2-D conventional mammography and hide pathologies are less likely to be obscured using tomosynthesis. The cross-sectional 3-D slice allows a clearer visualization of the lesion.³⁶ Digital breast tomosynthesis differs from other 3-D imaging modalities in that orthogonal multiplanar reconstructions such as sagittal, axial, and coronal views from the transverse tomo-synthesis image sets cannot be generated. Instead, cranial-caudal (CC) and medio-lateral oblique (MLO) views are obtained with DBT. Because breast compression is necessary in DBT in order to minimize tissue superposition, reduce X-ray scatter signal, and increase the amount of breast tissue in the field of view, processing of DBT projections in order to reconstruct a 3-D breast volume is not straightforward due to the lack

of orthogonal multiplanar views.^{36,37,38} Development of tridimensional reconstruction algorithms of DBT projections is beyond the scope of this work, and therefore, realistic breast modeling was alternatively carried out in a 2-step process in order to deal with the breast-deformation issue of DBT due to tissue compression.

First, the presence of tumors and the main tissues (tumoral tissue, fibroglandular tissue, and fatty tissue) in the region of interest were determined and marked out by physicians in both CC and MLO views in which dimensions, breast density, and the center of the tumor were determined. Tumor segmentation and 3-D reconstruction were carried out in 3-D Slicer in the original DBT images. Second, numerical breast phantoms available in a repository³⁹ and derived from T1-weighted magnetic resonance images of patients with no malignancy or other abnormalities were used to provide a decompressed model for the rest of the tissues of interest (fibroglandular and fatty tissue). Each phantom consists of a 3-D grid of cubic voxels of 0.5 0.5 0.5 mm. The database of numerical phantoms was classified based on the standard tissue composition descriptors used by radiologists to classify X-ray mammograms according to the radiographic density of the breast. Four categories were defined according to the breast imaging reporting and data system (BI-RADS): (1) almost entirely fat (<25% glandular tissue), (2) scattered fibroglandular (25%-50% glandular), (3) heterogeneously dense (51%-75% glandular), and (4) very dense (>75% glandular).^{40,41}

In this work, a computational phantom was radiologically assigned to each patient based on the correlation of patient breast density grading with the categories of the BI-RADS. Breast tissue consists mainly of glandular parenchyma, connective tissue, and fatty tissue. Breast tissue and glandular parenchyma are radiologically considered as dense tissue. Patient 1 DBT images showed whitish appearance that pointed to a major glandular parenchyma proportion; hence, a very dense phantom was selected for this patient. A scattered fibroglandular phantom was used for patient 2, since dense tissue in DBT images showed a scattered pattern, which corresponded to a minor amount of glandular parenchyma. On the other hand, nondense mammographic areas (dark regions) were observed for patient 3, and therefore, a mostly fatty phantom was selected to represent this case. Three main tissues were considered for the phantoms, that is, skin, fibroconnective/glandular tissue, and fatty tissue for segmentation. Finally, in order to build a model of a realistic-anatomical breast with malignancies, the scale of the tumor segmentation corresponding to each patient was adjusted to fit the dimensions of the selected phantom; then, the reconstructed tumor was embedded into the selected computational breast phantom, keeping its original position inside the breast. This position was determined in its corresponding DBT image. This methodology allowed the development of a 3-D anatomical model of a patient-specific decompressed breast as shown in Figure 1. Table 1 shows the patients' and tumors' anatomical properties considered in order to build the breast models.

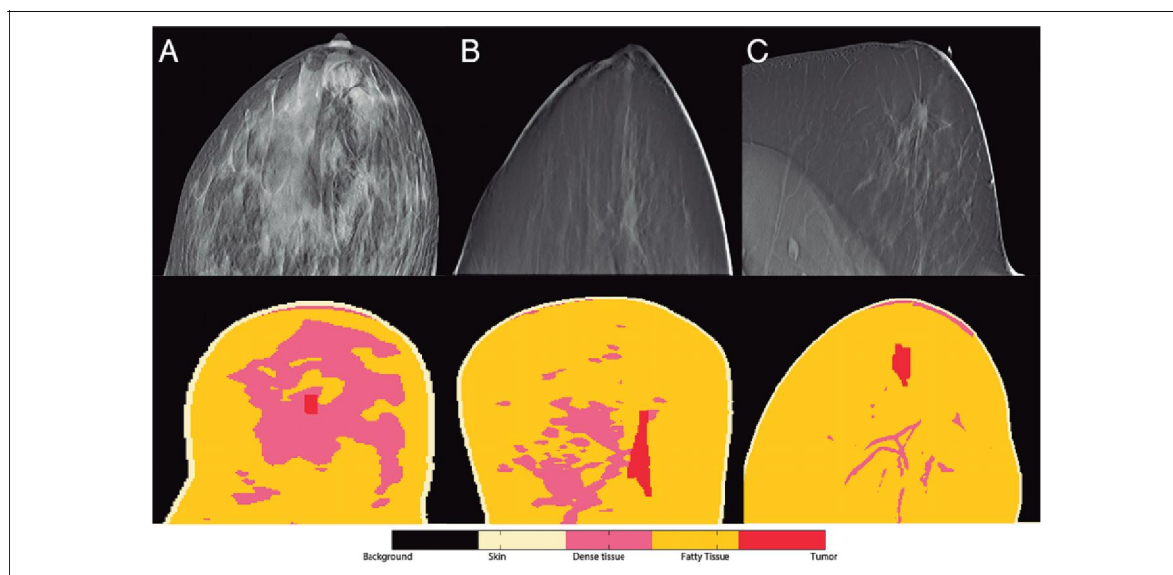


Figure 1. Breast Models. A, Craniocaudal (CC) view of a digital breast tomosynthesis of patient 1 and corresponding axial view of a very dense phantom analogue to CC view. B, Craniocaudal view of patient 2 and corresponding axial view of a scattered fibroglandular phantom. C, Medio-lateral-oblique view of patient 3 and corresponding sagittal view of a mostly fatty phantom analogue to medio-lateral oblique (MLO) view.

Table 1. Properties of the Anatomical Breast Models.

P ^a	Age	Location	Tumors			Phantom		
			#	Size, mm	Volume, cm ³	Type	Density	Volume Size, pixels
1	67	Left breast	1	4.49.1 11.5	0.46	III	Very dense	215 328 212
2	55	Left breast	1	389.6 8.5	3.10	II	Scattered fibroglandular	258 253 251
3	54	Left breast	1	299.5 18.5	5.10	I	Almost entirely fat	310 355 253

^aPatient.

Patient-Specific Treatment Planning

An efficient treatment of deep-seated invasive tumors with surgical resection requires the eradication of 10 mm of tissue surrounding the target tumor in order to reduce the probability of recurrences.⁴² This surrounding tissue is considered as a safety margin, and it must be taken into account along with the breast target tumor in each patient to develop the patient-specific treatment planning with electrochemotherapy.

Clinical cases differ from patient to patient in tumor size, tumor location, breast density, and dielectric properties of the tissues of interest; therefore, it was our purpose to determine first whether deep-seated invasive ductal carcinomas along with tissue into a safety margin of 10 mm may be eligible for their treatment with electrochemotherapy through the use of an universal electrode array, and second, the most effective electrode configuration and the electric protocol to be applied in that particular case. For this purpose, 3 sets of electrodes corresponding to 12 electrode arrays were proposed in this work. Electrode arrays in the different sets own the same number of

needles (4, 5, and 6) and the arrangement of needles (delta, diamond, and star), but they differ in distance among the electrodes as described in Figure 2 and Table 2. Number of needles ranges from 4 to 6 in order to investigate whether a sufficient electric field can be generated through the minimal number of electrodes and hence requiring fewer needle punctures. Variation in distance among the electrodes was proposed to fulfill a complete coverage of the tumors in the 3 patients according to their particular dimensions and geometries. However, it is our purpose to establish a suitable electrode array with a fixed-geometry configuration, which may cover target tissues in any clinical scenario of patients with IDC, based on the analysis of the 12 electrode arrays in the 3 patients reported in this work. In the clinical practice, handle of electrodes must remain the same for all electrode arrays, and selection of a particular electrode array shall depend on the dimensions of the target tumor. Needles' diameter in all arrays was 1.2 mm, and their active length varied depending on the tumor size as shown in Table 2, where C-P refers to the distance from the intratumoral-central electrode to the peripheral electrodes, P-P refers to the distance

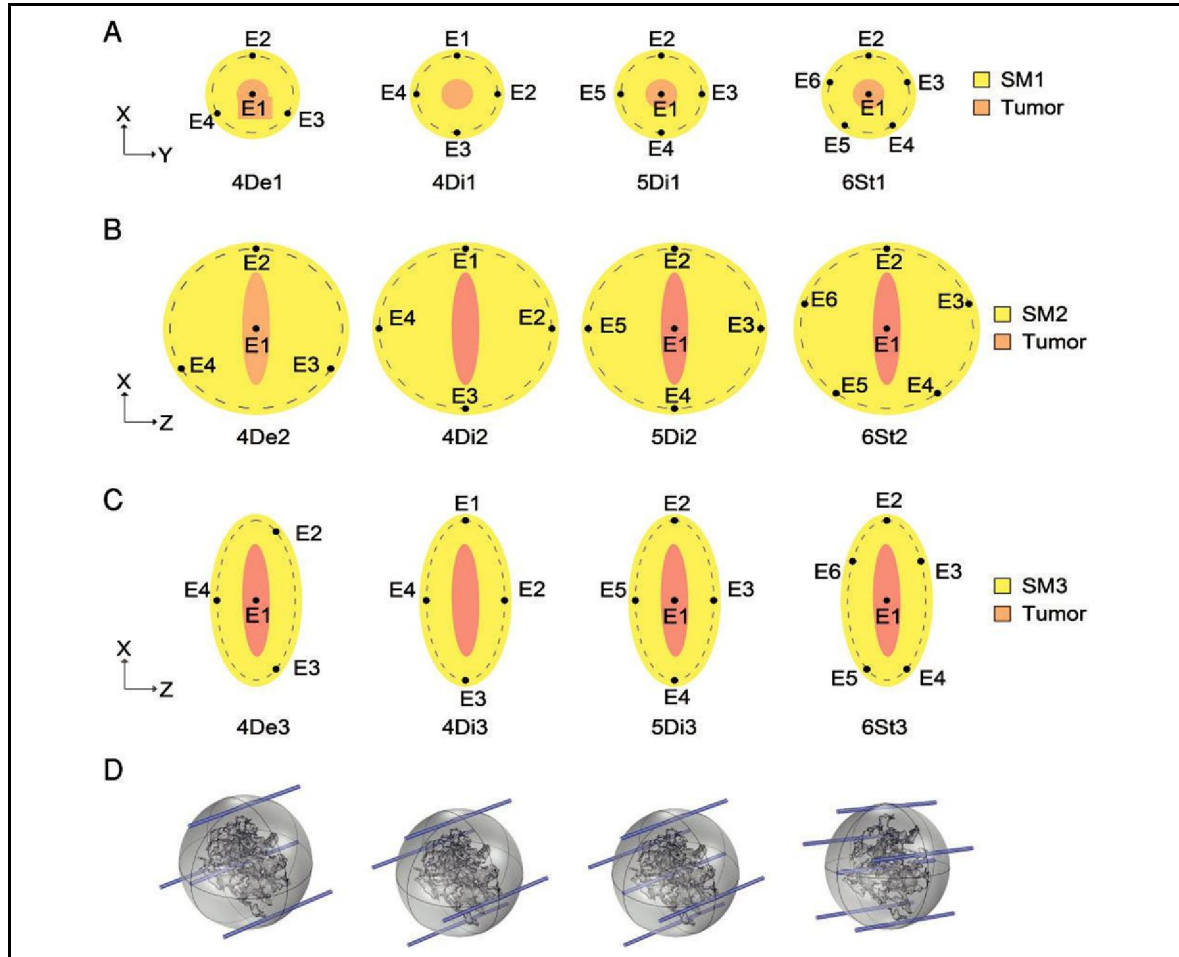


Figure 2. Topside view of (A) electrode set 1 for the treatment of a breast tumor (red) in patient 1 and a spherical safety margin tissue (SM1). (B) Electrode set 2 for the treatment of a breast tumor (red) in patient 2 and a spherical safety margin tissue (SM2). (C) Electrode set 3 for the treatment of a breast tumor (red) in patient 2 and an elliptic safety margin tissue (SM3). (D) Three-dimensional visualizations of the tumor embedded into a safety margin and the 4 electrode configurations; delta configuration, 4-needle diamond configuration, 5-needle diamond configuration, and 6-needle star configuration.

between peripheral electrodes only, and D refers to the distance between electrodes forming diagonals.

Electrode Arrays

In order to determine a suitable treatment protocol with electrochemotherapy for every clinical case and establish the coverage of the 3 target tissues, 4 needle-electrode configurations were used as an initial basis for each patient. Target tissues included the tumoral tissue in addition to the fatty and breast tissue comprised within a surrounding safety margin of 10 mm in diameter. Based on the number of needles (4, 5, or 6) and their configuration geometry (delta [De], diamond [Di], and star [St]), these original arrays were called 4De1, 4Di1, 5Di1,

and 6St1, Figure 2A. It is worth noting that for the diamond configuration, 2 electrode arrays were derived, that is, a 4-needle array without a central needle (4Di1) and a 5-needle array considering an intratumoral needle (5Di1). The safety margin for this set was considered as a sphere placed in the tumor center. Dimensional properties of these arrays are listed in Table 2. It can be seen that the distance between electrodes in the original array was appropriate to cover the tumoral volume of the first patient. However, tumors of the second and third patients were bigger, so in order to improve target coverage, the distance between the needles was increased resulting in 2 additional arrays. Electrode set 2 consists of an enlarged version of the electrode set 1 considering the safety margin as a sphere. Electrodes in this set were called 4De2, 4Di2, 5Di2, and 6St2 as

Table 2. Properties of the Needle-Electrode Arrays.

No.	Needles Configuration	Array	Symbol ^a	Active Length, mm	Distance ^b , mm			
					C-P	P-P	D	
4	Delta	Original	4De1	15	13.0	22.5	–	
		Enlarged	4De2	20	27.0	46.8	–	
		Ellipse	4De3	20	24.1	29.7	–	
	Diamond	Original	4Di1	15	–	18.4	26.0	
		Enlarged	4Di2	20	–	38.2	54.0	
		Ellipse	4Di3	20	–	29.6	54.0	
	5	Diamond	Original	5Di1	15	13.0	18.4	–
			Enlarged	5Di2	20	27.0	38.2	–
			Ellipse	5Di3	20	27.0	29.6	–
6	Star	Original	6St1	15	13.0	15.3	–	
		Enlarged	6St2	20	27.0	31.7	–	
		Ellipse	6St3	20	27.0	17.4	–	
						17.0	36.7	–
						24.1	12.5	–

^aSymbols indicate the number of needles (4, 5, 6), the array configuration (De ¼ Delta, Di ¼ Diamond, St ¼ Star), and the electrode set marker (1 refers to the original electrode array, 2 refers to the enlarged electrode array, 3 refers to the ellipse electrode array).

^bC-P refers to the distance from the central-intratumoral electrode to the peripheral electrodes, P-P refers to the distance between peripheral electrodes, and D refers to the distance between opposite electrodes in diamond configuration.

shown in Figure 2B. Based on the dimensions of the tumor of patients 2 and 3, a safety margin with an ellipsoidal geometry was used in set 3, since it fit better the boundaries of the tumor. Electrode arrays in this set were called 4 needle-delta configuration-set 3 (4De3), 4 needle-diamond configuration-set 3 (4Di3), 5 needle-diamond configuration-set 3 (5Di3), and 6 needle-star configuration-set 3 (6St3) as shown in Figure 2C.

Electric Field Calculation

One of the objectives of this work was to determine whether it was feasible to treat deep-seated invasive ductal carcinomas effectively with electrochemotherapy through the use of a set of electrodes of fixed geometry. It has been reported that in order to achieve a successful ECT, reversible electroporation of tumor cells must be reached, so chemotherapeutic drugs are allowed to enter the cell and cause its death. Furthermore, IRE cannot be avoided, mostly in the periphery of the electrodes; therefore, contribution of IRE in cell death may be significant, but it may still be tolerated for ECT.³¹ Taking this into consideration, pairs of needles in the different electrode arrays were sequentially set to voltage until all combinations of unique pairs were activated, setting boundary conditions for voltage as an anode and a cathode during each simulation. For the electrode configurations with a central needle, the central needle was first set as an anode paired off with peripheral needles considered as cathodes in the safety margin; subsequently, only

Table 3. Dielectric Properties of Tissues in the Breast Models.

Tissue	Initial conductivity (s0) [S/m]	Final conductivity sf [S/m]	Threshold Electric Field [V/cm]	
			RE ^a	IRE ^b
Skin	0.170	0.170	400	800
Fibroconnective/glandular	0.085	0.340		
Fatty	0.025	0.100		
Tumor	0.425	1.700		

^aThreshold electric field for reversible electroporation in breast models.

^bThreshold electric field for irreversible electroporation in breast models.

peripheral electrodes were switched as anode and cathode, respectively. For configurations lacking a central needle (ie, 4Di1, 4Di2, and 4Di3), electrodes were commuted as anode and cathode in 6 possible combinations formed by adjacent and opposite needles. Initial voltage values were applied between each pair of electrodes in the different arrays. Depending on the tissue coverage resulting from this first simulation, voltage was varied until the target volumes were covered by an electric field magnitude above the reversible electroporation threshold in order to find the most appropriate treatment protocol for each patient.

Depending on the location of the tumor in the breast and the ease of needle insertion into the target tissue, the arrays were determined to be inserted normal to the axial plane for patients 1 and 2 and normal to the sagittal plane for patient 3. All models were computed in COMSOL Multiphysics (version 5.0, COMSOL, Sweden) with an algorithm written in Matlab (version R2013b; Mathworks, Natick, Massachusetts, USA) in order to establish the electric field distribution in the regions of interest. Visualization approach reported by Zupanic et al was used to extract the results and quantitatively compare the models based on the electroporation cross-section images, and the cumulative coverage of tissues by electric fields after the complete sequence of pulses has been applied. Cumulative coverage was displayed as an electric field histogram similar to dose-volume histograms used in radiation therapy planning. Electric field histograms were calculated for the 3 target tissues. All tissues were considered as isotropic with electrical conductivity values reported in the literature,^{31,43-45} and changes in conductivity due to electroporation were taken into account as shown in Table 3.

Results

Different electroporation protocols for each 1 of the 12 electrode arrays were used for the treatment of breast malignancies and surrounding tissue inside a safety margin of 1 cm around the tumor edge. The volumes of target tissues corresponding to the safety margin for each patient depended on the breast density and the phantom type used; total volumes of each tissue are listed in Table 4. Global electroporation results obtained for each patient are shown in Supplemental Table A. In

Table 4. Volumes of Target Tissues.

Patient	Volume of Target Tissues[cm ³]		
	Breast Tissue	Fatty Tissue	Tumor
1	10.20	3.76	0.46
2	5.16	19.73	3.10
3	1.05	26.58	5.10

Supplemental Table A, the first column shows the corresponding patient, and acronyms in the second column indicate the number of needles which we assumed as an indicator of invasiveness. Voltages between the different pairs of electrodes in the third column show the activation of electrode pairs. Percentage of tissue coverage in the fourth column indicates reversibly and irreversibly electroporated tissues, where breast and fat tissue correspond to the safety margin volume. Finally, the last column reports electric current obtained for each electroporation protocol. The most efficient treatment protocols obtained for each patient and each 1 of the 12 electrode arrays regarding the generation of an electric field magnitude above to the reversible electroporation threshold, and the coverage percentage of the 3 tissues of interest are shown highlighted in light red.

It has been reported that successful medical application of ECT requires the achievement of optimal parameters in the whole target tissue while keeping healthy tissue damage at a minimum.³¹ Nevertheless, in this work, healthy tissue constituting the safety margin was subjected to electroporation for the treatment of potential micro-metastases or tumor outgrowths not visible in imaging. The most efficient electrode array was selected for each patient hierarchically, taking into account the following criteria: (1) percentage of tumor volume reversibly electroporated; (2) percentage of tumor volume irreversibly electroporated; (3) percentage of treated safety margin volume; (4) minimal invasiveness, that is, minimal number of electrodes; (5) minimal activated electrode pairs; and (6) minimal electric current. Selection criteria are in accordance with the literature.³¹ The best electrode arrays are listed in Table 5, according to the hierarchic selection criteria applied to the global results reported in Supplemental Table A. The best electric protocols are reported as the voltage applied between central electrodes and peripheral electrodes (C-P), peripheral electrodes (P-P), and opposite electrodes (D, in 4-needle diamond configuration). The percentage of the target tissue covered between reversible and IRE thresholds and the average electric current between all pairs of activated electrodes are reported. It can be seen that for a small tumor in patient 1, a 4-needle electrode array in diamond configuration (4Di1) was suitable to reversibly cover the complete tumor and more than 90% of the safety margin. Good results were obtained with a 4-needle electrode array in delta configuration (4De2) and

6-needle electrode array in star configuration (6St2), as they 7 covered 100% of the tumor and more than 85% of the safety margin. For patient 2, 5-needle electrode array in diamond configuration (5Di2), 6St2 and 4De2 showed comparable results regarding reversibly electroporated tissue coverage. 5Di2 electrode array generated the minor IRE. Similarly, for patient 3, 6St2, 5Di2, and 4De2 resulted to be the most efficient electrode arrays in a comparable manner, but 5Di2 electrode array required fewer pairs of active electrodes.

The most effective electroporation protocols from Table 5 were 1000 V and 2000 V pulses between peripheral and opposite needles, respectively, in 4Di1 electrode array for patient 1, 2000 V pulses between C-P needles in 5Di2 electrode for patient 2, and 3000 V pulses between C-P needles in 6St2 electrode for patient 3. These protocols were used to determine the electric field histograms for the 3 target tissues (tumor, fatty, and breast tissue in the safety margin) as shown in Figures 3 to 5. Electric field histograms show the volume fraction of tissue (1/4 100%) covered at a certain electric field strength. A complete coverage was expected to be reached above 400 V/cm, whereas the tissue volume covered above 800 V/cm had to be kept at the minimum to minimize IRE. Tumor coverage in Figure 3 shows that an efficient electroporation (100% coverage above 400 V/cm) of a small tumor in patient 1 may be achieved with electrode 4Di1. Tumors from patients 2 and 3 were bigger than that from patient 1 and hence more difficult to reversibly electroporate, covering 98.9% and 98.6% of these tumors with 5Di2 and 6St2, respectively, with an electric field above 400 V/cm. It is worth noting that coverage of the tissues in the safety margin changed for the different breast densities due to the different dielectric properties of the tissues. Fatty tissue was easier to cover completely by fields above the reversible electroporation threshold (shown in Figure 4) than breast tissue (shown in Figure 5). At the same time, fatty tissue was also more susceptible to IRE than breast tissue.

Electroporation color maps obtained for the most efficient protocol applied to each of the 3 breast models are shown in Figure 6. Irreversibly electroporated areas are marked in magenta, color blue represents reversibly electroporated areas in the tumors, and green shows reversibly electroporated areas in the safety margin tissues. Nontreated areas, that is, points where reversible electroporation threshold was not reached, appear uncolored.

Discussion

Twelve electrode arrays corresponding to 4 different configurations were used to evaluate the feasibility of treatment of invasive ductal breast carcinomas with electrochemotherapy. The results listed in Supplemental Table A show that the appropriate electrode array differs from patient to patient depending on the anatomical properties of the tissues of interest, that is, tumor size, breast density, and dielectric properties. This table also shows that a different efficient electric protocol was obtained for every patient. On the one hand, the treatment of

Table 5. Effective Electroporation Protocols for the Treatment of Target Tissues.

Pa	Electrode Array	Voltage ^b [V]			Tissue Coverage [%]						c [A]
		C-P	P-P	D	Tumor		Breast		Fat		
					RE ^c	IRE ^d	RE	IRE	RE	IRE	
1	4Di1	–	1000	2000	100	0	95.1	22.9	99.8	48.4	3.5
	4De2	2000	1500	–	100	30.2	85.3	11.0	90.6	10.1	3.2
	6St2	1500	3000	–	100	33.5	85.0	6.2	91.8	6.6	4.3
2	5Di2	2000	–	–	98.9	9.7	96.7	16.9	99.2	28.1	7.9
	6St2	2500	2000	–	99.9	29.9	100	51.0	100	64.0	5.8
	4De2	3000	3000	–	99.8	60.3	99.6	48.8	99.8	62.3	7.5
3	6St2	3000	–	–	98.6	14.9	94.0	29.0	100	80.5	8.2
	5Di2	3000	–	–	97.8	15.4	92.1	27.5	100	74.9	8.2
	4De2	3000	3000	–	95.7	14.2	88.2	22.7	100	59.4	6.1

^aPatient.

^bVoltage applied between central electrodes and peripheral electrodes (C-P), peripheral electrodes (P-P), and opposite electrodes (D) in 4-needle diamond configuration.

^cPercentage of tissue covered at the reversible electroporation threshold (RE ¼ 400 V/cm).

^dPercentage of tissue covered at the irreversible electroporation threshold (RE ¼ 800 V/cm).

^eAverage electric current between activated pairs of needles.

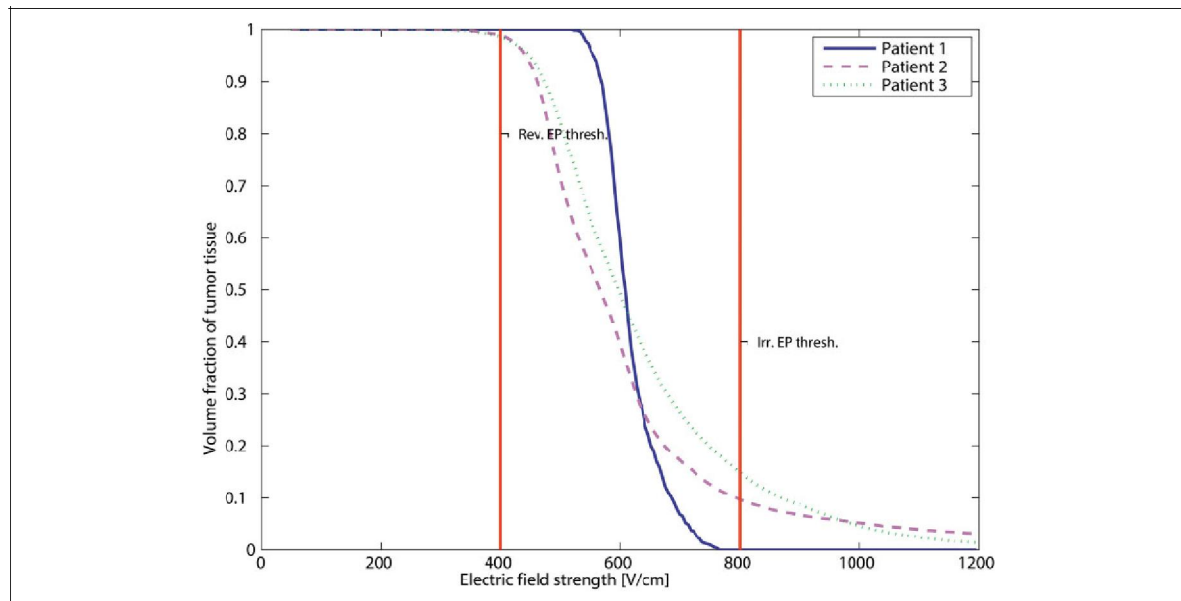


Figure 3. Most efficient coverage of tumors in the 3 patients. Electrode 4Di1 covered 100% of tumor in patient 1 with 1000 V and 2000 V between peripheral and opposite needles. Electrode 5Di2 covered 98.9% of tumor in patient 2 with 2000 V between C-P needles. Electrode 6St2 covered 98.6% of tumor in patient 3 with 3000 V between C-P needles.

whole tissues of interest. In addition, delta and star configuration (4De2 and 6St) in electrode set 2 resulted in effective target coverage. It is worth noting that as the tumors become bigger, as for the cases for patients 2 and 3, this electrode array (4Di1, set 1) was the least efficient configuration, since none of the tissues of interest got completely covered. On the other hand, efficient protocols for patient 2 were obtained with arrays in set 2 (6St2 and 4De2) and set 3 (4De3 and 6St3). It was

observed that the use of an electrode array following a tumor-specific safety margin geometry which was in turn selected based on the tumor dimensions (ideally elliptic for tumor in patient 2) resulted in optimal outcomes. Effective coverage for patient 3 was obtained with electrode arrays in set 2 (6St2, 5Di2, 4De2). Contrary to the results obtained for patient 1 with the array 4Di1, 4-needle diamond configuration in any of the sets, that is, 4Di1, 4Di2, and 4Di3, resulted in the least effective

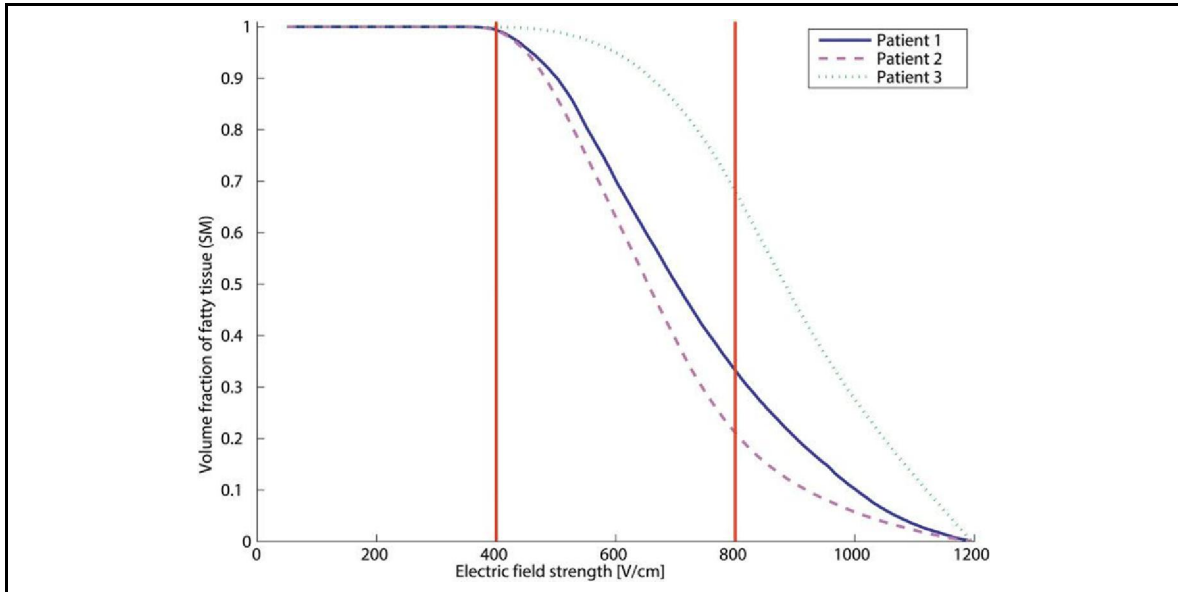


Figure 4. Most efficient coverage of fatty tissue in the safety margin for the 3 patients. Electrode 4Di1 covered 99.8% of fatty tissue in patient 1 with 1000 V and 2000 V between peripheral and opposite needles. Electrode 5Di2 covered 99.2% of fatty tissue in patient 2 with 2000 V between C-P needles. Electrode 6St2 covered 100% of fatty tissue in patient 3 with 3000 V between C-P needles.

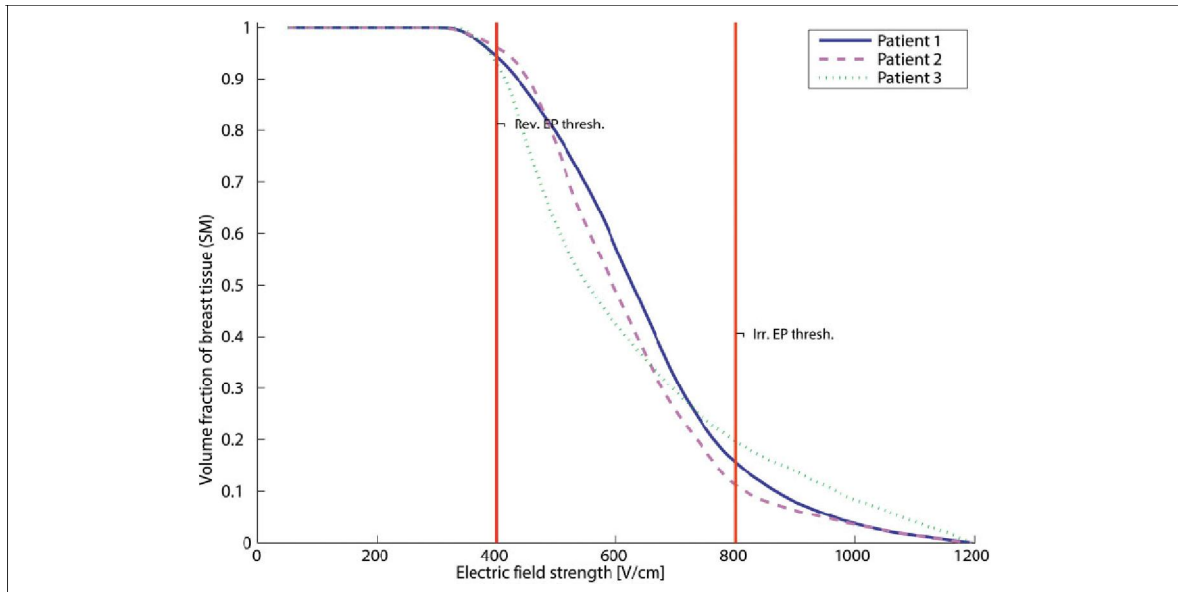


Figure 5. Most efficient coverage of breast tissue in the safety margin for the 3 patients. Electrode 4Di1 covered 95.1% of breast tissue in patient 1 with 1000 V and 2000 V between peripheral and opposite needles. Electrode 5Di2 covered 96.7% of breast tissue in patient 2 with 2000 V between C-P needles. Electrode 6St2 covered 94% of breast tissue in patient 3 with 3000 V between C-P needles.

arrays for the treatment of the target lesions even if the voltage was increased to the maximum value (3000 V) provided by current electroporation systems. Noticeably, an enlarged

version of the original electrode set used in patient 1, was the most appropriate set of electrodes for both patients 2 and 3 and a good alternative for patient 1 also. It is worthy to mention that

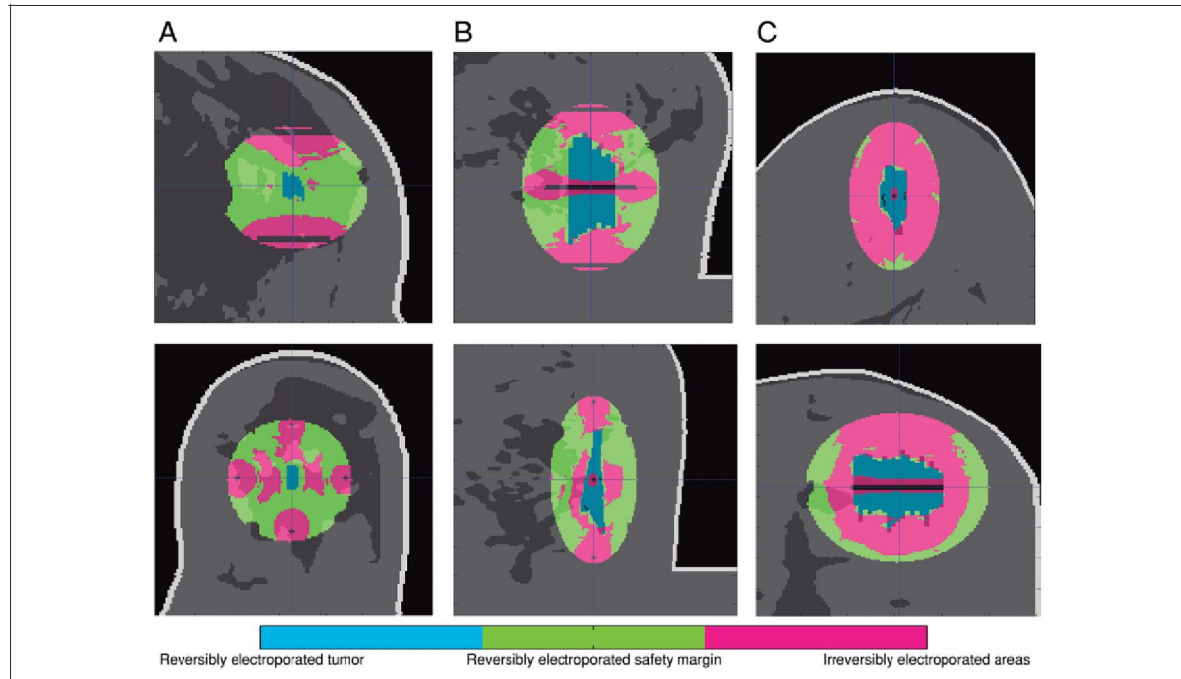


Figure 6. Visualization of electroporation reached in the target tissues of (A) patient 1, (B) patient 2, and (C) patient 3. Magenta color represents irreversibly electroporated regions, green shows reversibly electroporated regions in the safety margin (fatty tissue and breast) and blue indicates reversibly electroporated areas in the tumors. Nontreated areas in the models are uncolored.

for big tumors such as those in patients 2 and 3, a complete coverage of target tissues was harder to obtain if compared to the coverage of small tumors, but efficient coverage is possible to achieve.

Tissue dielectric property ratios used in this work were considerable $(\frac{s_{\text{tumor}}}{s_{\text{breast tissue}}} = \frac{5s}{17}; \frac{s_{\text{tumor}}}{s_{\text{fatty tissue}}} = \frac{5s}{17})$,

making electroporation a challenging process and hence requiring high-voltage values to achieve an efficient treatment. Based on the results reported in this work, it would be possible to use a fixed set of electrodes (4De2, 5Di2, and 6St2) to effectively treat invasive breast ductal carcinomas in the range of 1 to 5 cm³ with electrochemotherapy. Regarding the electrode-manufacturing issue, our results indicate that producing 2 electrode arrays (4De2 and 6St2) would be enough to treat invasive breast ductal carcinoma. This reduces meaningfully the complexity of manufacturing and device certification processes.

Further efforts aimed at imaging reconstruction of DBT views are required so that more accurate breast models can be obtained, since the breast models presented in this work consisted of interpolations of data in the DBT images in order to deal with the tissue compression issue. In addition, research with variations in the electrode positioning is encouraged in order to compare the results with the outcomes presented here. A comparison between the most effective electrode arrays (4De2, 5Di2, and 6St2) and the commercial hexagonal

electrode array with a central needle, manufactured by IGEA S.p.a (Carpi, Italy),⁸ would be useful in order to determine whether the number of needles may be reduced without jeopardizing the effectiveness of the treatment.

There are 2 articles addressing the treatment of primary breast cancer with ECT. Tumors in both cases can be reached by commercial electroporators and electrodes.^{29,30} Future acceptance of electrochemotherapy into medical practice as a first-line treatment of primary deep-seated breast tumors and possible replacement of conventional neoadjuvant chemotherapy and surgical procedures shall take into account advantages, drawbacks, and limitations of this procedure. Advantages include the reduction in antineoplastic drug dosage, local therapy administration instead of a systemic route, and hence the reduction in adverse effect of conventional chemotherapy (myelosuppression), potential displacement of neoadjuvant chemotherapy and/or radical mastectomy, treatment enhancement of triple negative lesions for which hormone therapy, and use of drugs that target estrogen, progesterone, and HER-2 receptors are ineffective, an apoptotic process would be induced in the major part of the target tissues contributing to a beneficial immune response.

Drawbacks

Drug resistance contribution through activation of multiple drug resistance pumps due to low-drug concentration if

multiple ECT sessions are required and inflammatory response associated with necrosis achieved in irreversibly electroporated regions.

Limitations

Determination of patient-specific breast dielectric properties in order to accurately model electroporation of target tissues, accomplishment of image-guided electrode positioning according to the treatment planning, and development of suitable hardware and electrodes that provide enough energy to deliver the electric protocol determined by the treatment planning.

Conclusion

The development of realistic breast models combining the use of computational breast phantoms and patient-specific tumor reconstruction is presented in this work as a novel approach to the modeling of electroporation of invasive breast ductal carcinomas diagnosed by DBT imaging. In order to achieve a sufficient electric field distribution in the tumor and a surrounding safety margin composed of fibroglandular breast tissue and fatty tissue, 3 sets of electrodes consisting of 12 electrode arrays were investigated.

The outcomes showed that an efficient average coverage percentage of the tissues of interest (tumor and safety margin) in the 3 patients was achieved with 3 main electrode arrays: 4 needles in a delta configuration 4De2 (tumor: 98.50%, breast tissue: 91.03%, fatty tissue: 96.80%), 5 needles in a diamond configuration 5Di2 (tumor: 98.76%, breast tissue: 86.53%, fatty tissue: 95.50%), and 6 needles in a star configuration 6St2 (tumor: 99.50%, breast tissue: 92.96%, fatty tissue: 97.20%). Consequently, we can conclude that a single-electrode array seems unlikely to treat effectively all breast ductal carcinomas with electrochemotherapy, but a group of 3 electrode arrays may be sufficient to cover the target tissues when treating this disease. Although a complete coverage of target tissues in large tumors, as it was the case for patients 2 and 3, was difficult to achieve, it should be considered that these tumor dimensions are representative of most of the current stages detected in Mexican patients with breast cancer. These outcomes could probably be extrapolated to any population with an effective response to the treatment; however, its effectiveness may be potentiated if the disease is detected at an early stage. Finally, outcomes obtained in this work encourage the use of electrochemotherapy, which has fewer unwanted side effects than the systemic chemotherapy, such as high toxicity and myelosuppression, for the treatment of invasive breast ductal carcinoma. We imply that it is possible that in future this method may displace neoadjuvant chemotherapy and/or surgery in the treatment of breast cancer and probably be considered as a first-line treatment of primary tumors. Nevertheless, enrollment of patients and experimental application of the method presented in this work conducting a clinical trial will be required to validate this hypothesis.

Acknowledgments

The research was conducted in the scope of LEA EBAM (French-Slovenian European Associated Laboratory: Pulsed Electric Fields Applications in Biology and Medicine). Study was performed within Infrastructure Programme: Network of research infrastructure centers at University of Ljubljana (MRIC UL IP-0510).



Declaration of Conflicting Interests

The author(s) declared the following potential conflicts of interest with respect to the research, authorship, and/or publication of this article: Damijan Miklavc'ic holds patents on electrochemotherapy that have been licensed to IGEA S.p.a (Carpi, Italy) and is also consultant to various companies with interest in electroporation based technologies and treatments. The other authors have no competing interests.

Funding

The author(s) disclosed receipt of the following financial support for the research, authorship, and/or publication of this article: A.L. Vera Tizatl thanks the National Council for Science and Technology (CONACYT, Mexico) for the scholarship granted. Authors thank the National Council for Science and Technology (CONACYT, Mexico) for the support received with project CONACYT-F-Salud 2013-I-201590, 201256, project CSIC-COOPB20166 and Project EMHE-CSIC 200022. The authors acknowledge the financial support from the Slovenian Research Agency (ARRS (research core funding No. P2-0249, and project "Development and validation of treatment planning methods for treating cancer with electroporation based therapies" Z3-7126).

ORCID iD

Damijan Miklavc'ic, PhD  <http://orcid.org/0000-0003-3506-9449>
Bor Kos, PhD  <http://orcid.org/0000-0001-6219-7046>

Supplemental Material

Supplemental material for this article is available online.

References

1. Masson Doyma, M'xico SA, ed. *Consenso Mexicano sobre diagnóstico y tratamiento del cáncer mamario*. Mexico City, Mexico: Elsevier; 2015.
2. Types of breastcancer. <http://www.breastcancer.org/symptoms/types>. Updated November 9, 2016, Accessed December 14, 2016.
3. Stewart BW, Wild C, eds. *World Cancer Report 2014*. Lyon, France: International Agency for Research on Cancer; 2014.
4. Rems L, Miklavc'ic D. Tutorial. *Electroporation of cells in complex materials and tissue*. *J Appl Phys*. 2016;119(20):201101.
5. Davalos RV, Mir IL, Rubinsky B. Tissue ablation with irreversible electroporation. *Ann Biomed Eng*. 2005;33(2):223-231. doi:10.1007/s10439-005-8981-8.
6. Sersa G, Miklavcic D, Cemazar M, Rudolf Z, Pucihar G, Snoj M. Electrochemotherapy in treatment of tumours. *Eur J Surg Oncol*. 2008;34(2):232-240. doi:10.1016/j.ejso.2007.05.016.
7. Orłowski S, Belehradek J, Jr, Paoletti C, Mir LM. Transient electroporability of cells in culture. Increase of the cytotoxicity of anticancer drugs. *Biochem Pharmacol*. 1988;37(24):4727-4733. doi:10.1016/0006-2952(88)90344-9.

8. Miklavcic D, Mali B, Kos B, Heller R, Sersa G. Electrochemotherapy: from the drawing board into medical practice. *Biomed Eng Online*. 2014;13(1):29. doi:10.1186/1475-925x-13-29.
9. Sersa G, Cemazar M, Miklavcic D. Antitumor effectiveness of electrochemotherapy with cis-Diamminedichloroplatinum(II) in mice. *Cancer Res*. 1995;55(15):3450-3455.
10. Yarmush ML, Golberg A, Sersa G, Kotnik T, Miklavcic D. Electroporation-based technologies for medicine: principles, applications, and challenges. *Annu Rev Biomed Eng*. 2014; 16(1):295-320. doi:10.1146/annurev-bioeng-071813-104622.
11. Kamensek U, Cemazar M, Lamprecht Tratar U, Ursic K, Sersa G. Antitumor in situ vaccination effect of TNF α and IL-12 plasmid DNA electrotransfer in a murine melanoma model. *Cancer Immunol Immunother*. 2018;67(5):785-795. doi:10.1007/s00262-018-2133-0.
12. Mir LM, Orlowski S, Belehradec J, Jr, Paoletti C. Electrochemotherapy potentiation of antitumor effect of bleomycin by local electric pulses. *Eur J Cancer*. 1991;27(1):68-72. doi:10.1016/0277-5379(91)90064-k.
13. Sersa G, Miklavcic D, Cemazar M, et al. Electrochemotherapy in treatment of tumours. *Eur J Surg Oncol*. 2008;34(2):232-240. doi: 10.1016/j.ejso.2007.05.016.
14. Marty M, Sersa G, Garbay JR, et al. Electrochemotherapy—An easy, highly effective and safe treatment of cutaneous and subcutaneous metastases: results of ESOPE (European Standard Operating Procedures of Electrochemotherapy) study. *EJC Suppl*. 2006;4(11):3-13. doi:10.1016/j.ejcsup.2006.08.002.
15. Mali B, Jarm T, Snoj M, Sersa G, Miklavcic D. Antitumor effectiveness of electrochemotherapy: a systematic review and meta-analysis. *Eur J Surg Oncol*. 2013;39(1):4-16. doi:10.1016/j.ejso.2012.08.016.
16. Haberl S, Miklavcic D, Sersa G, Frey W, Rubinsky B. Cell membrane electroporation-Part 2: the applications. *IEEE Electrical Insulation Magazine*. 2013;29(1):29-37. doi:10.1109/mei.2013.6410537.
17. Campana LG, Galuppo S, Valpione S, et al. Bleomycin electrochemotherapy in elderly metastatic breast cancer patients: clinical outcome and management considerations. *J Cancer Res Clin Oncol*. 2014;140(9):1557-1565. doi:10.1007/s00432-014-1691-6.
18. Wichtowski M, Murawa D, Kulcenty K, Zaleska K. Electrochemotherapy in breast cancer—discussion of the method and literature review. *Breast Care*. 2017;12(6):409-414. doi:10.1159/000479954.
19. Matthiessen LW, Johannesen HH, Hendel HW, Moss T, Kamby C, Gehl J. Electrochemotherapy for large cutaneous recurrence of breast cancer: a phase II clinical trial. *Acta Oncol*. 2012;51(6): 713-721. doi:10.3109/0284186x.2012.685524.
20. Miklavcic D, Sersa G, Breclj E, et al. Electrochemotherapy: technological advancements for efficient electroporation-based treatment of internal tumors. *Med Biol Eng Comput*. 2012; 50(1):1213-1225.
21. Edhemovic I, Breclj E, Gasljevic G, et al. Intraoperative electrochemotherapy of colorectal liver metastases. *J Surg Oncol*. 2014; 110(3):320-327. doi:10.1002/jso.23625.
22. Cadossi R, Ronchetti M, Cadossi M. Locally enhanced chemotherapy by electroporation: clinical experiences and perspective of use of Electrochemotherapy. *Future Oncol*. 2014;10(5):877-890. doi:10.2217/fon.13.235.
23. Granata V, Fusco R, Piccirillo M, et al. Electrochemotherapy in locally advanced pancreatic cancer: preliminary results. *Int J Surg*. 2015;18:230-236. doi:10.1016/j.ijso.2015.04.055.
24. Bianchi G, Campanacci L, Ronchetti M, Donati D. Electrochemotherapy in the treatment of bone metastases: a phase II trial. *World J Surg*. 2016;40(12):3088-3094. doi:10.1007/s00268-016-3627-6.
25. Wichtowski M, Potocki P, Kufel-Grabowska J, Streb J, Murawa D. Electrochemotherapy in the treatment of massive, multisite breast cancer metastasis to the skin and subcutaneous tissue: a case report. *Breast Care (Basel)*. 2016;11(5):353-355. doi:10.1159/000450869.
26. Kalavathy G, Sasi KS, Manohar PE, Sundararajan R. Electrochemotherapy makes resectable from unresectable and pain reduction in chest wall recurrence breast cancer of two patients. *J Cancer Prev Curr Res*. 2015;3(2):00074. doi:10.15406/jepcr.2015.03.00074.
27. Schmidt G, Juhasz-Bo'ss I, Solomayer EF, Herr D. Electrochemotherapy in breast cancer: a review of references. *Geburtshilfe Frauenheilkd*. 2014;74(6):557-562. doi:10.1055/s-0034-1368538.
28. Sersa G, Cufer T, Paulin SM, Cemazar M, Snoj M. Electrochemotherapy of chest wall breast cancer recurrence. *Cancer Treat Rev*. 2012;38(5):379-386. doi:10.1016/j.ctrv.2011.07.006.
29. Cabula C. Neoadjuvant electrochemotherapy of breast cancer: our experience on first case treated in Italy. *Updates Surg*. 2012; 65(4):325-328. doi:10.1007/s13304-012-0170-3.
30. Denzi A, Strigari L, Di Filippo F, et al. Modeling the position-ing of single needle electrodes for the treatment of breast cancer in a clinical case. *Biomed Eng Online*. 2015;14(suppl 3): S1. doi:10.1186/1475-925x-14-s3-s1.
31. Neal RE, 2nd, Davalos RV. The feasibility of irreversible electroporation for the treatment of breast cancer and other heterogeneous systems. *Ann Biomed Eng*. 2009;37(12):2615-2625. doi:10.1007/s10439-009-9796-9.
32. Neal RE, 2nd, Singh R, Hatcher HC, Kock ND, Torti SV, Davalos RV. Treatment of breast cancer through the application of irreversible electroporation using a novel minimally invasive single needle electrode. *Breast Cancer Res Treat*. 2010;123(1):295-301. doi:10.1007/s10549-010-0803-5.
33. Zhang W, Wang W, Chai W, et al. Breast tissue ablation with irreversible electroporation in rabbits: a safety and feasibility study. *PLoS One*. 2017;12(7):e0181555. doi:10.1371/journal.pone.0181555.
34. Deipolyi AR, Golberg A, Yarmush ML, Arellano RS, Oklu R. Irreversible electroporation: the evolution of a laboratory technique to be used in interventional oncology. *Diagn Interv Radiol*. 2014;20(2):147-154. doi:10.5152/dir.2013.13304.
35. Zupanic A, Kos B, Miklavcic D. Treatment planning of electroporation-based medical interventions: electrochemotherapy, gene electrotransfer and irreversible electroporation. *Phys Med Biol*. 2012;57(17):5425-5440. doi:10.1088/0031-9155/57/17/5425.
36. Smith A. Fundamentals of breast tomosynthesis: improving the performance of mammography, 2012, 78967-12_WP-00007_

- FundmntlsTomo. <http://web.psmedical.it/DOC/Fundamentals.pdf>. Updated 2008, Accessed June 23, 2018.
37. Ertas M, Yildirim I, Kamasak M, Akan A. Digital breast tomosynthesis image reconstruction using 2D and 3D total variation minimization. *Biomed Eng Online*. 2013;12(1):112. doi:10.1186/1475-925x-12-112.
 38. Sechopoulos I. A review of breast tomosynthesis. Part II. Image reconstruction, processing and analysis, and advanced applications. *Med Phys*. 2013;40(1):014302. doi:10.1118/1.4770281.
 39. Zastrow E, Davis SK, Lazebnik M, Kelcz F, Van Veen BD, Hagness SC. Development of anatomically realistic numerical breast phantoms with accurate dielectric properties for modeling microwave interactions with the human breast. *IEEE Trans Biomed Eng*. 2008;5(12):2792-2800. doi:10.1109/tbme.2008.2002130.
 40. Numerical Breast Phantoms Repository. <http://uwcem.ece.wisc.edu/MRIdatabase/>. Accessed October 12, 2017.
 41. Sickles EA, D'Orsi CJ, Basset LW, et al. ACR BI-RADS[®] Mammography. In: ACR BI-RADS[®] Atlas. Breast Imaging Reporting and Data Syste. Reston, VA: American College of Radiogy; 2013.
 42. Moran MS, Schnitt SJ, Giuliano AE, et al. Society of Surgical Oncology–American Society for Radiation Oncology Consensus Guideline on Margins for Breast-Conserving Surgery With Whole-Breast Irradiation in Stages I and II Invasive Breast Cancer. *Int J Radiat Oncol Biol Phys*. 2014;88(3):553-564. doi:10.1016/j.ijrobp.2013.11.012.
 43. Jossinet J. Variability of impedivity in normal and pathological breast tissue. *Med Biol Eng Comput*. 1996;34(5):346-350. doi:10.1007/bf02520002.
 44. Surowiec AJ, Stuchly SS, Barr JB, Swarup A. Dielectric properties of breast carcinoma and the surrounding tissues. *IEEE Trans Biomed Eng*. 1988;35(4):257-263. doi:10.1109/10.1374.
 45. Gabriel S, Lau RW, Gabriel C. The dielectric properties of biological tissues: III. Parametric models for the dielectric spectrum of tissues. *Phys Med Biol*. 1996;41(11):2271-2293. doi:10.1088/0031-9155/41/11/003.

APPENDIX D: CONFERENCE PAPER (PRODUCTIVITY)



2016 GLOBAL MEDICAL ENGINEERING PHYSICS EXCHANGES/PAN AMERICAN HEALTH CARE EXCHANGES (GMEPE / PAHCE)

Review of Electrochemotherapy-based Treatment of Cutaneous, Subcutaneous and Deep-seated Tumors towards Specific Treatment Planning

A. L. Vera Tizatl¹, S. Rodríguez Cuevas², L. Leija Salas¹ and A. Vera Hernández¹
¹CINVESTAV-IPN, Mexico D.F., Mexico

²Instituto de Enfermedades de la Mama, FUCAM, Mexico

Abstract — Electrochemotherapy is an electroporation-based treatment successfully used in palliation of cutaneous and subcutaneous tumors. Its high response rate encourage further research on electrochemotherapy applied in deep tissues as a minimally invasive procedure for primary tumors. In order to assess electrochemotherapy effectiveness in breast primary tumors in Mexico, it is presented a review of background, current aspects and perspectives of this technique reported in Europe thus the identification of technological requirements to be attended are discussed.

Keywords — deep-seated tumor, electrochemotherapy, electroporation, treatment planning

I. INTRODUCTION

In 1982, the term Electroporation (EP) was introduced to describe the increased permeability of a cell to otherwise low permeant or nonpermeant molecules that do not diffuse across the plasma membrane and for which there are no active transporters. Demonstration of this phenomenon requires the “electropermeabilization” of cell. The most common electroporation theory trying to explain cell electropermeabilization is the one developed by Eberhard Neumann which points out that normal fluctuations of the cell membrane are enlarged by an induced transmembrane potential difference, thus causing its exposure to an intense external electric field resulting in large hydrophobic pores which then become hydrophilic [1, 2]. Regarding cell viability, there are two types of EP: reversible electroporation (REP) in which cell membrane recovers after electric pulse application and irreversible electroporation (IRE) in which conversely, cell death is induced because of impossibility of maintaining cell homeostasis [1]. In spite of the progress reached by many groups of research regarding EP, there is still a large lack of

knowledge on the mechanism of cell electropermeabilization [1]. All data available up to the moment have been obtained as an indirect evidence of membrane electropermeabilization such as conductivity changes measurements and observations of molecular transport through the cell membrane [2, 3]. Nevertheless, EP is currently used in biotechnological applications (for microbial deactivation and shelf time prolongation of beverages) and in medical applications such as gene transfection, gene therapy, DNA vaccination, cell electrofusion and electrochemotherapy (ECT) [2, 4]. This latter is used for improved drug delivery for cancer

treatment and was carried out for the first time *in vivo* by L. M. Mir in 1989 and consists in the combination of REP with the use of cytotoxic chemotherapeutic drugs in order to increase its uptake through the cellular membrane. Since then many treatment protocols and high voltage pulse generators were developed [5, 6] and ECT have been successfully used in Europe in the treatment of cutaneous and subcutaneous solid tumors regardless its histological origin [3].

In order to standardize ECT application, standard operating procedures (SOP) in the clinical practice were developed, thus two projects were founded by the European Commission based on the experience of the leading European cancer centers on ECT: a medical grade device for EP, CliniporatorTM (IGEA, Spa, Italy) in 2000 and the ESOP (European Standard Operating Procedures of Electrochemotherapy) in 2003. The main aim of SOP is to offer oncologists a decision tree for safe and convenient treatment of cutaneous and subcutaneous metastatic tumors not deeper than 1 cm through selection of the adequate administration route of cytotoxic drug, type of anesthesia and the type of electrode to be used according to the number (< 20) and thickness (< 2cm) of tumors to be treated [7, 8, 9]. SOP describe as well inclusion and exclusion criteria for patient selection and are currently followed by 120 oncological centers in 18 European countries [7, 3]. Due to effectiveness of this technique, there is a current interest in spreading its use to the treatment of deep-seated tumors [3] and to this purpose technology has been modified for application of ECT in larger and deeper lesions [8]. Therefore, a new generation of the Cliniporator device (Cliniporator Vitae, IGEA, Spa, Italy) has been developed along with three new needle electrodes types [4, 8] and ECG synchronization capabilities concerned to the treatment of tumors located near the heart [8, 10]. Despite technology already existent, it is mandatory the development of new standard protocols based on individual treatment planning [8].

Since the use of medical devices such as Cliniporator is restricted to European Union, the goal of this review is to describe the most relevant aspects of EP and ECT to identify the technological advances and the current trends of its use in the treatment of deep-seated tumors which have to be considered for the development of an electroporation system aimed to assessment of ECT in primary breast cancer in Mexico. It is our purpose to identify parameters influencing

ECT effectiveness thus background, current issues and perspectives of ECT are described.

II. BACKGROUND OF ELECTROCHEMOTHERAPY

A. Biophysics aspects of Electroporation

In order to describe electroporation phenomenon, many theoretical models have been developed among which the transient aqueous pore model is the most accepted [2]. This model states that exposition of cells (either in a culture medium or in tissue) to an external electric field leads to the reorientation of electrical charges on the cell membrane by inducing a transmembrane potential which superimposes to the normal transmembrane potential of cell and provides free energy necessary for structural rearrangement of membrane phospholipids, causing an increase in membrane permeability [2, 8, 9]. When a sufficiently strong electric field is reached, there is a hydrophilic pore formation in a small fraction of the lipid bilayer, arising from expansion of hydrophobic pores formed in turn by spontaneous thermal fluctuation of membrane lipids. Hydrophilic pores allows then the passage of non-permeant molecules into the cell. The electric field distribution can be determined by solving the Laplace equation [3, 12] and the induced transmembrane voltage leading to a consequent increased conductivity follows Schwan equation [2, 8]. Theoretical values obtained by this equation were observed experimentally with potentiometric dyes in spherical single-cells for which EP occurs when transmembrane potential exceeds 1.5 V [2, 8, 9]. EP is affected by three main parameters; electric pulse parameters, chemical composition of the media used and traits of the cells exposed to the external electric field. The electric pulse parameters to be used depend on the desired application of EP (i. e., introduction of different molecules into the cell, electrofusion, water sterilization or food preservation) [2, 4].

EP can be considered as a threshold phenomenon since depending on the pulse electric parameters, EP can be either reversible (REP) or irreversible (IRE). In the case of REP, induced pores are transient, hence membrane restoration is possible. Conversely in IRE, induced pores are permanent, thus leading to cell death because of impossibility of maintaining cell homeostasis. REP consists of three main phases; pore formation (lasting a few microseconds), time dependent expansion of pore size (lasting throughout the duration of the pulse) and pore resealing (taking place after electric pulse application). There have been stated electric field threshold values of 460 V/cm and 700 V/cm for REP and IRE respectively [2, 3].

B. Electrochemotherapy process

ECT is a particular medical application of the reversible electroporation, in which besides the exposition of cell

membrane to intense electric pulses, the administration of poorly permeant hydrophilic chemotherapeutic drugs is used for the treatment of cancerous tissue [8, 11]. Therefore, ECT takes advantage of electroporation to enhance intracellular drug accumulation. Several studies regarding the potentiation of diverse drugs (29) in combination of EP have been carried out *in vitro* and *in vivo* from which bleomycin (BM) and cisplatin (cis-diammine-dichloroplatinum (II) - CDDP) resulted to be the most potentiated by factors of around 5000 and 12 fold respectively [8, 11]. Both of these drugs acts upon DNA by hampering its synthesis. Under non-permeabilized conditions, BM transport through the plasma membrane is achieved by carrier proteins reaching a systemic absorption of about 45% (for BM) and 20% (for CDDP) [8, 11].

Experimentally, it has been stated that for introduction of small molecules such as cytotoxic drugs, a train of short electric pulses in the range of tens to hundreds of microseconds are generally used. On the other hand during EP, medium heating depends on its composition and the pulse length. For short electric pulses in the range of microseconds, joule heating in high conductivity media is negligible whereas for long pulses in the range of milliseconds, joule heating becomes more pronounced in high conductivity media than in low conductivity media. In addition, pulses must be applied with a repetition frequency ranging from 0.5 to 10 Hz in order to ensure pore resealing and thus cell viability [2].

In order to control the ablation zone caused by cytotoxic drug uptake, electric field distribution needs to be determined. Electric field threshold for ECT depends on several physical, biological and electric pulse parameters and a value of 460 V/cm for REP and thus for ECT was determined experimentally in liver and muscle by comparison of histological changes in tissue observed before and after ECT [4, 13, 14].

C. Standard Operating Procedures

SOP were developed to standardize parameters used in ECT application in accessible cutaneous and subcutaneous tumors and are suggested to be used along with the medical grade EP-device CliniporatorTM [12]. A map of decision for clinicians is the major contribution of SOP allowing determination of electrode type to be used among the tree offered by the device (I: plate shaped for cutaneous lesions less than 1cm, II: parallel needle electrode lesions less than 4 mm and III: hexagonal array of needle electrodes bigger than 1 cm), the route administration of cytotoxic drug (Intratumoral for bleomycin and cisplatin and intravenous for bleomycin only), anesthesia and electrical parameters of pulse depending on tumor diameter (less than 2 cm), depth in the case of subcutaneous tumors (less than 1 cm) and the number of lesions (less than 20) [7, 12]. Therefore SOP

offer 4 treatment protocol (TA: local anesthesia and intratumoral route, TB: local anesthesia and intravenous route, TC: general anesthesia and intratumoral route, TD: general anesthesia and intravenous route). Exclusion criteria for ECT use is based on patient clinic history including heart diseases (cardiac arrhythmia, previous cardiac events and pacemaker presence), pulmonary fibrosis, allergies to BM or CDDP, cumulative BM dosage of 400,000 IU/m², INR > 1.5 (in the case of invasive protocols, i. e., the use of needle electrodes) and creatinine > 150 mol/L (in order to dismiss renal failure) [7]. Regarding electric pulsing parameters, the protocol suggested consist of a train of eight 100 s-long monopolar pulses applied with repetition frequency of 1 Hz and 5 kHz [7, 8, 9, 13, 14]. It is worthy to remark that no theoretical justification supports the use of this pulsing protocol and it was suggested based on the experimental experience of the European cancer centers on ECT [8, 9].

D. Outcomes obtained in cutaneous and subcutaneous tumors

The use of ECT as a local tumor treatment for superficial tumors have proved to be effective even for a single -session ECT and quantitative effectiveness was determined through the assessment of the response of different treated tumors in clinical trials before (592 tumors) and after (1664 tumors corresponding to approximately 3000 patients until August 2013) ESOPE publication in 2006 [15]. Response was classified as complete response (CR), partial response (PR), objective response (OR = CR + PR) and no response (NR = no change + progressive disease) reported in percentage. Comparison showed that OR and PR increased (from 77.4% to 88.8% and from 16.3% to 26.9% respectively) and NR significantly decreased (from 22.6% to 11.2%). In turn, CR remained almost unaltered (from 61.1 % to 62.0%) [3, 4, 8, 9]. ECT has been used as treatment for squamous cell carcinoma, melanoma, adenocarcinoma, Kaposi sarcoma, transitional cell carcinoma of the urinary bladder and head and neck tumors and the highest effectiveness has been achieved on basal cell carcinoma. Current predominant uses of ECT in superficial tumors are the palliation of metastasis in patient who have undergone many previous unsuccessful procedures, treatment of tumors located in the head and neck area where optimal cosmetic outcome influence patient quality of life [8, 9].

E. Parameters influencing electrochemotherapy effectiveness

The effectiveness of ECT depends upon many physical and biological factors as it is on electrical traits of high-pulse delivery protocol (Table I). The main goal of ECT is to ensure the highest uptake of drug into tumor cells and the least uptake into healthy cells. In addition, uptake depends on local availability of the drug which is related in turn to intratumoral distribution, membrane permeabilization level

which depends on induced transmembrane potential. Therefore, parameters influencing effectiveness are related to each other and the induced electric field is the most important parameter. A method of ensuring that drug reaches the target is to administer it before applying high-voltage pulses. If drug is intratumorally injected, the maximal extracellular concentration can be obtained. Nonetheless, due to heterogeneity of tissue, drug administration route cannot guarantee that enough concentration is achieved everywhere inside the tumor [4]. Time between drug administration and treatment protocol delivery appear to be calculated based on pharmacokinetic and pharmacodynamic studies of a particular drug.

F. Electrochemotherapy advantages

Outcomes regarding cutaneous and subcutaneous ECT-based treatment awake increasing interest in spreading its use to the treatment of deep -seated tumors. Some of its advantages are high response rate in local tumor control, increased response rate for repetitive sessions of ECT, limited effect on healthy tissue, lower drug concentrations requirements, immune response preservation, effectiveness on previous unsuccessfully treated tumors, minimal invasiveness, few secondary effects (muscle contraction), “heat sink” effect absence which allows it to be used near major vessels [4]. ECT has been particularly accepted for the treatment of head and neck tumors since systemic treatments in this type of lesions show limited efficacy and local procedures in turn, compromise patient quality of life due to mutilating possibility [9].

III. STATE OF ART OF ELECTROCHEMOTHERAPY IN DEEP SEATED TUMORS

Since SOP were developed for cutaneous and subcutaneous tumors, they are not expected to be efficient in the treatment of deep-seated tumors which are likely to be bigger and more irregular than cutaneous and subcutaneous tumors. In addition, internal tumors might be located near vital organs, thus special attention must be paid to safety considerations [12, 16]. In addition, significant variation on the electrical properties of target and the surrounding tissue is another aspect to be minded [12]. Therefore, patient-specific treatment planning must be designed along with the development of the appropriate technology to reach deep tissues. If it is considered that in radiotherapy, interaction between a physical agent (radiation) and biological tissue is to be determined, an analogy of ECT with this procedure is possible if it is assumed that in this case the physical agent results to be the external electric field. Based on this analogy, steps suggested to reach a patient-specific treatment planning are [3, 12];

offer 4 treatment protocol (TA: local anesthesia and intratumoral route, TB: local anesthesia and intravenous route, TC: general anesthesia and intratumoral route, TD: general anesthesia and intravenous route). Exclusion criteria for ECT use is based on patient clinic history including heart diseases (cardiac arrhythmia, previous cardiac events and pacemaker presence), pulmonary fibrosis, allergies to BM or CDDP, cumulative BM dosage of 400,000 IU/m², INR > 1.5 (in the case of invasive protocols, i. e., the use of needle electrodes) and creatinine > 150 mol/L (in order to dismiss renal failure) [7]. Regarding electric pulsing parameters, the protocol suggested consist of a train of eight 100 s-long monopolar pulses applied with repetition frequency of 1 Hz and 5 kHz [7, 8, 9, 13, 14]. It is worthy to remark that no theoretical justification supports the use of this pulsing protocol and it was suggested based on the experimental experience of the European cancer centers on ECT [8, 9].

D. Outcomes obtained in cutaneous and subcutaneous tumors

The use of ECT as a local tumor treatment for superficial tumors have proved to be effective even for a single-session ECT and quantitative effectiveness was determined through the assessment of the response of different treated tumors in clinical trials before (592 tumors) and after (1664 tumors corresponding to approximately 3000 patients until August 2013) ESOPE publication in 2006 [15]. Response was classified as complete response (CR), partial response (PR), objective response (OR = CR + PR) and no response (NR = no change + progressive disease) reported in percentage. Comparison showed that OR and PR increased (from 77.4% to 88.8% and from 16.3% to 26.9% respectively) and NR significantly decreased (from 22.6% to 11.2%). In turn, CR remained almost unaltered (from 61.1 % to 62.0%) [3, 4, 8, 9]. ECT has been used as treatment for squamous cell carcinoma, melanoma, adenocarcinoma, Kaposi sarcoma, transitional cell carcinoma of the urinary bladder and head and neck tumors and the highest effectiveness has been achieved on basal cell carcinoma. Current predominant uses of ECT in superficial tumors are the palliation of metastasis in patient who have undergone many previous unsuccessful procedures, treatment of tumors located in the head and neck area where optimal cosmetic outcome influence patient quality of life [8, 9].

E. Parameters influencing electrochemotherapy effectiveness

The effectiveness of ECT depends upon many physical and biological factors as it is on electrical traits of high-pulse delivery protocol (Table I). The main goal of ECT is to ensure the highest uptake of drug into tumor cells and the least uptake into healthy cells. In addition, uptake depends on local availability of the drug which is related in turn to intratumoral distribution, membrane permeabilization level

which depends on induced transmembrane potential. Therefore, parameters influencing effectiveness are related to each other and the induced electric field is the most important parameter. A method of ensuring that drug reaches the target is to administer it before applying high-voltage pulses. If drug is intratumorally injected, the maximal extracellular concentration can be obtained. Nonetheless, due to heterogeneity of tissue, drug administration route cannot guarantee that enough concentration is achieved everywhere inside the tumor [4]. Time between drug administration and treatment protocol delivery appear to be calculated based on pharmacokinetic and pharmacodynamic studies of a particular drug.

F. Electrochemotherapy advantages

Outcomes regarding cutaneous and subcutaneous ECT-based treatment awake increasing interest in spreading its use to the treatment of deep-seated tumors. Some of its advantages are high response rate in local tumor control, increased response rate for repetitive sessions of ECT, limited effect on healthy tissue, lower drug concentrations requirements, immune response preservation, effectiveness on previous unsuccessfully treated tumors, minimal invasiveness, few secondary effects (muscle contraction), “heat sink” effect absence which allows it to be used near major vessels [4]. ECT has been particularly accepted for the treatment of head and neck tumors since systemic treatments in this type of lesions show limited efficacy and local procedures in turn, compromise patient quality of life due to mutilating possibility [9].

III. STATE OF ART OF ELECTROCHEMOTHERAPY IN DEEP SEATED TUMORS

Since SOP were developed for cutaneous and subcutaneous tumors, they are not expected to be efficient in the treatment of deep-seated tumors which are likely to be bigger and more irregular than cutaneous and subcutaneous tumors. In addition, internal tumors might be located near vital organs, thus special attention must be paid to safety considerations [12, 16]. In addition, significant variation on the electrical properties of target and the surrounding tissue is another aspect to be minded [12]. Therefore, patient-specific treatment planning must be designed along with the development of the appropriate technology to reach deep tissues. If it is considered that in radiotherapy, interaction between a physical agent (radiation) and biological tissue is to be determined, an analogy of ECT with this procedure is possible if it is assumed that in this case the physical agent results to be the external electric field. Based on this analogy, steps suggested to reach a patient-specific treatment planning are [3, 12];

TABLE I
PARAMETERS INFLUENCING ECT EFFECTIVENESS [3, 8, 12]

Physical	Biological	Electrical	Others
Cell shape	Cytoskeleton structure	Amplitude	Drug administration route
Cell size	Membrane composition	Length	Time between drug administration and treatment delivery
		Number	Insertion depth of needle
		Repetition frequency	

1) *Specific anatomical model to EP*: obtained from medical images (CT, RMI) for segmentation and subsequent 3D reconstruction, this model of EP is aimed to be analyzed and post-processed by numerical methods such as finite element method (FEM) [3, 12, 16].

2) *Treatment planning*: aimed to suggest the optimal number of electrodes, its positioning and electric potential to be applied in order to obtain the numerical prediction of the electroporated regions by the use of numerical methods in order to cover the complete tumor and the minimal healthy surrounding tissue. Input parameters to numerical method comprise electric conductivity of target and surrounding tissue, electric field threshold values for EP. Modern models consider conductivity changes in tissue during the pulse delivery [3, 4, 12, 16].

3) *Set-up verification*: regarding intraoperative positioning of electrodes based on the configuration suggested by the treatment planning step [3, 4, 12, 16].

4) *Treatment delivery*: once patient and electrodes are positioned, electrodes are connected to the corresponding outputs of the EP device and pulses are delivered [3]. Surprisingly SOP protocols are reported to be used in the same way for deep-seated tumors [3, 4]. In case many tumors are to be treated a therapeutic window (based on mean life of cytotoxic drug) must be determined in order to ensure effective uptake [3, 16].

5) *Postsurgical response assessment*: evaluated radiologically and by histological analyses, 4 to 8 weeks after ECT application [3, 4, 16].

Current technological development are focused on treatment of deep-seated tumors. For this purpose, the Cliniporator Vitae™ (IGEA, Carpi, Italy) was developed as an extended version of Cliniporator™. It offers three novel electrodes designed to reach specific deep lesions

(Table II) and 6 outputs for needle electrodes which can be activated in pairs (only two at a time) [patient-spe]. On the other hand, delivery of electric pulses is synchronized with ECG through the AccuSync 42 (AccuSync Medical Research Corp. Milford, CT, USA) in order to avoid the pulse delivery during the vulnerable period of ventricles [3, 17, 18]. Nevertheless, recent studies demonstrate weaknesses of the synchronization protocol and suggest R wave of ECG as the best time of delivering of ECT protocol [10]. Amplitude voltage of pulses (up to 3000 V) and delivery protocols remains the same as in Cliniporator™.

IV. ELECTROCHEMOTHERAPY ROLE IN MEXICO

Regarding primary and metastatic skin tumors, a clinical trial using ECT with intralesional BM was carried out in 2001. It was approved by the Scientific and Ethics Committee of the Hospital de Oncologia in Mexico. 34 metastatic nodules (in 15 patients) previously treated by radiotherapy and chemotherapy showing no response, were treated by ECT. Electroporation device for this study was developed by the Biomedical Engineering Department. A single session of 4 pulses of 100 s and 1 Hz frequency repetition were applied. Response rates were reported to be: CR = 50%, PR = 17% and NR = 33%. Outcomes in skin tumors encouraged further research on the use of ECT as treatment of primary deep-seated tumors [18]. On the other hand, breast cancer in Mexico is reported to be the first cause of death due to cancer in women. Ordinary treatment for this disease are invasive procedures such as radiotherapy, chemotherapy and mutilating surgical resection causing undesirable secondary effects like hair loss, nausea and fibrotic tissue formation due to healing processes. Therefore, development of alternative treatment procedures based on selective minimally invasive ablation techniques such as ECT are current subject of study.

TABLE II
ELECTRODES FOR CLINIPORATOR VITAE [4,8]

Electrode type	Appearance		
	Material	Dimensions [mm]	Tumor Location
Long needle	Stainless steel	Diameter: 1.2 Length: 127 (insulating sleeve), 30 (active tip)	Metastases of colorectal tumors in liver. Bone metastases Soft tissue sarcomas
Endoluminal (plate)	Stainless steel	Electrode: 10x26 Separation: 10	Colorectal, gastric and esophageal tumors
Expandable	Stainless steel	--	Brain tumors

Since the use of medical grade electroporation devices is restricted to Europe only, it was designed an electroporation system to be used in deep breast tumors in which low resistivity values range from 100 cm to 1 K cm depending on the type of tissue and the operation frequency. Electroporation system includes a high voltage source (200 V to 1000 V) a high voltage pulse generator providing rectangular pulses variable in width (50 s to 500 s) and frequency repetition (1 Hz to 10 kHz) and c) a communication interface allowing the selection of a specific protocol [19, 20, 21]. Further studies aimed to the assessment of this EP system are required and owing to this fact, our research group is currently focused on the technological optimization of the Electroporation system in order to generate rectangular pulses of up to 1500 V. In addition it is our goal to design adequate electrodes aimed to reach deep breast tumors by minimal invasiveness. Prior to the delivery of the treatment it is our interest to develop a method of treatment planning based on 3D reconstruction of lesions imaging and its numerical processing.

V. DISCUSSION

In spite of accurate prediction of the electric field on a spherical single-cell calculated by solving the Laplace equation, effective prediction of electric field distribution *in vivo* demands much more realistic models since tissues are composed of different cellular types which are irregularly shaped, vascularized and present different electrical properties. Consequently, this realistic model should take into consideration changes in conductivity while ECT is performed. Nevertheless it represents a current challenge since a main problem regarding conductivity measurement *in vivo* is the inhomogeneous distribution of electric field due to inhomogeneous and anisotropic properties of the tissue [1, 2, 3, 4, 8, 9, 10]. The effective ECT-based treatment of deep-seated tumors requires strict design of treatment planning specific to each patient in order to minimize damage to healthy tissue. Leading treatment planning into clinical practice require optimization of the procedure. First, segmentation of medical images require special attention since target tissue (e. g., tumor, kidney, liver, brain, etc.) is commonly heterogeneously texturized hence intensities that describes these objects vary. An appropriate three-dimensional model generated from image segmentation is required for suggesting the number and positioning of electrodes to be used. Currently the achievement of exact positioning of electrodes with respect to suggestion obtained from the treatment planning is not efficient. Some reasons include the deformable nature of tissues and the manual positioning of electrodes. The number of electrodes to treat deep -seated tumors has not been formally settled and up to the moment it is based on surgeon suggestion depending on the possible routes of positioning. However, it must be determined considering both the complete coverage of neoplastic tissue and the

preservation of the minimal invasiveness desired for the procedure (i. e., the least number of electrodes). New electrodes might be designed in order to be ultrasound-visible and guided, thus materials used to this purpose need to be considered along with the scattering effect in correlation with electrodes under ultrasound since surgical materials show very high acoustic impedance. This new electrodes might allow use of ECT in unresectable lesions or tumors localized near vital organs [4]. Conductivity monitoring in real-time should be performed so it could be re-inserted into the numerical model for modification of electrode positioning according to conditions found *in situ* and so further recalculation of electric field distribution could be achieved. Up to the moment, the prediction models of EP are based on the determination of the applied electric field distribution dismissing stochastic nature of EP phenomenon due to cellular heterogeneity, cellular density and cellular communication, which should be inserted in the specific-patient model [3, 8, 9, 10, 17, 18].

On the other hand, the determination of EP threshold values for deep tissues and the development of statistical model of EP in tissue are required to obtain further increased response rate of ECT. Despite the demonstrated effectiveness of ECT as palliation procedure in the treatment of metastatic cutaneous and subcutaneous tumors, there is still lack of evidence for using ECT as curative treatment of primary tumors thus future clinical trial must be carried out. It is suggested to explore further combination of cytotoxic drugs with recently developed tyrosine kinase inhibitors to assess possibility of effectiveness increase. In addition, it is important to explore the use of other drugs in case BM or CDDP are contraindicated or cumulative dose of BM is reached [3, 8, 12]. Contrary to the impressive success of the electroporation techniques, molecular membrane processes of electroporation are not yet well understood and require active investigation. Treatment planning is on its early stages and future optimization is required in order to simplify the procedure [8, 9, 10].

V. CONCLUSION

Nowadays, ECT represent an effective minimally invasive palliation treatment for cutaneous and subcutaneous tumors in Europe in spite of the lack of theoretical justification supporting experimental outcomes obtained from clinical trials. Our research group is fond of the assessment of electrochemotherapy effectiveness in breast primary tumors in Mexico. For this purpose, technological challenges must be overcome including the development of an electroporation system, the design of new electrodes in order to reach the target tissue by imaging guidance while preserving the minimally invasiveness of the procedure and the implementation of a treatment planning algorithm considering electric field distribution, insertion

depth of electrodes and kinetic analyses of the drug which seem to be crucial parameters to control ablation zone and to achieve higher complete response rates. Special emphasis regarding numerical methods has to be made since they represent the only current way of prediction of electric field distribution applied to deep-seated tumors which are most likely to be non-homogeneous, non-linear and anisotropic, thus dielectric properties of target and surrounding tissue must be accurately determined. For deep-seated tumors, time in which treatment is to be applied becomes a critical factor when considering time required for electrode positioning and half time of the cytotoxic drug to be administered. The review of current clinical trials aimed to the assessment of ECT in deep tissues, reveals that treatment protocols suggested by SOP are used for this purposes even though they were developed for the treatment of cutaneous lesions. Since distribution of external electric field is the most important factor to predict in order to control ablation zone, appropriate electrical parameters of pulse must be determined for specific deep tissues. In turn, based on this parameters, new electric field threshold values for ECT in deep tissue must be calculated in addition to new standard protocols of treatment.

ACKNOWLEDGMENT

Authors thank the National Council for Science and Technology (CONACYT, Mexico) for the support received for the project CONACYT-Salud 2013-I-201590, 201256, Joint Cooperation México-Uruguay (SRE-AUCI) 2012-2013 and CSIC-COOPB20166.

REFERENCES

- [1] L. M. Mir, "Application of Electroporation Gene Therapy: Past, Current and Future" in *Electroporation Protocols preclinical and Clinical Gene Medicine*, S. Li, Ed. Totowa, NJ: Humana Press, 2008, ch. 1, pp. 3-18.
- [2] M. Kanduser, D. Miklavcic, "Electroporation in Biological Cell and Tissue: An Overview" in *Electrotechnologies for Extraction from Food Plants and Biomaterials*, N. Lebovka, E. Vorobiev, Ed. N.Y: Springer, 2008, ch. 1, pp. 1-37.
- [3] D. Pavliha, B. Kos, A. Zupanic, M. Marcan, G. Sersa and D. Miklavcic, "Patient-specific Treatment Planning of Electrochemotherapy: Procedure Design and possible pitfalls", *Bioelectrochemistry*, vol. 87, pp. 265-273, Jan. 2012
- [4] D. Miklavcic et. al, "Electrochemotherapy: technological advancements for efficient electroporation-based treatment of internal tumors", *Med. Biol. Eng. Comput.*, vol. 50, no. 10, pp. 1213-1225, Nov. 2012.
- [5] A. G. Hofmann, S. Dimmer, G. S. Nanda, "Electroporation therapy: A new Approach for the Treatment of Head and Neck Cancer", *IEEE Trans. Biomed. Eng.*, vol. 46, no. 6, pp. 752-759, 1999.
- [6] A. Ivorra, "Tissue Electroporation as a Bioelectric Phenomenon: Basic Concepts" in *Irreversible Electroporation*, B. Rubinsky, Ed. Berkeley California: Springer, 2009, ch. 2, pp. 23-62.
- [7] L. M. Mir et al, "Standard operating procedures of the electrochemotherapy: instructions for the use of bleomycin or cisplatin administered either systemically or locally and electric pulses delivered by the Cliniporator™ by means of invasive or non-invasive electrodes", *EJC Supplements*, vol. 4, pp. 14-25, Aug. 2006.
- [8] D. Miklavcic, B. Mali, B. Kos, R. Heller and G. Sersa. (2014). Electrochemotherapy: from the drawing board into medical practice. *BioMedical Engineering* [Online]. 13(29). Available: <http://www.biomedical-engineering-online.com/content/13/1/29>.
- [9] R. Cadossi, M. Ronchetti, M. Cadossi, "Locally enhanced chemotherapy by electroporation: clinical experience and perspective of use of ECT", *Future Concol*, vol. 10, no. 5, pp. 877-890, 2014.
- [10] B. Mali, D. Miklavcic, G. Sersa, "Comparison of protocols for synchronized electroporation pulse deliver" in *Proc. 6th European Conference of the International Federation for Medical and Biological Engineering*, vol. 45, Switzerland, 2015 pp. 586-589.
- [11] G. Sersa, M. Cemazar, M. Snoj, "Electrochemotherapy of tumors" *Current Oncol*, vol. 16, no. 2 pp. 34-35, 2009.
- [12] B. Kos, A. Zupanic, T. Kotnik, M. Snoj, G. Sersa, D. Miklavcic, "Robustness of treatment planning for electrochemotherapy of deep-seated tumors", *J. Membrane Biol*, vol. 236, pp. 147-153, 2010.
- [13] D. Miklavcic, D. Sermov, H. Mekid, L. Mir, "A validated model of in vivo electric field distribution in tissues for electrochemotherapy and for DNA electrotransfer for gene therapy", *Biochim. Biophys. Acta Gen. Subj*, vol. 1523, pp. 73-83, 2000.
- [14] S. Corovic, A. Zupanic, S. Kranjc, B. Al Sakere, A. Leroy-Willing, L. Mir et al., "The influence of skeletal muscle anisotropy on electroporation: in vivo studying and numerical modeling", *Med. Biol. Eng. Comput.* vol. 48, pp. 637-648, 2010.
- [15] B. Mali, T. Jarm, M. Snoj, G. Sersa, D. Milavcic, "Antitumor effectiveness of electrochemotherapy: a systematic review of meta-analysis", *Eur. J. Surg. Oncol.* vol. 19, pp. 4-16, 2013.
- [16] D. Pavliha, B. Kos, M. Marcan, A. Zupanic, G. Sersa, D. Milavcic. "Planning of electroporation-based treatments using web-based treatment planning software", *J. Membrane Biol.* vol. 246, pp. 833-842, 2013.
- [17] A. Deodhar, T. Dickfeld, G. Single, W. Hamilton, R. Thornton, C. Sofocleus, et al., "Irreversible electroporation near the heart: ventricular arrhythmias can be prevented with ECG synchronization", *Am. J. Roentgenol.* vol. 196, pp. 330-335, 2011.
- [18] B. Mali, T. Jarm, S. Corovic, M. Paulin-Kosir, M. Cemazar, G. Sersa et al., "The effect of electroporation pulses on functioning of the heart", *Med. Biol. Eng. Comput.* vol. 46, pp. 745-757, 2008.
- [18] S. Rodriguez-Cuevas, S. Barroso-Bravo, J. Almanza-Estrada, L. Cristóbal-Martínez, E. González-Rodríguez., "Electrochemotherapy in primary and metastatic skin tumors: phase II clinical trial using intralesional bleomycin", *Archives of Medical Research.* vol. 32, pp. 273-276, 2001.
- [19] A. L. Vera-Tizatl, "Desarrollo de un sistema de electroporación para ser aplicado en tejido canceroso", M. of A. T. dissertation, Programa en Tecnología Avanzada, UPHITA-IPN. Mexico city, Mexico, 2013.
- [20] A. L. Vera-Tizatl, L. I. Garay-Jiménez, R. R. Horta-Olivares, J. H. Peralta-Zepeda, "Diseño y modelado de un Sistema de electroporación para ser aplicado en tejido canceroso profundo", presented at the XXXVI Biomedical Engineering National Congress. Aguascalientes, Mexico. 2013.
- [21] A. L. Vera-Tizatl, L. I. Garay-Jiménez, S. A. Rodríguez-Cuevas, A. Vera-Hernández, P. R. Hernández-Rodríguez, "3D Model and simulation of electroporation application on healthy and tumoral breast tissue", presented at the 10th International Conference on Electrical Engineering, Computing Science and Automatic Control (CCE), Mexico city, Mexico, 2013.

APPENDIX E: CONFERENCE PAPER (PRODUCTIVITY)

2016 13th International Conference on Electrical Engineering, Computing Science and Automatic Control (CCE),
September 26-30, 2016, Mexico, City, Mexico.

Electric Field Distribution Obtained by Using the Finite Element Method and 3D Reconstruction of a Breast Carcinoma: Approach to the Electroporation of Deep-seated Tumors by Using Two Needle Electrodes

A. L. Vera Tizatl^{1,*}, C. A. Ramírez Martínez¹, C. E. Vera Tizatl¹, M. I. Gutiérrez², L. Leija Salas¹, P. R. Hernández Rodríguez¹, A. Vera Hernández¹, S. A. Rodríguez Cuevas³

¹Departamentos de Ingeniería Eléctrica y de Infectómica y Patogénesis Molecular, CINVESTAV, Mexico City, Mexico

²CONACYT – Instituto Nacional de Rehabilitación, Subdirección de Investigación Biotecnológica, Mexico City, Mexico

³Instituto de Enfermedades de la Mama- FUCAM, Mexico City, Mexico

*Corresponding author. E-mail address: veradit@hotmail.com

Abstract—Electrochemotherapy (ECT) is an application of reversible electroporation currently used in the European clinical practice to enhance absorption of chemotherapeutic drugs successfully used in the treatment of cutaneous and subcutaneous tumors. High response ratings obtained in these tumors encourages further investigation about the application of ECT in deep-seated tumors. As an approach to real anatomical modeling of target lesions, required in patient-specific treatment planning, it is presented in this work, the electric field distribution in a volume corresponding to a 3D reconstruction of a deep-seated breast carcinoma by applying electric potentials amplitudes from 100 V to 1500 V through two needle electrodes. Results obtained with the Finite Element Method (FEM) analysis show that for the breast carcinoma modeled, the electric potential suggested to be applied between the electrodes must be lower than 500 V to cause reversible electroporation and hence to control ablation regions while preserving the minimal invasiveness.

Keywords—*deep-seated tumor; 3D reconstruction; FEM modeling; electroporation; breast tissue.*

I. INTRODUCTION

Electroporation (EP) consists in the exposure of a cell to an intense pulsatile electric field to activate hydrophilic pore formation in the cell membrane [1]. Among the applications of EP, microbial ablation in biotechnology, gene transfection, gene therapy, DNA vaccination, cellular electrofusion and insertion of non-permeant molecules into the cell, can be mentioned [2]. Electrochemotherapy (ECT) is an application of EP used to increase absorption of heavy poorly-permeant cytotoxic drugs into cancerous cells [2, 3].

Nowadays, efforts are aimed to the development of patient-specific treatment planning for deep-seated tumors treated by ECT [5]. The steps suggested by many authors to achieve a patient-specific treatment planning include: a) a specific anatomical model to EP based on medical images processing, b) treatment protocol planning (electric protocol and positioning of electrodes) based on Finite Element Method (FEM) analysis, c) set-up verification regarding intraoperative conditions compliance, d) treatment delivery, and e) postsurgical response assessment [4, 5, 6, 7]. A detailed review of these steps, including the research, carried out by our group in Mexico, can be found in [8]. Up to now, these steps represent an active field of research and we focus in this paper only on the deep-seated tumors modeling, based on a 3D reconstruction of medical images corresponding to real patients.

Since anatomical models are required to obtain an actual approximation of real clinical cases, it is presented in this work a simplified FEM model of the electric field distribution in a breast tumor. The tumoral volume was obtained from a 3D reconstruction based on medical interpretation, segmentation, and processing of DICOM (Digital Imaging and Communication in Medicine) data available in [9]. This data is provided online by the Cancer Imaging Archive [9, 10]. Our group of research is focused in ECT technique to evaluate its effectiveness in deep-seated tumors, particularly in the treatment of breast neoplasia since it represents the first cause of death in women older than 20 years [4, 5, 12, 13, 14].

II. METHODOLOGY

A. Image Data Obtention

The Cancer Imaging Archive (TCIA) provides on-line DICOM data collections corresponding to different cancer types and anatomical site locations. Among these imaging data, The Cancer Genome Atlas (TCGA) supplies public collections belonging to 500 patients per cancer type. Since our target tissues are breast tumors, 164 studies conforming The Cancer Genome Atlas Breast Invasive Carcinoma (TCGA-BRCA) were analyzed, which were obtained to assess breast cancer response to neoadjuvant chemotherapy. The scanning modality for these studies is Magnetic Resonance Imaging (MRI) with and without contrast agent and spin-echo (SE) sequence using a Siemens 3T TIM Trio system [9, 10]. Each study is made of some sequences of the axial, sagittal and coronal planes. All the studies were analyzed over clinician guidance to select useful cases to be considered for further modeling and hence to be a basis for reaching a specific treatment planning of deep-seated-tumors.

B. Image Data Selection

Selection criteria of image sequences take into account adequate contrast, optimal resolution of images in each anatomical plane and visible neoplasia. It was selected only one sequence corresponding to a T2 left breast of a woman. The series were taken on December 20th 2003. Files provided by the Cancer Imaging Archive have .jnlp format, therefore, Java Runtime Environment are required in order to download DICOM data [9, 10]. In order to visualize and analyze medical images, it has been used the 3D Slicer 4.5 (National Cancer Institute, USA) software which is an open source platform available in multiple operating systems. It is worthy to remark that this software was developed as a tool for research hence it owns no Food and Drug Administration (FDA) approval. After loading DICOM data, axial, sagittal and coronal planes can be displayed. In Fig. 1(a), it is shown the sagittal plane in which it can be observed a hypodense image corresponding to a fibrocystic pattern, suggestive of a tumoral mass localized in the top right quadrant. Another suggestive image of a tumoral mass and a hyperdense image are found in the bottom right quadrant. This latter is consistent with a cystic lesion. Such interpretation is inferred based on a visual inspection due to the lack of data regarding the clinical history of the patient.

C. 3D Reconstruction of Breast Tumor

We have previously published ideal geometries in order to simulate the electric field distribution in healthy breast tissue and tumoral breast tissue [15]. In this work, we focus on the use of a geometry closer than can be found in the clinical practice regarding specific-patient analysis. Hence is it our purpose to reconstruct a volume based on clinical images corresponding to real neoplasia. For the collection selected, semiautomatic segmentation based on threshold application was not possible, due to the low resolution of medical images, pixels corresponding to breast tissue, fat tissue, and skin own similar intensities. Consequently, voxels in the different volumes overlap. Therefore, manual segmentation of 52 slices

was carried out. Three labels were used to differentiate the tissue: fat (blue), breast (green) and tumoral (yellow), as shown in Fig. 1(b). From the three volumes generated in 3D Slicer 4.5 [16], only the tumor volumes could be exported for its analysis with FEM since all faces were adequately parameterized. The volume imported to further analysis with FEM corresponding to the tumoral tissue is shown in Fig. 2.

D. Analysis of the Anatomical Model using FEM

It is of our interest to know the distribution of the electric field in biological tissues, specifically inside the tumor, caused by the application of an intense pulsatile electric field in order to establish an optimal electric potential to cause reversible EP and consequently an adequate ECT protocol hence the tumoral volume were modeled with FEM. In order to simulate the exposure of the biggest tumor to an external electric field, two conductive cylinders with a diameter of 1 mm corresponding to steel needle electrodes were inserted into the tumor. The simulated electrical properties of tumoral tissue are shown in Table I [15, 16].

Equations governing electric field distribution relating heat transfer are [17]:

$$\mathbf{E} = -\nabla V \quad (1)$$

$$\nabla \cdot \mathbf{J} = Q_j \quad (2)$$

$$\mathbf{J} = \sigma \mathbf{E} + \mathbf{J}_e \quad (3)$$

$$\rho C_p \mathbf{u} \cdot \nabla T = \nabla \cdot (k \nabla T) + Q \quad (4)$$

where $\mathbf{E} \equiv$ Electric field, $V \equiv$ electric potential, $\mathbf{J} \equiv$ electric current density, $Q_j \equiv$ heat generation, $\mathbf{J}_e \equiv$ external electric current density, $T \equiv$ temperature of the tissue, and $Q \equiv$ metabolic heat generation.

Regarding boundary conditions, one electrode was set to a range of electric potential (100 V – 1500 V) and the second one grounded to generate the external field. Initial condition given to the modeled geometry includes a temperature of the tumor which was set at 37 °C [17]. The amplitude of electric pulses was varied in increments of 100 V, therefore 15 studies were carried out.

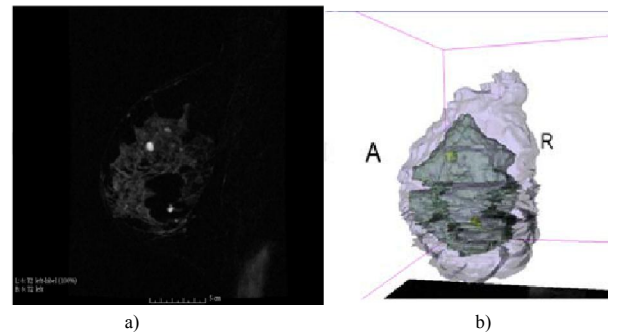


Fig. 1. a) MRI of a left breast, b) volumes reconstructed from DICOM data.

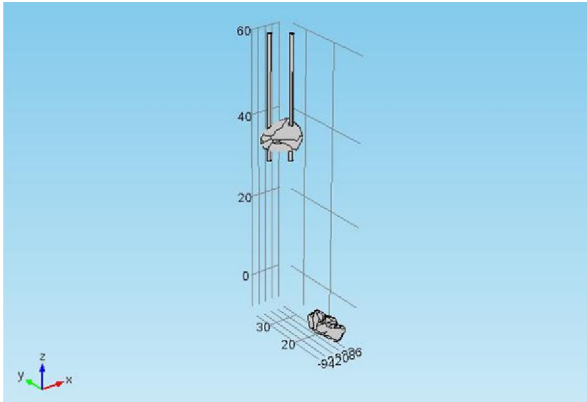


Fig. 2. FEM geometry of breast carcinoma and two cylindrical conductive electrodes.

TABLE I. ELECTRIC PROPERTIES OF BREAST CARCINOMA.

Property	Value		Unit
	Symbol	Tumor	
Heat capacity	C_p	3700	J/(kg·K)
Density	ρ	1044	Kg/m ³
Thermal conductivity	k	0.564	W/(m·K)
Electrical conductivity	σ	0.5	S/m

The electric field resulting from the application of an electrical potential pulse of 100 μ s can be considered as quasi-stationary, since cellular membrane polarization due to its exposure to an external electric field is only about 1.1 μ s. Therefore, for our FEM analysis, it was used a stationary study. The electroporation system developed by our research group offers a variable output voltage ranging from 20 V to 1500 V programmed by I²C communication protocol. This range of voltage is used to apply protocols offered by commercial ECT devices used in clinical practice for cutaneous and subcutaneous tumors, therefore, there were simulated electric potentials ranging from 100 V to 1500 V with increments of 100 V [1, 5].

III. RESULTS

A. Electric field distribution

The electric field distribution inside the reconstructed tumor, resulting from the simulation based on a breast carcinoma reconstruction is shown in Fig 3. The maximum electric field obtained is 1.22x10E6 V/m. It can be appreciated that the highest magnitudes of the electric field are located throughout the interface electrode-tumor. The values resulting from the simulation are enough to cause electroporation of tumoral tissue.

In Fig. 4, it is shown a slice plot to appreciate the electric field distribution throughout the greatest tumor, along the “yz” and “xz” planes.

There were 11170 solved degrees of freedom. The solution time for the study was 8 s. Based on the edges constituting the

geometry of the tumoral volume, the edges on the “xy” plane of it were considered to obtain a line graph to get a quantitative electric field distribution as shown in Fig. 5, which contrasts the generated electric field versus the applied electric potential. Blue and red line correspond to the anterior and rear edges of the tumor geometry. On the other hand, the minimum, maximum, and average electric field in the volume of the greatest tumor were calculated, for the different values of the applied electric potential ranging from 100 V to 1500 V.. They were generated through an electroporation system based on protocols for ECT reported in [1] and [5]. The results are shown in Table I.

IV. DISCUSSION

It can be seen in Fig. 3 and Fig. 4 that the electric field is generated throughout the tumor and the regions exposed to the greatest magnitudes of the electric field and located in the vicinity of the electrodes. Based on the software used to carry out the finite element analysis, it can be stated that the size of the reconstructed tumor is approximately 0.8 cm x 1.0 cm x 0.7 cm. Due to the irregular geometry of the reconstructed tumor, the edges defining the boundaries of this tissue are consequently irregular. Hence, the electric field distribution is non-symmetric. As it can be seen in Fig. 4, the electric field in the neighborhood of the electrodes is more intense and varies with a non-uniform pattern inside the tumor.

The dependence of the electric field distribution with the electric potential applied in the periphery of the tumoral volume is shown in Fig. 5. This periphery is constituted by anterior and rear edges of the tumoral volume on the “xy” plane. It can be appreciated in Fig. 5 that the magnitudes of the electric field reached values greater than 60000 V/m (0.6×10^5 in y axis). This latter magnitude is reported to be the maximal electric field required to achieve reversible electroporation, avoiding irreversible electroporation in a tissue regardless their histology [3, 5].

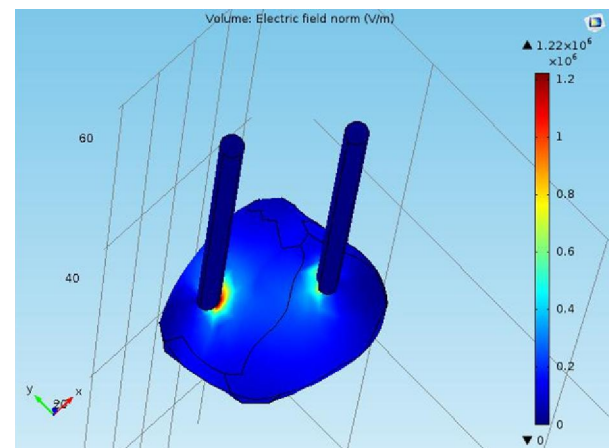
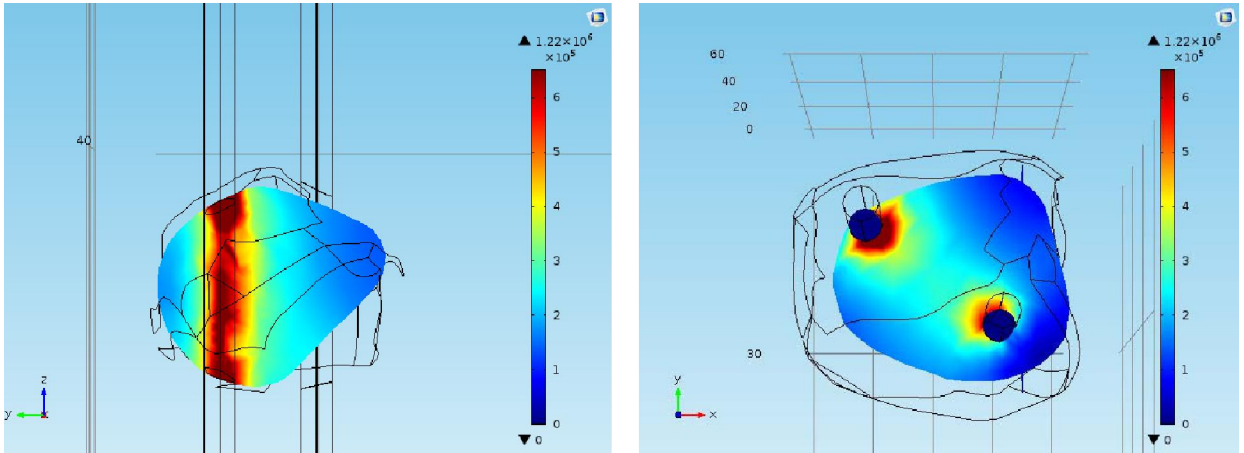


Fig. 3. Electric field distribution in breast carcinoma and two cylindrical conductive electrodes. On the right, it is shown a chromatic scale corresponding to electric field in V/cm.



a)++ b) Fig. 4. Electric field distribution in breast carcinoma in a) “yz” plane and b) “xz” planes.

This work is aimed to determine the electric field distribution to reach a reversible electroporation in a clinical scenario while preserving minimal invasiveness by using only two electrodes. Data displayed in Table II correspond to the magnitude of the electric field obtained in the complete volume of the tumoral tissue when electric potential amplitudes of 100 V to 1500 V are applied. It can be seen that for the size of the reconstructed tumor, the current positioning of the electrodes and for the material properties of Table I, the electric potential suggested to be applied between the electrodes must be lower than 500 V. This value is suggested to cause reversible electroporation, necessary to the delivery of ECT. Even if there are regions in which it is evident the generation of a possible irreversible electroporation, it is generated throughout the tumor which is the tissue we must damage.

V. CONCLUSION

The work presented here represents an approach to a patient-specific anatomical model of a deep-seated breast carcinoma useful to assess the electric field distribution generated by using needle electrodes. Two tumoral volumes were reconstructed but just the biggest volume was solved by using FEM, aimed to reduce computational requirements. Based on the volume of the tumoral volume reconstructed, only two needle electrodes were used to preserve minimal invasiveness principle.

Acquisition of medical images possessing correct resolution is crucial to carry out an adequate segmentation of them. If clinical condition of patients allows it, a manual segmentation is recommended because guidance of a physician interpretation from the different slices constituting a sample is strongly suggested to locate the right region of interest.

The results listed in Table II show that it is possible to reach the electroporation phenomenon in a breast carcinoma with dielectric properties showed in Table I and dimensions of 0.8 cm x 1.0 cm x 0.7 cm for electric potential amplitudes lower than 500 V. Nevertheless, experimental application of EP is required to compare and contrast the results obtained in the present model.

This work is aimed to obtain an anatomical model of a target tissue, which is the first step towards a complete patient-specific treatment planning as the basis to lead the application of ECT in deep-seated tumors.

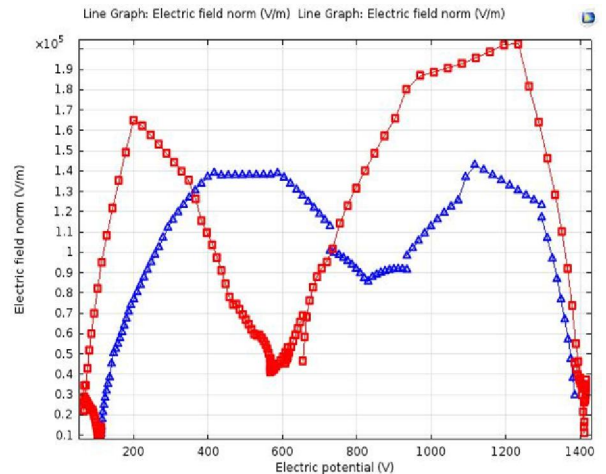


Fig. 5. Dependence of electric field distribution in breast carcinoma on the applied electric potential. Blue and red line corresponds y to the anterior and rear edges of the tumor periphery on the “xy” plane respectively.

TABLE II. ELECTRIC FIELD DISTRIBUTION IN A BREAST CARCINOMA MODEL

applied Voltage [V]	Electric Field in Volume[V/m]		
	Average	Minimum	Maximum
100	13076	087	171419
200	26153	174	342839
300	39229	261	514259
400	52305	348	685679
500	65382	435	857098
600	78459	522	1028528
700	91535	609	1199938
800	104612	697	1371358
900	117688	784	1542777
1000	130765	871	1714197
1100	143841	958	1885617
1200	156918	1045	2057037
1300	169994	1132	2228456
1400	183071	1219	2399876
1500	196147	1307	2571296

ACKNOWLEDGMENT

Authors thank the National Council for Science and Technology (CONACYT, Mexico) for the support received for the project CONACYT-Salud 2013-I-201590, 201256, Project Joint Cooperation México-Uruguay (SRE-AUCI) 2012-2013 and Project CSIC-COOPB20166. A. L. Vera Tizatl and C. A. Ramírez Martínez thank the National Council for Science and Technology (CONACYT, Mexico) for the scholarship granted.

REFERENCES

[1] M. Kanduser, D. Miklavcic, "Electroporation in Biological Cell and Tissue: An Overview" in *Electrotechnologies for Extraction from Food Plants and Biomaterials*, N. Lebovka, E. Vorobiev, Ed. N.Y.: Springer, 2008, ch. 1, pp. 1-37.

[2] A. G. Pakhomov, D. Miklavcic, M. S. Markov. *Advanced electroporation techniques in biology and medicine*. USA. CRC Press. 2010.

[3] G. Sersa, M. Cemazar, M. Snoj, "Electrochemotherapy of tumors" *Current Oncol*, 2009, vol. 16, no. 2 pp. 34-35.

[4] S. Corovic, A. Zupanic, and D. Miklavcic, "Numerical Model and Optimization of Electric Field Distribution in Subcutaneous Tumor Treated with Electrochemotherapy Using Needle Electrodes"

[5] D. Pavliha, B. Kos, A. Zupanic, M. Marcan, G. Sersa and D. Miklavcic, "Patient-specific Treatment Planning of Electrochemotherapy: Procedure Design and possible pitfalls", *Bioelectrochemistry*, vol. 87, pp. 265-273, Jan. 2012.

[6] B. Kos, A. Zupanic, T. Kotnik, M. Snoj, G. Sersa, D. Miklavcic, "Robustness of treatment planning for electrochemotherapy of deep-seated tumors", *J. Membrane Biol.*, vol. 236, pp. 147-153, 2010.

[7] D. Pavliha, B. Kos, M. Marcan, A. Zupanic, G. Sersa, D. Milavcic. "Planning of electroporation-based treatments using web-based treatment planning software", *J. Membrane Biol.* vol. 246, pp. 833-842, 2013.

[8] A. L. Vera-Tizatl, S. A. Rodríguez-Cuevas, L. Leija Salas and A. Vera-Hernández. "Review of electrochemotherapy-based Treatment of Cutaneous, Subcutaneous and Deep-seated Tumors towards Specific Treatment Planning", presented at the Global Medical Engineering Physics Exchanges/Pan American Health Care Exchanges (GMEPE/PAHCE), Madrid, Spain, April 4-9, 2016

[9] Smith K, Clark K, Bennett W, Nolan T, Kirby J, Wolfsberger M, Moulton J, Vendt B, Freymann J. Radiology Data from The Cancer Genome Atlas Breast Invasive Carcinoma [TCGA-BRCA] collection <http://dx.doi.org/10.7937/K9/TCIA.2016.AB2NAZRP>

[10] Clark K, Vendt B, Smith K, Freymann J, Kirby J, Koppel P, Moore S, Phillips S, Maffitt D, Pringle M, Tarbox L, Prior F. The Cancer Imaging Archive (TCIA): Maintaining and Operating a Public Information Repository, *Journal of Digital Imaging*, Volume 26, Number 6, December, 2013, pp 1045-1057. (paper)

[11] S. Harberl, D. Miklavcic, G. Sersa, W. Frey, B. rubinsky. "Cell Membrane Electroporation-Part 2: The Applications", *IEEE Electrical Insulation Magazine*, 2013, vol. 29, no 1, pp 29-37

[12] D. Miklavcic et. al. "Towards Treatment Planning and Treatment of Deep-seated Solid Tumors by Electrochemotherapy", *BioMedical Engineering OnLine*, 2010, 9:10

[13] B. Rubinsky, "Irreversible Electroporation", Germany, Springer. 2010

[14] R. E. Neal and R. V. Dávalos, "The Feasibility if Irreversible electroporation for the Treatment of Breast Cancer and Other Heterogeneous Systems", *Annals of biomedical Engineering*, vol 37, pp 2615-2625, Sept 2009C. Gabriel, S. Gabriel and E. Corthout, "The dielectric properties of biological tissues: I. Literature survey", *Phys. Med. Biol.* Vol. 41, pp. 2231-2249. 1996.

[15] A. L. Vera-Tizatl, L. I. Garay-Jiménez, S. A. Rodríguez-Cuevas, A. Vera-Hernández, P. R. Hernández-Rodríguez, "3D Model and simulation of electroporation application on healthy and tumoral breast tissue", presented at the 10th International Conference on Electrical Engineering, Computing Science and Automatic Control (CCE), Mexico city, Mexico, 2013.

[16] Fedorov A., Beichel R., Kalpathy-Cramer J., Finet J., Fillion-Robin J-C., Pujol S., Bauer C., Jennings D., Fennessy F., Sonka M., Buatti J., Aylward S.R., Miller J.V., Pieper S., Kikinis R. 3D Slicer as an Image Computing Platform for the Quantitative Imaging Network. *Magnetic Resonance Imaging* 2012; July PMID: 22770690. <http://www.slicer.org>

[17] R. N. Lawson, M. S. Chuchtai. "Breast cancer and body temperature", *Canad. Med. Ass. J.*, vol. 88, pp. 68-70, 1963.

[18] J. Ghazanfarian , R. Saghatchi, D. V. Patil. "Implementation of Smoothed-Particle Hydrodynamics for non-linear Pennes' bioheat Transfr Equation", *Applied Mathematics and Computation*, 2015, vol. 259, pp. 21-31.

APPENDIX F: CONFERENCE PAPER (PRODUCTIVITY)

APPENDIX G: CONFERENCE PAPER (PRODUCTIVITY)

Electric Field Distribution Generated by Two Needle Electrodes in an Anatomical Model of a Deep-Seated Breast Carcinoma

Adriana L. Vera Tizatl¹, Carlos A. Ramírez Martínez¹, Arturo Vera Hernández¹, Lorenzo Leija Salas¹, Pablo R. Hernández Rodríguez¹, Sergio Rodríguez Cuevas²; ¹ *Department of Electrical Engineering, Bioelectronics, CINVESTAV, Av. Instituto Politécnico Nacional 2508, MX-07360 Mexico City, MEXICO* ² *Institute of Breast Diseases, FUCAM, Av. Bordo 100, MX-04980 Mexico City, MEXICO*

INTRODUCTION

In Mexico, breast cancer is reported to be the first cause of death in women and current treatments include highly invasive techniques. Outcomes obtained with electrochemotherapy (ECT) encourage the development of minimally invasive treatment techniques. The design of an electroporation system to be used in a deep-seated breast carcinoma, corresponding to a real clinical case, is presented in this work [1, 2].

METHODOLOGY

In order to build a high voltage source, three regulated high voltage DC to DC programmable converters with an output voltage ranging from 0 V to 500 V are used. The connection in series of these modules allows to generate 1500 V. The control of these converters was carried out by using isolated Inter-Integrated Circuit (I²C) communication. The control of each module has a resolution of 12 bits. The generation of pulses is made by a PWM and a power switching MOSFET.

Based on the anatomical model presented in [3], the reconstruction of the surrounding breast healthy tissue was added to the model as shown in Fig. 1. The finite element method (FEM) (COMSOL Multiphysics®) was used to determine electric field distribution caused by the application of the electric potential generated by the electroporation system designed.

RESULTS

Based on the outcomes previously reported in [3], the application of maximum electric voltage of 500 V was used. Electric conductivity of 0.05 S/m and 0.5 S/m for healthy breast tissue and tumoral tissue respectively, were simulated. The resultant electric field magnitudes for each tissues are shown in Table 1. The electric field distribution can be observed in Fig 2.

Table 1: Electric field magnitude generated in the model.

Electric Field [V/cm]	Healthy breast tissue	Breast Carcinoma
Average	2.37	651.26
Minimum	0	9.35
Maximum	43.17	900.42

CONCLUSION

The anatomical model presented in this work represents an approach to a patient-specific treatment planning. It can be seen that an average electric field magnitude of 651.26 V/cm (651.26 V/cm) is achieved when applying 500 V through just two needle electrodes. Assuming that an electric field of 400

V/cm is necessary for the ECT treatment of tumors and based on results showed in Table 1, an electric voltage lower than 500 V is suggested for this specific model.

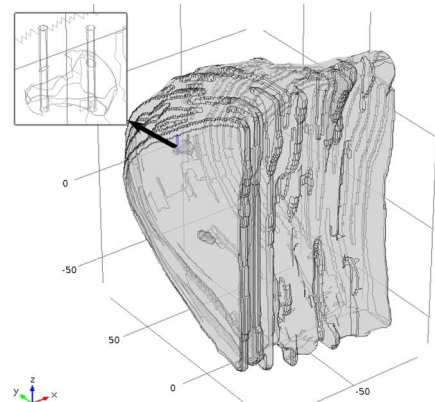


Figure 1: Model of a left breast and two needle electrodes.

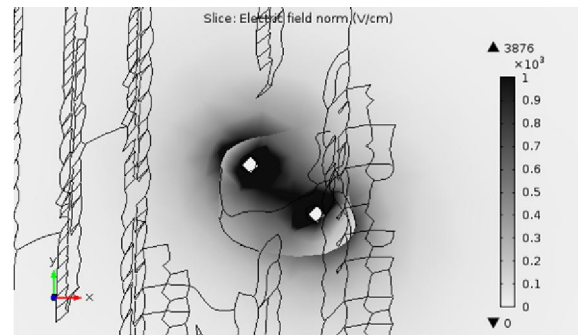


Figure 2: Electric field distribution in the complete model.

REFERENCES

- [1] A. L. Vera-Tizatl, S. A. Rodríguez-Cuevas, L. Leija Salas and A. Vera-Hernández, "Review of electrochemotherapy-based Treatment of Cutaneous, Subcutaneous and Deep-seated Tumors towards Specific Treatment Planning", GMEPE/PAHCE, Madrid, Spain, April 4-9, 2016.
- [2] D. Pavliha, B. Kos, A. Zupanic, M. Marcan, G. Sersa and D. Miklavcic, "Patient-specific Treatment Planning of Electrochemotherapy: Procedure Design and possible pitfalls", *Bioelectrochemistry*. vol. 87, pp. 265–273, Jan. 2012.
- [3] A. L. Vera Tizatl et. Al, "Electric Field Distribution in an Anatomical Model with the Finite Element Method based on the 3D Reconstruction of a Breast Carcinoma", 13th. International Conference on Electrical Engineering, Computing Science and Automatic Control (CCE), Mexico City. Sept. 26-30, 2016.

APPENDIX H: CONFERENCE PAPER (PRODUCTIVITY)



2017 GLOBAL MEDICAL ENGINEERING PHYSICS EXCHANGES/PAN AMERICAN HEALTH CARE EXCHANGES (GMEPE / PAHCE)

Investigation of numerical models for planning of electrochemotherapy treatments of invasive ductal carcinoma

A. L. Vera-Tizatl^{1*}, B. Kos², D. Miklav i², A. Vera-Hernández¹, L. Leija-Salas¹, C. E. Vera-Tizatl¹, S. A. Rodríguez-Cuevas³

¹CINVESTAV-IPN, Mexico D.F., Mexico

²Faculty of Electrical Engineering, University of Ljubljana, SI, Slovenia ³Instituto de Enfermedades de la Mama-FUCAM, Mexico D.F., Mexico Email: veradit@hotmail.com, damijan.miklavcic@fe.uni-lj.si

Abstract — Three numerical models are presented in this work i. e., a reference model and interpolated models varying geometrical traits, material properties, boundary conditions and mesh size to establish their effects in the resultant electric field during electrochemotherapy. For static conductivity the results show that the use of an interpolation function grid of 1 mm and a normal mesh are suitable for further more complex models. On the other hand an iterative increasing conductivity behavior describes better the increasing conductivity phenomenon reported to be caused by electroporation. The results reported in this work could be useful in further modeling of breast tumors and development of treatment planning for electrochemotherapy based on invasive ductal carcinoma.

Keywords — Electrochemotherapy, Electroporation, Invasive Ductal Carcinoma, Numerical Modeling

I. INTRODUCTION

From 2006, breast cancer represents in Mexico the first cause of death due to malignant tumors in women older than 25 years. Its recurrence has increased 49.5% during the last two decades. About 45% of total cases are diagnosed in stages III and IV and 11% are younger than 40 years. The survival rate for this latter group is lower compared to the one for older population. Geographically, the higher death rates occur in the north and center states of the country [1]. The most common histologic subtypes of breast cancer are ductal carcinoma, *in situ* (DCIS) and invasive (IDC) and lobular carcinoma, *in situ* (LCIS) and invasive (ILC). Both of them represent 80% and 10% of all breast cancer types respectively [1,2]. The detection methods combine imaging and corroboration techniques (biopsy with histopathologic studies). Imaging monitoring include mammography, ultrasound (US), magnetic resonance (MR), positron emission tomography (PET) and digital breast tomosynthesis (DBT). Mammography has been used as the primary solving tool for breast abnormalities but despite its benefits it is limited by tissue superimposition. On one hand, overlying dense tissues can mask tumors, potentially leading to a missed cancer and on the other, overlapping structures can mimic the appearance of a tumor and thereby cause a false-positive. Therefore, DBT is becoming increasingly accepted since it can reduce the tissue overlap effect and structure noise in single slice two-dimensional mammography imaging [3,4]. DBT is a three-dimensional

method in which images are acquired at a limited number of different x-ray source angles while the breast is statically compressed [4]. It differs from other 3D imaging modalities in that orthogonal multiplanar reconstructions such as sagittal and coronal views from the transverse tomosynthesis image sets cannot be generated. Instead, Cranial-caudal (CC) and Medio-lateral oblique (MLO) views are obtained with DBT [4]. Regarding the treatment techniques used for breast cancer, neoadjuvant chemotherapy, radiotherapy, hormonal therapy and surgical procedures including lumpectomy and mastectomy may be mentioned. Since breast cancer has become a rising problem concerning public health, current efforts are aimed to the control of known risk factors, establishment of early detection programs and the development of new minimally invasive and conservative treatment procedures to this disease [1].

It is known that electrochemotherapy (ECT) is considered as a minimally invasive technique that consists of the combination of high voltage short duration electric pulses and a cytotoxic drug like bleomycin and cisplatin. ECT is reported to be highly effective in the treatment of cutaneous and subcutaneous tumors. Because of its benefits such as high specificity for targeting cancer cells and capacity for preserving the innate immune response its use is therefore extending to the treatment of internal tumors [5]. Clinical experiences regarding treatment of liver and bone metastases, soft tissue sarcomas, brain tumors, and colorectal and esophageal tumors have been reported [5]. For this purpose, numerical modeling is nowadays the only efficient way to predict the electric field distribution in target and surrounding tissues. A combination of numerical modeling and optimization methods has been reported to be used for treatment planning electroporation-based treatments like ECT, to set the optimal electrode positioning and electric pulse amplitude for a complete tumor eradication based on the processing of medical images [6-10].

Based on the increasing need of effective minimally invasive treatments for breast cancer in Mexico and the outcomes obtained with ECT in the treatment of different tumor types, our research group is interested in assessing the benefits of ECT in the treatment of IDC. The role of ECT in Mexico and a review of the steps required to this purpose in

addition to the modeling of breast carcinomas as an approach to further development of patient-specific treatment planning for breast cancer have been previously reported by our group [11- 14]. Three numerical models are presented in this work, considering the variation of different parameters to be used in further treatment planning of IDC corresponding to Mexican women treated in the FUCAM.

II. METHODOLOGY

In order to investigate the effects that the variation of parameters such as geometrical traits, material properties, boundary conditions and mesh size may have in the resultant electric field generated by electric pulses used in ECT, a comparison between a reference model created in COMSOL Multiphysics (version 5.0) and a model manipulated in Matlab (version R2013a) was carried out. Both models consist of two geometries i.e., a sphere embedded in a block simulating a tumoral volume and a surrounding healthy tissue volume respectively in addition to four cylinders to simulate needle electrodes inserted into the healthy tissue very close to the tumor. The electrodes were activated sequentially in pairs. The models were solved using the Electric Currents module to obtain the Electric Field distribution for each pair of active electrodes. Two approaches are described in this work. The first one consider static conductivity values and the second one takes into account conductivity changes during the delivery of electric pulses in electroporation.

1) *Reference model*: A model consisting of a 2 cm diameter sphere embedded in a block of 4 cm x 4 cm x 4 cm was created in the COMSOL Multiphysics User Interface. Four cylinders of 1 mm of diameter and 4 cm length simulate the electrodes positioned orthogonally into the block 2.5 mm away from sphere quadrants as it is shown in Fig. 1. The electric conductivity assigned to tumoral and healthy tissue were 0.1 S/m and 0.5 S/m respectively. Regarding boundary conditions, each pair of electrodes (E1E2, E2E3, E3E4, E4E1, E1E3 and E2E4) was set to 1500 V. Two mesh quality allowed by the software were used i. e., a normal mesh and a finer mesh.

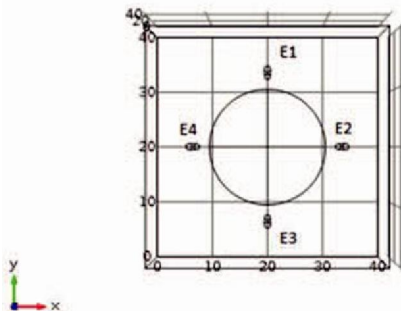


Fig. 1. Reference model of a tumor embedded in healthy surrounding tissue and four needle electrodes (E1, E2, E3 and E4).

MARCH 20–25, 2017, CHIAPAS, MEXICO

2) *Interpolated Model*: In order to assign arbitrary material properties to the tissues, interpolation functions containing conductivity values at discrete points were created in Matlab as grids. These grids were programmed to define a 2 cm diameter spherical tumor with conductivity of 0.5 S/m and a block of 4 cm x 4 cm x 4 cm with conductivity of 0.1 S/m. The distance between the points in the interpolation function grid was varied from 0.5 mm, 1 mm, 2 mm, and 4 mm. The interpolated function grids are shown in Fig. 2. The positioning of electrodes, their activation and the boundary conditions remained as those used in the reference model. The comparison between both models is based on the correlation factor, the normalized crossed-correlation factor and the root mean square error calculation.

3) *Electric Field Dependent Conductivity Models*: Current accepted models for electroporation and the effect of electroporation pulses on tissue conductivity consider the conductivity as a function of the local electric field magnitude [15, 16]. Therefore, a dynamic conductivity behaviour of tissue was used to compare its effects on the electric field distribution obtained on one hand through sigmoid functions defined in COMSOL Multiphysics and on the other, through increasing conductivity functions programmed in Matlab.

Fig. 3 shows the two sigmoid functions used for the geometry described in 1). Electric field magnitudes of 400 V/cm and 800 V/cm were considered as threshold values for reversible and irreversible electroporation respectively as suggested in [7] and [8]. Since electroporation phenomenon has been reported to increase tissue conductivities from three to four times the initial values, the step functions parameters considered for this model are shown in Fig. 3. On the other hand, a code in Matlab was written defining an iterative ramp function to simulate an increasing conductivity behavior for the tumoral and the surrounding tissue in addition to the sequential activation of electrodes and the creation of a conductivity interpolation function for each active pair. The programmed ramp functions are described in (1) and (2).

$$\text{---} \quad (1)$$

$$\text{---} \quad (2)$$

where $n = 1, 2, 3, 4$ and define the number of iterations programmed, $\sigma_0 = 0.5$, $\sigma_1 = 1.5$ define initial and final tumoral conductivity and $\sigma_0 = 0.1$ and $\sigma_1 = 0.3$ are the initial and final peripheral healthy tissue conductivity. and E_{th} represent the threshold electric field values for reversible and irreversible electroporation, respectively.

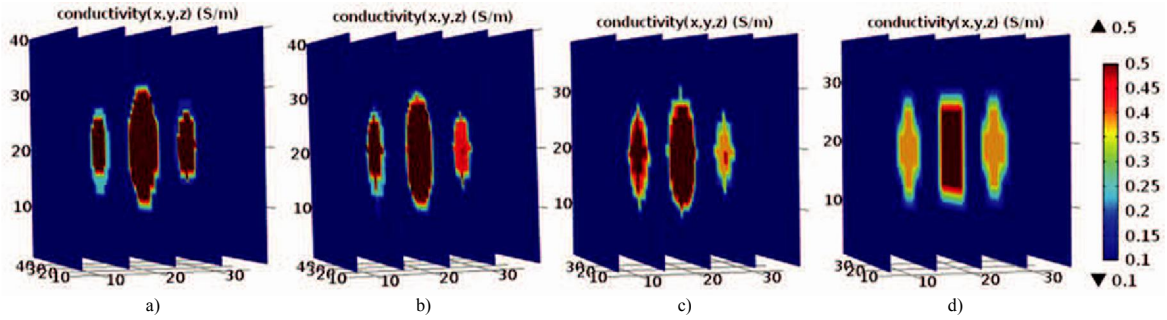


Fig. 2. Interpolation function for a grid of conductivity values with spacing of a) 0.5 mm, b) 1 mm, c) 2 mm and d) 4 mm.

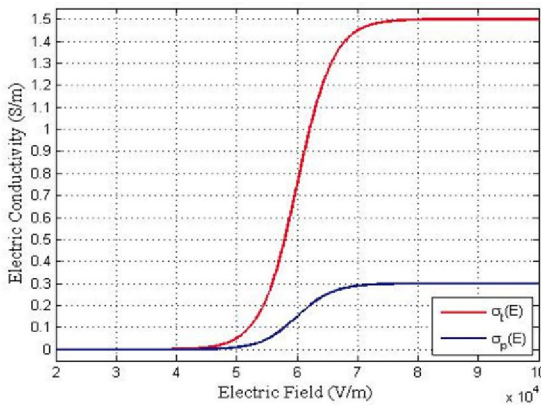


Fig. 3. Electric conductivity as a function of the electric field defined through a step function for a tumoral volume (red curve) and healthy surrounding tissue (blue curve). Note different ranges of conductivity for both tissues.

III. RESULTS

A. Static Conductivity

The resultant electric field for each model was read in the Matlab prompt through the use of LiveLink™ for Matlab. The electric field distribution for the reference model and for the models with interpolation functions are shown quantitatively in Table I and graphically in Fig. 4. Fig. 4b, Fig. 4c show that a grid of conductivities with a spacing of 0.5 mm and 1 mm produce an electric field distribution that approximate better to the one obtained for the reference model (Fig. 4a). Despite the distorted geometry generated by the coarser grids of 2 mm and 4 mm (Fig. 4d, Fig. 4e) the electric field magnitudes were similar for all the grids. In order to describe quantitatively the differences between the models, the correlation factor shown in Fig. 5 and the root mean squared error, shown in Fig. 6, between the electric distribution corresponding to the reference and interpolation function models, were calculated in Matlab according to (3) and (4). Two mesh types were used for each model to

determine the effects of the mesh quality on the results. In Fig. 5 and Fig. 6 a normal mesh is denoted as NM and the finest mesh that COMSOL multiphysics may handle is denoted as FM.

$$\text{---} \quad (3)$$

$$\text{---} \quad (4)$$

where $i=1, \dots, 6$ defines the active pair of electrodes, α_i is the correlation factor calculated for each active pair of electrodes, E_{ref} is the electric field magnitude of the reference model, E_i is the electric field magnitude corresponding to the interpolation functions.

TABLE I
ELECTRIC FIELD DISTRIBUTION FOR REFERENCE AND INTERPOLATED MODELS

Active Pair of Electrodes	Comsol mesh	Maximum Electric Field (V/m) $\times 10^6$				
		Ref. Model	0.5 mm	1 mm	2 mm	4 mm
E1E2	Normal	1.48	2.12	2.13	2.13	2.14
E2E3	Normal	2.57	2.40	2.37	2.28	2.34
E3E4	Normal	2.60	2.39	2.41	2.45	2.47
E4E1	Normal	1.07	2.11	2.16	2.28	2.25
E1E3	Normal	2.42	2.26	2.24	2.15	2.20
E2E4	Normal	1.39	0.76	0.78	0.80	0.77
E1E2	Finer	2.93	1.66	1.67	1.67	1.68
E2E3	Finer	1.97	1.67	1.65	1.59	1.66
E3E4	Finer	1.96	1.64	1.66	1.70	1.74
E4E1	Finer	2.94	1.63	1.67	1.77	1.75
E1E3	Finer	2.74	1.57	1.57	1.67	1.65
E2E4	Finer	2.94	1.63	1.67	1.77	1.75

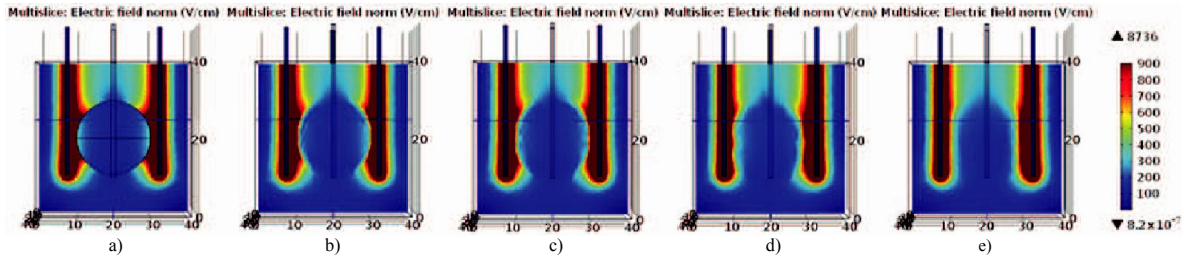


Fig. 4. Electric field distribution obtained for a) the reference model and for b) 0.5 mm, c) 1 mm, d) 2mm and e) 4 mm grid spacing interpolation functions.

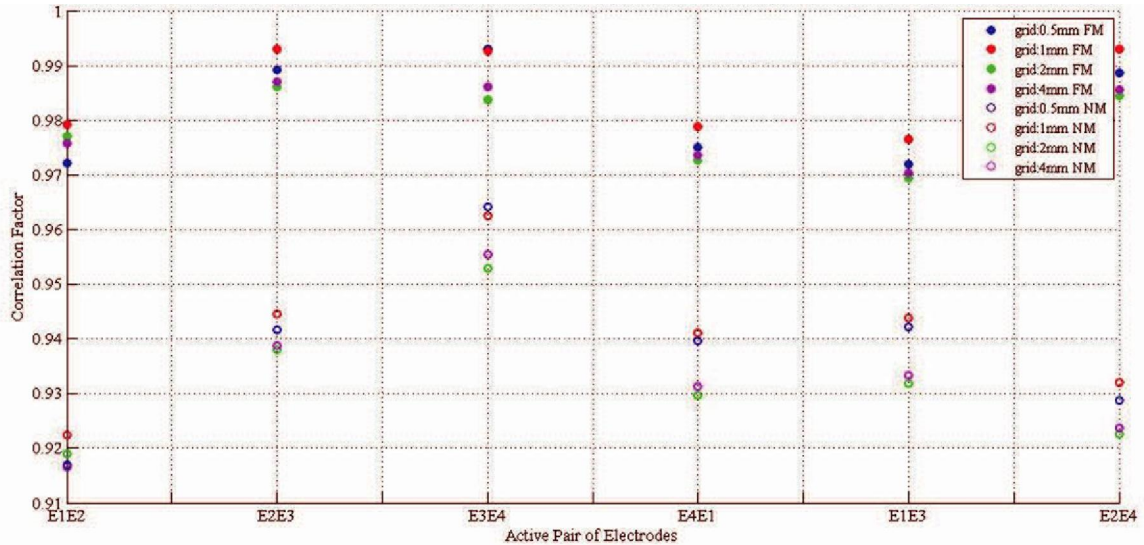


Fig. 5. Correlation factor calculated for the electric field distribution of the reference model and those obtained for the interpolation functions and meshes.

In Fig. 5 and Fig. 6 it can be seen that the most accurate results are obtained for the interpolation function grids of 0.5 mm and 1 mm and the finest mesh. Despite the high correlation factors obtained for the finest mesh, its use seems unsuitable due to the longer solution time that the use of a finer mesh demands. The solution time increased from 15 s to 3.5 min when the geometry mesh was varied from a normal mesh to a finer mesh. In order to determine the similarity between the reference model and the interpolated model with a 1 mm grid, the normalized cross correlation (NCC) was calculated using a normal mesh as shown in Fig. 7. NCC was calculated along the z axis with a 1 mm spacing for 40 slices representing the complete geometry. E12, E23, E34, E41, E13 and E24 denote the active pair of electrodes E1E2, E2E3, E3E4, E4E1, E1E3 and E2E4 respectively.

B. Electric field dependent conductivity

The best results showing the similarity between the reference model and the interpolated model were obtained by using a grid spacing of 1 mm and a normal mesh based on the high correlation factors, low root square error values and the solution time of the models. Therefore, an iterative dynamic conductivity study according to (1) and (2) was carried out only for a spacing grid of 1 mm. For the first iteration, is the resultant electric field corresponding to the static conductivity study in 1). A new increased conductivity matrix is generated after each iteration depending on the conditions stated in (1) and (2). Electric field, and are obtained after solving the model for the conductivity matrix generated in their precedent iterations. The electric field dependent conductivity for the reference model and the iterative increased conductivity programmed in Matlab are shown in Fig. 8. It can be seen that a smoother incremental behavior is obtained through iterative processes (Fig. 8b) compared to the increased conductivity obtained with step functions defined in COMSOL user interface (Fig. 8a).

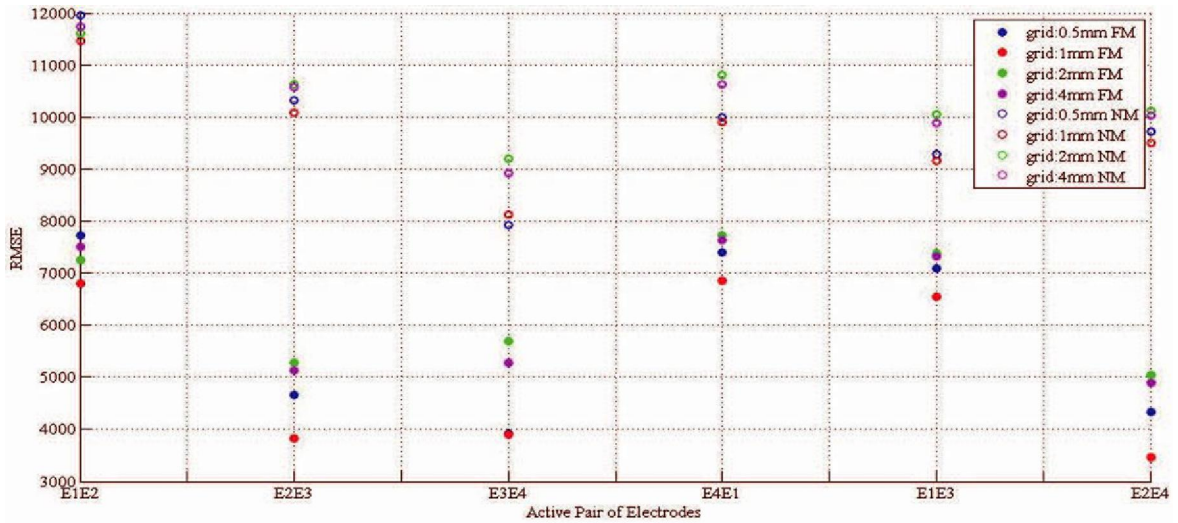


Fig. 6. RMSE calculated for the electric field distribution of the reference model and those obtained for the interpolation functions and meshes.

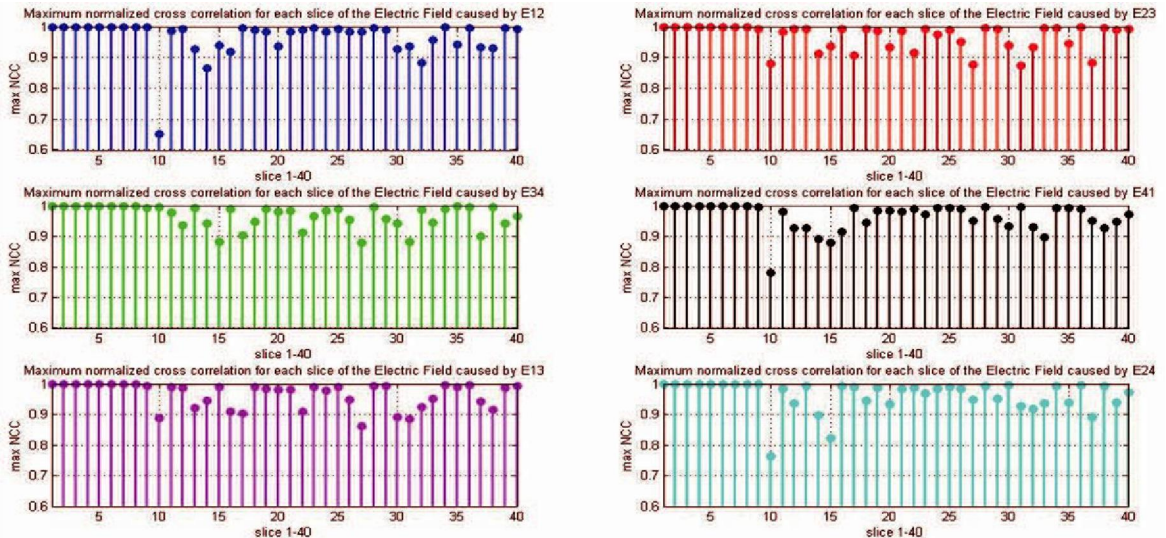


Fig. 7. Normalized cross-correlation (NCC) for the electric field distribution between the reference model and the interpolation functions.

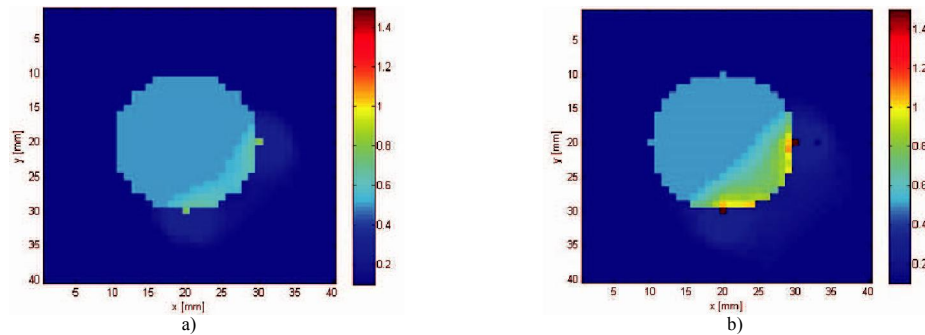


Fig. 8. Electric field dependent conductivity for a) COMSOL Multiphysics step functions and for b) the iterative increasing conductivity in Matlab.

IV. DISCUSSION

The spacing grid for interpolation functions presented in this work determine the electric conductivity in different points in the model geometry. For static conductivity, parameters including the spacing grid for interpolation functions, the activation of electrodes pairs, and the mesh quality to be used for solving the models were varied. The results show that the use of an interpolation function grid of 1 mm and a normal mesh are suitable for further more complex models considering the solution time for the electric field distribution calculation and the similarity between the models created in the COMSOL user interface and the ones manipulated in Matlab.

Based on the outcomes reported in [17] describing permeabilization on tissue level as a dynamic process in which electric field distribution is dependent on the local conductivity, an iterative increasing conductivity behavior was programmed in Matlab. Results in Fig. 8 show that an iterative increasing conductivity is preferred over the step functions that can be defined in the COMSOL Multiphysics user interface since it describes better the increasing conductivity phenomenon caused by electroporation.

V. CONCLUSION

The results reported in this work can be used in further modeling of breast tumors which are geometrically much more complex than the spherical tumor used in this study. Breast carcinoma models of real clinical cases must be based on image processing corresponding to specific-patient lesions. The development of a treatment planning for invasive ductal carcinoma based on processing and reconstruction of DBT data represents new challenges because of the nature of its views (MLO and CC) differing from MRI or CT images and hence their incomplete data sampling and the considerations reported in this work should be taken into account for the development of treatment planning for invasive ductal carcinoma.

ACKNOWLEDGMENT

A. L. Vera Tizatl thanks the National Council for Science and Technology (CONACYT, Mexico) for the scholarship granted. Authors thank the CONACYT, Mexico for the support received for the project CONACYT-Salud 2013-I-201590, 201256, Project Joint Cooperation México-Uruguay (SRE-AUCI) 2012-2013 and Project CSIC-COOPB20166.

REFERENCES

- [1] 2015 Masson Doyma México S.A. Consenso Mexicano sobre diagnóstico y tratamiento del cáncer mamario.
- [2] <http://www.breastcancer.org>.

- [3] I. Reiser and I. Sechopoulos, "A review of digital breast tomosynthesis", *Med. Phys. Int. Journal.*, vol. 2, no. 1, pp. 57–66, 2014.
- [4] A. Smith, "Fundamentals of breast tomosynthesis: Improving the performance of mammography", *78967-12_WP-00007_FundmntlsTomo.*, March 2012.
- [5] D. Miklav i *et al.*, "Electrochemotherapy: technological advancements for efficient electroporation-based treatment of internal tumors", *Med. Biol. Eng. Comp.*, vol. 50, no. 10, pp. 1213–1225, Nov. 2012.
- [6] A. Zupanic, B. Kos and D. Miklav i, "Treatment planning of electroporation-based medical interventions: electrochemotherapy, gene electrotransfer and irreversible electroporation", *Phys. Med. Biol.* vol. 57, no. 17, pp. 5425–5440, Aug. 2012.
- [7] D. Miklav i *et al.*, "Towards Treatment Planning and Treatment of Deep-seated Solid Tumors by Electrochemotherapy", *BioMedical Engineering OnLine*, Sept. 2010.
- [8] S. Corovic, A. Zupanic, and D. Miklav i, "Numerical Model and Optimization of Electric Field Distribution in Subcutaneous Tumor Treated with Electrochemotherapy Using Needle Electrodes", *IEEE Transactions on Plasma Science*, vol. 36, no. 4, Aug. 2008.
- [9] D. Pavliha, B. Kos, A. Zupanic and D. Miklav i, "Patient-specific Treatment Planning of Electrochemotherapy: Procedure Design and Possible Pitfalls", *Bioelectrochemistry*, vol. 87, pp. 265-273, Jan. 2012.
- [10] B. Kos, A. Zupanic, T. Kotnik, M. Snoj, G. Sersa, D. Miklav i, "Robustness of treatment planning for electrochemotherapy of deepseated tumors", *J. Membrane Biol.*, vol. 236, pp. 147-153, 2010.
- [11] A. L. Vera-Tizatl, L. I. Garay-Jiménez, S. A. Rodríguez-Cuevas, A. Vera-Hernández, P. R. Hernández-Rodríguez, "3D Model and simulation of electroporation application on healthy and tumoral breast tissue", presented at the 10th International Conference on Electrical Engineering, Computing Science and Automatic Control (CCE), Mexico city, Mexico, 2013.
- [12] A. L. Vera-Tizatl, S. A. Rodríguez-Cuevas, L. Leija Salas and A. Vera-Hernández. "Review of electrochemotherapy-based Treatment of Cutaneous, Subcutaneous and Deep-seated Tumors towards Specific Treatment Planning", presented at the Global Medical Engineering Physics Exchanges/Pan American Health Care Exchanges (GMEPE/PAHCE), Madrid, Spain, April 4-9, 2016.
- [13] A. L. Vera-Tizatl *et al.*, "Electric Field Distribution Obtained by Using the Finite Element Method and 3D Reconstruction of a Breast Carcinoma: Approach to the Electroporation of Deep-seated Tumors by Using Two Needle Electrodes", presented at the 13th International Conference on Electrical Engineering, Computing Science and Automatic Control (CCE), Mexico city, Mexico, 2016.
- [14] A. L. Vera-Tizatl, C. A. Ramírez-Martínez, A. Vera-Hernández, L. Leija-Salas, S. A. Rodríguez-Cuevas, P. R. Hernández-Rodríguez. "Electric Field Distribution Generated by Two Needle Electrodes in an Anatomical Model of a Deep-Seated Breast Carcinoma", presented at the Electroporation Based Technologies and Treatments (EBTT), International Scientific Workshop and postgraduate course, Ljubljana, Slovenia 2016
- [15] J. Langus, M. Kranjc, B. Kos, T. Šuštar and D. Miklav i, "Dynamic finite-element model for efficient modelling of electric currents in electroporated tissues", *Sci. Rep.*, 6, 26409; doi: 10.1038/srep26409, May 2016.
- [16] S. Corovic, I. Lackovic, P. Sustaric, T. Sustar, T. Rodic and D. Miklav i, "Modeling of electric field distribution in tissues during electroporation", *BioMedical Engineering OnLine*, 2013, 12:16.
- [17] D. Sel, D. Cukjati, D. Batiuskaite, T. Slivnik, L. Mir and D. Miklav i, "Sequential Finite Element Model of Tissue Electroporation", *IEEE T. Biomed. Eng.* vol. 52, pp. 816-827, 2005.

APPENDIX I: CONFERENCE PAPER (PRODUCTIVITY)

Comparison of different electrode arrays for treatment of breast tumors with electrochemotherapy

Adriana Leticia Vera Tizatl¹, Arturo Vera Hernández¹, Lorenzo Leija Salas¹, Bor Kos², Damijan Miklavčič²

¹Department of Electrical Engineering, CINVESTAV-IPN, Mexico City, Mexico

²Faculty of Electrical Engineering, University of Ljubljana, Ljubljana, Slovenia
damijan.miklavcic@fe.uni-lj.si

Abstract—Four electrode arrays are proposed in this work in order to determine the most efficient configuration and develop a protocol to treat breast tumors and surrounding safety margin of 10 mm with electrochemotherapy. To achieve the therapeutic endpoint, electric fields of at least 400 V/cm need to be established in the whole target volume. Numerical modeling of the electric field distribution in the tissues of interest and their coverage was carried out through the finite element method in COMSOL Multiphysics (version 5.0) and Live link for Matlab. The outcomes obtained suggest that a 4-electrode array would be suitable for the treatment of a breast tumor and a safety margin of 10 mm while preserving a minimally invasiveness due to a reduced number of electrode insertion. An effective protocol for this particular electrode configuration results for 2500 V between an electrode inserted in the center of the tumor and three electrodes positioned 8 mm apart from the center of the tumor and 2000 V applied in the electrodes inserted into the safety margin tissue. Nevertheless, a 6-electrode array shows a higher coverage with lower electric current requirement compared with the 4-electrode array.

Keywords—breast tumor; electric-field coverage; electrochemotherapy; electrode array; safety margin

I. INTRODUCTION

Electrochemotherapy is a promising medical application of reversible electroporation used as a nonthermal local antitumor treatment in which electric pulses are applied to a target tumor after injection of a membrane-impermeant cytotoxic drug such as Bleomycin or Cisplatin [1]. Electroporation of cell membrane is caused by the application of an external electric field of sufficient magnitude [2] leading to an exchange of molecules originally non-permeable to the cell membrane [3]. Since electroporation increases the permeability of the cell membrane, the dose and in consequence, the side effects of chemotherapeutic agents can be reduced by using Electrochemotherapy (ECT). For efficient ECT, it is necessary that the entire tumor tissue is subjected to a local electric field in the range between reversible and irreversible electroporation threshold values [4, 5, 6]. The effective outcomes obtained with Electrochemotherapy application for the treatment of cutaneous and subcutaneous tumors regardless of histological origins, encourage the treatment of internal tumors [7, 8]. For this purpose, new standard operating procedures for deep-seated tumors are needed and hence,

treatment planning design has been developed taking as a basis radiotherapy treatment planning [9, 10]

Breast cancer is the second most common cancer worldwide, it is the most frequent cancer among women and it ranks as the fifth cause of death from cancer overall. Neoadjuvant chemotherapy, radiotherapy, hormonal therapy and surgical procedures including lumpectomy and mastectomy may represent the most common treatments for this disease [11]. Since breast cancer has become a rising problem concerning public health, current efforts are aimed to the control of known risk factors, the establishment of early detection programs and the development of new minimally invasive and conservative treatment procedures to this disease.

It has been suggested that it is possible that any target tissue in any location may be treated by Electrochemotherapy with appropriate electrodes and an accurate positioning provided by image guided assistance since tissue electroporation depends on local electric field distribution and this is in turn a function of the electrode geometry and positioning, tissue anatomy and tissue dielectric properties [4]. This can be done through numerical modelling of electroporation which represents currently the only efficient way to predict electric field distribution in biological tissues. Combined with medical imaging analysis and optimization methods, finite element modelling can be used for developing patient-specific treatment planning of electroporation-based treatments by determining the minimal number of electrodes to be inserted, their optimal positioning and electric pulse amplitude to cover the whole target lesion [4, 8, 12].

The purpose of this work is comparing four different electrode arrays for the treatment of breast tumors and a surrounding safety margin of surrounding tissue. Different voltage scenarios were considered to establish the most convenient protocol to assure a complete coverage of the target tissues [4, 13, 14].

II. METHODOLOGY

A. Model Geometry

The model geometry used in the work consists of a spherical tumor of 10 mm in diameter. In the clinical practice, eradication of a safety margin surrounding tumoral tissue measuring at least 10 mm from the tumor edge is required, hence a sphere of 30 mm in diameter was modeled as the safety margin. Both spheres are embedded in a 50 mm x 50 mm x 50 mm block of surrounding healthy tissue. Cylinders of 1.2 mm diameter and 30 mm length are used to simulate the electrodes.

B. Numerical modeling

Four arrays of needle electrodes were used to determine the configuration producing a complete coverage of the tissues of interest as shown in Fig. 1. For three cases (triangle, diamond and star configuration), an intratumoral electrode was considered in the center of the tumor and the rest of the electrodes are inserted equidistant to it into the safety margin, 8 mm away from the tumor edge. Additionally, a 4-electrode (diamond) configuration with all the needles inserted into the safety margin 8 mm away from the tumor edge, was analyzed. Boundary conditions for voltage are set on pairs of electrodes. Initial conductivity values of the tumor, safety margin and healthy-breast surrounding tissue were conferred in each point of the model by interpolation functions as 0.4 S/m, 0.03 S/m respectively. An electric field dependent conductivity was considered as suggested in [15, 16] hence final conductivity values for the tumor, safety margin and healthy-breast surrounding tissue were 1.2 S/m, 0.09 S/m respectively. Modeling was performed in COMSOL Multiphysics (version 5.0) and Live link for Matlab as reported in [14]. A built-in free tetrahedral meshing algorithm for a normal quality mesh was used. For the configurations in Fig. 1b, 1d, and 1e, electrodes are activated considering first the electrode pairs formed by the central electrode and the electrodes into the safety margin tissue and then the electrode pairs into the safety margin only. On the other hand, electrodes corresponding to the configuration in Fig. 1c, are activated in the 6 possible combinations in order to cover the complete regions of interest. The distance between the electrodes and the applied voltage for all the arrays are shown in Table 1. After voltages on all of them are computed, the total coverage of the tumor and the safety margin with electric field between reversible (400 V/cm) and irreversible (800 V/cm) electroporation thresholds values [17, 18] are determined. For all the electrodes arrays, an initial voltage protocol is first simulated. The resulting tissue coverage obtained for this first simulation allows the adjustment of the voltage to improve the tissue coverage. Therefore, different voltage values are simulated until an efficient coverage close to the reversible electroporation threshold for both tissues of interest is obtained. The outcomes for this efficient coverage are referred in Table 1 as final simulation.

C. 4-Electrode (triangle) array

Activation of the electrode pairs for this array is E1E2, E1E3, E1E4 (central-peripheral pairs) and E2E3, E3E4, E2E4 (peripheral-peripheral pairs) sequentially. An initial voltage of 2000 V between all electrode pairs was applied.

D. 4-Electrode (diamond) array

This configuration consists of 4 electrodes placed into the safety margin, 8 mm apart from the tumor edge with no intratumoral electrode. Adjacent electrodes are first activated, i. e., E1E2, E2E3, E3E4, E1E4, followed by the electrodes forming diagonals E1E3 and E2E4.

E. 5-Electrode (diamond) array

Activation of the electrode pairs for this array is E1E2, E1E3, E1E4, E1E5 (central-peripheral pairs) and E2E3, E3E4, E4E5 and E2E5 (peripheral-peripheral pairs) sequentially. Since the distance between the electrodes into the safety margin is shorter than the distance resulting in the 4-electrode (triangle) array, an initial voltage of 2500 V and 2000 V, resulting as the best protocol for the 4-electrode (triangle) array, was applied between the electrodes activated with the intratumoral electrode and the electrodes inserted into the safety margin respectively.

F. 6-Electrode (star) array

Activation protocol for this electrode array is E1E2, E1E3, E1E4, E1E5, E1E6 (central-peripheral pairs) and E2E3, E3E4, E4E5, E5E6 and E2E6 (peripheral-peripheral pairs) sequentially. A voltage of 2000 V and 1000 V between the electrodes activated with the intratumoral electrode and the electrodes inserted into the safety margin was first considered and then the values were reduced based on the results in order to improve the coverage.

III. RESULTS

The computed electric current for all the electrode arrays and the voltage protocols are listed in Table I where C-P refers to the electrode pair including the central electrode and the electrodes into the safety margin, referred further on as peripheral electrodes, hence P-P refers to the pulses applied between electrodes outside the tumor. Electrodes forming diagonals in the 4-electrode (diamond) array are described by D. In addition, the electric field for a complete coverage of the tissues of interest is reported for 100% of the tumor volume and the safety margin volume which represents 13.6 cm³ of the total model volume.

It can be seen that for the 4-electrode (triangle) array, the most efficient protocol regarding the complete coverage of the tissues of interest (tumor and the safety margin tissue) and the electric current required for this purpose, is achieved with 2500 V and 2000 V between C-P and P-P, respectively. On the other hand, with a 4-electrode (diamond) array very high voltages need to be used in order to ensure tumor coverage, which leads to very high fields in the safety margin.

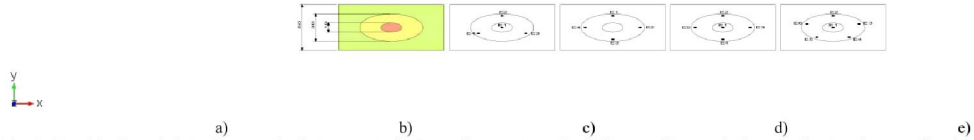


Fig. 1. Topside view of electrode arrays for the treatment of a 5 mm diameter tumor (red), 10 mm safety margin tissue (yellow) and surrounding tissue (green). a) model geometry, dimensions are in mm, b) 4-electrode array (triangle configuration), c) 4-electrode array (diamond configuration) and d) 6-electrode array (star configuration).

TABLE II. Electroporation Protocols used for Coverage of Tumor and Safety Margin with 4-Electrode Arrays

Electrode array		Active pairs	Distance [mm]	Initial Simulation				Final Simulation			
# needles	Conf.			Voltage [V]	Average current [A]	Cumulative coverage [V/cm]		Voltage [V]	Average current [A]	Cumulative coverage [V/cm]	
						Tumor	Safety Margin			Tumor	Safety Margin
4	triangle	C-P	13.0	2000	6.60	341.2	527.4	2500	8.56	403.3	513.1
		P-P	22.5	2000	4.10			2000	4.10		
	diamond	P-P	18.4	2000	4.58	283.9	422.4	3500	8.91	412.8	737.4
		D	26.0	2500	5.04			4000	9.20		
5	diamond	C-P	13.0	2500	8.60	460.6	670.6	1950	6.43	403.3	494.0
		P-P	18.4	2000	4.58			---	---		
6	star	C-P	13.0	2000	6.67	427.1	594.2	1700	5.44	412.8	522.6
		P-P	15.3	1000	1.96			---	---		

For the 5-electrode (diamond) array, the optimal coverage was obtained for a voltage of 1950 V between C-P. It is worth noting that no electric potential is required between P-P for this configuration. For the 6-electrode array, a voltage value of 1700 V applied between C-P electrodes, is enough to achieve a complete coverage of the tissues of interest.

The cumulative coverage curves for the tissues of interest corresponding to the most efficient protocols for each electrode array in Table I are shown graphically in Fig. 3, and Fig. 4 where each line represents the coverage produced by each pair of electrodes sequentially activated. Similar to the dose-volume histograms used in radiotherapy, the cumulative coverage curves in Fig. 3 and Fig. 4 show the volume fraction of the tumor and the volume of safety tissue (which represents for this tumor geometry 13.6 cm³ of the total volume) covered by an electric field of at least the value indicated on the x axis. An effective coverage is considered when the total tissue volume is completely covered by an electric field ranging from 400 V/cm and 800 V/cm.

In Fig. 3a, it can be seen that more than 50 % of the tumor might be irreversibly electroporated by using the 4-electrode (triangle) array. On the other hand, coverage of the tumor with less than 20 % irreversibly electroporated, is obtained by using a 4-electrode array with no intratumoral electrode. However, the electric current requirements and high voltage values to get this coverage are very high and would not be feasible with currently available clinical pulse generators. 5-electrode and 6-electrode arrays show a more efficient coverage based on the volume amount of tumoral tissue irreversibly electroporated and the lower electric currents compared with the two previous arrays. Fig. 4 shows that for all electrode configurations, the

safety margin is exposed to higher electric fields than the tumor due to the difference in conductivity considered in this model.

IV. DISCUSSION

The electric field distribution was solved for four electrode arrays proposed in a configuration aimed to the treatment of two target tissues, i. e., a breast tumor and a safety volume tissue. The dimensions of 10 mm from the tumor edge corresponding to a safety margin was established by oncologists. In order to reduce the distance between the electrodes while assuring an electric field above the reversible electroporation threshold, an electrode inserted into the target tumor was considered for three electrode arrays and the remaining electrodes were inserted into the safety margin whereas a fourth array consisting of four electrodes positioned into the safety margin tissue and no electrode inside the tumor were considered. An initial protocol of 2000 V pulses applied to all electrode pairs in a 4-electrode (triangle) array was first modeled. The results demonstrate an insufficient tumor coverage (below 400 V/cm) therefore the voltage was increased up to 2500 V and 2000 V between C-P and P-P electrodes. The outcomes for this array show an effective minimal invasive scenario due to the reduced number of electrodes but the required electric current is higher than the 5-electrode and 6-electrode arrays. For the 5-electrode configuration, the optimal protocol of 2500 V and 2000 V used for the 4-electrode (triangle) configuration, was considered as the first protocol to simulate since the distance between the electrodes is shorter for this configuration. As the

voltage was reduced, it was observed that a complete coverage may be obtained by activating the C-P electrode pairs only, i. e., the pairs of electrodes formed by the needles outside the tumor may remain inactive. Similarly, for the 6-electrode array, 1700 V in the C-P configuration is enough to completely cover the tissues of interest. Alternatively, the use of electrodes inserted only into the safety margin tissue and no electrode into the tumor, leads to a higher demand of voltage and consequently to the highest electric current required for the complete coverage of the tissue volume compared to the arrays containing an intratumoral electrode.

The electrode arrays presented in this work may offer a guideline to further electroporation modeling of realistic breast tumors and a safety margin tissue. Nevertheless, voltage protocols and electric current requirements shall be likely to differ from the outcomes showed in Table I depending on the size of the tumor and the corresponding safety margin size. In addition, non-homogeneity of breast was not assumed in this work and hence, electric field distribution in models containing fatty tissue, fibroglandular breast tissue, skin and neoplastic tissue, will lead to outcomes contrasting those in Table I.

V. CONCLUSION

Based on the electrode arrays presented in this work, we may conclude that a 4-electrode array would be suitable for the treatment of a breast tumor and a safety margin of 10 mm while preserving a minimally invasiveness due to a reduced number of electrode insertion. Nevertheless, a 6-electrode array shows a higher coverage with lower electric current compared with the 4-electrode array so the decision on what array to use shall depend on the tumor location and the electroporation hardware. It is worth noting that the efficiency of the treatment depend on an accurate positioning of the electrodes since a variation in the positioning lead to a considerably variation in coverage of the target tissue [19]. The electrode arrays proposed in this work for the treatment of breast tumors and a safety margin tissue of 10 mm can be used as basis for further modeling of electroporation of realistic breast tumors. In future work anatomical models of breast tumors based on medical imaging will be developed and combined with breast models and computational breast phantoms in order to a develop a more realistic breast model.

ACKNOWLEDGMENT

A. L. Vera Tizatl thanks the National Council for Science and Technology (CONACYT, Mexico) for the scholarship granted. This research was supported in part by the Slovenian Research agency (Grants P2-0249 and Z3-7126). It has been performed within the scope of LEA EBAM.

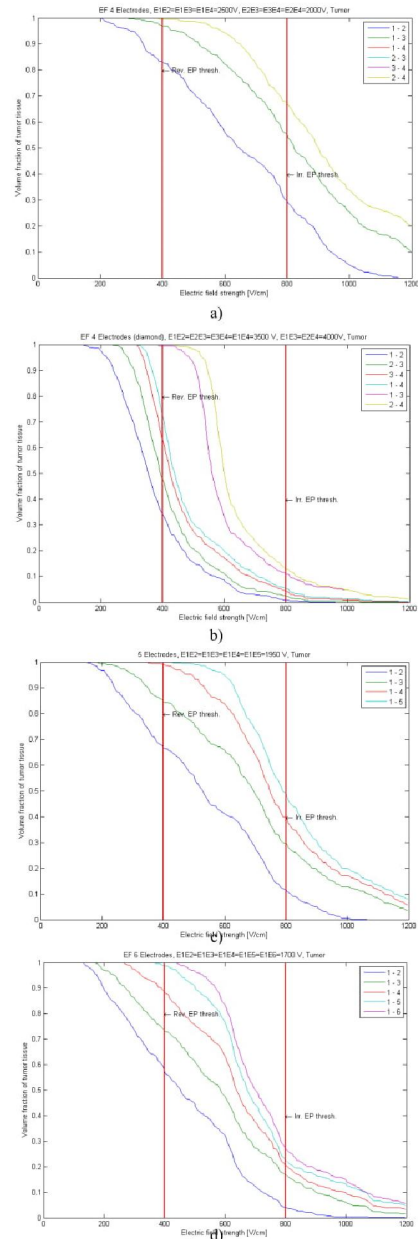


Fig. 3. Cumulative coverage of the tumor volume for the a) 4-electrode (triangle) array, b) 4-electrode (diamond) array, c) 5-electrode (diamond) array and d) 6-electrode (star) array

REFERENCES

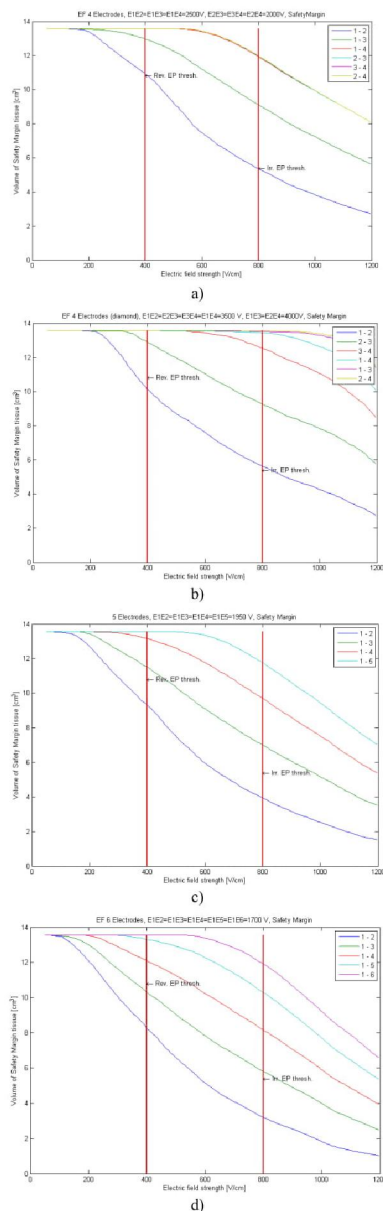


Fig. 4. Cumulative coverage of the safety margin volume for the a) 4-electrode (triangle) array, b) 4-electrode (diamond) array, c) 5-electrode (diamond) array and d) 6-electrode (star) array

- [1] Orłowski S, Belehradek J, Paoletti C and Mir L. M. (1988). Transient electroporability of cells in culture, increase of the cytotoxicity of anticancer drugs, *Biochemical Pharmacology*, 37(24), 4727-4733.
- [2] Rems L. and Miklavcic D. (2016). Tutorial: Electroporation of cells in complex materials and tissues. *Journal of Applied Physics*, 119, 201101
- [3] Kotnik T, Kramar P, Pucihar G, Miklavcic D, and Tarek M. (2012). Cell Membrane Electroporation-Part 1: The Phenomenon, *IEEE Electrical Insulation Magazine*, 28(5), 14-23
- [4] Zupanic, A., Kos, B., & Miklavcic, D. (2012). Treatment planning of electroporation-based medical interventions: electrochemotherapy, gene electrotransfer and irreversible electroporation. *Physics in Medicine and Biology*, 17(57), 5425-5440.
- [5] Haberl, S. et al. (2013). Cell Membrane Electroporation-Part2: The Applications. *IEEE Electrical Insulation Magazine*, 29(1), 29-37.
- [6] Miklavcic D., Pavselj N, and Hart F. X. (2006), *Electric Properties of Tissues*. Wiley Encyclopedia of Biomedical Engineering.
- [7] Mali B., Jarm T., Snoj M., Sersa G. and Miklavcic D. (2013). Antitumor effectiveness of electrochemotherapy: A systematic review and meta-analysis. *EJSO*, 39, 4-16.
- [8] Miklavcic, D. et al. (2012). Electrochemotherapy: technological advancements for efficient electroporation-based treatment of internal tumors. *Med. Biol. Eng. Comput*, 1213-1225.
- [9] Pavliha, D. et al. (2012). Patient-specific treatment planning of electrochemotherapy: Procedure design and possible pitfalls. *Bioelectrochemistry* 87, 265-273
- [10] Pavliha, D. et al. (2013). Planning of electroporation-based treatments using web-based treatment planning software. *J. Membrane Biol.*, 246, 833-842.
- [11] Masson Doyma México S. A. . (2015). Consenso Mexicano sobre diagnóstico y tratamiento del cáncer mamario
- [12] Edhemovic I. et al. (2014). Intraoperative Electrochemotherapy of Colorectal Liver Metastases. *Journal of Surgical Oncology*. 110, 320-327.
- [13] Vera Tizatl, A. L. et al. (2017). Investigation of numerical models for planning of electrochemotherapy treatment of invasive ductal carcinoma. presented at the Global Medical Engineering Physics Exchanges/Pan American Health Care Exchanges (GMEPE/PAHCE), Chiapas, Mexico, March 20-25, 2017.
- [14] Marcan M, Pavliha D, Kos B, Forjanič T, and Miklavčič D. (2015). 'Web-Based Tool for Visualization of Electric Field Distribution in Deep-Seated Body Structures and Planning of Electroporation-Based Treatments'. *Biomedical Engineering Online* 14 Suppl 3.
- [15] J. Langus, M. Kranjc, B. Kos, T. Šuštar and D. Miklavčič. (2016), Dynamic finite-element model for efficient modelling of electric currents in electroporated tissues, *Sci. Rep.*, 6, 26409.
- [16] S. Corovic, I. Lackovic, P. Sustaric, T. Sustar, T. Rodic and D. Miklavčič, (2013). Modeling of electric field distribution in tissues during electroporation, *BioMedical Engineering OnLine*, 12-16.
- [17] Sel, D., Cukjati D., Batuskaite D., Slivnik T., Mir L. M., and Miklavcic D.. (2005). Sequential Finite Element Model of Tissue Electroporability. *IEEE Transactions on Biomedical Engineering* 52(5), 816-27.
- [18] Kranjc M, Markelc B, Bajd F, Čemažar M, Serša I, Blagus T, and Miklavčič D. (2015). In Situ Monitoring of Electric Field Distribution in Mouse Tumor during Electroporation. *Radiology*, 274(1), 115-123,
- [19] Kos, B. et al. (2010). Robustness of treatment planning of electrochemotherapy of deep seated tumors. *J Membrane Biol*, 174-153.

APPENDIX J: CONFERENCE PAPER (PRODUCTIVITY)

2018 15th International Conference on Electrical Engineering, Computing Science and Automatic Control (CCE)
Mexico City, Mexico, September 5-7, 2018

Establishment of Electroporation Protocols in BT-20 and SKOV-3 Cell Lines based on Finite Element Modeling

C. E. Vera-Tizatl^{1*}, A. L. Vera-Tizatl², J. C. Osorio-Trujillo¹, P. Talamás-Rohana¹, S. Rodríguez-Cuevas³, L. Leija-Salas², A. Vera-Hernández²

¹Departamento de Infectómica y Patogénesis Molecular, CINVESTAV, Mexico City, Mexico

²Departamento de Ingeniería Eléctrica, CINVESTAV, Mexico City, Mexico

³Sociedad Mexicana de Oncología, Mexico City, Mexico.

* Corresponding author. E- mail: cavera@cinvestav.mx

Abstract—A current treatment method of cutaneous and subcutaneous tumors is based on an application of electroporation, known as Electrochemotherapy (ECT). We infer, from the outcomes reported on these malignancies, that ECT might be utilized for eradication of primary deep-seated breast malignancies. The aim of this work is therefore, to establish an electroporation protocol specific for breast tissue, based on a finite element model of electroporation of BT-20 cells, and *in vitro* electroporation. These electroporation protocols were compared with those obtained with a second cell line SKOV-3, an ovarian carcinoma derived cell line, in order to determine whether the cellular origin has an effect on efficiency of an electroporation protocol predicted by computational models simulating *in vitro* conditions. Efficiency was verified through the determination of propidium iodide uptake and cell viability by epifluorescence microscopy and MTT assay. The results show that a protocol of 8 pulses of 150 V, pulse width of 100 μ s, and pulse repetition frequency of 1 s, leading to a cell viability of 98.7 % in SK-OV-3 cell line is in accordance with the computational model predictions. Nonetheless, this protocol must be modified to a protocol of 8 pulses of 140 V, pulse width of 100 μ s, and pulse repetition frequency of 1 s, so that a maximal cell viability of 89.1 % in BT-20 cell line can be obtained. A limitation of the methodology in this work is the atypical use of suspended SK-OV-3 and BT-20 cell, since they are adherent i.e., these cells require a substratum to keep their epithelial and morphological features which may lead to significant variations whether electroporation of attached cells was carried out. Nevertheless, the contribution of this research is the determination of a first specific protocol of reversible electroporation for a human breast cancer cell line. Consequently, the establishment of organ-specific electroporation protocols planned prior to experimental application is encouraged.

Keywords—breast cancer, electroporation, epifluorescence microscopy, finite element modeling, MTT assay.

I. INTRODUCTION

Electroporation or electroporation (EP) consist in the formation of temporary hydrophilic pores in the cell membrane because of induction of an increased transmembrane potential difference (>200 mV) after cell

exposure to pulsed electric fields ranging from 300 to 3000 V/cm [1,2]. These structural changes in the membrane are reflected in an increased permeability to non-permeant and large molecules such as exogenous DNA, immunoglobulins, proteins and drugs [3, 4]. Intense electric fields caused by high-voltage pulses, when combined with antineoplastic drugs, lead to a phenomenon known as Electrochemotherapy (ECT). It has been established as a local treatment at an oncological level in both, humans and animals for the eradication of cutaneous and subcutaneous tumors independent of the histological type [5,6]. ECT is mainly used in the European Union (EU) as a palliative alternative of skin metastases derived from melanoma, breast, Kaposi's sarcoma, squamous and basocellular carcinoma, all of them responsible of ulceration, bleeding and pain [7-10].

In Mexico, breast cancer represents a major disease because of its mortality rate [11]. Therefore, implementation of ECT for the eradication of the primary breast tumor could address the inadequate dosage in the region of interest and avoid side effects of conventional chemotherapy. Nevertheless, due to the lack of protocols targeted to breast cancer treatment, our group of research is focused on the establishment of threshold values specific for mammary cells. In this work we present a comparison between computational simulations and *in vitro* assays carried out in a breast cancer cell line and in an ovarian cancer cell line, in order to determine whether electroporation protocols could be predicted and extrapolated to both cases.

II. MATERIALS AND METHODS

A. Cell cultures

The human breast cancer cell line BT-20 (ATCC® HTB-19™) was grown in Eagle's Minimum Essential Medium (EMEM) ATCC® 30-2003™). The human ovarian cancer cell line SK-OV-3 (ATCC® HTB-77™) was grown in McCoy's 5A Medium (Corning™ cellgro™). 10% fetal bovine serum was added to both cell lines in a humidified environment (95% air, 5% CO₂) at 37 °C. For all experiments, the cell suspensions were prepared from

confluent cultures with a 0.25% trypsin solution comprising 0.034% ethylene diamine tetraacetic acid (EDTA). The ensuing pellet was resuspended in new medium. The assays for both cell lines consist of 4 samples, each containing 150,000 cells for their further exposure to electroporation. Each experiment was repeated three times. Two groups were considered; a) a control group without electric stimulation and b) an experimental group exposed to electric stimulation. Initial electrical conductivity in the 40 ml total volumes of SKOV-3 and BT-20 cells in suspension was measured at 37 °C with a conductivity meter HANNA HI8633, EMC deviation: $\pm 2\%$. The conductivity meter was calibrated prior measurement with a HI 7030 calibration solution of 1.288 S/m. Measured values were 0.75 S/m in SKOV-3 cell suspension, and 0.71 S/m in BT-20 cell suspension. All the volume samples of each cell line to undergo electroporation were taken from the total volume.

B. Numerical model of electroporation in cell suspension

A finite element model of cells suspension of 500 μ l contained in an electroporation cuvette (12 mm x 12 mm x 40 mm) was created in COMSOL Multiphysics 5.1, on an Intel(R) Core(TM) i5 -6500, 3.20GHz, 4 -core processor. The aim of modeling the electroporation of cell suspensions by the finite element method is to establish the pulse amplitude which will generate an electric field strength in the cell suspensions ranging from 400 V/cm to 800 V/cm, and hence causing reversible electroporation in cells [12, 13]. The cuvette and cell suspension were modeled as 3D domains as shown in Fig. 1. Two parallel plates (4 mm x 12 mm x 20 mm) inside the cuvette geometry simulate the electrodes. One plate is set as a voltage terminal and the second plate is grounded to simulate application of pulses.

Materials were assigned as; aluminum for the electrodes (Fig. 1.a), water for the culture medium (Fig. 1.b) with a relative permittivity of 80.1, and an electrical conductivity value in accordance with its prior measurement and air for the cuvette volume without medium (Fig. 1. c). The governing equation of electroporation phenomenon defining the transmembrane potential distribution is described by Eq. 1 [14]:

$$\frac{\partial \varphi}{\partial t} = \nabla \cdot (\sigma \nabla \varphi) \quad \text{Eq. (1)}$$

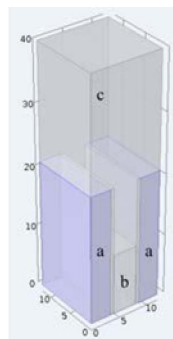


Fig. 1. Computational model of electroporation cuvette. a) parallel aluminum plates, b) cell suspension and c) air.

where, φ represents the electric potential, and σ indicates the electrical conductivity. During electroporation, cells undergo an increase of electrical conductivity due to cell membrane permeabilization [15, 16], therefore an increasing conductivity dependent on electric field E is assumed through a smoothed step function [17] as shown in Eq. (2) and Fig. 2.

$$\sigma(E) = \begin{cases} \sigma_0 & E < E_{rev} \\ \frac{\sigma_f - \sigma_0}{E_{irr} - E_{rev}} E & E_{rev} \leq E \leq E_{irr} \\ \sigma_f & E > E_{irr} \end{cases} \quad \text{Eq. (2)}$$

where, $E_{rev} = 400$ V/cm and $E_{irr} = 800$ V/cm show reversible and irreversible electroporation threshold respectively, σ_0 is the initial electrical conductivity of culture medium (0.75 S/m and 0.71 S/m for SKOV-3 and BT-20 respectively) and, $\sigma_f = 3\sigma_0$ is the final electrical conductivity of culture medium. A parametric study was considered in the model, varying the voltage amplitude from 50 V up to 400 V in increments of 50 V. Solutions for both cell suspension models converged at 10 s by using 18190 free tetrahedral mesh and a parametric non-linear solver.

C. Application of electric stimulation

The cell suspensions (200 μ l of 1.4×10^5 cells per ml) were cultured in electroporation cuvettes (0.4 cm electrode gap, Gene Pulser®/Micropulser™). Propidium iodide (5 μ l) (PI, P4170, Sigma–Aldrich) was utilized as a fluorescent dye in order to visualize exogenous molecules uptake. Cell suspensions were exposed to electric pulses delivered by a BTX830 Square Wave Electroporation System (ECM® 830). For both SK-OV-3 and BT-20 cell lines, voltage was varied in a range from 100 V to 250 V in increments of 50 V. For each voltage value, 4 and 8 pulses were applied. Pulse width of 100 μ s and pulse repetition frequency of 1 s were used for all cell suspensions. After application of electric pulses, cell suspensions were transferred to 24-well plates.

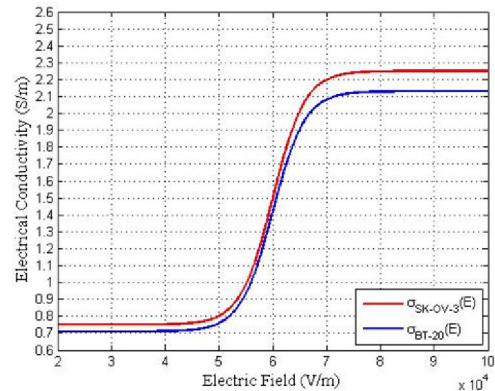


Fig. 2. Smoothed step function describing the increasing conductivity of SK-OV-3 cell line (red line) and BT-20 cell line (blue line).

TABLE I. SIMULATED ELECTROPORATION PROTOCOLS.

Voltage [V]	Electric Field [V/cm]
50	125
100	250
150	375
200	500
250	625
300	750
350	875
400	1000

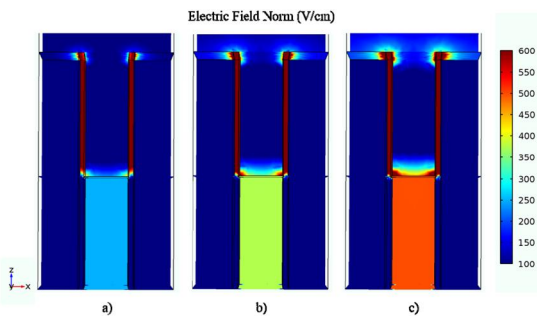


Fig. 3. Electric field distribution generated in cell suspensions due to the application of a) 100 V, b) 150V and c) 200 V.

D. Cell viability assay

Forty-eight h after electric pulses exposure, cell viability measurement was done through the methylthiazolyldiphenyltetrazolium bromide (MTT) assay (Sigma-Aldrich, St. Louis, MO, USA) at 570 nm. The accurate way of determining cell viability is through the reduction by metabolically active cells of yellow tetrazolium salts, MTT (3-(4, 5-dimethylthiazolyl-2)-2,5diphenyltetrazolium bromide) to its insoluble formazan, which has a purple color [18]. The absorbance readings obtained in each of the three repetitions were averaged to determine percentage of cell viability.

E. Visualization of permeated molecules

PI uptake by electroporated cell membranes was monitored immediately after electric field exposure through epifluorescence microscopy and 48 h after electroporation.

III. RESULTS

The electric field distribution calculated by computational simulations of electroporation in cuvettes point out that voltage values ranging from 150 V to 300 V, generate an electric field within a reversible electroporation threshold (400 V/cm – 800 V/cm) as shown in Table I. Electric field distribution generated in suspended cells, is shown in Fig. 3, where it can be seen that a voltage of 100 V seems to be not enough to cause a reversible electroporation,

TABLE III. EXPERIMENTAL ELECTROPORATION PROTOCOL 1

Voltage [V]	Number of Pulses	Cell viability [%]		Electric field magnitude [V/cm]
		SK-OV-3 cell line	BT-20 cell line	
100	4	100	70	250
100	8	100	68.2	
150	4	100	59.7	375
150	8	98.7	52	
200	4	97.1	28.2	500
200	8	92	24.4	
250	4	100	21.6	625
250	8	94.3	17.6	

TABLE II. EXPERIMENTAL ELECTROPORATION PROTOCOL 2

Voltage [V]	Number of Pulses	Cell viability in BT-20 cell line [%]	Electric field magnitude [V/cm]
120	4	71	300
120	8	70	
140	4	82.5	350
140	8	89.1	
160	4	57.8	400
160	8	65.5	
180	4	24.9	450
180	8	27.1	

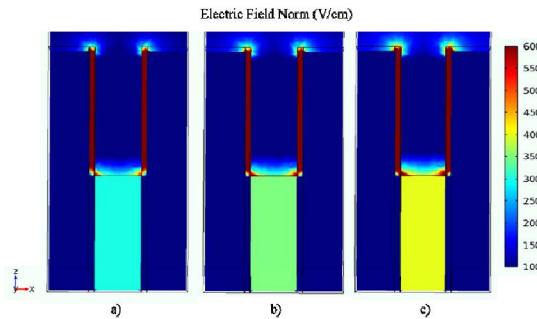


Fig. 4. Electric field distribution generated in BT-20 cell suspension due to the application of a) 120 V, b) 140 V and c) 160 V.

moreover voltages exceeding 150 V are more likely to generate a reversible electroporation. In the case of SK-OV-3 cell line we found out an efficient electroporation protocol consisting of 8 pulses of 150 V, pulse width of 100 μ s, and pulse repetition frequency of 1 s, resulting in the maximum cell viability percentage of 98.7 % along with the maximum PI uptake as shown in Table II. Nonetheless, the voltage values obtained from computational simulations were



Fig. 5. Propidium Iodide (PI) uptake of SK-OV-3 cell line after exposure to electric pulses of: a) 100 V, b) 150 V, c) 200 V, d) 250 V and e) control of electroporation without exposure. The PI uptake by electroporated cells is shown as white spots. Images taken with a Nikon diaphot inverted phase contrast microscope. Objective 40 X.

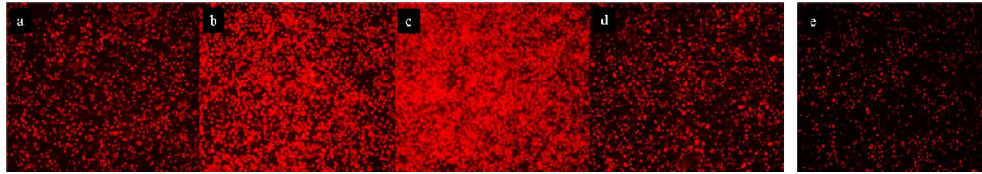


Fig. 6. Propidium Iodide (PI) uptake of BT-20 cell line after exposure to electric pulses of: a) 120 V, b) 140 V, c) 160 V, d) 180 V and e) control of electroporation without exposure. The PI uptake by electroporated cells is shown as red spots. Images taken with Nikon Eclipse Ti-U. Objective 40 X.

modified for the BT-20 cell line due to the lower percentage of cell viability obtained through MTT assay. Therefore, this cell suspension was exposed to a second electroporation protocol, i.e., pulse amplitude was ranged from 120 V to 200 V in increments of 20 V. Four and 8 pulses were applied for each voltage value. Pulse width of 100 μ s and pulse repetition frequency of 1 s were used. The electric field distribution obtained for this protocol is shown in Fig. 4. For this cell line, the maximum percentage of cell viability of 89.1 % was obtained with 8 pulses of 140 V corresponding to an electric field of 350 V/cm, 100 μ s pulse width, and pulse repetition frequency of 1 s, as shown in Table III.

The PI uptake obtained with different voltages in the electroporation protocol 1 for SK-OV-3 cell line and in electroporation protocol 2 for BT-20 cell line is shown in Fig. 5 and Fig. 6 respectively. On one hand, the maximum PI uptake in SK-OV-3 cells was obtained with 250 V (Fig. 5d). On the other hand, the maximum PI uptake in BT-20 cells was obtained with 160 V (Fig. 6c). The negative electroporation controls for both SK-OV-3 (Fig. 5e) and BT-20 cells (Fig. 6e) show a slight uptake of PI due to the trypsinization process. Nevertheless, it is possible to appreciate differences between experimental conditions and controls.

IV. DISCUSSION

Breast cancer treatment with ECT has been previously addressed by our group of research through the finite element computational modeling. Nevertheless, we consider that the establishment of finer and accurate electroporation protocols specific for particular tissues is required in order to achieve a more efficient treatment. The outcomes obtained in this work show that computational modeling represents a useful tool for predicting electric field distribution in cell suspensions of known electrical conductivity as shown in Table I. In spite of this, there are some parameters that cannot be modeled, e. g., the number

of pulses, since the duration of the pulse (100 μ s) implies a static phenomenon.

It can be seen in Table II, that the most effective electroporation protocol for SKOV-3 cells is in accordance with the protocol predicted by the simulation in Table I. However, this protocol resulted in a non-efficient electroporation of BT-20 cells regarding PI uptake and cell viability. The results show that an efficient electroporation protocol must take into account the maximum PI uptake along with the maximum cell viability percentage besides the electric field distribution. Though voltage values in computational modeling generate an electric field distribution within reversible electroporation threshold, experimental results show high rate of cell death as it is the case of 180 V with 27.1 % of cell viability for BT-20 cell line. Differences between computational modeling and experimental results might be due to the features of the cells conforming tissues, such as size, shape and organizational level in epitheliums.

V. CONCLUSION

Computational modeling provides an initial guidance for determining a reversible electroporation protocol prior to experimental assays which accuracy relies on the knowledge of dielectric properties of the cell type of interest.

The results show experimentally that there exist differences between the two cell lines used in this work regarding the most effective electric protocol based on PI uptake and cell viability. Though, differences in voltage values for the two cell lines seem to be non-representative, it has been shown that these slight differences of 10 V, lead to a dramatic decrease of cell viability. Therefore, the establishment of electroporation protocols specific for a particular tissue of interest is mandatory.

ACKNOWLEDGMENT

Authors thank MSc. José Hugo Zepeda for his support to carry out conductivity measurements in this work. C. E. Vera-Tizatl and A. L. Vera-Tizatl thank the National Council for Science and Technology (CONACYT, Mexico) for the scholarship granted. Authors appreciate the funding for the development of the work presented project: CSIC-COOPB20166, ERAnet-EMHE 200022 and CYTED-DITECROD-218RT0545.

REFERENCES

- [1] SH. Meglič, T. Kotnik. Electroporation-Based Applications in Biotechnology. Handbook of Electroporation. 2017:2153-2169.
- [2] J. Escoffre, J. Teissié, M. Rols. Gene Transfer: How can the biological barriers be overcome. The Journal of Membrane Biology. 2010; 236(1):61-74. doi:10.1007/s00232-010-9275-0.
- [3] ML. Yarmush, A. Golberg, G. Serša, T. Kotnik, D. Miklavčič. Electroporation-based technologies for medicine: principles, applications, and challenges. Annual Review of Biomedical Engineering. 2014; 16(1):295-320.
- [4] U. Kamensek, M. Cemazar, UL. Tratar, K. Ursic, G. Sersa. Antitumor in situ vaccination effect of TNF α and IL-12 plasmid DNA electrotransfer in a murine melanoma model. Cancer Immunology, Immunotherapy. 2018. doi:10.1007/s00262-018-2133-0
- [5] F. Ricotti, K. Giuliadori, I. Cataldi et al. Electrochemotherapy: an effective local treatment of cutaneous and subcutaneous melanoma metastases. *Dermatologic Therapy*. 2013; 27(3):148-152. doi:10.1111/dth.12098.
- [6] J. Escoffre, M. Rols. Electrochemotherapy: Progress and prospects. *Current Pharmaceutical Design*. 2012; 18(23):3406-3415
- [7] Electrochemotherapy for metastases in the skin from tumours of non-skin origin and melanoma | Guidance and guidelines | NICE. Niceorguk. 2017. Available at: <https://www.nice.org.uk/guidance/ipg446/chapter/1-Guidance>. Accessed May 24, 2018
- [8] V. Seccia, L. Muscatello, et al. Electrochemotherapy and its controversial results in patients with head and neck cancer. *Anticancer research*. Vol 34, pp. 967-972, 2014.
- [9] L. Matthiessen, H. Johannesen, H. Hendel, T. Moss, C. Kamby, J. Gehl. Electrochemotherapy for large cutaneous recurrence of breast cancer: A phase II clinical trial. *Acta Oncologica*. Vol. 51, No. 6, pp. 713-721, 2012.
- [10] JL. Vásquez, P. Ibsen, H. Lindberg, J. Gehl. In Vitro and In Vivo Experiments on Electrochemotherapy for Bladder Cancer. *The Journal of Urology*. No. 193, Vol 3, pp. 1009 – 1015, 2015.
- [11] Cancer fact sheets: all cancers excluding non-melanoma skin cancer. *Gcoiarefr*. 2017. Available at: <http://gco.iarc.fr/today/data/pdf/fact-sheets/cancers/cancer-fact-sheets-29.pdf>. Accessed May 23, 2018
- [12] D. Miklavčič et al., "Towards Treatment Planning and Treatment of Deep-seated Solid Tumors by Electrochemotherapy", *BioMedical Engineering OnLine*, 2010.
- [13] S. Corovic, A. Zupanic, and D. Miklavčič, "Numerical Model and Optimization of Electric Field Distribution in Subcutaneous Tumor Treated with Electrochemotherapy Using Needle Electrodes", *IEEE Transactions on Plasma Science*, vol. 36, 2008.
- [14] A. Ivorra, B. Al-Sakere, B. Rubinsky, and L. M. Mir. In vivo electrical conductivity measurements during and after tumor electroporation: conductivity changes reflect the treatment outcome. *Phys. Med. Biol.* 54:5949–5963, 2009.
- [15] J. Langus, M. Kranjc, B. Kos, T. Šuštar and D. Miklavčič, "Dynamic finite-element model for efficient modelling of electric currents in electroporated tissues", *Sci. Rep*, 6, 26409; doi: 10.1038/srep26409, May 2016.
- [16] S. Corovic, I. Lackovic, P. Sustaric, T. Sustar, T. Rodic and D. Miklavčič, "Modeling of electric field distribution in tissues during electroporation", *BioMedical Engineering OnLine*, vol 12, 2013.
- [17] A. L. Vera-Tizatl et al., "Investigation of numerical models for planning of electrochemotherapy treatments of invasive ductal carcinoma", presented at the Global Medical Engineering Physics Exchanges/Pan American Health Care Exchanges (GMEPE/PAHCE), Chiapas, Mexico, 2017.
- [18] IA. Cree. *Cancer Cell Culture: Methods and Protocols*. Totowa: Humana Press; 2011

APPENDIX K: CONFERENCE PAPER (PRODUCTIVITY)

Pilot Study on the Enhancement of Pharmacological Effect of Paclitaxel with Electrochemotherapy for Breast Cancer Treatment

C. E. Vera-Tizat¹, A. L. Vera-Tizat², P. Talamás-Rohana¹, A. Vera-Hernández², S. Rodríguez-Cuevas³.
¹Department of Infectomics and Molecular Pathogenesis, ²Department of Electrical Engineering, Bioelectronics, CINVESTAV, Av. Instituto Politécnico Nacional 2508, MX-07360 Mexico City, MEXICO
³ Mexican Society of Oncology, SMEO, Vértiz Narvarte, 03600 Mexico City, MEXICO.

INTRODUCTION

Invasive ductal breast carcinoma is the most common cancer type in México. Based on the poor outcome to conventional therapies and the successful clinical response to electrochemotherapy (ECT) of different cancer types [1], ECT optimization for breast cancer is encouraged [2]. Hence, the determination of cell-specific electroporation (EP) thresholds for an efficient permeabilization in adhered cells, and the results obtained for ECT *in vitro* are presented in this work.

METHODOLOGY

In silico prediction of the electric field distribution due to the application of EP was carried out through the finite element method (FEM). Subsequently, the outcomes were experimentally validated taking into account cell viability and external molecule uptake to establish the most efficient EP protocol. Cell viability was measured by the MTT assay, and molecular uptake was monitored through epifluorescence microscopy.

ECT was performed using the selected protocol along with the taxane Paclitaxel in two breast cancer cell lines, BT-20 and MCF-7. Cell death was determined to assess drug effectiveness improvement. The pharmacological effect of paclitaxel was evaluated through the Annexin V and the Ethidium Homodimer III (EthD-III) recognition.

RESULTS

The optimal electric field for the permeabilization of MCF-7 cells, was in agreement with simulations. Conversely, BT-20 cells were permeabilized with a lower electric field than the simulated [Table 1]. The molecule uptake is shown in Figure 1.

MCF-7 cells showed an increased response to the ECT with a higher cell death through apoptosis than chemotherapy alone. In contrast, BT-20 cells showed a poor response to ECT only exhibiting a faster triggering of apoptosis with a similar cell death compared to chemotherapy.

CONCLUSION

Based on the results, EP may potentiate paclitaxel efficacy in hormonal cancer cells (MCF-7) resulting in an adjuvant therapy. Regarding triple negative cells (BT-20), the low cell viability due to EP suggests that irreversible electroporation could be a more effective treatment without the need to use an antineoplastic drug.

Table 1: Electroporation protocols

Cell line	Pulse amplitude [V]	Electric field [V/cm]		Cell viability [%]
		<i>In silico</i>	<i>In vitro</i>	
BT-20	160	415	332	50
MCF-7	200	415	415	100

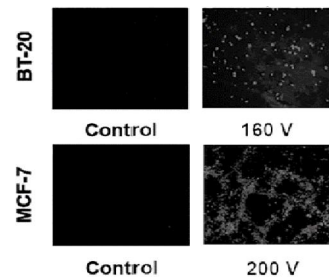


Figure 1: Cell-specific electroporation protocol based on external molecule uptake.

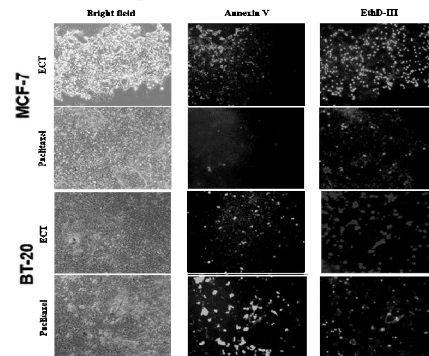


Figure 2: Recognition of apoptotic cells after ECT by Annexin V and EthD-III.

REFERENCES

- [1] G. Sersa and D. Miklavcic, "Electrochemotherapy of Tumours," Journal of Visualized Experiments, no. 22, 2008.
- [2] C. E. Vera-Tizat, A. L. Vera-Tizat, J. C. Osorio-Trujillo, P. Talamas-Rohana, S. Rodríguez-Cuevas, L. Leija-Salas, and A. Vera-Hernandez, "Establishment of Electroporation Protocols in BT-20 and SKOV-3 Cell Lines based on Finite Element Modeling," 2018 15th International Conference on Electrical Engineering, Computing Science and Automatic Control (CCE), 2018.

12. REFERENCES

- Agoramurthy P., Campana L., and Sundararajan R., (2011), "Finite element modeling and analysis of human breast tissue for electrochemotherapy", Annual Report Conference on Electrical Insulation and Dielectric Phenomena, Cancun, 2011, pp. 191-194.
- Arena C. B, Szot C. S, Garcia P. A, Rylander M. N, Davalos R. V. (2012), "A Three-Dimensional In Vitro Tumor Platform for Modeling Therapeutic Irreversible Electroporation", 2012, Biophysical Journal, 103:2033-2042.
- Batista N. & Miklavcic, D. (2018). In vitro electroporation detection methods - An overview. Bioelectrochemistry, 120, 166-182.
- Bianchi G, Campanacci L, Ronchetti M, Donati D. (2016), Electrochemotherapy in the treatment of bone metastases: a phase II trial. World J Surg.40(12):3088-3094.
- Bronzino J. D. (1995). The Biomedical Engineering Handbook. Boca Raton: CRC Press: IEEE Press, 2862 p
- Cabula C. (2012), Neoadjuvant electrochemotherapy of breast cancer: our experience on first case treated in Italy. Updates Surg. 65(4):325-328.
- Cadossi, R. et al. (2014). Locally enhanced chemotherapy by electroporation clinical experience and perspective of use of ECT. *Future Concol*, 10(5), 877-890.
- Caliari S. R. and Burdick J. A, (2016), "A practical guide to hydrogels for cell culture", Nat Methods. 13(5): 405–414.
- Campana LG, Galuppo S, Valpione S, et al. (2014), Bleomycin electrochemotherapy in elderly metastatic breast cancer patients: clinical outcome and management considerations. J Cancer Res Clin Oncol.;140(9):1557-1565.
- Clark , K., Vendt, B., Smith, K., Freymann , J., Kirby, J., Koppel , P., . . . Prior, F. (2013). The Cancer Imaging Archive (TCIA): Maintaining and Operating a Public Information Repository. *Journal of Digital Imaging*, 26(6), 1045-1057.
- Corovic, S, I. Lackovic, P. Sustaric, T. Sustar, T. Rodic and D. Miklavčič, (2013). Modeling of electric field distribution in tissues during electroporation, BioMedical Engineering OnLine, 12-16.
- Corovic, S., Zupanic, A., & Miklavcic, D. (2008). Numerical Modeling and Optimization of Electric Field Distribution in Subcutaneous Tumor

Treates With Electrochemotherapy Using Needle Electrodes. *IEEE Transactions on Plasma Science*, 36(4), 1665-1672.

- Denzi A, Strigari L, Di Filippo F, et al. (2015), Modeling the positioning of single needle electrodes for the treatment of breast cancer in a clinical case. *Biomed Eng Online*. 14(suppl 3): S1.
- Dong S, Wang H, Zhao Y, Sun Y, Yao Y, (2018). First Human Clinical Trial of High-Frequency Irreversible Electroporation Therapy for Prostate Cancer. *Technology in Cancer Research & Treatment*, 17:1-9.
- Edhemovic I, Brecelj E, Gasljevic G, et al. (2014). Intraoperative electrochemotherapy of colorectal liver metastases. *J Surg Oncol*. 110(3):320-327.
- Ertas M, Yildirim I, Kamasak M, Akan A. (2013), Digital breast tomosynthesis image reconstruction using 2D and 3D total variation minimization. *Biomed Eng Online*. 12(1):112.
- Gabriel S, Lau RW, Gabriel C. (1996). The dielectric properties of biological tissues: III. Parametric models for the dielectric spectrum of tissues. *Phys Med Biol*. 41(11):2271-2293
- Gothelf A, Mir L. M, Gehl J, (2003), Electrochemotherapy: results of cancer treatment using enhanced delivery of bleomycin by electroporation. *Cancer Treatment Reviews*, 29:5:371-387.
- Granata V, Fusco R, Piccirillo M, et al. (2015), Electrochemotherapy in locally advanced pancreatic cancer: preliminary results. *Int J Surg*. 18:230-236.
- Haberl, S. et al. (2013). Cell Membrane Electroporation-Part2: The Applications. *IEEE Electrical Insulation Magazine*, 29(1), 29-37.
- Hofmann A. G, Dimmer S, Nanda G. S, (1999), "Electroporation therapy: A new Approach for the Treatment of Head and Neck Cancer", *IEEE Trans. Biomed. Eng.*, vol. 46, no. 6, pp. 752–759.
- Ivey J. W, Latouche E. L, Sano M. B, Rossmeis J. H, Davalos R. V. and Verbridge S. S. (2015). "Targeted cellular ablation based on the morphology of malignant cells", *Sci. Rep*. 5, 17157.
- Ivorra A, (2009). "Tissue Electroporation as a Bioelectric Phenomenon: Basic Concepts" in *Irreversible Electroporation*, B. Rubinsky, Ed. Berkeley California: Springer, ch. 2, pp. 23-62.
- Jourabchi N, Beroukhim K, Tafti B. A, Kee S. T. and Lee E. W. (2014) Irreversible electroporation (Nanoknife) in cancer treatment. *Gastrointest Interv*, 3:8-18.

- Jossinet J. Variability of impedivity in normal and pathological breast tissue. (1996). *Med Biol Eng Comput.* 34(5):346-350
- Kalavathy G, Sasi KS, Manohar PE, Sundararajan R. (2015), Electrochemotherapy makes resectable from unresectable and pain reduction in chest wall recurrence breast cancer of two patients. *J Cancer Prev Curr Res.*3(2):00074.
- Kamensek U, Cemazar M, Lampret T, Ursic U, and Sersa, G. (2018). Antitumor in situ vaccination effect of TNFalpha and IL-12 plasmid DNA electrotransfer in a murine melanoma model. *Cancer Immunol Immunother*, 67, 785-795.
- Kanduser M, Miklavcic D, (2008), "Electroporation in Biological Cell and Tissue: An Overview" in *Electrotechnologies for Extraction from Food Plants and Biomaterials*, N. Lebovka, E. Vorobiev, Ed. N.Y: Springer, ch. 1, pp. 1–37.
- Kos, B. et al. (2010). Robustness of treatment planning of electrochemotherapy of deep seated tumors. *J Membrane Biol*, 174-153.
- Kos B. (2017), Treatment Planning for Electrochemotherapy and Irreversible Electroporation of Deep-Seated Tumors. In: Miklavcic D. (eds) *Handbook of Electroporation*. Springer.
- Kotnik T, Rems L, Tarek M and Mikavcic D. (2019). Membrane electroporation and electropermeabilization: Mechanisms and Models. *Annu. Rev. Biophys*, 48:63-91
- Kotnik T, Frey W, Sack M, Haberl Meglic S, Peterka M and Miklavcic D. (2015). Electroporation-based applications in biotechnology. *Trends Biotechnol*, 33, 480-8.
- Kotnik T, Kramar P, Pucihar G, Miklavcic D. and Tarek M. (2012). Cell membrane electroporation- Part 1: The phenomenon. *IEEE Electrical Insulation Magazine*, 28, 14-23.
- Langus, J, Kranjc, M, Kos, B, Šuštar, T, and Miklavčič, D. (2016), Dynamic finite-element model for efficient modelling of electric currents in electroporated tissues, *Sci. Rep*, 6, 26409.
- Larkin J. O., C. G. Collins, S. Aarons, M. Tangney, M. Whelan, S. O'Reily, O. Breathnach, D. M. Soden and G. C. O'Sullivan. (2007). Electrochemotherapy: aspects of preclinical development and early clinical experience. *Ann Surg* 245: 469-479.

- Maček A, Serša G, Kranjc S, Groslej A, and Miklavčič D. (2002). Optimisation of Pulse Parameters *In Vitro* for *In Vivo* Electrochemotherapy. *Anticancer Research* 22: 1731-1736.
- Marcan M, Pavliha D, Kos B, Forjanič T, and Miklavčič D. (2015). 'Web-Based Tool for Visualization of Electric Field Distribution in Deep-Seated Body Structures and Planning of Electroporation-Based Treatments'. *Biomedical Engineering Online* 14 Suppl 3.
- Masson Doyma México S. A. (2015). *Consenso Mexicano sobre diagnóstico y tratamiento del cáncer mamario*.
- Matthiessen LW, Johannesen HH, Hendel HW, Moss T, Kamby C, Gehl J. (2012), Electrochemotherapy for large cutaneous recurrence of breast cancer: a phase II clinical trial. *Acta Oncol.* 51(6): 713-721.
- Meijerink M. R, Scheffer H. J, Narayanan G. (2018), Irreversible Electroporation in Clinical Practice, Springer, Switzerland. ISBN 978-3-319-55113-5
- Miklavcic D., D. Semrov, H. Mekid and L. M. Mir. (2000). A validated model of in vivo electric field distribution in tissues for electrochemotherapy and for DNA electrotransfer for gene therapy. *Biochim Biophys Acta* 1523: 73-83.
- Miklavcic D. and Davalos V. R. (2015), Electrochemotherapy (ECT) and irreversible electroporation (IRE) -advanced techniques for treating deep-seated tumors based on electroporation. *Biomedical Engineering Online*, 14 (Suppl 3): 11
- Miklavcic D. et al. (2010). Towards treatment planning and treatment of deep-seated solid tumors by electrochemotherapy. *Biomed Eng Online*, 23; 9:10.
- Miklavcic D. et al. (2012). Electrochemotherapy: technological advancements for efficient electroporation-based treatment of internal tumors. *Med. Biol. Eng. Comput*, 1213-1225.
- Miklavcic, D. et al. (2014). *Electrochemotherapy: from the drawing board into medical practice*. Retrieved from BioMedical Engineering [Online]: <http://www.biomedical-engineering-online.com/content/13/1/29>
- Mimics Student Edition Course Book*. (n.d.). Retrieved from <http://uc.materialise.com/mimics>
- Mir, L. M. et al. (2006). Standard operating procedures of the electrochemotherapy: instructions for the use of bleomycin or cisplatin administered either systemically or locally and electric pulses delivered

by the Cliniporator™ by means of invasive or non-invasive electrodes. *EJC Supplements*, 4, 14-25.

- Mir L. M. (2008). "Application of Electroporation Gene Therapy: Past, Current and Future" in *Electroporation Protocols preclinical and Clinical Gene Medicine*, S. Li, Ed. Totowa, NJ: Humana Press, ch. 1, pp. 3–18.
- Moran MS, Schnitt SJ, Giuliano AE, et al. (2014), Society of Surgical Oncology–American Society for Radiation Oncology Consensus Guideline on Margins for Breast-Conserving Surgery With Whole-Breast Irradiation in Stages I and II Invasive Breast Cancer. *Int J Radiat Oncol Biol Phys*. 88(3):553-564
- Neal R. E, Davalos R. V. (2009). The feasibility of irreversible electroporation for the treatment of breast cancer and other heterogeneous systems. *Ann Biomed Eng*. 37(12):2615-2625.
- Neal R. E, Singh R, Hatcher H. C, Kock N. D, Torti S. V, Davalos R. V. (2010), Treatment of breast cancer through the application of irreversible electroporation using a novel minimally invasive single needle electrode. *Breast Cancer Res Treat*. 123(1):295-301.
- Numerical Breast Phantoms Repository. <http://uwcem.ece.wisc.edu/MRI/database/>. Accessed October 12, 2017.
- Pavliha, D, B. Kos, A. Zupanic, M, Marcan, G. Sersa and D. Miklavcic. (2012). Patient-specific treatment planning of electrochemotherapy: Procedure design and possible pitfalls. *Bioelectrochemistry* 87, 265-273.
- Pavliha, D. et al. (2013). Planning of electroporation-based treatments using web-based treatment planning software. *J. Membrane Biol.*, 246, 833-842.
- Pavlin M., M. Kanduser, M. Rebersek, G. Pucihar, F. X. Hart, R. Magjarevic and D. Miklavcic. (2005). Effect of cell electroporation on the conductivity of a cell suspension. *Biophys J* 88: 4378-4390.
- Pavselj, N., & Miklavcic, D. (2008). Numerical modeling in electroporation-based biomedical applications. *Radiol Oncol*, 3(42), 159-168.
- Probst U, Fuhrmann I, Beyer L and Wiggermann P, (2018), Electrochemotherapy as a New Modality in Interventional Oncology: A Review. *Technol Cancer Res Treat*. 17, 1-12.
- Pucihar G., T. Kotnik, B. Valic and D. Miklavcic. (2006). Numerical determination of transmembrane voltage induced on irregularly shaped cells. *Ann Biomed Eng* 34: 642-652.

- Reiser, I., & Sechopoulos, I. (2014). A review of digital breast tomosynthesis. *Medical Physics International Journal*, 2(1), 57-66.
- Ringel-Scaia V. M, et. al., (2019), High-frequency irreversible electroporation is an effective tumor ablation strategy that induces immunologic cell death and promotes systemic and anti-tumor immunity. *EBioMedicine*, 44:112-125.
- Rubinsky B. (2007), Irreversible electroporation in medicine, Technol. In Cancer Research Treatment, ISSN 1533-0346, 6: 255-259.
- Sersa G. and D. Miklavcic. (2008). Electrochemotherapy of tumours. *J Vis Exp* 15;(22). pii: 1038.
- Sersa G, Cufer T, Paulin SM, Cemazar M, Snoj M. (2012;), Electrochemotherapy of chest wall breast cancer recurrence. *Cancer Treat Rev.* 38(5):379-386.
- Smith, A. (2012). Fundamentals of breast tomosynthesis: Improving the performance of mammography. *WP-FundamentalsTomo*.
- Schmidt G, Juhasz-Boss I, Solomayer EF, Herr D. (2014), Electrochemotherapy in breast cancer: a review of references. *Geburtshilfe Frauenheilkd.*74(6):557-562.
- Smith, K. et al. (n.d.). *Radiology Data from The Cancer Genome Atlas Breast Invasive Carcinoma [TCGA-BRCA] collection*. Retrieved from <http://dx.doi.org/10.7937/K9/TCIA.2016.AB2NAZRP>.
- Spugnini E. P., G. Arancia, A. Porrello, M. Colone, G. Formisano, A. Stringaro, G. Citro and A. Molinari. (2007). Ultrastructural modifications of cell membranes induced by "electroporation" on melanoma xenografts. *Microsc Res Tech* 70: 1041-1050.
- Surowiec A. J, Stuchly S. S, Barr J. B, Swarup A. (1988), Dielectric properties of breast carcinoma and the surrounding tissues. *IEEE Trans Biomed Eng.* 35(4):257-263
- Vera-Tizatl A. L, C. E. Vera-Tizatl, A. Vera-Hernández, L. Leija-Salas, S. Rodríguez Cuevas, B. Kos, D. Miklavčič, (2018), “**Computational Feasibility Analysis of Electrochemotherapy with Novel Needle-Electrode Arrays for the Treatment of Invasive Breast Ductal Carcinoma**”, *Technology in Cancer Research and Treatment*, 17.
- Vera Tizatl A. L. (2013). *Desarrollo de un sistema de un sistema de electroporación para ser aplicado en tejido canceroso*. Mexico city,

Mexico: M. of A. T. dissertation, Programa en Tecnología Avanzada, UPIITA-IPN.

Vera Tizatl, A. L et al., (CCE). (2016). Electric Field Distribution Obtained by Using the Finite Element Method and 3D Reconstruction of a Breast Carcinoma: Approach to the Electroporation of Deep-seated Tumors by Using Two Needle Electrodes. *13th International Conference on Electrical Engineering, Computing Science and Automatic Control (CCE)*. Mexico City, Mexico.

Vera Tizatl A. L. et al (EBTT). (2016). Electric Field Distribution Generated by Two Needle Electrodes in an Anatomical Model of a Deep-Seated Breast Carcinoma. *Electroporation Based Technologies and Treatments (EBTT), International Scientific Workshop and postgraduate course*. Ljubljana, Slovenia.

Vera Tizatl, A. L., Kos, B., Miklavcic, D., Vera Tizatl , C. E., Vera Hernández , A., Leija Salas , L., & Rodríguez Cuevas, S. (2017). Investigation of numerical models for planning of electrochemotherapy treatments of invasive ductal carcinoma. *Global Medical Engineering Physics Exchanges (GMEPE) & Pan American Health Care Exchanges (PAHCE)*. Chiapas, Mexico.

Vera-Tizatl, A. L, Vera-Hernández, A, Leija-Salas, A, Kos, B, Miklavčič. D. (2017) **“Comparison of different electrode arrays for treatment of breast tumors with electrochemotherapy”**, 26th International Electrotechnical and Computer Science Conference (ERK), 25, 26/09/2017, Portorož, Slovenia.

C. E. Vera-Tizatl, A. L. Vera-Tizatl, J. C. Osorio Trujillo, P. Talamás Rohana, A. Vera-Hernández, L. Leija-Salas, S. Rodríguez Cuevas. **“Establishment of Electroporation Protocols in BT-20 and SKOV-3 Cell Lines based on Finite Element Modeling”**, 15th International Conference on Electrical Engineering, Computing Science and Automatic Control (CCE). 05-07/09/2018. Mexico City.

Wichtowski M, Murawa D, Kulcenty K, Zaleska K. (2017), Electrochemotherapy in breast cancer—discussion of the method and literature review. *Breast Care*. 12(6):409-414.

Wichtowski M, Potocki P, Kufel-Grabowska J, Streb J, Murawa D. (2016) Electrochemotherapy in the treatment of massive, multisite breast cancer metastasis to the skin and subcutaneous tissue: a case report. *Breast Care (Basel)*. 11(5):353-355.

- Zastrow E, Davis S. K, Lazebnik M, Kelcz F, Van Veen B. D, Hagness S. C. (2008), Development of anatomically realistic numerical breast phantoms with accurate dielectric properties for modeling microwave interactions with the human breast. *IEEE Trans Biomed Eng.* 5(12):2792-2800.
- Zhang W, Wang W, Chai W, et al. (2017), Breast tissue ablation with irreversible electroporation in rabbits: a safety and feasibility study. *PLoS One.* 12(7)
- Zhao, D, Wu M, Huang D, Liang Z, Wei Z. & Li Z. (2018). Parametric optimization of electric field strength for cancer electrochemotherapy on a chip-based model. *Theranostics*, 8, 358-368.
- Zupanic, A., Kos, B., & Miklavcic, D. (2012). Treatment planning of electroporation-based medical interventions: electrochemotherapy, gene electrotransfer and irreversible electroporation. *Physics in Medicine and Biology*, 17(57), 5425-5440.